ELECTROMIGRATION-INDUCED FAILURE CHARACTERISTICS OF GMR SPIN-VALVES AND MAGNETIC MULTILAYERS FOR THE ELECTRICAL RELIABILITY OF SPINTRONIC DEVICES

JING JIANG

(M. Eng., Hefei University of Technology, P. R. China)

A THESIS SUBMITTED

FOR THE DEGREE OF DOCTOR OF PHILOSOPHY

DEPARTMENT OF ELECTRICAL & COMPUTER ENGINEERING

NATIONAL UNIVERSITY OF SINGAPORE

January 2011

ACKNOWLEDGEMENT

I would like to take this opportunity to thank all those who have helped and supported me in completing the work within this dissertation. First and foremost, I would like to give my utmost gratitude to my supervisor, Assistant Professor Seongtae Bae, for his kind and consistent concern, support and guidance in the project and also all the valuable discussion on the experimental results. He is a generous and caring mentor, always willing to offer a helping hand when I encountered difficulties over the past few years. Moreover, his active attitude and precise spirit of doing research have great influence on my personality. I do appreciate his precious advice and counseling. Without his encouragement and understanding, I would not have been able to achieve this research goal.

I am also grateful to be in a caring, supportive and cooperative research team. I'd like to thank Dr Sunwook Kim, Dr Howan Joo, Mr. Minghong Jeun, Ms. Naganivetha Thiyagarajah, Ms. Lin Lin, and Ms. Ping Zhang for their help in carrying out the experiment. I would especially like to thank Mr. Dinggui Zeng working closely with me in BML, Mr. Bee Ling Tan in DSI helping me do the AES characterization and Dr Hojun Ryu from ETRI (Korea) helping me do the TEM analysis. Their valuable assistance and support have been indispensable for my research work.

I would also like to express my heartfelt appreciation for all the staffs in BML and ISML for their efforts in maintaining the functionality of the equipments, caring for the welfare of the students, and making our life here safe and pleasant. In addition, deep appreciation also goes to my friends in Singapore and China for having faith in me and

encouraging me to pursue my research goal.

Last but not least, I would not have survived the PhD process without the support and understanding from my parents. Equally noble and important is my beloved husband Yongshan Yuan, who accompanies me throughout the most severe time. Without his patience, continuous support and encouragement, all these things would have never been possible.

TABLE OF CONTENTS

SUMMARY

Electromigration (EM) and thermally-induced inter-diffusion are considered as the crucial factors limiting the lifetime and performance of magnetoresistance (MR) heads. Different FM/Cu chemical interfaces (FM is $Ni_{81}Fe_{19}$, Co or $Co_{90}Fe_{10}$) and varying spacer and diffusion barrier layer thickness are used in this project to investigate the detrimental effect of EM-induced inter-diffusion on the reliability of NiFe/(Co or CoFe)/Cu/(Co or CoFe)/ NiFe/($Fe_{50}Mn_{50}$) based magnetic multi-layers (MLs) and GMR spin valve (SV) devices and to verify the blocking effect of Co and CoFe diffusion barrier on improving their lifetime and magnetic performance.

EM-induced inter-diffusion is demonstrated to be the dominant failure mechanism in NiFe/Cu/NiFe/FeMn based GMR devices. By decreasing the Cu spacer thickness, the lifetime of patterned NiFe/Cu/NiFe tri-layers was dramatically increased. The obvious shorter lifetime of NiFe/Cu/NiFe tri-layers compared to that of Co/Cu/Co tri-layers could be attributed to the formation of current shunting paths from Cu to NiFe layers due to Ni-Cu intermixing. In addition, the failure mechanism of NiFe/Cu/NiFe tri-layers showed “bi-modal failure characteristics” and the critical current density (J_c) was determined to be 7×10^7 A/cm^2. The current density dependence factor, "n" values, are determined at 5.4 and 1.3, respectively, when the applied current density is below or above J_c.

An ultrathin Co (or CoFe) film is inserted between Cu and NiFe layers for reducing the Cu inter-diffusion. The optimal thickness of diffusion barrier layer is demonstrated to be beyond 0.5 nm. The activation energy of the patterned NiFe/Cu/NiFe magnetic multi-layered devices (MMLD) was increased from 0.52±0.2 eV to 1.17±0.16 eV by inserting a 0.5-nm Co diffusion barrier. Electrically stressed NiFe/Cu/NiFe tri-layers

showed a maximum reduction of 41% in the magnetic moment, and an obvious shift of interlayer coupling characteristics. In contrast, no detectable magnetic degradation was observed in the NiFe/Co/Cu/Co/NiFe SV-MLs. The obvious improvement of electrical and magnetic properties could be attributed to the dramatically reduced "current shunting paths" and the development of "self-healing process" resulted from the effectively controlled Ni-Cu intermixing. Further investigation on the EM and thermomigration (TM)-induced magnetic degradation of NiFe/(Co or CoFe)/Cu/(Co or CoFe)/NiFe/FeMn top exchange biased GMR (EBGMR) SV devices confirmed that the effectively reduced Mn atomic inter-diffusion at the NiFe/FeMn interface and the well maintained interfacial spin dependent scattering resulted from the control of EM and TM-induced Cu spacer inter-diffusion were the main physical reasons for enhancing the device reliability. CoFe thin films are found to be more effective than Co thin films in controlling the Cu inter-diffusion.

The effect of magnetic field on accelerating the EM-induced failures in SV-MLs was also investigated. The observed failure characteristics suggested that the magnetic field leads to accelerating Cu spacer atomic migration to the adjacent magnetic layers. Furthermore, theoretical analysis results confirmed that Hall effect-induced Lorentz force driven to the perpendicular-to-the-film-plane direction is primarily responsible for the severe acceleration of EM failures due to its dominant contribution to abruptly increasing local temperature and current density. The proposed failure model and the theoretical calculations were demonstrated to agree well with the experimental observation.

LIST OF FIGURES

LIST OF TABLES

CHAPTER 1 INTRODUCTION

This chapter starts from a brief review of the previous studies on electromigration (EM) in the interconnect metallization and magnetic thin films. In the first part (Section 1.1), we also introduce our motivation to study the EM-induced failure characteristics of GMR spin-valves and magnetic multilayers for the electrical reliability of spintronic devices. In the second and third parts, the objective of this project and synopsis of this thesis are described.

1.1 Background and Motivation

Electromigration (EM) is the name given to the mass transport caused by atomic migration when the high electrical current density imposed on metallic stripes, which causes electrostatic force and electron wind force (Fiks, 1959; Huntington, 1961) to activate atomic flux divergence and also results in temperature gradient due to current crowding effect induced joule heating (Gupta, 1988). It is one of the major failure phenomena in thin film technology and integrated circuits (ICs). Early experiments have shown that EM progressed most rapidly along grain boundaries, with depletion and accumulation of the migrating atoms occurring primarily at grain boundary triple-points (Hummel, 1977). After sufficient migration, the depleted regions are macroscopically observable as voids which lead to increasing current density, high resistance, hot spots, thermal runaway, and ultimately destroy the electrical continuity or even result in catastrophic failure from melting. On the other hand, in thin films without dielectric overlayers, the atoms that are removed from the void regions are typically

driven to the surface where they form “hillocks” or “whiskers”, which could cause shorting between closely spaced layers and lines.

Since the late 1960s when EM was identified as the fatal factor causing the failure of aluminum (Al) metallization lines of very-large-scale integration (VLSI) (Blech, 1967), a flurry of activities have been stimulated to study the EM-induced “cracked stripe” problem in the microelectronic ICs. Electromigration in polycrystalline metallic thin films has been considered as one of the major failure mechanisms responsible for the degradation of the high-density integrated semiconductor circuits (d’Heurle, 1978; Ogawa, 2002; Strehle, 2009). At moderate temperature of about half the absolute melting point ($<0.5T_{melt}$), the atomic mass transport is mainly through grain boundaries and therefore obeys the well established diffusion equations. The basic equation governing EM flux, J, is given by Eq. 1-1 (Trang, 1994),

$$J = \frac{ND}{kT} F \tag{1-1}$$

where N is atomic concentration, D is the diffusion coefficient, which is temperature dependent, T is absolute temperature and k is Boltzmann’s constant, F is the total driving force, which can be expressed as $F = Z^* e \rho j$, eZ^* is effective charge, j is the applied current density, and ρ is the resistivity.

The most general failure characteristics induced by EM is the formation of voids and hillocks (or extrusion). However, the occurrence of EM-induced failures (EIF) has two basic prerequisites: carrying a current density higher than the threshold current density (e.g. 2×10^5 A/cm^2 for Al and Au conductor lines) (Tang, 1990) and non-zero atomic flux divergence. The free-electron model of conductivity of metals assumes that the

conduction electrons are free to move in the metallic, unstrained by the perfect lattice of ions except for scattering interactions due to phonon vibration. For example, a diffusion atom at its activated state possesses a very large scattering cross section. If the carrying current density is above 10^5 A/cm^2 or even higher (depending on the material and structure of thin films), the scattering will enhance atomic migration and results to mass transport. Nonzero atomic flux divergence is another compulsory requirement for EIFs. It exists at the places where the number of atoms flowing into the area is not equal to the number of atoms flowing out per unit time (Attardo, 1971; Venables, 1972). Microstructural inhomogeneities, temperature gradient and concentration gradient are the three primary factors responsible for the nonzero flux divergence. The former includes the grain size distribution, the distribution of grain boundary misorientation angles and the inclination of grain boundaries with respect to electron flow and so on. Previous studies indicate that in most cases, the junction of three grains which is called the triple points or saddle points in the grain boundaries can serve as the centers of atomic flux divergence. At these grain boundary intersections, there could be an abrupt change in grain size, which produces a change in the number of paths for mass transport. The atomic diffusivity could also be different due to variation in grain boundary microstructure. In addition to the microstructural inhomgeneities, the temperature variation in the metallic thin films can be the most important factor in accelerating EM induced degradation because of the exponential dependence of the atomic diffusivity on temperature. With the nonzero atomic flux divergence, there will be either a mass depletion (divergence > 0) or accumulation (divergence < 0), resulting in formation of

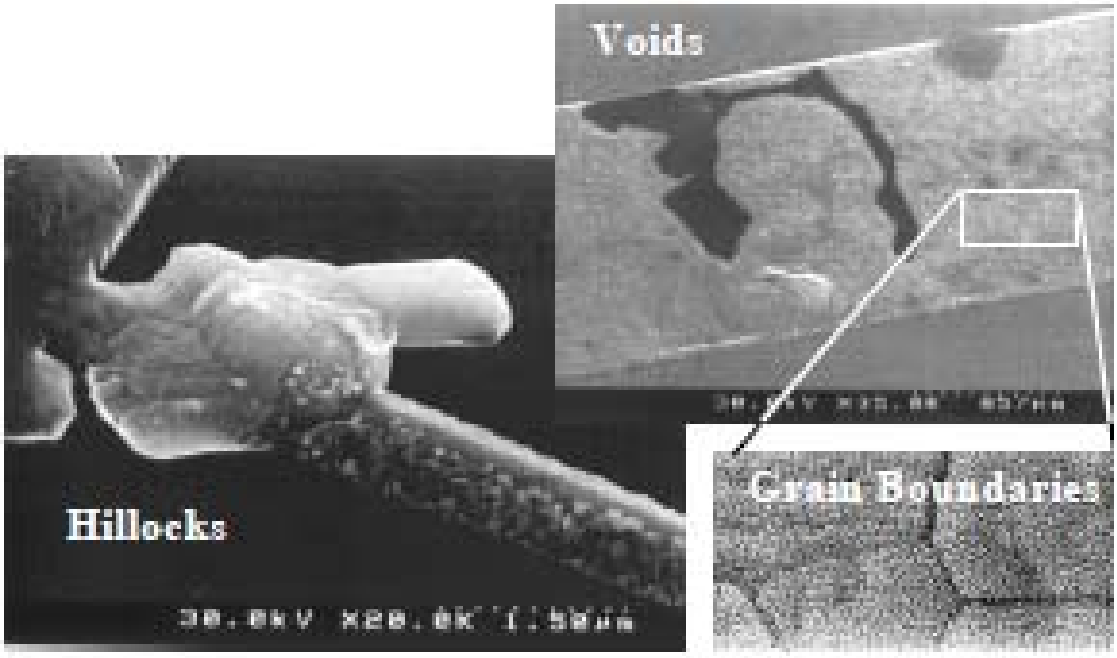

Fig. 1.1 Hillocks and voids (or cracks) formation due to electromigration (Jens Lienig, 2003)

voids (or cracks) and hillocks (or whiskers) as shown in Fig. 1.1. As the damage starts to form, the additional Joule heating generated by current crowding further increases the temperature. The temperature gradient in turn accelerates the growth rate of the voids/hillocks. When the voids collapse into a narrow slit across the width of the line or when the surface extrusion builds up the channel between adjacent layers or interconnects, the final irreversible failure of electrical discontinuities or short circuits occur. Empirically, electrical resistance is monitored with time and the EIFs in metallic thin films are usually determined by measuring the Time-to-Failure (TTF) or the Mean-Time-to-Failure (MTTF), t_{50}. The general expression for MTTF obeys the "Black equation" (Black, 1969) derived from the "Arrenius diffusion equation" and usually follows a lognormal distribution. Such behavior suggests that EIFs in thin films are mainly due to the inter-diffusion through grain boundaries resulting from defects

(including point, line, and volume defects) inhomogeneities in grains and localized temperature gradients after initializing EM. This phenomenon is especially significant in applications where high current densities are used and its damage to metallic thin films increases as the typical structure size decreases.

Since the "giant magnetoresistive" (GMR) effect was discovered by two European scientists working independently: Gruenberg Peter of the KFA research institute in Julich, Germany and Fert Albert of the University of Paris-Sud (Gruenberg, 1986; Albert, 1988) in 1980s, GMR spin valve (SV) devices have been widely used in the heads of hard disk drives (HDDs). However, the problem due to EM-induced failures (EIFs) is becoming serious because these SV devices are operated at current densities one order of magnitude higher than the maximum current density in Al or Cu interconnects in VLSI. GMR is a quantum mechanical effect observed in composed alternating layers of ferromagnetic and nonmagnetic layers. When the magnetic moments of the ferromagnetic layers are parallel, the spin-dependent scattering of the carriers is minimized, and the material has its lowest resistance, while when the ferromagnetic layers are anti aligned, the spin-dependent scattering of the carriers is maximized, and the material has its highest resistance. In December 1997, IBM introduced its first HDD using GMR heads. As archival storage devices, the minimum life of HDD is required to be longer than 5 years. As we can see in Fig. 1.2 and Fig.1.3 (Hitachii, 2003), the trend toward the extremely high information-storage density requires the GMR read heads to be miniaturized in an astonishing rate. For today’s 200 Gbytes longitudinal HDDs, the stripe height and width of GMR read heads has been

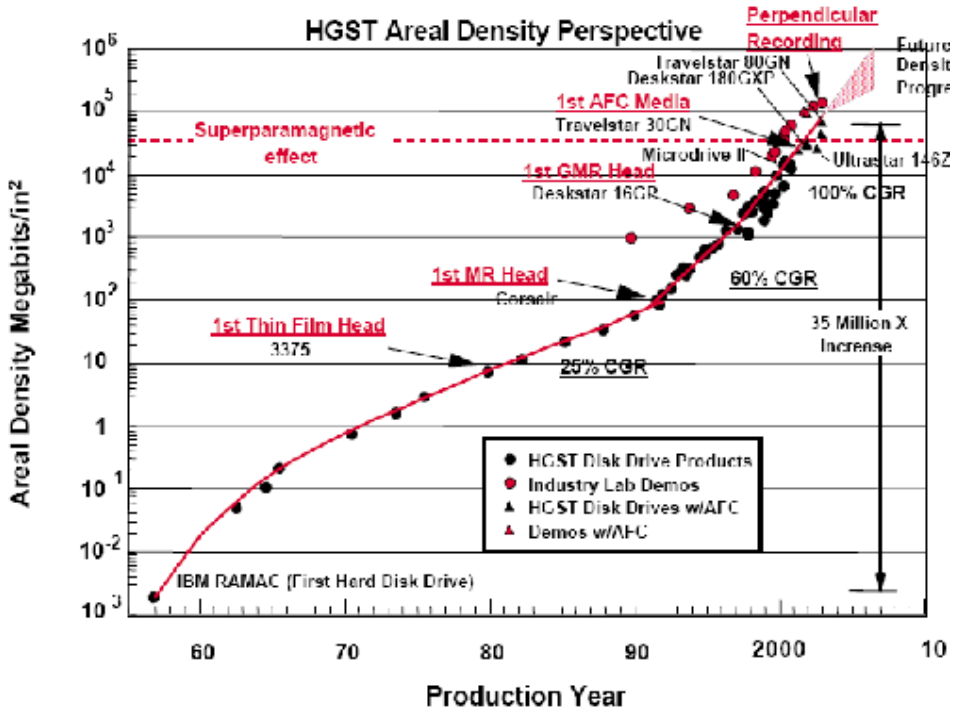

Fig.1.2 HDD technology roadmap based on Hitachi products, indicating large increases in areal density growth rates with the introduction of new technology. (Hitachii, 2003).

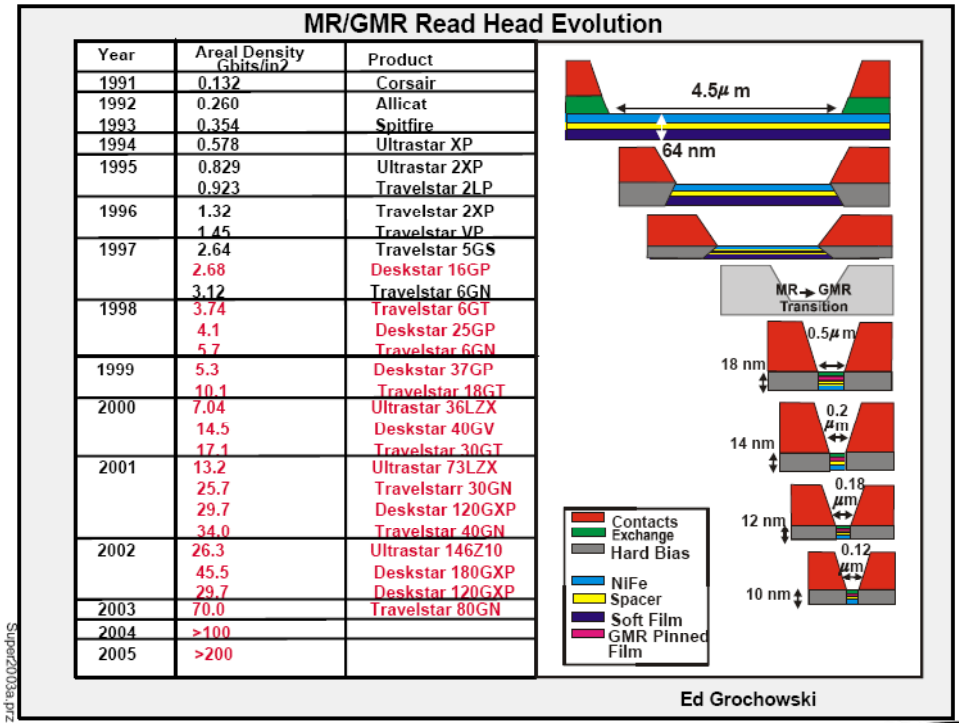

Fig.1.3 The MR/GMR read head evolution correspondingly with the increase of areal density since 1990s. (Hitachii, 2003).

dramatically scaled down to be 100 and 50 nm respectively and the "fly height" of read heads flying over the recording media is also reduced to 10 nm (McFadyen, 2006), and correspondingly the operating current density applied to the read sensors could reach ~ 10^8 A/cm^2 in order to maintain an adequate signal-to-noise ratio (SNR) (Childress, 2005). Therefore, electromigration of metals and inter-diffusion between thin layers due to the pronounced electron wind force and joule heating at such a high biasing current density may cause the electrical resistance of these GMR spin valves (SVs) to be increased by an unacceptable amount and also lead to degradation of magnetic performance. In the worst case, catastrophic failure may occur if the operating current density is high enough to cause total melting of the head metallurgy.

Although the lifetime measurement and physical mechanisms for the EM of magnetic single or multi-layers (MLs) and thermally induced inter-diffusion, thermomigration (TM) in the magnetic MLs and GMR SVs (Gurp, 1977; Cross, 1994; Sauto, 1998; Kos, 1997; Tsu, 1999; Bae, 2002; Zhao, 2007; Gafron, 2000; Hawraneck, 2008) have been investigated from 1970s, the failure mechanism for the EM-induced degradation of electrical and magnetic properties in FM/NM/FM (FM: ferromagnetism; NM: non-magnetic spacer) based GMR SV spintronic devices, especially under the combined stress of electrical and magnetic field, are still poorly understood. Thereafter, it is highly desirable to find out the physical mechanism behind it and to find an effective solution for improving the electrical and magnetic stability of these GMR SV devices.

In addition to the electron wind force directly related to the high electrical stress, the

temperature gradient in magnetic MLs or GMR SV devices is also an important driving force in accelerating EM and EM-induced inter-diffusion because of the exponential dependence of the atomic diffusivity on temperature. According to Eq. 1-2, high current density indicates serious joule heating. In addition, current crowding is the primary factor inducing joule heating and abnormal temperature distribution.

$$Q_{joule} = I^2 R \tag{1-2}$$

As we have discussed in the previous part, void formation is the typical signature of the early-stage EM and the micro cracking voids lead to current crowding. Actually, for the FM/NM/FM/AFM (FM: $Ni_{81}Fe_{19}$, Co, or $Co_{90}Fe_{10}$) based GMR ML devices, current crowding effect is more serious compared to that in the general conductors used in ICs. For an instance, considering the "current sinking effect" (Gurney, 1997) describing that more than 2/3 of applied current can flow through the Cu spacer in the NiFe/(Co or CoFe)/Cu/(Co or CoFe)/NiFe pesudo SVs due to the film resistivity difference between the high-conductivity Cu spacer and low conductivity magnetic thin films (the corresponding resistivity is listed in Table 1-1 (Jarratt, 1997; Brückner, 2000; Ko, 2003; Williams, 2000; Yang, 2004; Sousa, 2004), the temperature of Cu spacers is much higher than that of the magnetic layers initially. As a result, additional flux divergence in the direction perpendicular-to-the-plane may be initiated by the local temperature gradient resulted from the different film resistivity of each layer. Although in the current-in-the-plane (CIP) ICs (Schwartzenberger, 1988) and magnetic read sensors (Zeng, 2010), the flux divergence due to TM is smaller than that caused by EM, temperature gradients are actually important sources of atomic flux divergence. For

Table 1-1. The resistivity of different metallic thin films used in the NiFe/(Co or CoFe)/Cu/(Co or CoFe)/NiFe/FeMn MMLDs.

Thin film	Cu	$Ni_{81}Fe_{19}$	Co	$Co_{90}Fe_{10}$	$Fe_{50}Mn_{50}$
Resistivity (Ohm-m)	2.2×10^{-8}	2.1×10^{-7}	4.5×10^{-6}	2×10^{-7}	1.3×10^{-6}

example, at 200 °C in aluminium, a 5 °C change in temperature results in a change of more than 10% in the EM atomic flux (Schwartzenberger, 1988).

FM/Cu/FM/FeMn (FM: NiFe, Co, or CoFe) is a basic and core structure of the most often studied GMR SV read sensors, and so it's very critical to investigate the reliability problems relevant to the electrical and magnetic degradation of FM/Cu/FM/FeMn based GMR read heads caused by EM and thermally induced inter-diffusion, thermomigration (TM), across the multi-layered interfaces. Besides being operated at the current densities increased by 10 fold compared to that applied to the high conducting metals such as Al, Ag and Cu, magnetic read sensors and toggle switching GMR MRAMs are generally operated susceptible to an external magnetic fields retrieved from the recording media or R/W lines, as shown in Fig. 1.4. This geometrically-induced Hall-effect, which can exert an extra Lorentz force in the direction of perpendicular-to-the-plane, would further exacerbate the thermally induced atomic migration. Even though considerable research efforts were attempted to provide an insight into the physical mechanism responsible for the EM-induced failures under the accelerated electrical stress and different ambient temperature conditions, none of the previous authors (Gurp, 1977; Cross, 1994; Tsu, 1999; Bae, 2002; Zhao, 2007; Gafron, 2000) have reported the physical effect of applied magnetic field including dc and pulsed dc magnetic field on

the EM-induced failure lifetime and its characteristics.

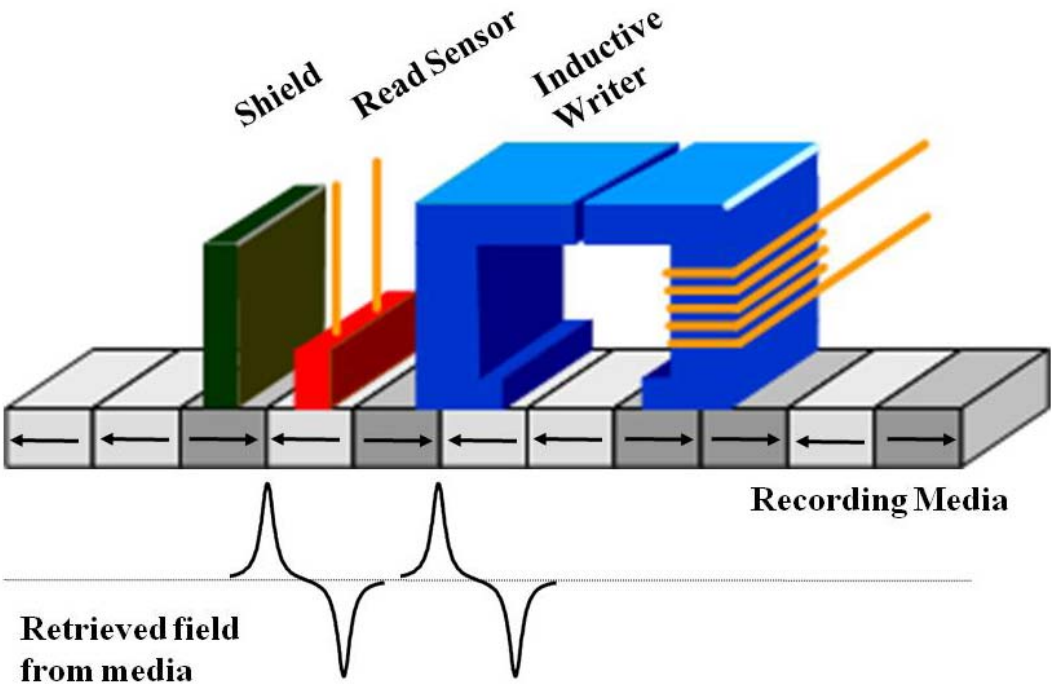

Fig. 1.4 Schematic illustration of a magnetic recording system.

1.2 Objectives and Work Done

Focusing on the implications of accelerated EM-induced failures of FM/Cu/FM/(FeMn) based GMR read sensors and interfacial mixing, local temperature gradient as well as Hall voltage, we have done the following research work:

(1) Study the EM-induced failure characteristics of NiFe/(Co)/Cu/(Co)/NiFe based GMR SV devices. Different FM/Cu chemical interfaces (FM: NiFe or Co) and varying Cu spacer thickness (from 1.8 to 4 nm) are used to investigate the effect of Cu inter-diffusion on the failure characteristics of the FM/Cu/FM tri-layers. Since the EM-induced failure characteristics could be an unacceptable resistance increase or melting of total metallurgy depending on the applied electrical stress, a “bi-modal failure characteristics” is developed and numerical data of the current dependence

factor of NiFe/Cu/NiFe and NiFe/Co/Cu/Co/NiFe MLs is graphically determined at the current densities below or above the critical current density (J_c) to find out the contribution of electrostatic force (or electron wind force) accelerated Cu inter-diffusion and joule heating at different current densities. Activation energy values of NiFe/Cu/NiFe and NiFe/Co/Cu/Co/NiFe MLs are also obtained by varying the ambient testing temperature from ambient temperature to 280 °C in order to show the controlled diffusion behavior by inserting an ultra-thin Co layer. Scanning electron microscopy (SEM), auger electron spectroscopy (AES), and Energy Dispersive X-ray (EDX) techniques are used to directly observe the failure characteristics and characterize the interfacial mixing.

(2) Investigate the relationship between magnetic degradation and EM as well as thermally induced inter-diffusion. Vibrating sample magnetometer (VSM) is employed to characterize the reduction of magnetic moment and the shift of interlayer coupling of electrically stressed NiFe/(Co)/Cu/(Co)/NiFe magnetic MLs, and a four-point probe MR measurement system is used to analyze the degradation of MR ratio and exchange bias field of electrically stressed NiFe/(Co or CoFe)/Cu/(Co or CoFe)/NiFe/FeMn GMR SV devices. Atomic force microscopy (AFM), high-resolution transmission electron microscopy (HR-TEM) and its attached EDX are also employed to compare the microstructure change of the different FM/Cu and Cu/FM (FM: NiFe or Co) interfaces.

(3) Optimize the electrical and magnetic stability of NiFe/Cu/NiFe/(FeMn) based GMR top SV structures by inserting a diffusion barrier such as Co and CoFe thin films. The dependence of mean-time-to-failure (MTTF) on the Co film thickness is measured to find out the optimized diffusion barrier thickness. The physical mechanism responsible for the effect of controlling atomic migration of Mn and Ni

atoms into Cu spacer on the improvement of electrical and magnetic reliability is explored. Comparison of blocking effect is also carried out between Co and CoFe diffusion barriers.

(4) For systematically investigating the effect of applied magnetic field on the EM-induced failure characteristics of magnetic read heads, the orthogonal electrical (current density is fixed at $J = 5 \times 10^7$ A/cm^2) and DC magnetic field (200~600 Oe) or pulsed DC magnetic field (H=200 Oe, duty factor is 0.3~1) are applied. MTTFs at different field strength and different duty factors are measured to evaluate the contribution of magnetic field-induced Hall voltage (Lorentz force) in accelerating the EM-induced failures. Failure characteristics analysis for the EM tested SV MLs under the electrical stress and combined electrical and magnetic stress is also carried out using HR-TEM.

(5) Theoretical calculation and thermo-electrical simulation are built to numerically predict the increased temperature gradient and atomic flux divergence caused by the high operating current density and magnetic field-induced current in the perpendicular-to-the-plane direction. A new physical model for interpreting the Hall-effect induced acceleration of EM failures in GMR SV devices needs to be developed and verified through the agreement of theoretical calculations with the experimental results.

1.3 The Outline of this Thesis

Chapter 2 provides a theoretical perspective of EM in the metallic thin films. Some significant previous research works on the EM phenomena in the conductor lines for the ICs and magnetic thin films for GMR SV devices are also summarized. In addition,

several important fundamentals related to this project are described, such as inter-diffusion in the magnetic MLs, Black equation, MR and Hall effect.

Chapter 3 describes the fabrication process of EM testing samples, lifetime measurement and failure criterion, as well as the key preparation and characterization techniques, such as AJA multi-target sputtering system, FE-SEM, TEM, AES, AFM, VSM and four-point probe MR measurement system.

Chapter 4 to Chapter 7 focuses on the results and discussion. Firstly, EM-induced failure characteristics of FM/Cu/FM (FM: NiFe, Co, or NiFe/Co) based GMR SV devices is presented. Lifetime and microstructure change of EM testing samples with different FM/Cu (and Cu/FM) interfaces and Cu spacer thickness will be compared, aiming to get a better understanding of the different failure mechanism dominant in NiFe/Cu/NiFe and NiFe/Co/Cu/Co/NiFe magnetic MLs. In addition, a “bi-modal failure characteristics” is proposed to interpret the different failure mechanism dominant at the different current density range below or above the critical current density (J_c). Secondly, magnetic degradation of NiFe/(Co)/Cu/(Co)/NiFe magnetic MLs caused by the EM and thermally induced inter-diffusion is studied. Topological coupling energy and oscillatory exchange coupling energy are also calculated to theoretically support the conclusion that controlling the chemical interface between NiFe and Cu and thus reducing the Cu inter-diffusion by inserting a thin Co film as diffusion barrier is quite effective for improving the electrical and magnetic reliability of NiFe/Cu/NiFe based SV devices. Thirdly, the physical reason responsible for the blocking effect of Co and CoFe diffusion barrier is investigated. Optimal diffusion barrier thickness is determined.

Comparison of blocking effect will also be carried out between CoFe and Co diffusion barriers, using the MR signal measurement and thermo-electrical simulation. Moreover, the reason for the reduction of MR ratio and exchange bias field strength will be discussed in detail. Finally, the magnetic field induced acceleration of EM-induced failures of NiFe/Co/Cu/Co/NiFe based GMR SV devices are demonstrated experimentally and theoretically. R-t curves and MTTFs of SV-ML devices stressed by both electrical and magnetic field are measured to show the strong dependence of EIF lifetime on the magnetic field strength and duty factors. A physical model is developed to numerically interpret the contribution of Hall voltage-induced Lorentz force to the abruptly increased temperature gradient and atomic flux divergence. This prediction will be verified both by the thermo-electrical simulation and microstructural analysis using HR-TEM.

Last but not the least, in Chapter 8, a summary of this work is provided, followed by a recommendation for future work.

References

Bae, S., Tsu, I-F., Davis, M., Murdock, E.S., Judy, J.H. (2002). EM study of magnetic thin Films for the electrical reliability of spin-valve read heads. IEEE Trans. Magn. **38**, 2655 - 2657.

Baibich, M.N., Broto, J. M., Fert, A., Nguyen van Dau, F., Petroff, F., Etienne, P., Creuzet, G., Friederich, A., and Chazelas, J. (1988). Giant magnetoresistance of (001)Fe/(001)Cr magnetic superlattices. Phys. Rev. Lett. **61 (21)**, 2472–2475.

Berenbaum, L. (1971). EM damage of grain-boundary triple points in Al thin films. J. Appl. Phys. **42**, 880-882.

Black, J.R. (1969). EM - a brief survey and some recent results. IEEE Trans. Electron Devices. **ED-16 (4)**, 338-347.

Blech, A. and Meieran, E.S. (1967). Appl. Phys. Lett. **11**, 263.

Brückner, W., Baunack, S., Heoker, M., Mönch, J.-I., van Loyen, L., and Schneider, C.M. (2000). Interdiffusion in NiFe/Cu/NiFe trilayers: Possible failure mechanism for magnetoelectronic devices. Appl. Phys. Lett. **77**, 358-360.

Childress, J.R., and Fontana Jr.,R.E. (2005) Magnetic recording read head sensor technology. C. R. Physique **6**, 997-1012.

Cross, R.W., Russek, S.E., and Sanders, S.C., Parker, M.R., Barnard, J.A., and Hossain, S.A. (1994). Size and self-field effects in giant magnetoresistive thin-film devices. IEEE Trans. Magn. **30**, 3825-3827.

d'Heurle, F.M., and Ho, P.S. In Thin Films: Interdiffusion and Reactions, edited by Poate, J.M., Tu, K.N., and Mayer, J.W. (New York: Wiley-Interscience, 1978), p.243.

Daughton, J. M. (1992). Magnetoresistive memory technology. Thin Solid Films **216**, 162-168.

Fiks, V.B. (1959). On the mechanism of the mobility of ions in metals. Soviet Physics – Solid State.**1**, 14 - 28.

Gafron, T.J., Burkett, S.L., and Russek, S.E. (2000). Current density limitations of spin valves. IEEE Trans. Magn. **36**, 2611-2613.

Genut, M., Li, Z., Mahajan, B.S., Tang, P.F., and Milnes, A.G. (1991). Characterization of early stages of EM at grain boundary triple junctions. Appl. Phys. Lett. **58**, 2354-

2356.

Gurney, B.A., Speriosu, V.S., Wilhoit, D.R., Lefakis, H., Fontana Jr.,R.E., Heim, D.E., and Dovek, M. (1997). Can spin valves be reliably deposited for magnetic recording applications?. J. Appl. Phys. **81**, 3998 (1-6).

Gurp, G. J. van. (1977). EM and hall effect in cobalt films. J. Phys. Chem. Solids. **38**, 627-633.

Grünberg, P., Schreiber, R., Pang, Y., Brodsky, M.B., and Sowers, H. (1986). Layered magnetic structures: evidence for antiferromagnetic coupling of Fe layers across Cr Interlayers. Phys. Rev. Lett. **57**, 2442–2445.

Hatachi HDD road map. (2003).

http://www.hitachigst.com/hdd/hddpdf/tech/hdd_technology2003.pdf

Hawraneck, W., Zimmer, J., Raberg, W., Prüg, K., Schmitt, S., Bever, T., Flege, S., and Alff, L. (2008). Diffusion based degradation mechanism in giant magnetoresistive spin valves. Appl. Phys. Lett. **93**, 012504-(1-3).

Hummel, R.E. (1977). Electromigration in thin films. In Electro- and thermo-transport in Metals and Alloys, Hummel, R.E., and Huntington, H.B. ed. (New York: Petroleum Engineerings, Inc.), 93-107.

Huntington, H.B., and Grone, A.R. (1961). Current induced marker motion in gold wires. J. Phys. Chem. Solids **20**, 76 - 87.

Jarratt, J.D., Klemmer, T.J., and Barnard, J.A. (1997). Electrical resistivity in sputtered $Co_{90}Fe_{10}$/Ag GMR MLs. J. Appl. Phys. **81**, 5793-5795.

Jiang, J., Bae, S., and Ryu, H., (2009). Magnetic instability of giant magnetoresistance spin-valves due to EM-induced inter-diffusion. Thin Solid Films **517**, 5557-5562.

Jiang, J., Zeng, D.G., Ryu, H., Chung, K.W., and Bae, S. (2010). Effects of controlling Cu spacer inter-diffusion by diffusion barriers on the magnetic and electrical stability of GMR spin-valve devices. J. Magn. Magn. Mater., **322**, 1834-1840.

Ko, Y.K., Park, D.S., Seo, B.S., Yang, H.J., Shin, H.J., Kima, J.Y., Lee, J.H., Lee, W.H., Reucroft, P.J., and Lee, J.G. (2003). Studies of cobalt thin films deposited by sputtering and MOCVD. Mater. Chem. Phys. **80**, 560-564.

Kos, A.B., Russek, S.E., Kim, Y. K., and Cross, R. W. (1997). High current density measurements of giant magnetoresistive spin-valves for magnetic recording and sensor applications. IEEE Trans. Magn. **33**, 3541-3543.

Lienig J. (2005). Invited talk: introduction to electromigration-aware physical design. Proceedings of SLIP'05, 81-88.

Massalski, T.B., Okamoto, H., Subramanian, P.R., Kacprzak, L. (1990). Binary Alloy Phase Diagram, 2nd edn. (OH: ASM International, Materials Park).

McFadyen, I.R., Fullerton, E.E., and Carey, M.J. (2006). State-of-the-art magnetic hard disk drives. MRS Bulletin **31**, 379-383.

Ogawa, E.T., Li, K.D., Blaschke V.A., and Ho, P.S. (2002). EM reliability issues in dual damascene Cu interconnections. IEEE Trans. Reliab. **51**, 403-419.

Parkin, S.S.P. (1994). Ultrathin Magnetics Structures II, edited by B. Heinrich and J. A. C. Bland (Berlin: Springer), Chap. 2.

Rosenberg, R., and Ohring, M. (1971). Void formation and growth during EM in thin films, J. Appl. Phys. **42 (13)**, 5671-5679.

Sauto, A.T., Iwasalu, H., Kamiguchi, Y., Fuke, H.N., and Sahashi, M. (1998).

Activation Energy of Interdrffusion and Interface Structure for CoFe/Cu Spin-valves. IEEE Trans. Magn. **34**, 1420.

Sousa, R.C., Prejbeanu, I.L., Stanescu, D., Rodmacq, B., Redon, O., Dieny, B., Wang, J.G., and Freitas, P.P. (2004). Tunneling hot spots and heating in magnetic tunnel junctions. J. Appl. Phys. **95**, 6783.

Strehle, S., Mezel, S., Jahn, A., Merkel, U., Bartha, J.W., and Wetzig, K. (2009). EM in electroplated Cu(Ag) alloy thin films investigated by means of single damascene Blech structures. **86**, 2396-2403.

Tang, P.F. (1990). Modeling of electromigration with applications to Au on GaAs. pp. 1, Ph.D thesis, Canegie Mellon University.

Tang, P.F. (1994). Simulation and computer models for electromigration. In Electromigration and electronic device degradation, Christou, A. ed. (New York: John Wiley & Sons, Inc.) p.33.

Tsu, I., Chang, C., and Edelman, H.S. (1999). Electrical reliability of giant magneto-resistive recording sensors. Mater. Res. Soc. Symp. Proc. **563**, 139-145.

Wang, S.X., and Li, G.X. (2008). Advances in giant magnetoresistance biosensors with magnetic nanoparticle tags: review and outlook", IEEE Trans. Magn. **44**, 1687-1702.

Williams, E.M., *Design and Analysis of Magnetoresistive recording heads*, (Wiley-IEEE Press, 2000).

Yang, Y., Shojaeizadeh, S., Bain, J.A., Zhu, J.G., and Asheghi, M. (2004). Detailed modeling of temperature rise in giant magnetoresistive sensor during an electrostatic discharge event. J. Appl. Phys. **95**, 6780-6782.

Zeng, D.G., Chung, K.W., and Bae, S. (2009). Thermomigration-induced magnetic degradation of current perpendicular to the plane giant magnetoresistance spin-valve read sensors operating at high current density. J. Appl. Phys., **106**, 113908 (1-6).

Zeng, D.G., Chung, K.W., Judy, J.H., and Bae, S. (2010). Numerical simulation of current density induced magnetic failure for giant magnetoresistance spin valve read sensors, J. Appl. Phys., **108**, 023903-(1-5).

Zhao, J., Garay, J.E., Tamburini, U.A., and Munir, Z.A. (2007). Directional EM-enhanced interdiffusion in the Cu-Ni system", J. Appl. Phys. **102**, 114902-(1-7).

CHAPTER 2 ELECTROMIGRATION AND GIANT MAGNETORESISTANCE - RELEVANT TOPICS

This chapter provides the theoretical background of the project. The first part (Section 2.1) will focus on introducing the essential theories on the electromigration (EM) in metallic thin films, which include the driving force for EM, grain boundary diffusion and atomic flux divergence, structural factor, current crowding effect and thermal gradient effect, as well as the self-healing effect. The second part (Section 2.2) will be devoted to discussing inter-diffusion in the magnetic multilayers (MLs) and its detrimental effect in the electrical and magnetic stability of GMR SV devices. After a detailed discussion on the theories relevant to EM and thermally induced inter-diffusion, the third part (Section 2.3) gives several methods for improving EM resistance. Finally, black equation, magnetoresistance (MR) and interlayer coupling are also described this chapter.

2.1 General Aspects of Electromigration in Thin Films

2.1.1 Theoretical Development of Electromigration

The enhanced atomic displacement and the accumulated effect of mass transport under the influence of electric field are defined as EM, which is the result of a combination of electrical and thermal effects on mass transport. Investigations of this phenomenon can be traced back to 150 years ago, when Geradin (Geradin, 1861) observed this diffusion-controlled phenomenon in molten alloys of lead-tin and

mercury-sodium. Although electromigration is a diffusion-controlled process, the driving force here is more complicated than what is involved in a pure diffusion process in which the concentration gradient of the moving species is the only component. By contrast, the electrical driving force for EM consists of the "electron wind force" and the electrostatic force (Ho, 1989; d'Heurle, 1978; Hesketh, 1979; Sorbello, 1985; Gupta, 1982). The theoretical studies for the driving force started from the early 1950's with the work of Seith and Wever (Seith, 1953). Their measurement on the mass transport across the phase diagram of some Hume-Rothery alloys provided the first evidence in terms of the nature of the driving force for EM, because they observed that the direction of atomic motion can be reversed and is correlated with the type of the majority charge carriers, instead of solely depending on the electrostatic force imposed by the applied electric field. In the semi-classical "ballistic" model, the concept of "electron wind" was first formulated by Fiks in 1959 (Fiks, 1959) as well as by Huntington and Grone in 1961 (Huntingto, 1961). Until the development of EM theory evolves into the ballistic model, the driving force for EM are believed to include two components: the electron wind force refers to the effect of momentum exchange between the moving electrons and the ionic atoms, and the electrostatic force is taken to be the force exerted by the electric field on the ionic atoms. The EM driving force can be rewritten as in Eq. 2-1 (Paul, 1989).

$$F = |e| EZ^* = |e| \rho j (Z^e + Z^w) = |e| \rho jZ[1 - \frac{1}{2} \frac{\rho_d N}{\rho N_d} \frac{m^*}{|m^*|}] \qquad (2\text{-}1)$$

where, $|e|$ is the absolute value of the electronic charge and E is the electric field, ρ_d is the extra resistivity created by a "defect" (i.e. a metal ion in a saddle point position or

magnetic metal atoms in the nonmagnetic spacer films), ρ is the metallic stripe resistivity, N_d is the defect density, N is the atomic density, j is the current density and m^* is the effective mass. The first term on the right is the electrostatic contribution and the second item is attributed to the momentum transfer. As we can see from Eq. 2-1, the direction of EM driving force is determined by the sign of m^*. For hole conductors the two terms are positive, which implies transport to the cathode. For electron conductors the momentum transfer term is negative.

When the current density, which is proportional to the electron flux density, is high enough (typically in the range of 10^5 to 10^7 A/cm^2), the electron wind becomes significant, although the ionic atoms also tend to move in the direction of the applied field if they are positively ionized. The migration direction is determined by the balance of these two forces. For the gold, aluminum and copper, the electron wind force overrides the electrostatic force and therefore the net electrical driving force is in opposite to the applied electrical field direction (Blech, 1975; Wang, 1998; Shao, 2005). But for transition metals such as Co, Ni, Fe etc. used in GMR spin valve MLs (SV-MLs) or devices studied in our project, the conduction takes place in two bands with holes and electrons, the momentum transfer term is composed of two contributions, with different values for m^*, ρ_d and ρ.

Irrespective of most investigations were concentrated on EM in bulk materials during that period, the interest as well as the direction of EM study took a drastic turn to the thin films in the late 1960s when research communities (Blech, 1966; Black, 1969) observed that EM is a primary source to induce failures of the Al semiconductor ICs and

Attardo's group recognize that the EM damage in Al film occurred mainly along the grain boundaries (Attardo, 1970). From 1970s to this century, with the booming-up of semiconductor industry as well as related increasingly miniaturization trend, EM has been regarded as one of the most serious and persistent reliability problem in the very-large-scale-integration (VLSI) of the interconnect metallization. Since d'Heurle et.al. (Shine, 1971; d'Heurle, 1975) demonstrated the effect of supersaturating the Al with Cu in strengthening the EM resistance of Al conductors, people working in this field gradually used Al-Cu or Al-Cu-Si alloy to replace the pure Al thin film because the solute atoms such as Cu, Si, etc. beyond their saturation in Al lattice matrix would segregate at the grain boundaries, partially "blocking" them as migration paths. Al-Cu or Al-Si-Cu alloy has been used as interconnect materials for Si-based IC metallization for many decades. However, as feature sizes of ICs are scaled down to nanometers for faster switching speed, the wiring current density keeps increasing and the line/via overlapping area (reservoir) keep reducing. In this case, a new material which can be loaded with the increasingly high current density while maintaining low internconnects resistance to reduce the transistor-to-wiring delay. Therefore, the industry has turned Cu as the interconnect lines since 1990s in terms of the smaller resistance-capacitance delay, higher electrical resistivity and higher EM resistance as compared to the previously used Al (Park, 1991; Frankovic, 1997).

In addition to make clear the failure mechanism and find out the ways to improve the reliability of metallic conductors, EM has also drawn intense attention from researchers studying on the reliability of magnetic thin film materials as well as spintronic devices

such as giant magnetoresistance (GMR) read heads for ultrahigh-density magnetic recording hard disk drives and magnetic random access memorys (MRAMs) (Gurp, 1977; Kos, 1997; Shingubara, 1999; Bae, 2002) since 1970s. The EM-induced inter-diffusion not only limits the lifetime of GMR SV read heads, but it also causes a remarkable degradation of their magnetic performance, because the inter-diffusion induced roughness in the interfaces between antiferromagnetic/pinned/free layers, magnetization reduction of the ferromagnetic (FM) layers as well as the spin status change in the pinned and pinning layers are detrimental to the interlayer coupling and GMR response. Considering the higher biasing current density (up to 1×10^8 A/cm^2) used in the spintronic devices compared to that applied to the microelectronic interconnects, the degradation of electrical and magnetic properties should be studied in terms of the EM and thermomigration (TM) focusing on the relationship between temperature gradient and inter-diffusion in magnetic MLs. Different from the microelectronic interconnects which only need to work under the electrical stress, the spintronic devices such as GMR read heads have to be operated under the concurrent action of electrical and magnetic stress and the latter certainly will lead to the increase of current density as well as the temperature gradient in the GMR read heads. The inter-diffusion in the GMR MLs and the existence of hall effects during their operation make the EM phenomena in the GMR spintronic devices to become more complicated as compared to that in the conductor interconnects and single layered magnetic thin films.

2.1.2 Grain Boundary Diffusion and Atomic Flux Divergence

A two-dimensional metallic thin film can be considered as an ensemble of grain

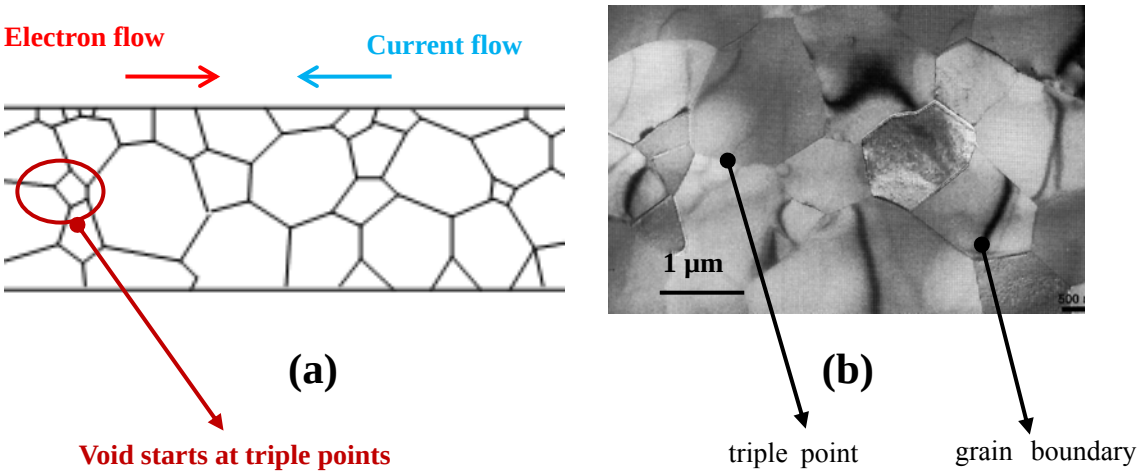

Fig. 2.1 (a) Sketch; (b) SEM image of a two-dimensional grain texture. (Cho, 1989).

boundaries and their intersections are illustrated in Fig. 2.1 (Cho, 1989). Because of the fine grain size in most as-deposited polycrystalline films compared to the width of films, atomic diffusion due to EM is dominated by grain boundary diffusion, at least at temperature less than one-half of the absolute melting temperature. Generally, as the average size of grains increase, EM decreases, if all else are unchanged. Two parameters need to be considered when we define the grain boundaries; the orientation of the bounding grains and the orientation of the boundary relative to one of the grains. For a given system and temperature, if the atomic concentration is assumed to be constant and is equal to its grain boundary value, $N_i = N_{gb}$ and the temperature is assumed to depend only on time and the position, namely $T_i = T(x, y, t)$, the diffusion coefficient in a grain boundary is determined by the grain boundary tilting angle (misorientation angle, θ. A commonly accepted expression for D_i is expressed as:

$$D_i = D_0 \sin\frac{\theta_i}{2} e^{-E_0/kT} \qquad (\theta_i < 37°) \qquad (2\text{-}2)$$

$$D_i = D_0 \sin 37° e^{-E_0/kT} \qquad (37° < \theta_i < 60°) \qquad (2\text{-}3)$$

where the subscript i denotes the *ith* grain boundary, D_0 and E_0 are the prefactor and the grain boundary activation energy of the films, respectively. (Schoen, 1980; Attardo, 1971; Li, 1961; Turnbull, 1954). E_0 is assumed to be constant over a film surface in the above Eq.s. If considering the variation of θ through the variation of activation energy over the entire ensemble of grain boundaries, the diffusion coefficient can also be rewritten as

$$D_i = D_0^* e^{-(E_0 + \Delta E_i(\theta_i))/kT} \tag{2-4}$$

where D_0^* is the prefactor, which is also assumed to be constant. $E_i = E_0 + \triangle E_i(\theta_i)$ is the total activation energy of the *ith* grain boundary and E_0 here is considered as the average grain boundary activation energy (Tang, 1989 & 1990). The dependence of diffusion coefficient on the microstructure can be understood in this way. Since θ varies from one boundary to another, the bonding force between ions varies, and thus the energy required to move an atom (or ion) along each boundary would also be different, resulting in the variation of diffusion coefficient.

EM-induced failures are mainly caused by atomic flux divergence (AFD) during high current density flowing through polycrystalline thin films in which grain boundary diffusion is dominant. In general, the atomic or ion flux J due to EM in the *ith* grain boundary is related to the total driving force F, as it is expressed in Eq. 2-5.

$$J_i = N_i v_{d,i} = \frac{N_i D_i}{kT_i} F_i \tag{2-5}$$

where, N_i is the atomic density and $v_{d,i}$ is the drift velocity, which can be related to the product of mobility and driving force. D_i is the diffusion coeffiecient, k is the Boltzmann constant, and T is the absolute temperature.

In addition to the local gradient resulting from the structural and chemical inhomogeneities, long-range thermal gradients because of Joule heating during the passage of current are another decisive factor responsible for the EM-induced failures. The driving force on the atoms (or ions) due to the applied electrical field, E, can be rewritten as in Eq. 2-6 (Tang, 1994) including the impact of thermal gradient.

$$F_i = |e| Z^* E \cos\phi_i = |e| Z^* \rho_0 j[1+\alpha(T-T_0)]\cos\phi_i \tag{2-6}$$

where $|e|$ and Z^* has the same meaning as they are in Eq. 2-1. ϕ_i is the inclination angle of the *ith* grain boundary with respect to the electron flow. ρ_0 is the resistivity of the film at the reference temperature and α is the temperature coefficient of the electrical resistivity, defining according to $\rho = \rho_0[1+\alpha(T-T_0)]$, T is the temperature at time τ and T_0 is the temperature of the substrate. Combining Eq. 2-5 and Eq. 2-6, the atomic flux can be rewritten as:

$$J_i = \frac{N_i D_0}{kT}|e| Z^* \rho_0 j[1+\alpha(T-T_0)]e^{-(E_0+\Delta E_i(\theta_i))/kT}\cos\phi_i \tag{2-7}$$

From the above Eq.s, it can be easily understood that, if the metal stripe is kept at a very low temperature (e.g. liquid nitrogen temperature), EM cannot occur because there is no atomic mobility. Defining

$$\Delta Y = \sum_{i=1}^{n_{gb}} e^{-\Delta E_i(\theta_i)/kT}\cos\phi_i \tag{2-8}$$

where n_{gb} is the number of grain boundaries defining a intersection, the flux divergence at this intersection then becomes

$$\nabla \cdot J = \sum_{i=1}^{n_{gb}} J_i = \frac{N_{gb} D_0}{kT}|e| Z^* \rho_0 j[1+\alpha(T-T_0)]\Delta Y e^{-E_0/kT}\cos\phi_i \tag{2-9}$$

Then the number of atoms (ions), N, flowing into an arbitrary intersection over a time

period Δt can be expressed as (Tang, 1994):

$$\Delta N = \delta h \nabla \cdot J \Delta t \tag{2-10}$$

where δ is the grain boundary width (~ tens of Å), h is the film thickness, and $\nabla \cdot J$ is the flux divergence at the intersection. Thus the growth rate of the volume (V) of the mass depletion or accumulation at the grain boundary intersection is (Tang, 1994):

$$\frac{\partial V}{\partial t} = \Omega_0 \frac{\partial (\Delta N)}{\partial t} = \delta h \Omega_0 \nabla \cdot J \tag{2-11}$$

where the Ω_0 is the atomic volume.

From Eq. 2-11, we can understand that if the atomic flux is continuous in the metal lines, that is, if there are no sites for AFD to occur, EM under the influence of an impressed electric field alone can not cause any mass depletion or accumulation. There are two physical mechanisms responsible for AFD: inhomogeneities in the microstructure and localized temperature gradients. Usually the former factor plays a much more crucial role in EM than the latter factor, however, once the applied current density up to higher scale (Misra, 2006; Zhang, 2007; Zeng, 2009), the influence of Joule heating effect due to the localized temperature gradients becomes dominant.

2.1.3 Structural Factor

ΔY, defined in Eq. 2-8, can be named as the structural factor, since it reflects the effects of grain boundary microstructure on EM and plays an important role in forming AFD. From Eq. 2-8, it is clear that the larger the variation in θ's and ϕ's, the greater the value of ΔY will be. Therefore ΔY characterizes the grain boundary structural inhomogeneities. The well-known microstructural inhomogeneities are those due to

localized variations in grain size including grain size and grain orientation distributions, those found at the junction of three grains named as triple or saddle points related to the structure factor reflecting the effects of GB microstructure on EM and playing a crucial role in causing AFD as well as those interfaces in the multilayered structures. These microstructure irregularities are the main sites for failure initiation. A triple junction shown in Fig. 2.2(a) can be equivalently described as shown in either Fig. 2.2(b) or Fig. 2.2(c) (Tang, 1994). In Fig. 2.2b, the triple junction is characterized by the three relative angles (ϕ_{ij}'s) between each pair of adjacent grain boundaries, an orientation angle (θ_0's) between a representative boundary mis-orientation angles (θ_i's). In Fig. 2.2(c), the same triple junction can also be characterized by the orientation angles of individual grain boundaries with respect to the electron flow (ϕ_i's) and θ_i's. With Fig. 2.2(b) as a reference, the structural factor can be re-expressed as

$$\Delta Y = e^{-\Delta E_1/kT}\cos\theta_0 + e^{-\Delta E_2/kT}\cos(\theta_0+\phi_{12}) + e^{-\Delta E_3/kT}\cos(\theta_0+\phi_{12}+\phi_{23}) \qquad (2\text{-}12)$$

where ϕ_{ij} is the relative angle between the ith and the jth grain boundary and i, j = 1, 2, 3. Based on Eq. 2-12, we know that there is no atomic flux divergence for any value of θ_0 if

$$\Delta E_1 = \Delta E_2 = \Delta E_3 \qquad (2\text{-}13)$$

and

$$\phi_{12} = \phi_{23} = \phi_{31} = 120° \qquad (2\text{-}14)$$

That means ΔY would be zero regardless of the orientation of the whole triple junction with respect to the direction of electron flow when the Eq. 2-13 and Eq. 2-14 are satisfied. Eq. 2-13 represents a case of uniform diffusion coefficient for all the grain

boundaries, while Eq. 2-14 is only to be met in a perfect hexagonal grain structure. However, due to the variation in crystal orientation in a polycrystalline film, the activation energy and thus the diffusion coefficient vary from one grain boundary to another. In addition, the relative angles between two adjacent grain boundaries in the real polycrystalline thin films are normally not 120° due to the variation of grain sizes (Berenbaum, 1971; Agarwala, 1970), as we can see in Fig. 2.1. Therefore, nonezero atomic flux divergence is likely to exist at the triple points where the number of atoms flowing into the area is not equal to the number of atoms flowing out per unit time. A

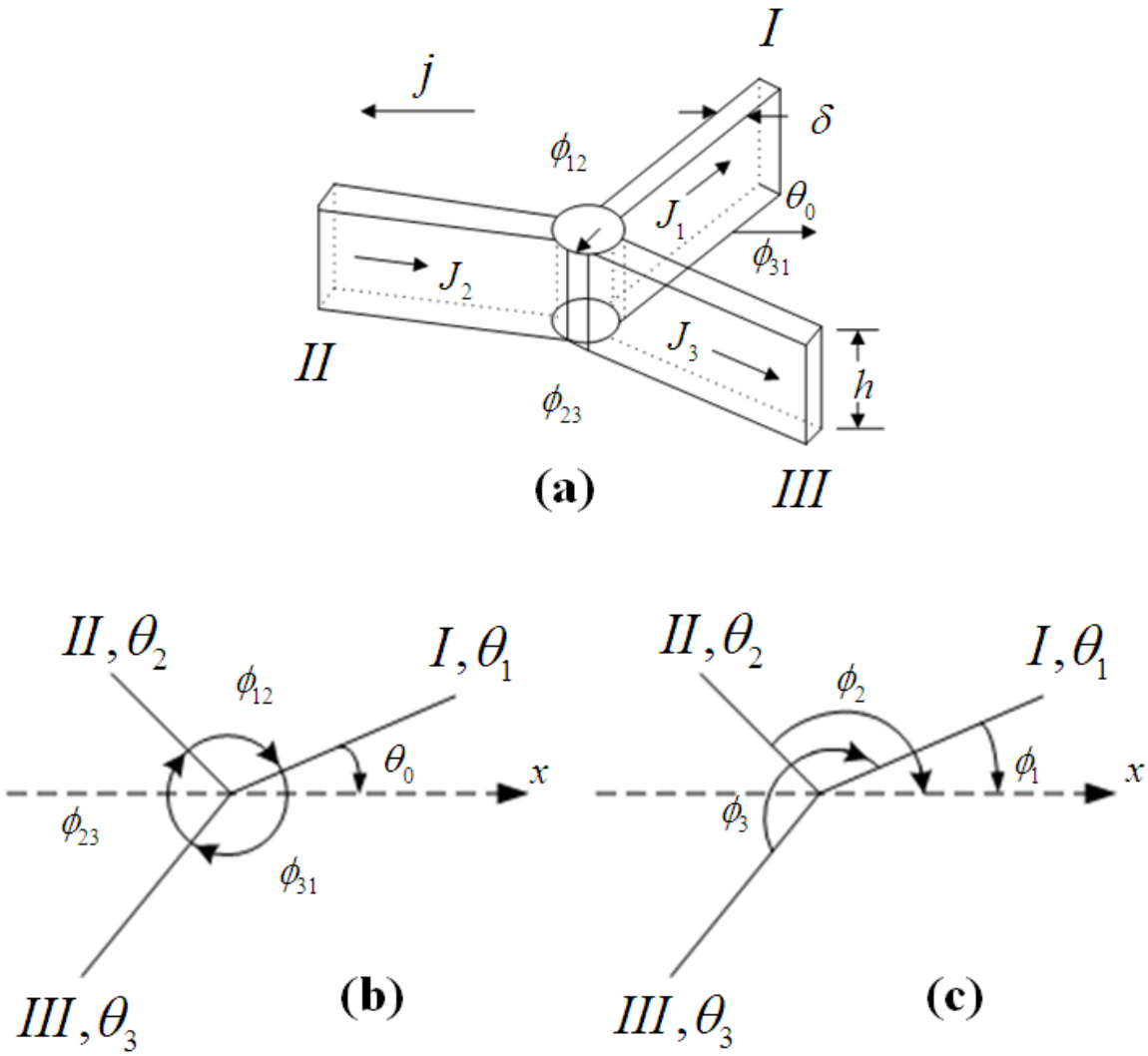

Fig. 2.2 Schematic illustration of (a) a triple junction defined by grain boundaries I, II, and III, (b)

and (c) the top view of the triple junction. x represents the direction of electron flow.

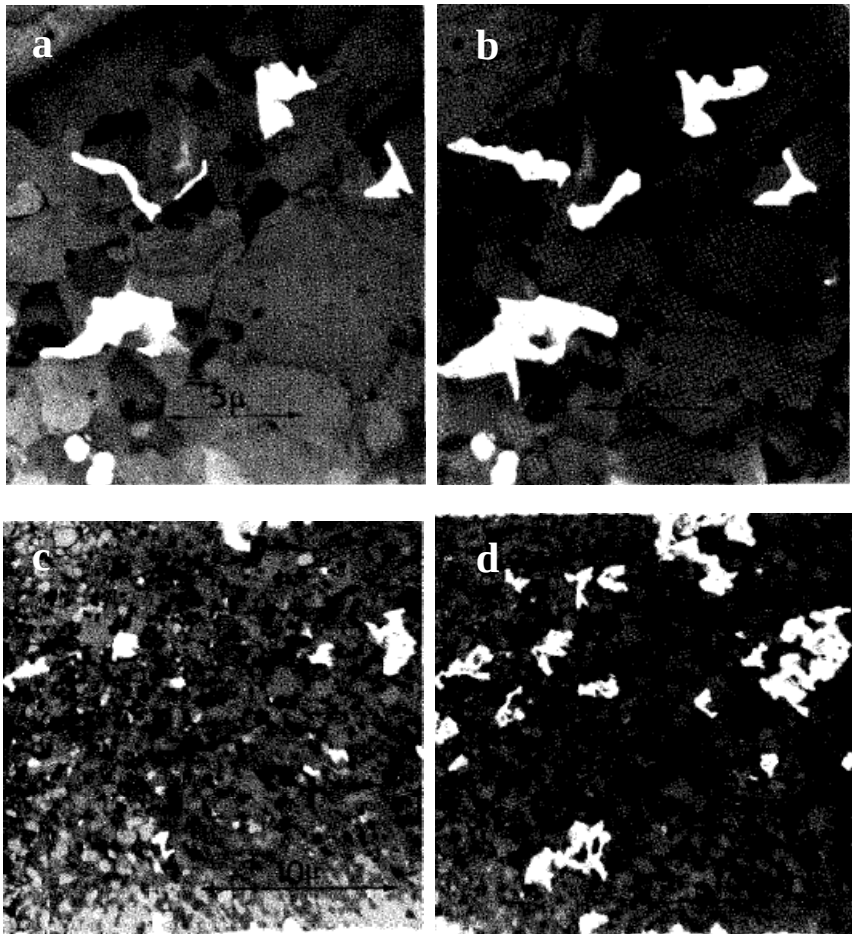

Fig. 2.3 Holes opening near cathode in large grained samples ((a) and (b)) and small grained samples ((c) and (d)): (a) j = 2.1 × 10^6 A/cm^2, 12 hours; (b) j = 2.1 × 10^6 A/cm^2, 17.5 hours; (c) j = 2.2 × 10^6 A/cm^2, 11.5 hours; (d) j = 2.2 × 10^6 A/cm^2, 15 hours. (Thickness of Al thin film is 260 nm) (Blech, 1969).

mass depletion ($\Delta Y < 0$) or accumulation ($\Delta Y > 0$) occurs depending on the sign of ΔY. As we can see in Fig. 2.3, an in-situ transmission electron microscope (TEM) study (Blech, 1969) of Al thin films with different grain sizes showed that voids usually nucleated at GBs or existing pinholes and grow into adjacent grains in the large-grained Al stripes. Compared with large-grained stripes, more voids were seen in the fine-grained Al stripes because of the existence of more nucleation sites. The corresponding activation energies were found to be 0.73 and 0.51 eV (Attardo, 1970) for large and

fine-grain films, respectively. The void edges are relatively straight due to the straightness of the grain boundaries in large-grained samples while the voids in fine-grained samples appear more irregular due to the large numbers of grains that are involved. Atomic flux divergences can also be caused by other structural discontinuities, e.g., at second-phase particles and at positions which have deviations in chemical composition. In addition, flux divergence can arise from variations in the atomic structure or defect concentration at the GB, for example, that caused by segregation of solute atoms or contaminants, which affects the atomic interactions between the migrated ions and the GB lattices, consequently altering the diffusivity parameters and the activation energy. The knowledge of ΔY is helpful for us to improve the EM resistance by reducing the value of structural factor. For example, applying high substrate temperature during film deposition, low energy deposition done by "ion beam sputtering" or "ionized cluster beam deposition", or high-temperature annealing of the metallization stripes to achieve a more uniform grain size and grain boundary misorientation (Tang, 1989; Kwon, 2005).

2.1.3 Current Crowding and Thermal Gradient Effects

As we have discussed in the previous paragraphs, besides the structural and chemical inhomogeneities, localized thermal gradient resulting from Joule heating during the passage of current is another significant driving force in causing AFD. Although we only discuss the EM under the D.C. electrical stress, the current density j in the AFD Eq. 2-9 is not constant. As soon as the EM-induced damage is initiated, current density becomes nonuniform due to the current crowding effect. Current crowding effect is a

nonhomogenous distribution of current density through a conductor or semiconductor, especially at the vicinity of the contacts and at the edge of voids (pinholes). Current crowding can lead to localized overheating and formation of thermal hot spots, in catastrophic cases leading to thermal runaway. Formation of voids increases the localized inhomogenity of current density over a metal stripe. Since the Joule heating is proportional to the square of the current density, the local temperature will also increase rapidly. Moreover, the increased resistance around the void also causes further localized temperature rise, which in turn accelerates the formation of the void. Therefore, the current crowding effect can cause an increase in the rate of failure propagation through the combined effect of the increase in current density and the subsequent increase in temperature.

The instantaneous current density field can be obtained by solving the two-dimensional Laplace Eq. for electrical potential (Marcoux, 1989) $u = u(x, y)$ at each time step:

$$\frac{\partial}{\partial x}(\sigma \frac{\partial u}{\partial x}) + \frac{\partial}{\partial y}(\sigma \frac{\partial u}{\partial x}) = 0 \tag{2-15}$$

where σ is the electrical conductivity, which is temperature dependent, defining according to $\sigma(T) = \frac{\sigma_0}{1 + \alpha T}$, where σ_0 is the electrical conductivity at the ambient temperature. In solving the above Eq., the existence of the voids can be considered by assigning $\sigma = 0$ to those regions where material has been depleted away and no current is being conducted. The current density is then obtained through the electrical potential according to Ohm's law:

$$j(x,y) = -\sigma\nabla \cdot u(x,y) \tag{2-16}$$

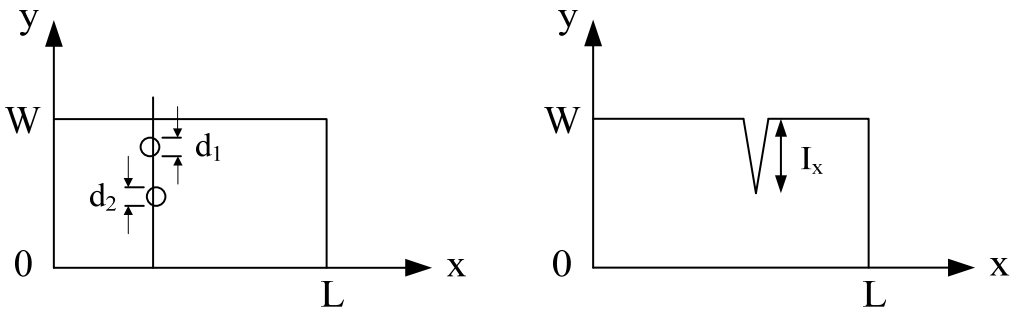

Fig. 2.4 Schemetic illustration of (a) cylindrical voids, and (b) crack in a conductor line of W wide and L long. (Tang, 1994)

For simplifying the simulation process, we first assume the current distribution is uniform within the undamaged regions. Secondly, the voids are assumed to be small cylinders perpendicular to the metal plane, and the current density in a particular cross section of the metal stripe, as illustrated in Fig. 2.4(a), can be expressed as

$$j_x = \frac{j_0}{1 - \sum_{i=1}^{n_c} \frac{d_i}{W}} \tag{2-17}$$

where j_0 is the initial current density, defined as $j_0 = \frac{I}{A}$ (I is the applied electric current flowing through the thin film, and A is the cross-sectional surface area of the film perpendicular to the current flow), j_x is the current density at the cross section at x, n_c is the number of voids that intercept the cross section, d_i is the chord of the *ith* void on the cross section, and W is the line width (Tang, 1989 & 1990). Alternatively, the voids are assumed to be mainly cracks growing from the edges to the inner region as shown in Fig. 2.4(b), the current density in the cross section where the crack is

formed becomes

$$j_x = \frac{j_0}{1 - \frac{l_x}{W}} \tag{2-18}$$

where l_x is the crack length at x (Sigsbee, 1973).

The temperature gradient in a metallic line is an important factor in accelerating EM-induced degradation because of the exponential dependence of the atomic diffusivity on temperature. In late 1960s, Blech et.al. observed EM-induced void formation in Al thin-film stripes due to temperature gradients via an in-situ TEM study (Blech, 1967 & 1969). Temperature gradient may exist before EM-induced void formation is started. For example, both ends close to the bonding pads are colder than the center region, and spacer layer of a SV is hotter than the ferromagnetic and anti-ferromagnetic layers due to the "current sinking effect" (Gurney, 1997) resulting from the film resistance difference of the metallic spacer versus magnetic thin films. As a consequence, AFD may occur solely due to the initial temperature gradient (Sigsbee, 1973; Ho, 1989; Zeng, 2010). After the damage caused by AFD starts to form, the additional Joule heating resulted from the current crowding effect further increases the temperature gradient and the temperature gradient in turn elevates the growth rate of the voids/hillocks following the positive feedback shown in Fig. 2.5.

As soon as the voids start to form, the effective cross-sectional area will correspondingly shrink, as it is indicated in Eq. 2-17 and 2-18. void formation has two contributions to the aggravated Joule heating effect: the first effect is an increase in the average current density which is inversely proportional to the remaining cross section of metal thin films as it is indicated in Eq. 2-18; the second one is the current crowding

effect which causes the current density to rise in the immediate vicinity of a defect to a value above the average. The localized temperature rise due to the joule heating led to an additional increase of the effective electrical field loaded onto the moving atoms, because of the corresponding increase of metal atoms mobility and the thermally-induced increase of film resistivity.

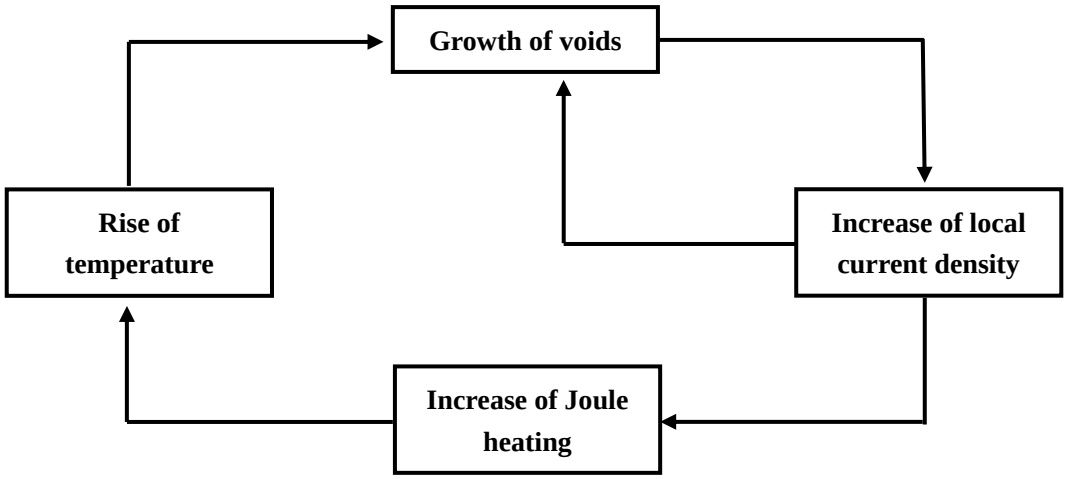

Fig.2.5 Thermal acceleration loop during electromigration. (Nikawa, 1981)

When we discuss the thermal effects in failure analysis, we have to consider both the heat generation and heat dissipation. Assuming constant boundary conditions, that is, constant substrate temperature T_0, the thermal Eq. can be written as (Lloyd, 1988):

$$K\frac{\partial^2 T}{\partial x^2}+Q-\frac{\lambda}{h}(T-T_0)=0 \qquad (2\text{-}19)$$

where K is the thermal conductivity, λ is the heat transfer coefficient between the film and the substrate, Q is the Joule heat generated in unit volume per unit time, which can be defined as:

$$Q=\sigma(\nabla u)^2 \qquad (2\text{-}20)$$

The term $\frac{\lambda}{h}(T-T_0)$ represents the heat dissipation through the film-substrate interface.

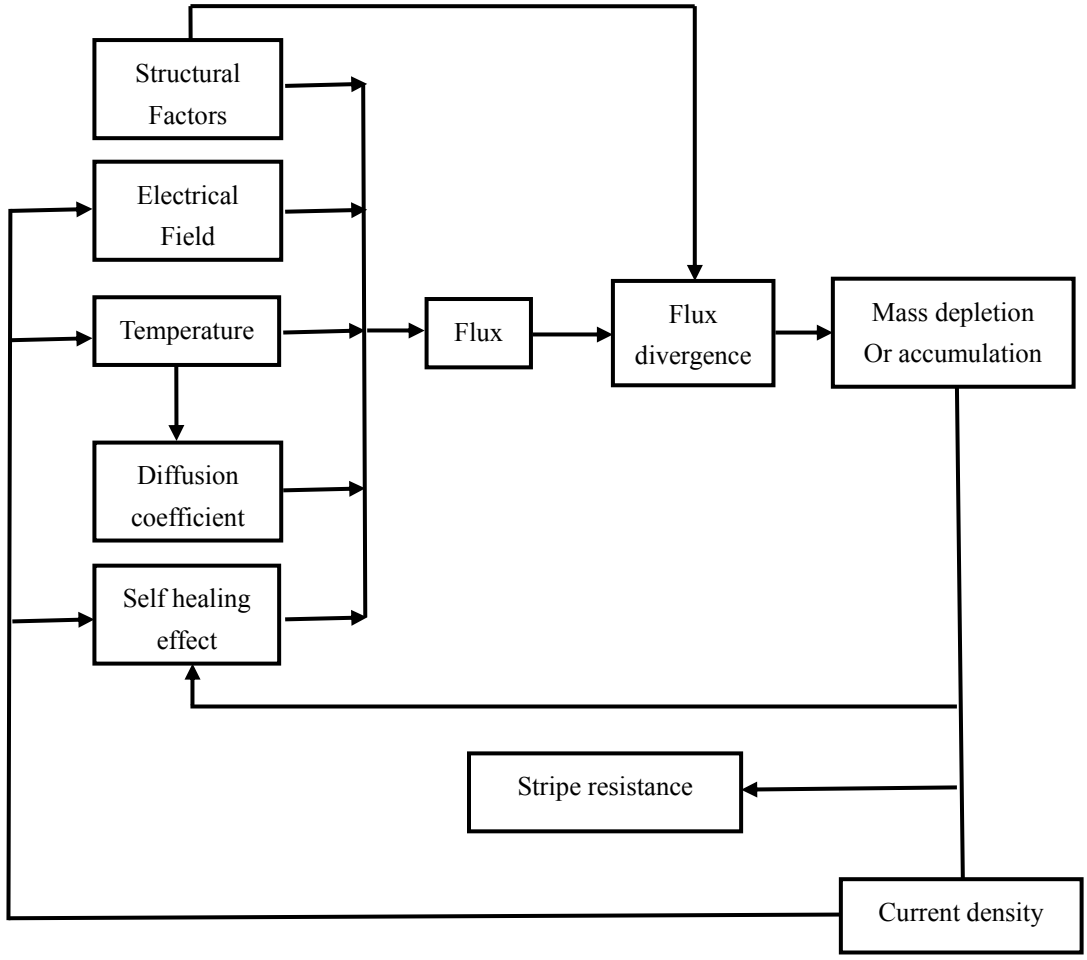

Fig.2.6 Summary of electromigration process.

2.1.4 Self Healing Effect

In a drift-velocity experiment, Blech studied the stress gradient across an Al stripe as a result of EM induced mass transport and he found that the mass accumulation and depletion formed at the two ends of the thin film stripe produce a concentration gradient between two ends, resulting in a force that generates an atom flow in the direction opposite to the stress gradient (Blech, 1976). This kind of backflow could

partially fill in the voids area and so it is named as self healing effect. In the NiFe/(Co or CoFe)/Cu/(Co or CoFe)/NiFe based GMR SV multilayers (MLs) or devices, we also found the self healing effect in another way. Due to the lower activation energy of Cu compared to NiFe and Co (CoFe) and the current sinking effect, the void-forming section on the Cu spacer would be melted by the high local temperature. Then the melted Cu would be quenched due to the suddenly dropped joule heating resulted from the crack damage caused electrical discontinuity. During this quenching process, the migration of locally melted Cu atoms to the adjacent NiFe layers is strictly limited by the diffusion barriers so that they could be solidified and subsequently make reconnection.

All the factors we have discussed which are decisive on the EM process are summarized in the flowchart shown in Fig. 2.6.

2.2 Inter-diffusion in Magnetic Multi-layers

Different from the EM process in the single layered Al, Cu or Ag conductors and NiFe, Co, Ni or FeMn magnetic thin films, we have to take into account the EM-induced inter-diffusion in the NiFe/(Co or CoFe)/Cu/(Co or CoFe)/NiFe based GMR SV MLs when we discuss about the EM-induced failures. Balgin and Poate (Balgin, 1978) declare that inter-diffusion in metallic thin films could happen by large-scale mass transport at low temperature. They found that diffusion time could be short because the films are thin and contain many defects such as grain boundaries and dislocations. For the most cases, diffusion takes place along grain boundaries (Benhenda, 1987; Iijima,

1977; Lefakis, 1983; Huang, 2003) and dominated by vacancy diffusion. In nature, inter-diffusion follows all the diffusion theory such as Fick's first and second law and Arrhenius equation, as shown in Eq. 2-21to Eq. 2-23.

$$F = -D\frac{\partial C}{\partial x} \tag{2-21}$$

$$\frac{\partial C}{\partial x} = D\frac{\partial^2 C}{\partial x^2} \tag{2-22}$$

$$D = D_0 \exp(-\frac{E}{k_B T}) \tag{2-23}$$

This phenomenon in the multilayered thin-film structures would increase the surface roughness and also change the thin film resistivity, therefore the degree of inter-diffusion is very crucial in limiting the magnetic and electrical properties of GMR SV devices. In this thesis, our studies on EM-induced failure characteristics in the GMR SV devices are started from the NiFe/Cu/NiFe ($Ni_{81}Fe_{19}$) tri-layers. Ni-Cu system is well known to be a continuous miscible system (Massalski, 1990) and the onset of inter-diffusion was observed to occur at about 200 °C (Brückner, 2000). Brückner et. al. (Brückner, 2000) found that around 8% of Cu diffused into NiFe layers at the annealing temperature of 400 °C which resulted in a Cu resistivity increase by 220%. Since the resistance of this tri-layer is mainly determined by that of Cu spacer due to the quite different resistivity of Cu and NiFe thin films ($\rho_{Cu} = 2.2\times10^{-8}\Omega\cdot m$, $\rho_{NiFe} = 2.1\times10^{-7}\Omega\cdot m$) (Brückner, 2000), the total effective resistance of this tri-layer would be increased remarkably and thus Joule heating as well thermal gradient effect become significant in accelerating the EM-induced failures.

In addition to changing the resistivity, the microstructural change caused by inter-

diffusion also plays an important role in accelerating the EM-induced failures in such a tri-layer. Cu-Ni intermixing region provides more current shunting paths from Cu to NiFe, and the increased Cu resistivity also leads to more current diverging through NiFe according to the current sinking effect. When the Ni-Cu intermixing region becomes thicker, more grain boundaries built in between NiFe/Cu or Cu/NiFe interfaces would also accelerate the Cu atom migration into the NiFe layers, until the NiFe/Cu/NiFe tri-layers become a single layered Ni-Fe-Cu alloy. Different from the complete miscibility of Ni-Cu system, the solid solubility of Co with Cu is less than 1 at.% below 422 °C, and the maximum of Cu can be dissolved in bcc Fe at 850°C is just 1.88±0.5 at.% (Massalski, 1990). Moreover, Co and CoFe have even higher activation energies than that of NiFe and Cu ($E_{NiFe} = 0.8 \pm 0.15eV$, $E_{Cu} = 0.5 \pm 0.2eV$, $E_{Co} = 1.4 \pm 0.2eV$, $E_{CoFe} = 0.9 \pm 0.1eV$) (Bae, 2002). Therefore, Co and CoFe are proposed to be inserted at the interface between NiFe and Cu as a diffusion barrier (van Loyen, 2000; Zeltser, 1998). The grain boundary diffusion coefficients (D_{gb}) and activation energies of Cu in Co and Ni as well as Ni in Cu and Co are listed in Table 2-1 (Huang, 2003; Barmak, 2000; Pellerin, 1994; Brandes, 1994; Lefakis, 1983; Svedberg, 2003). From this table we can easily have the conclusion that Cu diffusion in Ni is slightly slower than Ni diffusion in Cu. Also, the diffusion coefficient of Cu and Ni in the CoFe/Cu/CoFe sample was smaller than that in the Co/Cu/Co sample, because the addition of Fe in the CoFe/Cu/CoFe sample may slow down the Cu diffusion outwards and Ni diffusion into Cu.

In the previous study on the implication of inter-diffusion on the thermal stability of

Ta/NiFe/CoFe/Cu/CoFe/AF/Ta (AF is IrMn or PtMn) top spin valve (TSV) and Ta/NiFe/AF/CoFe/Cu/CoFe/NiFe/Ta bottom spin valve (BSV) (Anderson, 2000), two

Table 2-1. The calculated diffusion coefficients (D^{ex}) and the reported grain boundary diffusion coefficients (D_{gb}) of Cu and Ni in Co (host) are listed for comparison (unit: cm^2/s)

System	**Temperature**	E_{gb}	D_{gb}	**Note**
Cu/Co (host)	200 °C	No data	5.4×10^{-22}	Co/Cu/Co sample CoFe/Cu/CoFe sample
Ni/Co (host)	200 °C	No data	1.01×10^{-19}	Co/Cu/Co sample CoFe/Cu/CoFe sample
Ni/Cu (host)	280-405 °C 300-500 °C 650-915 °C	1.46eV	$2\times10^{-15}\sim6\times10^{-13}$ $2\times10^{-16}\sim1\times10^{-12}$ $2\times10^{-9}\sim2\times10^{-7}$	Cr/Cu/Ni sample
Cu/Ni (host)	280-405 °C 300-500 °C	1.3eV	$10^{-16}\sim1.5\times10^{-14}$ $5\times10^{-19}\sim1.5\times10^{-14}$	Cr/Cu/Ni sample
Cu/CoFe (host)	< 540 °C	0.90eV	1.91×10^{-17}	$(Cu/CoFe)_{25}$ sample

.

routes for inter-diffusion were detected: inter-mixing at Ta/NiFe interface and Mn inter-diffusion into the pinned and beyond. Here NiFe/Cu inter-diffusion has been effectively hampered by the CoFe diffusion barrier but the diffusion of Mn atoms into the pinned layer and even into Cu spacer or beyond become dominant. The solid solubility of Mn in Cu is around 20% at ambient temperature and it is completely soluble at high temperature (Iijima, 2009). The diffusivity of Mn atoms is even higher than that of Cu atoms in the Mn-Cu alloy, however, Mn-Cu is not as stable as other Cu alloy such as Ni-Cu and Ni-Fe-Cu alloys and thus Mn atoms may easily diffuse out and segregate at the surface of Cu layer. In Iwasaki et.al.'s Auger depth-profile analysis on CoZrNb/NiFe/Cu/CoFe/FeMn/Ta TSVs, it is found that Co and Cu atoms diffused into

the FeMn pined layer, and Mn atoms diffused to the Cu layer side. This indicates that not only the deterioration of the anisotropy field in the free layer due to the FeMn/CoFe inter-diffusion, but also spin dependent scattering deterioration caused by the diffusion of Mn impurity in the Cu spacer is responsible for the degradation of magnetic performance of these GMR SV-MLs.

2.3 Methods to Improve the EM Resistance

One of crucial goals of studying EM is to find out the methods of suppressing EM damage of these miniaturized thin-film microelectronic and spintronic devices and therefore increasing their lifetime. Based on the above discussion about the EM failure mechanism, the key for reducing EM-induced failures is to reduce the local divergence of atomic flux. This can be accomplished by either reducing the magnitude of the atomic flux and / or the inhomogeneity of the parameters controlling the mass transport. The magnitude of AFD is determined by the EM driving force and the grain boundary diffusivity. Therefore, what we can do is to reduce the driving force and / or diffusivity. Reduction of the driving force has some basic difficulties, since the current density and operating temperature is dictated by the device functional requirements. In this case, the only choice is to stop or slow down the grain boundary diffusion and control the inter-diffusion at interfaces. Here we discuss about three factors as well as their effect on EM: (1) grain size and bamboo structure; (2) addition of solutes; (3) diffusion barriers.

2.3.1 Grain Size and Bamboo Structure

The basic prerequisite for restraining the grain boundary diffusion is to minimize the local AFD. Long lifetimes in large grained Al or Al-Cu films (Attardo, 1970; Hong, 1993; Kwok, 1985) and large grained Al-Cu films with bamboo structure (Piece, 1981; Vaidya, 1980) have been reported. Attardo et.al. (Attardo, 1970) found that the median lifetime, t_{50}, could be increased by a factor of 4 if the grain size increases from 1.2 μm to 8 μm, and the activation energy for grain boundary diffusion is increased by 43% when the grain is induced to grow up from 2 μm to 8 μm, as shown in Fig. 2.7. An empirical relationship between the MTTF and the microstructure of Al – 0.5%Cu films was proposed by Vaidya and Sinha (Vaidya, 1981),

$$MTTF \propto \frac{D}{\sigma^2} \times \log[\frac{I_{(111)}}{I_{(200)}}]^3 \tag{2-24}$$

where D is the median grain size, σ is the standard deviation of the lognormal distribution of grain size, and $I_{(111)}$ and $I_{(200)}$ are X-ray intensities of the (111) and (200) peaks, respectively. In principle, grain boundary triple points (GBTP) are the most crucial sites for the divergence of atomic flux, therefore, reducing the number of triple points is a very direct and effective way of improving EM resistance of thin film metal stripe with respect to EM-induced failures. Increasing the grain size, D, or decreasing the grain size deviation, σ, of thin film metal stripes could correspondingly decrease the number of triple points. As we can see in Fig. 2.8 and Fig. 2.9 (Attardo, 1970; Kwon, 2005), the number of GBTP per unit length decreases with the decrease of ratio of line width (W) versus grain size (S). In Fig. 2.9, from type A to type B, with the line narrowing, the number of GBTPs is greatly decreased because some big grains ran

directly across the metal line and many interconnections between grains are interrupted. Until the line width is reduced to below the average grain size of the thin films, the

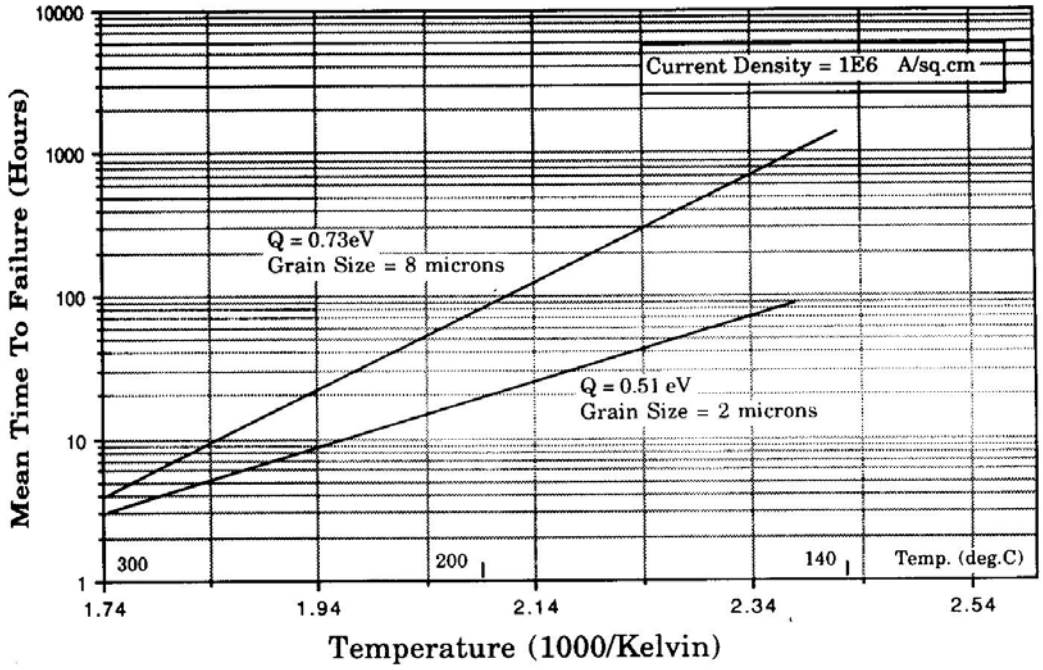

Fig. 2.7 Activation energy determined for fine and large-grain Al thin film conductors (Attardo, 1970).

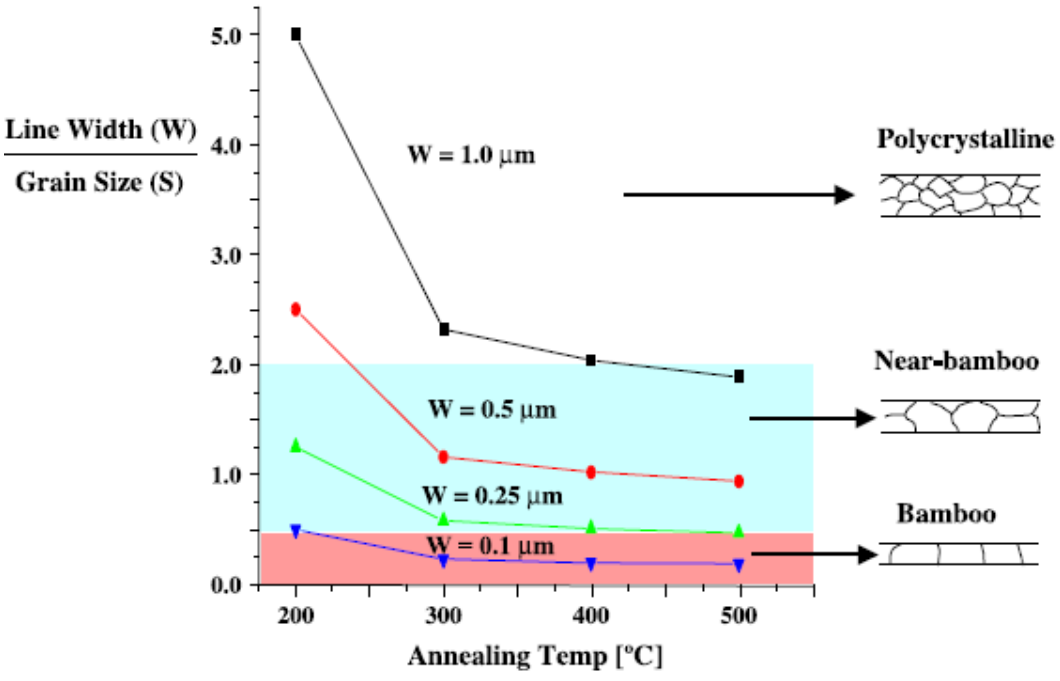

Fig. 2.8 Dependence of the line width/grain size ratio (W/S) of the electroplated Cu thin film on the

RTA temperature for different line widths (Kwon, 2005).

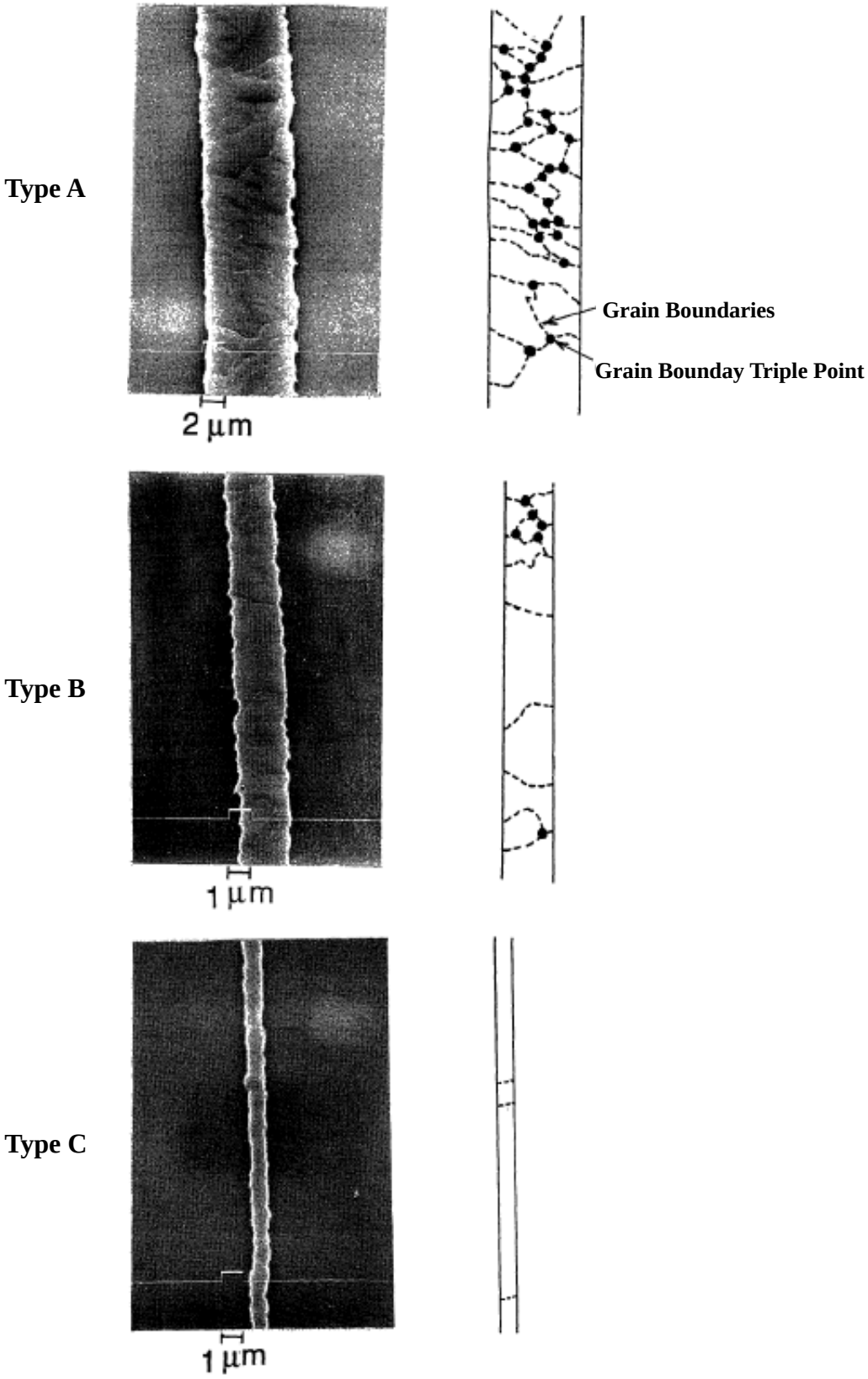

Fig. 2.9. Three types of grain boundary configuration in the samples (Hong, 1993).

polycrystalline microstructure transformed to a “bamboo structure” (type C in Fig. 2.9) and thus there is almost no GB diffusion. As a result, its EM resistance increases, despite an increase in current density. Another way to form a bamboo structure without the rise of current density is rapid thermal annealing, which could not only increase the grain size but also improve the grain size non-uniformity (Kwon, 2005).

2.3.2 Addition of Solutes

Another effective and reliable method to reduce the GB diffusion is the addition of a second element (d’Heurle, 1971; Kakar, 1973; Sideris, 1973) and it’s just the reason that Al-4 wt.% Cu or Al-1.1 wt.% Si-4 wt.% Cu alloy gradually replaced the plain Al conductors in VLSI industry (Ames, 1970; Learn, 1974). According to the study of d’Heurle et.al. (Shine, 1971; d’Heurle, 1971&1975), the addition of Cr, Cu, Mg or Ni can effectively improve the EM lifetime by two orders of magnitude, compared to that of plain Al thin films. The maximum activation energy for EM-induced failures is found to be about 0.8eV for a Cu content of 4 wt.% in Al (d’Heurle, 1972). Taking the Al - 4 at.% Cu alloy as an example, the solubility of Cu in Al is only 0.05 at. % at 230 °C, therefore, excess Cu atoms are likely to segregate at the Al GBs and block the short circuit paths for electrotransport. On the other hand, the excess Cu forms Al_2Cu precipitates in Al grain boundaries and these precipitates dissolve and serve as sources of Cu to replenish the loss of Cu in grain boundaries when EM depleted them by driving them the anode. Therefore, different kinds of solute atoms are tried by researchers for improving EM lifetime of metallic thin films. Table 2-2 (d’Heurle, 1978) listed the illustrative data of the alloying effect on the t_{50} of these thin film

conductors.

Table 2-2. Median failure times for Al, Au, and Cu conductor thin films as a function of alloying additions ($J = 2\times10^6$ A/cm^2) (d'Heurle, 1978)

Thin Film	Alloy, wt %	MTTF, hours
Al at 175 °C		30-45
Al at 175 °C	Si, 1.8	115
Al at 175 °C	Cu, 4	2500
Al at 175 °C	Cu, 4 & Si, 1.7	4000
Al at 175 °C	Ni, 1	3000
Al at 175 °C	Mg, 2	1000
Al at 175 °C	Cu, 4 & Mg, 2	10000
Al at 175 °C	Cu, 4 & Ni, 2 & Mg, 1.5	32000
Al at 175 °C	Au, 2	55
Al at 175 °C	Ag, 2	45
Au at 300 °C	Ta	4000
Au at 300 °C	Ni-Fe	800
Au at 300 °C	Mo	100
Au at 300 °C	W+Ti	25
Cu at 300 °C		180
Cu at 300 °C	Al, 1	300
Cu at 300 °C	Al, 10	6000
Cu at 300 °C	Be, 1.7	20000

2.3.3 Diffusion Barrier

As we have discussed in the previous paragraphs, inter-diffusion, especially the inter-diffusion at NiFe/Cu interfaces is very serious and detrimental. It would not only deteriorate the EM-induced failures, but it also leads to very significant degradation of magnetic performance of NiFe/Cu/NiFe based GMR SV devices, such as the drop of

interlayer coupling and reduction of magnetic moment as well as MR ratio (Yu, 2001; Huang, 1992: Hecker, 2002; Neamtu, 1999). Therefore, it is quite necessary to find an effective diffusion barrier to block or slow down the inter-diffusion. In this thesis, we will discuss about the feasibility of inserting an ultrathin Co or CoFe film between NiFe and Cu as a diffusion barrier as well as the self-healing effect because of these diffusion barriers.

2.4 Black Equation

The lifetime measurement of metal stripes is the most commonly used method for investigating the EM processes. The results usually follow a log-normal distribution and are given in terms of a median-time-to-failure (MTTF), t_{50}, which is the time to reach a failure of 50% of a group of identical conductor lines. The relationship between the testing sample lifetime and EM-induced failures due to the grain boundary diffusion under the electrical stress was first formulated by Black (Black, 1969) from an "Arrhenius-like empirical equation describing diffusion.

$$MTTF = Aj^{-n} \exp(E_a / kT) \tag{2-25}$$

here A is a parameter depending on thin film geometry, microstructure, and physical characteristics, E_a is the activation energy for grain boundary diffusion which is an very important parameter in evaluating the EM resistance of metallic thin films, the exponent value "n" is the current dependence factor, j, k and T have the same meaning as they are in the previous equations. For saving time, accelerating lifetime test conditions are generally used at the elevated temperature and with high current

Table 2-3. The "n"values of Al, Cu, Ta/Cu/Ta, NiFe, Co, CoFe thin film metal stripes at the given current density (j) range.

Materials	"n"	j	Reference
Al	1.5	10^5~10^6 A/cm^2	Attardo, 1970
Al	2~3	0.5×10^6 ~2.8×10^6 A/cm^2	Black, 1974
Al	1~3	10^5~10^6 A/cm^2	Venables, 1972
Al–1%Ge–0.5%Cu	3.4	10^6 A/cm^2	Kuniko, 1994
Al–1%Si–0.5%Cu	4.7	10^6 A/cm^2	Kuniko, 1994
Cu	1.7	1×10^6 ~1.5×10^8 A/cm^2	Bae, 2002
NiFe	3.1~3.3	1×10^6 ~1.5×10^8 A/cm^2	Bae, 2002
CoFe	6.1	1×10^6 ~1.5×10^8 A/cm^2	Bae, 2002

Table 2-4. The "E_a"values for grain boundary diffusion dominant EM-induced failures of Al, Cu, Ta/Cu/Ta, NiFe, Co, CoFe thin film metal stripes.

Materials	"E_a"	Reference
Al	0.55 eV	Aust, 1965
Al-Si or Al-Si-Cu	0.7 eV	Danso, 1981
Cu	0.65 eV	Chin, 2002
Cu	0.5±0.3 eV	Poate, 1978
Ta/Cu/Ta	0.77 eV	Chin, 2002
NiFe	0.8±0.15 eV	Bae, 2002
CoFe	0.9±0.1 eV	Bae, 2002
Co	1.4±0.2 eV	Bae, 2002

density stressing, but T is has to be below half of the melting point of the thin film stripes, otherwise the bulk diffusion to the mass transport will become dominant. Most studies on EM show that the distribution of lifetime data fits a straight line fairly well in the lognormal-scale R-t curves, at least in the 2% to 98% region of the distribution. The "n" and "E_a" values of Al, Cu, NiFe, Co, CoFe thin film metal stripes are summarized in Table 2-3 and Table 2-4. Theoretical studies (Venables, 1972) and empirical evidence (Black, 1969; d'Heurle, 1971) show that "n" itself is a function of the current density J. For Al thin film conductors, "n" in most literatures is found to be in the range of 1 to 3 when the current density J is in the range of 10^5~10^6 A/cm^2, while the "n" values higher than 2 might be attributed to Joule heating from a current density stressing higher than 1×10^6 A/cm^2 (Kwok, 1988).

2.5 Giant Magnetoresistance (GMR) and Interlayer Coupling in Magnetic Multi-layers

Ferromagnetism arises from the quantum mechanical exchange interaction of electrons in the material, thus giving a spin-split band structure in which the imbalance in the density of spin-up and spin-down electrons results in net magnetization (Jiles, 1998; Tsymbal, 2001). There are two prerequisites for GMR effect to appear: (1) at least two very thin ferromagnetic (FM) layers separated by a very thin nonferromagnetic layer such as Cr, Cu and Au, and (2) a way of changing the relative orientations of the magnetization in the adjacent FM layers. Different from anisotropic magnetoresistance (AMR) effect, which depends on the angle between the direction of electric current and

orientation of magnetic field, the GMR effect arises from differences in conduction electron scattering when its spin orientation is parallel or antiparallel to the magnetic moment of a FM layer. The mean free path is apparently short for antiparallel spins and long for parallel spins, so spin-up and spin-down electrons are differentially scattered, as shown in Fig. 2.10. GMR can be measured in the magnetic MLs with the current in the layer plane (CIP) as well as with the current perpendicular to the plane (CPP). In this thesis, we focused on the EM-induced failure characteristics in the CIP GMR devices.

In the late 1980s, the GMR effect was first discovered in a ML (ML) configuration (Grünberg, 1986; Baibich, 1988), in which two or more FM layers are separated by a very thin non-ferromagnetic spacer and at certain thicknesses, the antiferromagnetic (AFM) (Grünberg, 1986) interlayer coupling making it energetically preferable for the magnetizations of adjacent layers to align in anti-parallel (R_{AP}) in zero applied field, but can be aligned to be parallel (R_P) when an external magnetic field are applied. The AFM interlayer coupling is a particular case of interlayer exchange coupling, which is mediated by the itinerant electrons in the metallic spacer layer and is an analogue of the Ruderman-Kittel-Kasuya-Yosida (RKKY) interaction between localized magnetic moments in a nonmagnetic host metal. The interlayer exchange coupling oscillates between ferromagnetic (FM) and AFM as a function of the thickness of the nonmagnetic layer (Parkin, 1990). Therefore, the first way to have GMR effect is to choose an appropriate thickness of the non-ferromagnetic spacer corresponding to the 2^{nd} AFM peak in the oscillation of interlayer exchange coupling. As the schematic

representation of the GMR effect is shown in Fig. 2.11, the MR ratio, $\Delta R/R$ is generally expressed as

$$\frac{\Delta R}{R}(\%) = (R_{AP} - R_P)/R_P \times 100 \tag{2-26}$$

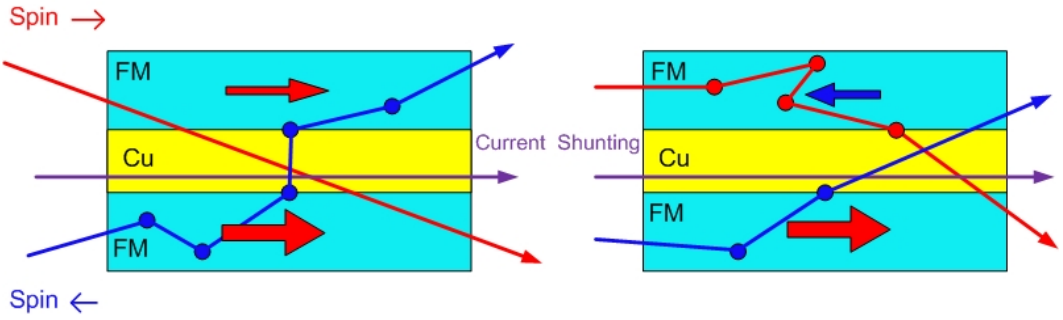

Fig. 2.10 Schematic of GMR pseudo SV structure in the CIP configuration, illustrating the two independent spin channels, and current shunting through the non-magnetic layer.

GMR requires that an antiparallel configuration of the magnetization in the MLs can be switched into a parallel one by applying a magnetic field. In addition to the AFM interlayer coupling, the team of Shinjo and Yamamoto (Shinjo, 1990) as well as Dupas et.al. (Dupas, 1990) demonstrated that GMR effect can also be obtained by introducing different coercivities of the successive ferromagnetic (FM) layers. In this case the magnetic moments of the soft and hard magnetic layers switch at different values of the applied magnetic field, providing a field range in which they are antiparallel and the resistance is higher. These exchange coupled MLs show large MR ratio, but the low-field sensitivity is not sufficiently high for the application of the MLs to magnetic read heads. Therefore, SV structures were proposed to realize high

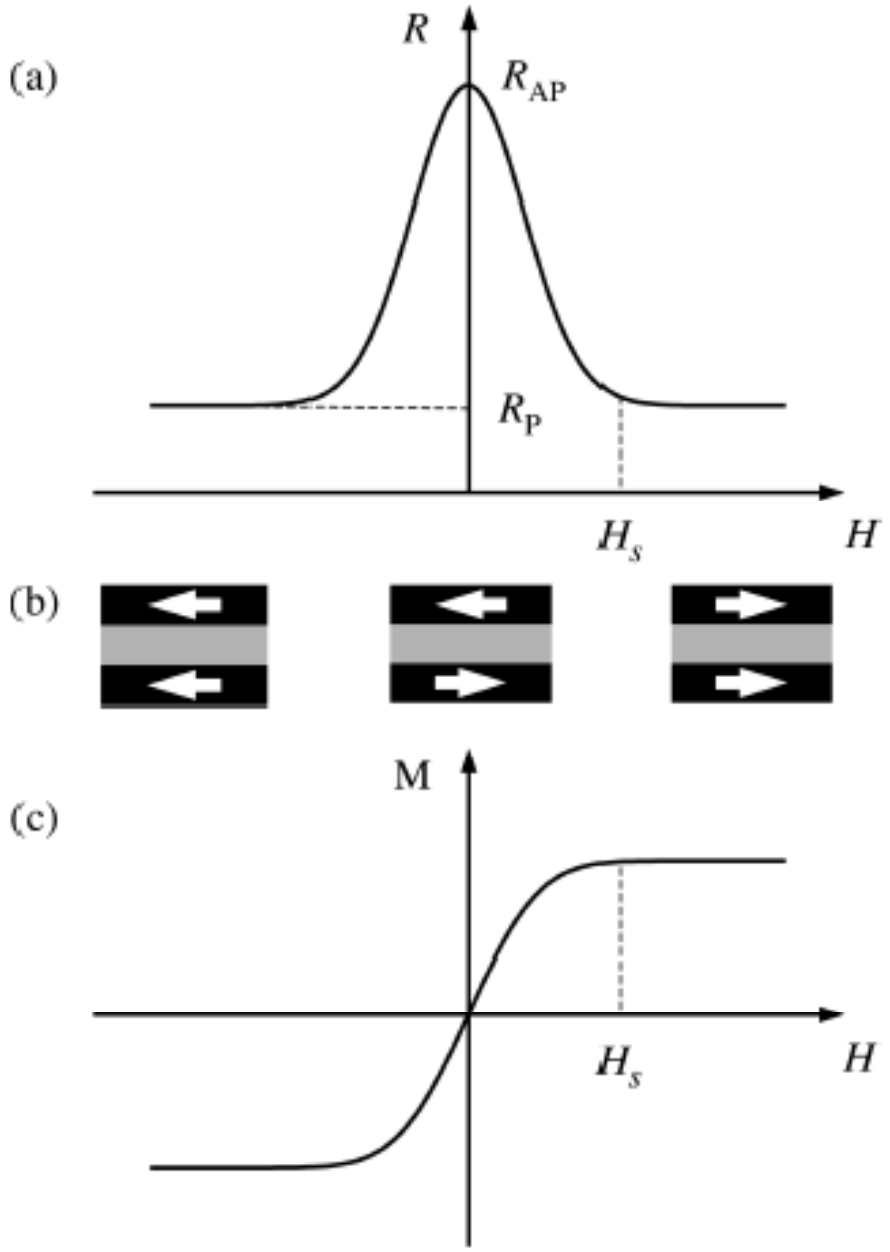

Fig. 2.11 Schematic representation of the GMR effect: (a) Change in the resistance of the magnetic ML as a function of applied magnetic field; (b) The magnetization configurations (indicated by the arrows) of the ML (trilayer) at various magnetic fields: The magnetizations are aligned antiparallel at zero field; the magnetizations are aligned parallel when the external magnetic field H is larger than the saturation field H_S; (c): The magnetization curve for the ML.

sensitivity of GMR MLs for small magnetic fields. As shown in Fig. 2.12, the simple SV structure is composed of a free magnetic layer (FL), a nonmagnetic spacer layer (NM), a pinned magnetic layer (PL), and an antiferromagnetic pinning layer (AF). The

FL is usually composed of soft magnetic materials so that it can change the magnetic direction with an application of a small magnetic field. The NM is a separator to eliminate the magnetic coupling between the FL and the PL and to realize free magnetic rotation in FL. The PL is AFM coupled with the AF across the interface between PL and AF and cause the exchange bias effect on the PL.

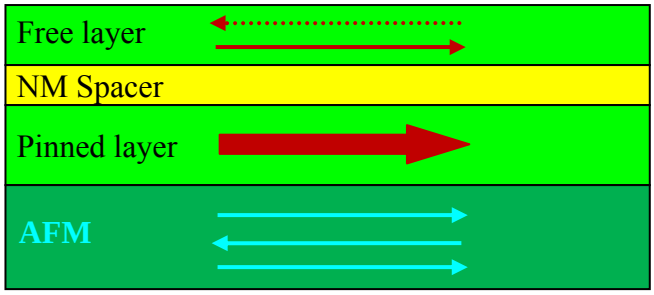

Fig. 2.12 Schematic of basic exchange biased SV structure.

As we have discussed in the above paragraphs, interlayer coupling field is a very important factor in determining the magnetic response of GMR MLs. In the previous studies, it has been reported that the interlayer coupling arises from two physical natures: one is FM coupling, originally described by Néel (Néel, 1962) and frequently called “orange peel” or “topological coupling (Chopra, 2000; Langer, 2001), and another is the oscillatory (RKKY-like) coupling (Petroff, 1991; Anthony, 1994). The Néel model describes the magnetostatic coupling caused by the correlated waviness of the magnetic layers in non-ideal films, while the oscillatory coupling is an indirect exchange interaction, resulting from the sharp cut-offs in momentum space due to the Fermi surface of the spacer layer. In their study on the interlayer coupling of NiFe/Cu/NiFe SV MLs, Kools et.al. (Kools, 1995) found that the Cu layer served to

decouple the FM layers and in the regime where the thickness of Cu spacer was less than about 1.7 nm, the FM coupling was so strong and it was proposed that NiFe bridges (pin holes) through Cu caused direct contact between two FM layers. As a consequent, two FM layers cannot rotate independently. The topological coupling energy and oscillatory exchange coupling energy per unit area (in centimeter-gram-second units) are in Eq. (2-27) and Eq. (2-28). (Williams, 2001)

$$E_{topo} = \frac{\pi^2}{\sqrt{2}} \frac{h^2}{\lambda} M_1 M_2 \exp\left(\frac{-2\pi\sqrt{2} t_S}{\lambda} \right) \tag{2-27}$$

$$E_{ex} = \frac{E_0}{\left(k_0 t_s\right)^2} \sin\left(\frac{2\pi t_s}{\Lambda} + \phi \right) \tag{2-28}$$

where M_1, M_2 is the saturation magnetization of two FM layers, h is the waviness amplitude of each film (can be determined from film roughness), λ is the wavelength of the surface variations (can be determined from grain size), E_0 is surface energy relevant to conduction electron potential, k_0 is wave number, ϕ is phase shift and Λ is the oscillatory coupling frequency, which is drastically influenced by the topological properties of the spacer of Fermi surface, and t_s is the spacer thickness.

The interaction field, which depends on the FM layer thickness and magnetization, is derived from the surface energy (Williams, 2001),

$$H_{\text{int}er} = \frac{E_{topo}}{M_s t_{FM}} \tag{2-29}$$

where M_s and t_{FM} are the saturation magnetization and thickness of two FM layers, respectively.

References

Agarwala, B.N., Attardo, M.J., and Ingraham, A.P. (1970). Dependence of electromigration-induced failure time on the length and width of aluminium thin-film conductors. J. Appl. Phys. **41**, 3954-3960.

Ames, I., d'Heurle, F.M., and Horstman, R. (1970). Reduction of electromigration in aluminum films by copper doping. IBM J. of Res. Develop., **4**, 461-463.

Anthony, T.C., Brug, J.A., Zhang, S.F. (1994). Magnetoresistance of symmetricspin valve structures. IEEE Truns.Mugn. **30**, 3819-3821.

Aust, K., and Rutter, J. (1965). Ultra high purity metals. American Society for Metals, (Ohio: Metals Park), 115.

Attardo, M.J., and Rosenberg, R. (1970). Electromigration Damage in Aluminum Film Conductors. J. Appl. Phys. **41**, 2381-2386.

Attardo, M.J., Rutledge, R., Jack, R.C. (1971). Statistical metallurgical model for electromigration failure in aluminum thin-film conductors. J. Appl. Phys. **42**, 4343-4349.

Bae, S., Tsu, I.F., Davis, M. Murdock, E.S., Judy, J.H. (2002). Electromigration study of magnetic thin films for the electrical reliability of spin-valve read heads. IEEE Trans. Magn. **38**, 2655-2657.

Baibich, M.N., Broto, J.M., Fert, A., Nguyen Van Dau, F., Petroff, F., Eitenne, P., Creuzet, G., Friederich, A., and Chazelas, J. (1988). Giant Magnetoresistance of (001)Fe/(001)Cr Magnetic Superlattices. Phys. Rev. Lett. **61**, 2472-2475.

Baglin, J.E.E., and Poate, J.M. (1978). Metal-Metal Inter-diffusion, Chap. 9 in Thin

Films Inter-diffusion and Reactions, Poate, J.M., Tu, K.N., and Mayer, J.W. eds. (New York: Wiley lnterscience).

Barmak, K., Lucadamo, G.A., Cabral Jr., C., Lavoie, C., and Harper, J.M.E. (2000). Dissociation of dilute immiscible copper alloy thin films. J. Appl. Phys., **87**, 2204-2214.

Chin, Y.L., Chiou, B.S., and Wu, W.F. (2002). Effect of the tantalum barrier layer on the electromigration and stress migration resistance of physical-vapor-deposited copper interconnect. Jpn. J. Appl. Phys. **41**, 3057-3064.

Berenbaum, L. (1971). Electromigration damage of grain-boundary triple points in Al thin films. J. Appl. Phys. **42**, 880-882.

Benhenda, S., Guglielmacci, J.M., Gillet, M., and Pech, T. (1987). Diffusion behaviour of Au/Ni bilayers deposited by electron beam evaporation and sputtering onto massive copper substrates. Appl. Surf. Sci. **28**, 215-223.

Black, J.R. (1969). Electromigration failure modes in aluminium metallization for semiconductor devices. Proceedings of the IEEE, **57**, 1587-1594; Electromigration - A brief survey and some recent results. IEEE Trans. on Electron Devices. **16,** 338-347.

Black, J.R. (1974). Physics of electromigration. Proceedings of the IEEE International Reliability Phhysics Symposium, 142-149.

Blech, I.A., and Sello, H. A study of failure mechanisms in silicon planar epitaxial Transistors. In Physics of Failure in Electronics, edited by Shilliday, T.S., and Vaccaro, J. (Rome Air Development Center, 1966). **5**, 496-505.

Blech, I.A., and Meieran, E.S. (1967). Direct transmission electron microscope observation of electrotransport in aluminum thin films. Appl. Phys. Lett., **11**, 263-266.

Blech, I.A., and Meieran, E.S. (1969). Electromigration in Al thin films. J. Appl. Phys., **40**, 485-491.

Blech, I.A., and Kinsbron, E. (1975). On the direction of electromigration in gold thin films. J. Appl. Phys. **46(2)**, 579.

Blech, I.A. (1976). Electromigration in thin film aluminum films on titanium nitride. J. Appl. Phys. Lett., **29**, 131-133.

Brandes, E.A., and Brook, G.B. (1994). Smithells Metals Reference Book, 7th Edn, (Oxford: Butterworth-Heinemann), Chapter 13.

Brückner, W., Baunack, S., Heoker, M., Mönch, J.-I., van Loyen, L., and Schneider, C.M. (2000). Inter-diffusion in NiFe/Cu/NiFe trilayers: Possible failure mechanism for magnetoelectronic devices. Appl. Phys. Lett. **77**, 358-360.

Brückner, W., Baunack, S., Thomas, J., Hecker, M., and Schneider, C.M. (2002). Inter-diffusion, stress, and microstructure evolution during annealing in Co/Cu/Co trilayers. J. Appl. Phys. **91**, 9696-9700.

de Miguel, J.J. Cebollada, A., Gallego, J.M., Ferrer, S., Miranda, R., Schneider, C.M., Bressler, P., Garbe, J.,Bethke, K., and Kirschner, J. (1989). Characterization of the growth processes and magnetic properties of thin ferromagnetic cobalt films on Cu (100). Surf. Sci. **211/212**, 732-739.

de Miguel, J.J., Cebollada, A., Gallego, J.M., Miranda, R., Schneider, C.M., Schuster, P., and Kirschner, J. (1991). Influence of the growth conditions on the magnetic properties of fcc cobalt films: from monolayers to superlattices. J. Magn. Magn. Mater. **93**, 1-9.

d'Heurle, F.M. (1971). The effect of copper additions on electromigration in aluminum thin films. Met. Trans., **2**, 683.

d'Heurle, F.M., Ainslie, N.G., Gangulee, A., and Shine, M.C. (1972). Activation energy for electromigration failure in aluminum films containing copper. J. Vac. Sci. Technol., **9**, 289-293.

d'Heurle, F.M. (1975). Electromigration in Thin Films: the effect of solute atoms on grain boundary diffusion. J. de Physique. **36**, (C4)191-(C4)199.

d'Heurle, F.M., and Ho, P.S. (1978). Electromigration in thin films. Thin films-inter-diffusion and reactions. (New York: Wiley).

Dupas, C., Beauvillain, P., and Chappert, C. Renard, J.P., Trigui, F., Veillet, P., Vélu, E., and Renard, D. (1990). Very large magnetoresistance effects induced by antiparallel magnetization in two ultrathin cobalt films. J. Appl. Phys. **67**, 5680.

Frankovic, R. and Bernstein, G.H. (1996). EM Drift and Threshold in Cu Thin-Film Interconnects. IEEE Trans. Electron Sensor **43**, 2233-2239.

Fiks, V.B. (1959). On the mechanism of the mobility of ions in metals. Sov. Phys. Solid State **1**, 14-28.

Geradin, M. (1961). De l'action des piles sur les sels de potasse et de soude et sur les alliages soumis a la fusion ignée, C. R. Acad. Sci. Paris **53**, 727-730.

Grünberg, P., Schreiber, R., Pang, Y., Brodsky, M.B., and Sowers, H. (1986). Layered magnetic structures: evidence for antiferromagnetic coupling of Fe layers across Cr interlayers. Phys. Rev. Lett. **57**, 2442-2445.

Gurney, A., Speriosu, V.S., Wilhoit, D.R., Lefakis, H., Fontana, Jr., R.E., Heim, D.E.,

and Dovek, M. (1997). Can spin valves be reliably deposited for magnetic recording applications? J. Appl. Phys., **81**, 3998-4003.

Gupta, R.P. (1982). Theory of electromigration in noble and transition metals. Phys. Rev. B **25(8)**, 5188.

Hecker, M., Tietjen, D., Wendrock, H., Schneider, C.M., Cramer, N., Malkinski, L., Camley, R.E., Celinski, Z. (2002). Annealing effects and degradation mechanism of NiFe/Cu/GMR MLs.

Hesketh, R.V. (1979). Electromigration: the electron wind. Phys. Rev. B **19(4)**, 1727-1733.

Ho, P.S., and Kwok, T. (1989). Electromigration in metals. Rep. Prog. Phys. **52**, 301-348.

Hong, C.F., Togo, M., and Hoh, K. (1993). Influence of grain boundary configuration in aluminum films on abrupt resistance changes during electromigration. Jpn. J. Appl. Phys., **32**, L247-L254.

Huang, R.T., Chen, F.R., Kai, J.J., Kai, W., Tsu, I.-F., and Mao, S. (2003). Diffusion behavior in spin valves studied by high resolution transmission electron microscopy and nanobeam technique. J. Magn. Magn. Mater., **260**, 28-36.

Huang, T.C., Nozieres, J.-P., Speriosu, V.S., Gurney, B.A., and Lefakis, H. (1992). Appl. Phys. Lett., **62**, 1478-1480.

Huntington, H.B., and Grone, A.R. (1961). Current induced marker motion in gold wires. J. Phys. Chem. Solids, **20**, 76-87.

Iijima, Y., Hirano, K.-I., and Sato K. (1977). Inter-diffusion in Cu-Mn alloys. J. Japan

Inst. Metals, **41**, 831-842.

Iijima, J., Fujii, Y., Neishi, K., and Koike, J. (2009). Resistivity reduction by external oxidation of Cu-Mn alloy films for semiconductor interconnect application. J. Vac. Sci. Technol. B, 27(4), 1963-1968.

Jile, D. (1998). Introduction to Magnetism and Magnetic Materials (Boca Raton, FL: CRC Press).

Kakar, A.K. (1973). Electromigration studies on aluminum-copper stripes, Solid State Technol., **16**, 47-62.

Kuniko, K., and Takamaro, K. (1994). Electromigration characteristics for Al-Ge-Cu. In Microelectronics Manufacturability, Yield, and Reliability. Vasquez, B., and Kawasaki, H. Eds. Proc. SPIE **2334**, 4-12.

Kwok, T. and Ho, P.S. (1988). Electromigration in metallic thin film. in Diffusion phenomena in thin films and microelectronic materials, Gupta, D. and Ho, P.S.ed. (New Jersey: Noyes Publications), p. 392.

Kwok, T., Ting, C.Y., and Han, J.U. (1985). Microstructure Studies of Al-Cu Submicron Interconnection. In Proceedings of the 2nd international Multilevel Interconnection Conference, Santa Clara, CA, 83.

Kwon, D., Park, H., and Lee, C. (2005). Electromigration resistance-related microstructural change with rapid thermal annealing of electroplated copper films. Thin Solid Films, **475**, 58-62.

Kools, J.C.S., Rijks, Th.G.S.M., De Veirman, A.E.M., and Coehoorn, R. (1995). On the ferromagnetic interlayer coupling in exchange-biased spin-valve MLs. IEEE Trans.

Magn. **31**, 3918-3920.

Chopra, H.D., Yang,D.X., Chen, P.J., Parks, D.C., Egelhoff, W.F. (2000). Nature of coupling and origin of coercivity in giant magnetoresistance NiO-Co-Cu-based spin valves. Phys. Rev. B, **61**, 9642-9652.

Kos, A.B., Russek, S.E., Kim, Y.K., and Cross. R.W. (1997). High current density measurement of giant magnetoresistive spin-valves for magnetic recording and sensor applications. IEEE Trans. Magn., **33**, 3541-3543.

Langer, J., Mattheis, R., Ocker, B., Maass, W., Senz, S., Hesse, D., and Krausslich, J. (2001). Microstructure and magnetic properties of sputtered spin valve systems. J. Appl. Phys., **90**, 5126-5135.

Learn, A.J. (1974). Electromigration effects in aluminum alloy metallization, J. Electron. Mater., **3**, 531-552.

Lefakis, H., Cain, J.F., and Ho, P.S. (1983). Low temperature interfiffusion in Cu/Ni thin films. Thin Solid Films, **101**, 207-218.

Li, C.M. (1961). High-angle tilt boundary - a dislocation core model. J. Appl. Phys., **32**, 525-541.

Lloyd, J.R., Shatzkes, M., and Challaner, D.C. (1988). Kinetic study of electromigration failure in Cr/Al-Cu thin film conductors covered with polyimide and the problem of the stress dependent activation energy. In Proceedings of the IEEE International Reliability Physics Symposium, 159-164.

Madakson, P. and Liu, J.C. (1990). Inter-diffusion and resistivity of Cu/Au, Cu/Co, Co/Au, and Cu/Co/Au thin films at 25-550 °C. J. Appl. Phys., **68**, 2121-2126.

Marcoux, P.J., Merchant, P.P., Naroditsky, V., and Pehder, W.D. (1989). A new 2D simulation model of electromigration. Hewlett-Packard J., June, 79-84.

Massalski, T.B., Okamoto, H., Subramanian, P.R., Kacprzak, L. (1990). Binary Alloy Phase Diagram, 2nd edn. (OH: ASM International, Materials Park).

Misra, E., Theodore, N.D., Mayer, J.W., Alford, T.L. (2006). Failure mechanisms of pure silver, pure aluminum and silver-aluminum alloy under high current stress. Microelectron. Reliab., **46**, 2096-2103.

Mott, N.F. (1936). The electrical conductivity of transition metals. Proc. R. Soc. A 153, 699-717.

Neamtu, J., Volmer, M., Coraci, A. (1999). Magnetoresistive properties and microstructure of NiFe/thin films and NiFe(t).Cu(s)/NiFe(t) ML films. Thin Solid Films, **343-344**, 218-221.

Néel, L., Hebd, C.R. (1962). A magnetostatic problem concerning ferromagnetic films. Seances Acad. Sci. **255**, 1545.

Nikawa, K. (1981). IEEE Int. Rel. Phys. Symp., **CH1619-6**, 175.

Paul, S.H., and Thomos K. (1989). Electromigration in metals. Rep. Prog. Phys., **52**, 301-348.

Park, C.W., and Vook, R.W. (1991). Activation Energy for EM in Cu films. Appl. Phys. Lett., **59**, 175.

Parkin, S.S.P., More, N., and Roche, K.P. (1990). Oscillations in exchange coupling and magnetoresistance in metallic superlattice structures: Co/Ru, Co/Cr and Fe/Cr. Phys. Rev. Lett., **64**, 2304-2307.

Pellerin, J.G., Anderson, S.G.H., Ho, P.S., Coffey, K.R., Howard, J.K., and Barmak. K. (1994). Grain boundary diffusion and its effects on the magnetic properties of Co/Cu and Co/Cr thin film bilayers. J. Appl. Phys., **75**, 5052-5060.

Petroff, F., Barthelemy, A., Mosca, D.H., Lottis, D.K., Fert, A., Schroeder, P.A., Pratt, W.P., Loloee, R., and Lequien, S. (1991). Oscillatory interlayer exchange and magnetoresistance in Fe/Cu MLs. Phys. Rev. B, **44**, 5355.

Pierce, J.M., Schmid, A.K., Atlan, D., Itoh, H., Heinrich, B., Ichinokawa, T., and Kirschner, J. (1993). Fast inter-diffusion in thin films: Scanning-tunneling-microscopy determination of surface diffusion through microscopic pinholes. Phys. Rev. B, **48**, 2855-2858.

Schneider, C.M., Bressler, P., Schuster, P., Kirschner, J., de Miguel, J.J., and Miranda, R. (1990). Curie temperature of ultrathin films of fcc-cobalt epitaxially grown on atomically flat Cu (100) surfaces. Phys. Rev. Lett., **64**, 1059-1062.

Schoen, J.M. (1980). Monte carlo calculations of structure-induced electromigration failure. J. Appl. Phys., **51**, 513-521..

Seith, W., and Wever, H. (1953). Uber einen neuen effekt bei der elecktrolytischen Überführung in festen Legierungen. Z. Elektrochem. **59**, 942.

Shao, W., Vairagar, A.V., Tung, C-H., Xie, Z-L., Krishnamoorthy, A., and Mhaisalkar, S.G. (2005). Electromigration in copper damascene interconnects: reservoir effects and failure analysis. Surf. Coating Tech., **198**, 257-261.

Shine, M.C., and d'Heurle, F.M. (1971). Activation energy for electromigration in aluminum films alloyed with copper. IBM J. Res. Dev., **15**, 378-383.

Shingubara, S., Takede, Y., Sakue, H., Takahagi, T., and Verbruggen, A.H. (1999). Electromigration reliability study of a GMR spin valve device. Mat. Res. Soc. Symp. Proc., 563, 145-150.

Shinjo, T., and Yamamoto, H. (1990). Large magnetoresistance of field-induced giant ferrimagnetic MLs. J. Phys. Soc. Jpn., 59, 3061.

Sideris, G. (1973). Power from transistors, Electronics, 46, 68-69.

Sigsbee, R.A. (1973). Electromigration and metallization lifetimes. J. Appl. Phys., **44**, 2533-2540.

Sorbello, R.S. (1985). Theory of the direct force in electroigration. Phys. Rev. B, **31(2)**, 798-804.

Tang, P.F. (1994). Simulation and computer models for electromigration. In Electromigration and electronic device degradation, Christou, A., ed. (New York: John Wiley & Sons, Inc.), p. 35-42.

Tang, P.F., Milnes, A.G., Bauer, C.L., and Mahajan. S. (1989). Electromigration in thin films of Au on GaAs. Proc. Mater. Res. Soc., **167**, 341; Tang, P.F. (1990). Modeling of electromigration with applications to Au on GaAs, Ph.D thesis, Dept. of ECE, Carnegie-Mellon University, Pitts-burgh, PA, April 30, 1990.

Tsybal, E.Y., and Pettifor, D.G. (2001). Solid State Physics: Perspectives of Giant Magnetoresistance, Ehrenreich, H. and Spaepen, F. ed. (Academic Press), **56**, 113.

Turnbull, D., and Hoffman, R.Z. (1954). The effect of relative crystal and boundary orientation on grain boundary diffusion rates. Acta metal., **2**, 419-426.

van Gurp, G.J. (1977). Electromigration and hall effect in cobalt films. J. Phys. Chem.

Solids. **38**, 627-633.

van Loyen, L., Elefant, D., Tietjen, D., Schneider, C.M., Hecker, M., and Thomas, J. (2000). Annealing of $Ni_{80}Fe_{20}$/Cu and Co/Cu MLs. J. Appl. Phys., **87**, 4852-4854.

Venables, J.D., and Lye, R.G. (1972). A statistical model for electromigration-induced failure in thin film conductors. Proceedings of the IEEE International Reliability Phhysics Symposium, 159-164.

Ventura, J., Sousa, J.B., Liu, Y., Zhang, Z., and Freitas, P.P. (2005). Electromigration in thin tunnel junctions with ferromagnetic/nonmagnetic electrodes: nanoconstrictions, local heating, and direct and wind forces. Phys. Rev. B, **72**, 094432-(1-7).

Wang, P.C., Cargill III, G.S., Noyan, I.C., and Hu, C.K. (1998). Electromigration-induced stress in aluminum conductor lines measured by x-ray microdiffraction. Appl. Phys. Lett., **72**, 1296-1298.

William, E.M. (2001). Thin Film Properties for MR Sensors. In Design and Analysis of Magnetoresistive Recording Heads-Thin Film Properties. (John Wiley & Sons, Inc.), p. 34-35.

Yu, G.H., Li, M.H., Zhu, F.W., Chai, C.L., Jiang, H.W., and Lai, W.Y. (2001). Magnetic property and interlayer segregation in spin valve metal MLs. Science in China, **45**, 140-145.

Zeng, D.G., Chung, K.W., Judy, J.H., and Bae, S. (2010). Numerical simulation of current density induced magnetic failure for giant magnetoresistance spin valve read sensors, J. Appl. Phys., **108**, 023903-(1-5).

Zeltser, A.M., Pének, K., Menyhárd M., and Sulyok, A. (1998). Thermal Stability of

CoFe, Co and NiFe/Co Spin Valves. IEEE Trans. Magn., **34**, 1417-1419.

Zhang, H., Wang, G., and Cargill III, G.S. (2007). Local melting during electromigration in Cu conductor lines. J. Electron. Mater., **36**, 117-122.

CHAPTER 3 EXPERINMENT AND CHARACTERIZATION TECHNIQUES

This chapter describes the key equipments and processes used in the preparation and characterization of the samples discussed in this chapter. Various measurement techniques have been used in this project to analyze the electrical and magnetic properties and characterize the microstructure of NiFe/(CoFe or Co)/Cu/(CoFe or Co)/NiFe/FeMn based GMR SV. JEOL-6700 field-emission scanning electron microscope (FE-SEM) was used to topographically detect the different failure characteristics formed under the different stressing conditions. Atomic force microscope (AFM) was conducted to quantitatively confirm the variation of surface roughness and the surface profiler is used to measure the film thickness. Auger electron spectroscopy (AES) depth profiles, nano-beam energy dispersive X-ray (EDX) depth profiles and cross sectional transmission electron microscopy (XTEM) are employed to investigate the interface of GMR SVs, especially the intermixing caused by Ni-Cu interdiffusion. The magnetic properties were analyzed from the M-H loops measured using a vibrating sample magnetometer (VSM) at ambient temperature and the R-H loops measured using an in-line 4 point probe and M-H loop tracer. Details for some of the important characterization methods will be presented in this chapter. A brief description of the fabrication process of the CIP-GMR SV devices would also be presented in this chapter.

3.1 Preparation of EM Test Samples

3.1.1 Input/Output Electrode Pad Design

All the EM test samples studied in this project are patterned using electron beam lithography (EBL) and optical lithography. In order to investigate the EM-induced failure behavior under different stressing conditions and find out the physical mechanism responsible for it, we fixed the aspect ratio of EM test stripe to be 1:10. EBL is used for "patterning" the magnetic thin films including the GMR MLs and the GMR SV whole stacks, and a Cr emerson glass mask is used for "lift-off" of input and output pad structures, which could be Al or Al/Cu/Al thin films. Figure 3.1 shows the test sample configuration. The electrode pads for the EM test samples are designed to be a "F" shape for the convenience to do four point measurement as well as wire bonding. The I/O pads are designed to have a continuously shrunken width from 150

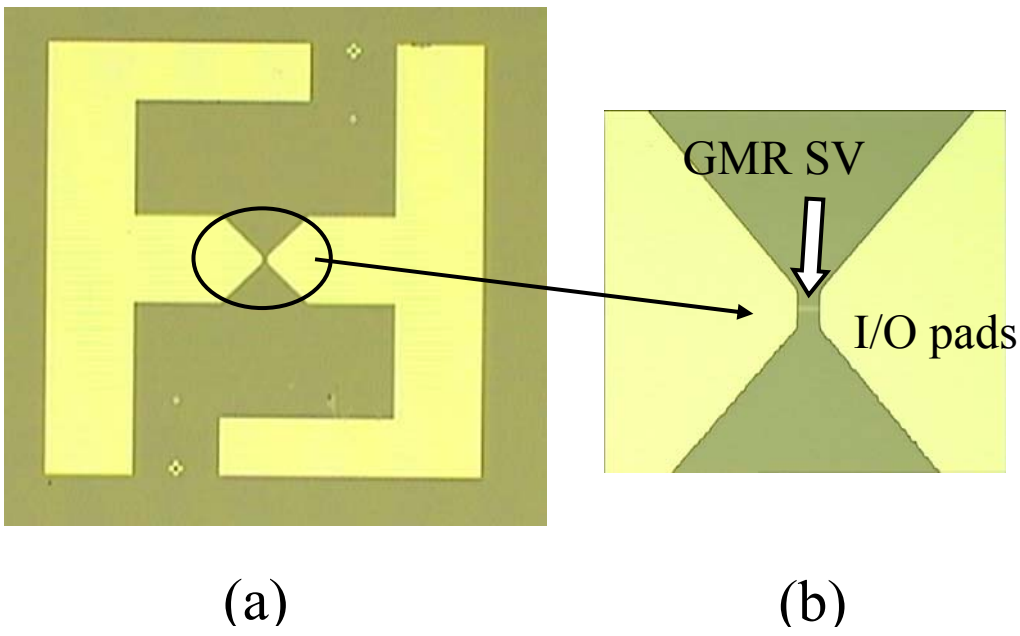

Fig. 3.1 (a) Optical microscopy image of EM test sample with the "F"-shape CIP electrodes; (b) enlarged top-view of the test sample with the CIP I/O electrode pads.

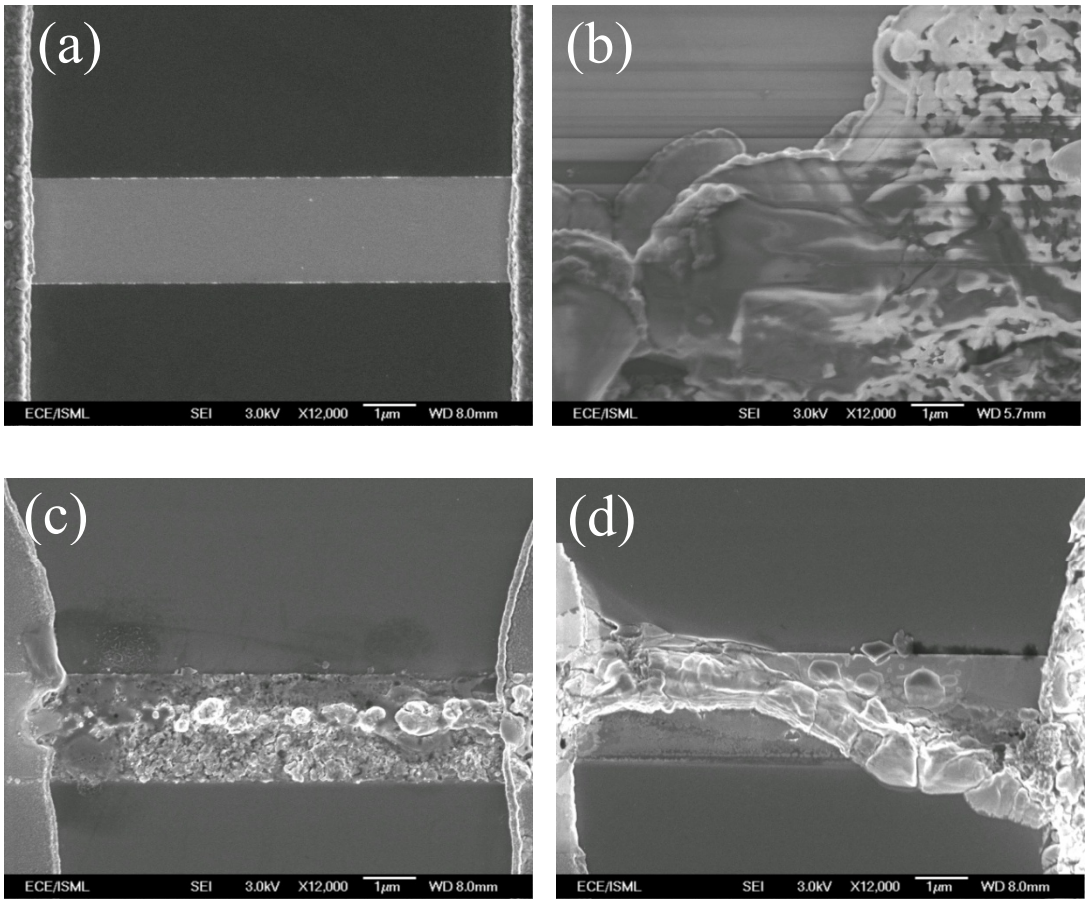

Fig.3.2 SEM images of the EM test samples: (a) both the magnetic multilayers and the Al I/O contact pads are as-deposit, no electrical stressing on it; (b) active region of EM test samples are covered by melted Al caused by Joule heating during EM test at the current density of J = 7×10^7 A/cm^2 (I = 48.3 mA); (c) EM-induced failure in the magnetic multilayered stripe after the EM testing at the current density of J = 7×10^7 A/cm^2 (I = 48.3mA); (d) Joule heating induced Al melt-short in the EM test samples at the current density of J = 1.2×10^8 A/cm^2 (I = 80 mA); all tests at ambient temperature.

μm to 12 μm so as to reduce the geometrically induced current crowding effect at both ends of test stripes connecting with contact pads.

From the discussion in the previous chapter, the industry has turned to Cu as the interconnect conductor in terms of resistance-capacitance delay, EM resistance and cost of fabrication. At first, in order to avoid the inter-diffusion at the Cu/NiFe interfaces as well as increase the wire bonding affinity, we consider Al (t = 300 nm) as

the contact pads. However, after the applied current density at the I/O contact pads is beyond 1.2×10^6 A/cm^2 (that is, I > 34.5 mA), the EM-induced melt-open failure in the Al contact pads, especially at the cathode end, occurred before the EM-induced failure or inter-diffusion in the magnetic multilayers can be observed. As it is shown in Fig. 3.2 (b), after EM testing under the current density of J = 7×10^7 A/cm^2 (I = 48.3 mA) at the ambient temperature, more than 80% of the active region of magnetic multilayered stripe is covered by the melted Al contact pads because the relatively much lower activation energy (0.4~0.8eV) and melting point of Al thin films. In order to solve this problem, we use the Al/Cu/Al trilayers to replace Al as the I/O contact pads. This optimized Al/Cu/Al trilayered contact pads can be loaded up to the biasing current of J=7×10^7 A/cm^2 (I = 48.3mA, see fig. 3.2 (c)), but less than J=1.2×10^8 A/cm^2 (I = 80 mA, see Fig. 3.2 (d)).

3.1.2 EM Test Device Patterning and Fabrication

All the magnetic thin films including $Ni_{81}Fe_{19}$, $Co_{90}Fe_{10}$, Co, and $Fe_{50}Mn_{50}$, and non magnetic thin films like Cu and Al used for the EM test samples were deposited by AJA sputtering machine onto the Si (100) substrates. The base vacuum pressure was in the range of 0.7 ~ 2 × 10^{-8} Torr, and the working gas pressure was fixed at 2 mTorr. The detailed information for the deposition conditions of these thin films are listed in Table 3-1. Two series of magnetic multilayer stacks are used in this project: NiFe/(CoFe or Co)/Cu/(CoFe or Co)/NiFe GMR magnetic multilayers (ML) or NiFe/(CoFe or Co)/Cu/(CoFe or Co)/NiFe/FeMn GMR SVs are shown in Fig. 3.3 (a) and (b).

Table 3-1 Deposition parameters for the different thin films used in this project.

Thin Film	Working gas pressure	Power	Deposition Rate
$Ni_{81}Fe_{19}$	2mTorr	13.2W or 50W	0.01nm/s or 0.028nm/s
$Co_{50}Fe_{50}$	2mTorr	12W	0.08nm/s
Co	2mTorr	50W	0.026nm/s
$Fe_{50}Mn_{50}$	2mTorr	12.2W	0.093nm/s
Ta	2mTorr	14.7W	0.01nm/s
Cu for spacer	2mTorr	14W or 30W	0.02nm/s or 0.04nm/s
Cu for I/O pads	2mTorr	100W	0.13nm/s
Al	2mTorr	100W	0.07nm/s

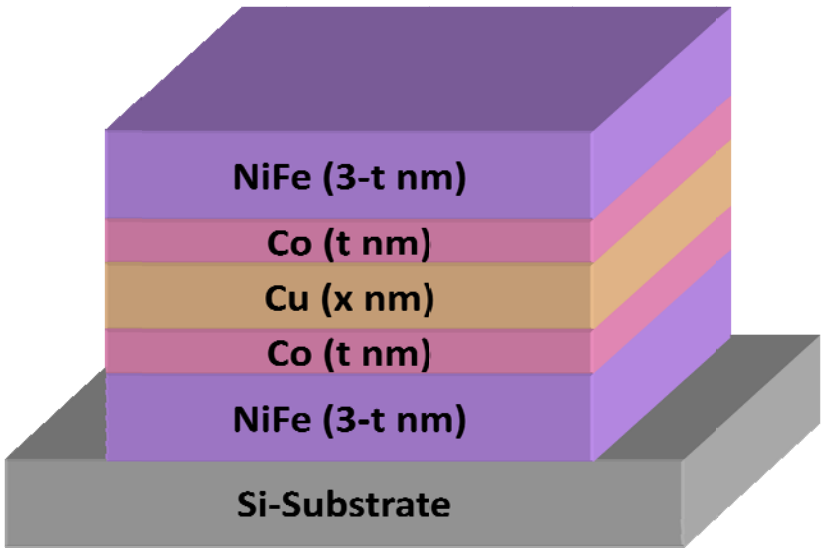

(a)

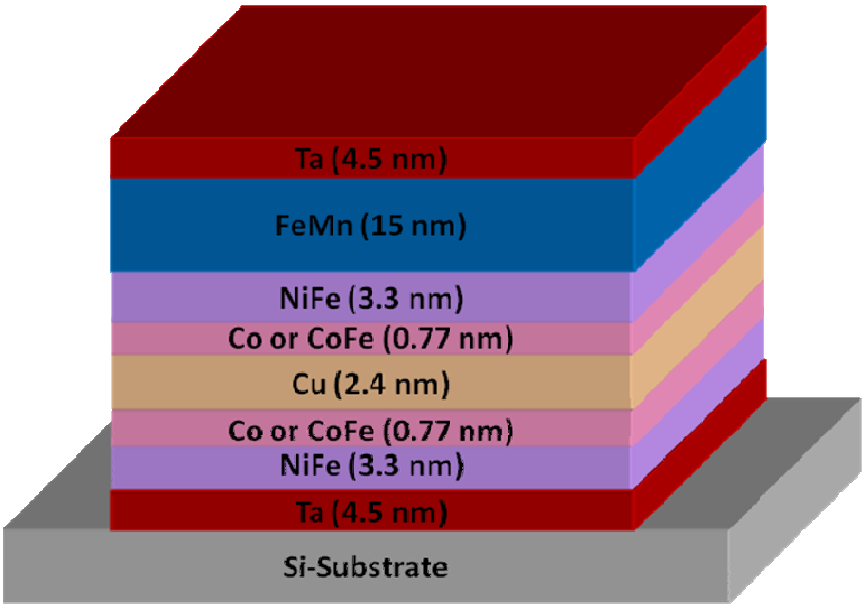

(b)

Fig. 3.3 3-D schematic configuration of (a) NiFe/(Co)/Cu/(Co)/NiFe GMR MLs; and (b) NiFe/(CoFe or Co)/Cu/(CoFe or Co)/NiFe/FeMn GMR SVs.

The active part of the EM test samples (in the following discussion, we called it as GMR SV spintronic devices, GMR SVSDs) were fabricated using either "EBL patterning – GMR whole stacks deposition – liftoff" technique or "GMR whole stacks deposition – EBL patterning – etching & removing the unwanted films" technique. For patterning the active part with the width of 2μm and length of 20 μm, two kinds of electron beam resist are coated onto the diced Si (100) substrate by spin coater, which are the positive PMMA950 with the thickness of 150~200 nm and negative maN2405 resist with the thickness of 300~500nm. The detailed experimental parameters are listed in Table 3-2. The patterning of the I/O contact pads are processed with the "standard photolithography technique". AZ 7220 photo-resist (PR) with a thickness of 0.2 μm was first spin coated onto the Si (100) substrate with the patterned GMR

Table 3-2. Parameters for the testing device patterning.

Resist	PMMA950 (ratio of PMMA to Anisole = 4:5)	maN2405
Spin Coat	3000 rpm, 40 s	6000 rpm, 45 s
Prebake	180 °C, 90s (hotplate)	100 °C, 120 s (hotplate)
Lithography	50 pA, 0.167 s	30 pA, 0.083 s
Developer	Diluted MIBK (MIBK:IPA=1:3), 40 s	maD532, 70~80 s
Rinse	IPA	DI water

SVSDs on it and then a soft baking was done for 30 minutes using an oven at the temperature of 90 °C. The PR-coated samples were then aligned and exposed in the UV atmosphere using a MA6 mask aligner. The mask contact was made using the "hard contact mode". The exposure dose and the gap between mask and test sample were selected as 130 mJ/cm^2, and 30 μm, respectively by considering PR thickness and sample geometries. A slight over-exposure condition was employed for the purpose of clean developing and lift-off of the contact pads. After masking alignment, the Al or Al/Cu/Al I/O contact pad materials were deposited using the AJA sputtering machine. We take several breaks to cool down the substrate during deposition of thick contact materials in order to avoid burning of the photo-resist due to overheating during long-time sputtering. In particular, in order to obtain uniform film thickness and to dissipate heat from the substrate easily, the substrate was rise to highest position and rotated at the maximum rate during deposition. The flow chart of EM test sample fabrication was shown in Fig. 3.4.

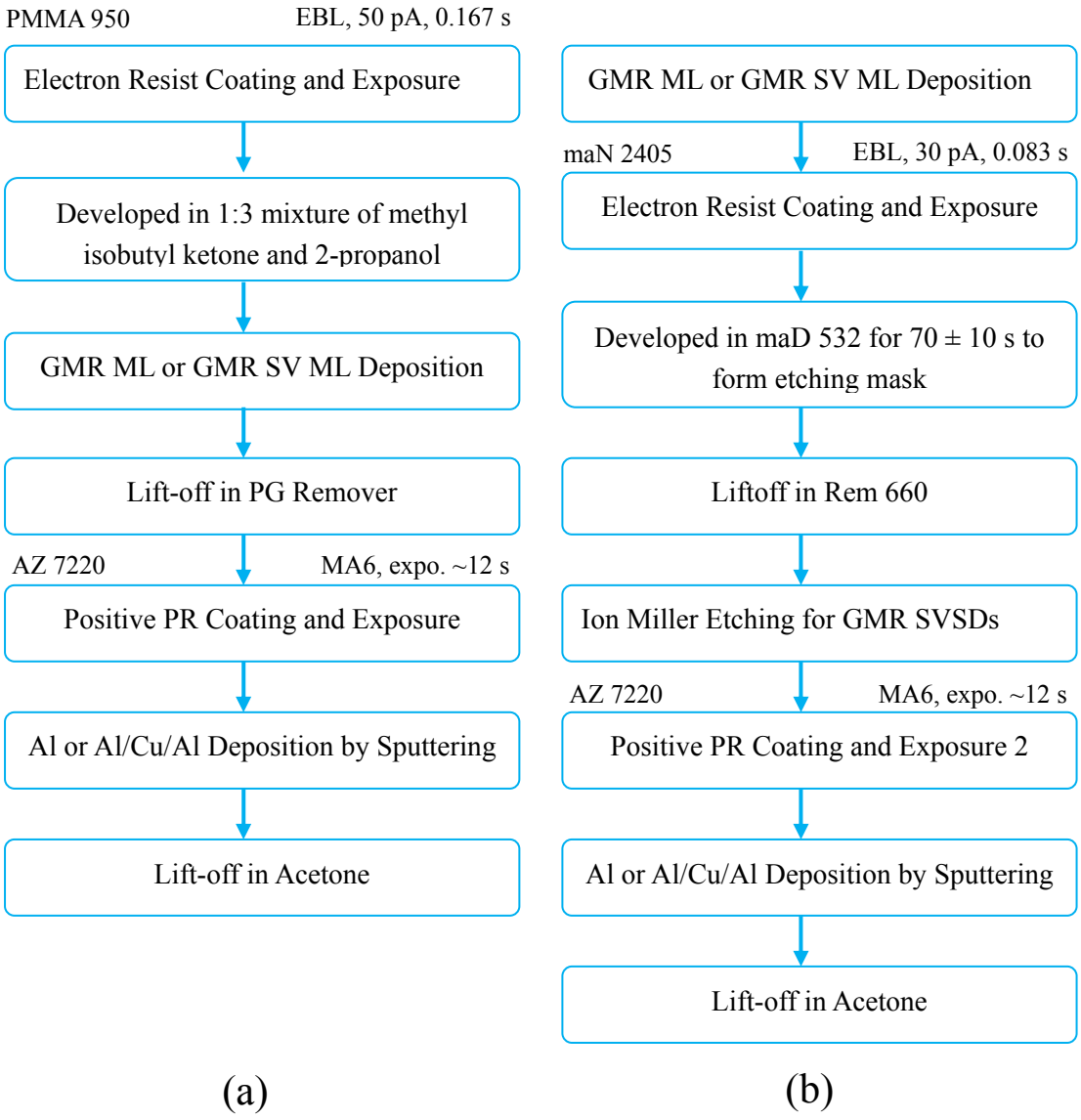

Fig.3.4 Optimal fabrication flow chart of EM test samples: (a) lift-off process with positive resist; (b) etching process with negative resist.

3.2 Lifetime Measurement and Failure Criterion

The lifetime measurement of metal stripes is the most commonly used method for investigating the EM processes. In this study, we compared the lifetime dependence on Cu spacer thickness, different FM/Cu interfaces, Co insertion layer thickness, and current densities. All the EM test devices for lifetime measurement we used in this

project have the identical shape and dimension (W = 2 μm and L = 20 μm). For different batch of EM test devices, the total thickness may be varied, but the applied biasing current density is same for each batch of test devices. The resistance measurement is carried out using program-controlled keithley source meter 2420. We always used constant dc current and fixed current densities for each measurement, and changed the input current value in accordance with the variation of total thickness so as to keep the same batch of EM test devices stressed at the same current density. The self-calibration function of program-controlled keithley source meter ensures the constant dc current density is applied during the whole testing process. Considering the magnetic field induced acceleration of EM failures in the GMR SVSDs, D.C. or pulsed D.C. magnetic field are also concurrently applied with the D.C. electrical field. Time-to-failure (TTF) in this report was defined as the time for the resistance of EM testing samples to increase by 100%. The results are usually given in terms of median time to failure (MTTF), or t_{50}, which is the time required for failure of 50% of a group of test samples. MTTF can be calculated from the equation 3-1.

$$MTTF, t_{50} = \exp \overline{\ln t_f}$$
$$\overline{\ln t_f} = \frac{\ln t_1 + \ln t_2 + \ln t_3 + ... + \ln t_n}{n} \quad (3\text{-}1)$$

where, t_n is the TTF of the n_{th} EM test sample, which can be measured using program-controlled keithley 2420 sourcemeter at four-wire mode I-V measurement.

Typically the result of lifetime measurements is plotted in a log-normal scale. In order to obtain the result of lifetime measurement in a reasonable time frame, the EM lifetime test is carried out under a set of accelerated test conditions at elevated

temperatures and with high D.C. current density stressing. The activation energy (E_a) of the test samples was obtained by varying the ambient testing temperature from ambient temperature to 280 °C. The current density dependence factor "n" value for analyzing the contribution of joule heating to EIF was determined from the slope of a plot ln (J) vs. ln (time-to-failure (TTF)) at ambient temperature by changing the D.C. applied current density in the range of $1\times10^7 \sim 1.5\times10^9$ A/cm^2. The magnitude of D.C. magnetic field is in the range of 200 to 600 Oe and the duty factor for pulsed magnetic field is 0.3, 0.5, 0.8 and 1. The electrical and magnetic field stress at different temperature was applied to the EM test samples using a lab-innovated microprobe station as shown in Fig. 3.5 together two computer controlled D.C. current source meters and one Agilent dual D.C. power supply.

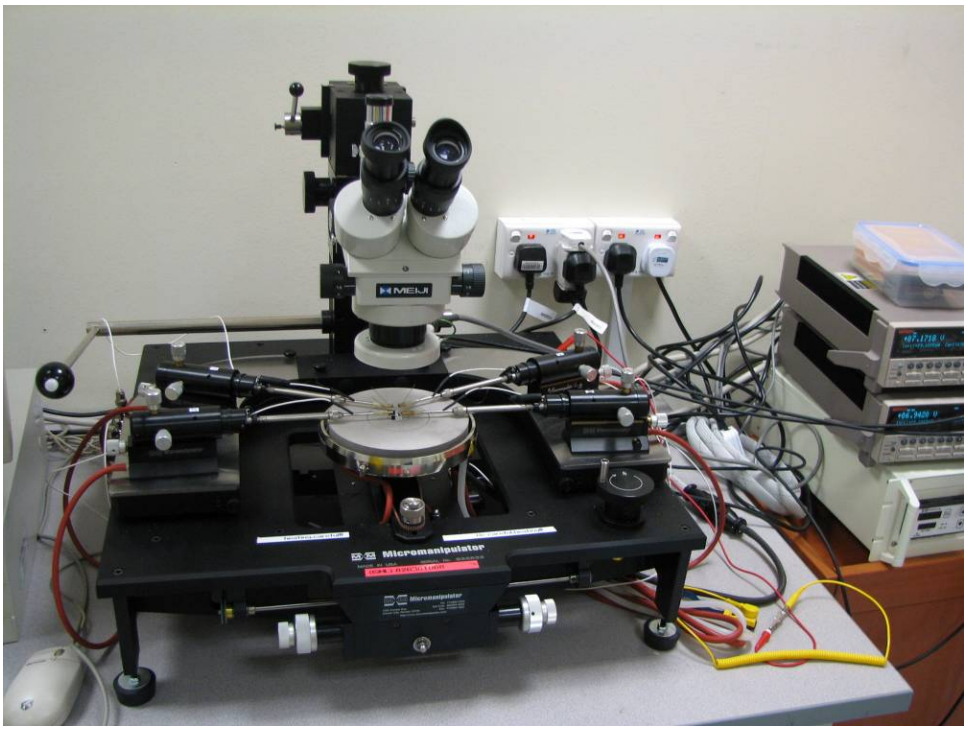

Fig. 3.5 Micromanipulator Probe Station used for measuring EM failure lifetimes.

3.3 Fabrication and Characterization Techniques

3.3.1 Deposition Technique - AJA multi-target Sputtering System

Physical vapor deposition (PVD) by sputtering is a term used to refer to a technique wherein atoms or molecules are ejected from a target material by high-energy particle bombardment so that the ejected atoms or molecules can condense on a substrate as a thin film. Although GMR has been discovered in 1988 by Fert's and Grünberg's group using molecular beam epitaxy (MBE) (Grünberg, 1986; Baibich, 1988), it's the later breakthrough on sputtering bringing GMR effect from laboratory to industry commercialization. At present, sputtering has become one of the most widely used techniques for depositing various metallic films on wafers, including metals, alloys, oxides, and all kinds of magnetic thin films.

As we all know, it is very important that the MLs have a clear and continuous layered structure with smooth interfaces to show the GMR effect owing to magnetic scattering at the interfaces between the magnetic and nonmagnetic layers. Therefore, for deposition of GMR MLs or GMR SV MLs, the sputtering method is better than the evaporation method since it is more suitable to prepare a flat and continuous layered structure, as the sputtered atoms have sufficient energy for migration, resulting in the growth of a layered structure while the evaporated atoms have small energy, resulting in the growth of an island structure. In this project, we choose AJA multi-target sputtering system for the deposition of all the magnetic, nonmagnetic and contact metallic thin films. It is found that an ultrathin Cu thin film deposited by sputtering

system, such as 0.9 nm, have a clear and continuous layered structure.

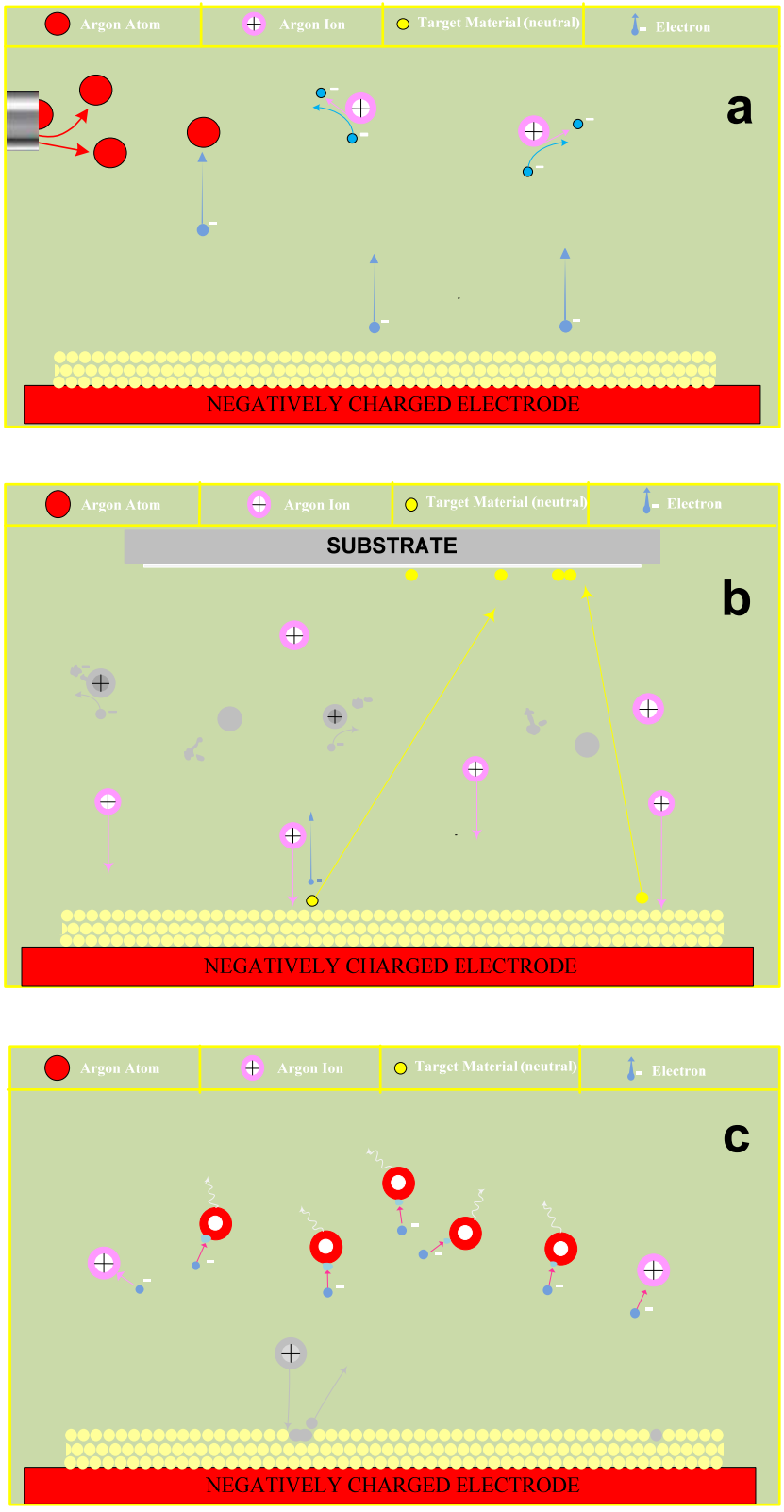

Fig. 3.6 Film formation mechanism of PVD using magnetron sputtering system.

Powering the electrode with D.C. voltage will result in "free electrons" which will immediately be accelerated away from the negatively charged electrode (cathode). These accelerated electrons will approach the outer shell electrons of neutral gas atoms in their path and, being of a like charge, will drive these electrons off the gas atoms. This leaves the gas atom electrically unbalanced since it will have more positively charged protons than negatively charged electrons - thus it is no longer a neutral gas atom but a positively charged "ion" (e.g. Ar +), as shown in Fig. 3.6 (a). At this time the positively charged ions are accelerated into the negatively charged electrode striking the surface and "blasting" loose electrode material (diode sputtering) and more free electrons by energy transfer, as shown in Fig. 3.6 (b). The additional free electrons feed the formation of ions and the continuation of the plasma. All the while free electrons find their way back into the outer electron shells of the ions thereby changing them back into neutral gas atoms, as shown in Fig. 3.6 (c). Due to the laws of conservation of energy, when these electrons return to a ground state, the resultant neutral gas atom gas gained energy and must release that same energy in the form of a photon. The release of these photons is the reason the plasma appears to be glowing.

Sputtering yield, or the number of atoms ejected per incident ion, is an important factor in sputter deposition processes, since it affects the sputter deposition rate. Sputtering yield primarily depends on three major factors: 1) target material; 2) mass of the bombarding particles; and 3) energy of bombarding particles. In the energy range where sputtering occurs (10 to 5000 eV), the sputtering yield increases with particle mass and energy.

3.3.2 Surface or Interface Characterization and Microstructure Analysis Techniques

Because the EM-induced failures and the magnetic properties such as coercivity H_c, remanent magnetic moment per unit area M_r, exchange biasing energy H_{ex} and internal exchange biasing H_{in} are closely related to the microstructure, texture, crystallite size and thickness of polycrystalline films, surface (or interface) and microstructure analysis has become one of the most decisive factors for studying and optimizing the EM reliability of the GMR SVSDs. The selected surface and structure observation and analysis techniques will be briefly discussed in this chapter.

3.3.2.1 Field-Emission Scanning Electron Microscope (FE-SEM)

The Field-Emission Scanning Electron Microscope (FE-SEM) is a type of electron microscope that images the sample surface by scanning it with a high-energy beam of electrons in a raster scan pattern. The electrons interact with the atoms that make up the sample producing signals that contain information about the sample's surface topography, composition and other properties such as electrical conductivity. It is a highly versatile instrument that is widely used for imaging, material characterization and failure analysis.

The types of signals produced by an SEM include secondary electrons, back scattered electrons (BSE), characteristic x-rays, light (cathodoluminescence), specimen current and transmitted electrons (Lee, 1983; Holt, 1989). The escape zones of different signals are shown in Fig. 3.7. These types of signal all require specialized detectors that are not usually all present on a single machine. The signals result from

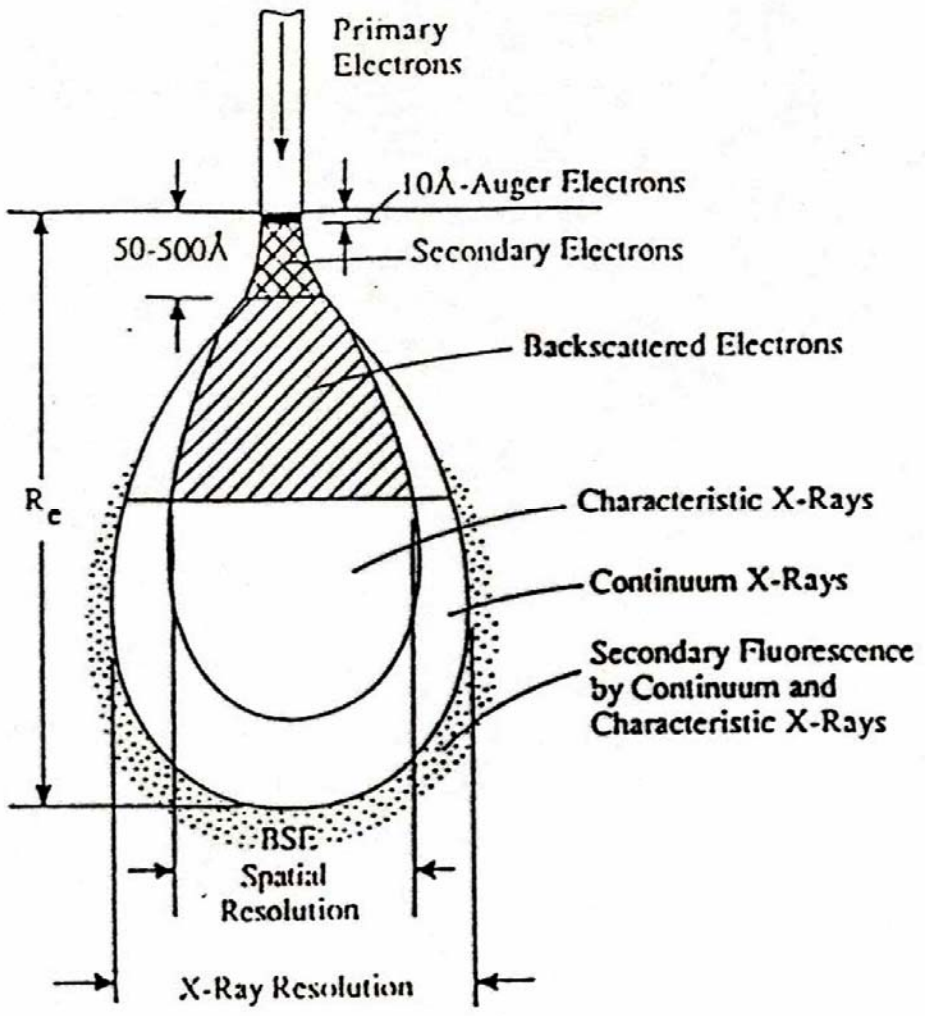

Fig. 3.7 Escape zones of various signals. SE provides information on surface topography. Used also in voltage contrast and magnetic contrast imaging. BSE provide information on topography and material (atomic number contrast imaging). AE provide information on chemical composition of thin films (used in surface analysis). Characteristic X-rays provide information on chemical composition (EDX/WDX). Emitted photons (CL or cathodoluminescence) provide information on crystal defects.

interactions of the electron beam with atoms at or near the surface of the sample. Due to the way these images are created, SEM micrographs have a very large depth of field yielding a characteristic three-dimensional appearance useful for understanding the surface structure of a sample. This is exemplified by the micrograph of pollen shown to the right. A wide range of magnifications is possible, from about x 25 (about equivalent to that of a powerful hand-lens) to about x 250,000, about 250 times the

magnification limit of the best light microscopes. Back-scattered electrons (BSE) are beam electrons that are reflected from the sample by elastic scattering. BSE are often used in analytical SEM along with the spectra made from the characteristic x-rays. Because the intensity of the BSE signal is strongly related to the atomic number (Z) of the specimen, BSE images can provide information about the distribution of different elements in the sample. Characteristic X-rays are emitted when the electron beam removes an inner shell electron from the sample, causing a higher energy electron to fill the shell and release energy. These characteristic x-rays are used to identify the composition and measure the abundance of elements in the sample.

3.3.2.2 Transmission Electron Microscopy (TEM)

The interface microstrctural variation and the degree of inter-diffusion are direct observed and qualitatively characterized by a cross-sectional TEM (XTEM, model is Tecnai G2 F30 S-Twin and the operating voltage is 300kV) as well as a nano-beam EDX with a nominal beam size of 2 nm attached to the TEM. TEM is unique in its capabilities to provide information about the structure and the local composition of a complicated, multilayered structure with a lateral resolution of about 1 nm. It directly shows a two-dimensional projection of all the crystals including the defects. The main TEM imaging modes are shown in Fig. 3.8, including both bright field (BF) mode and dark field (DF) mode. In BF mode, only the direct beam is allowed to pass through the objective aperture, while in DF mode, one or more diffracted beams are allowed to pass the objective aperture. (Chescoe, 1990; Reimer, 1997) Tilting electron beam is to minimize off-axis aberrations and beam stop is to correct for asymmetries in DF image.

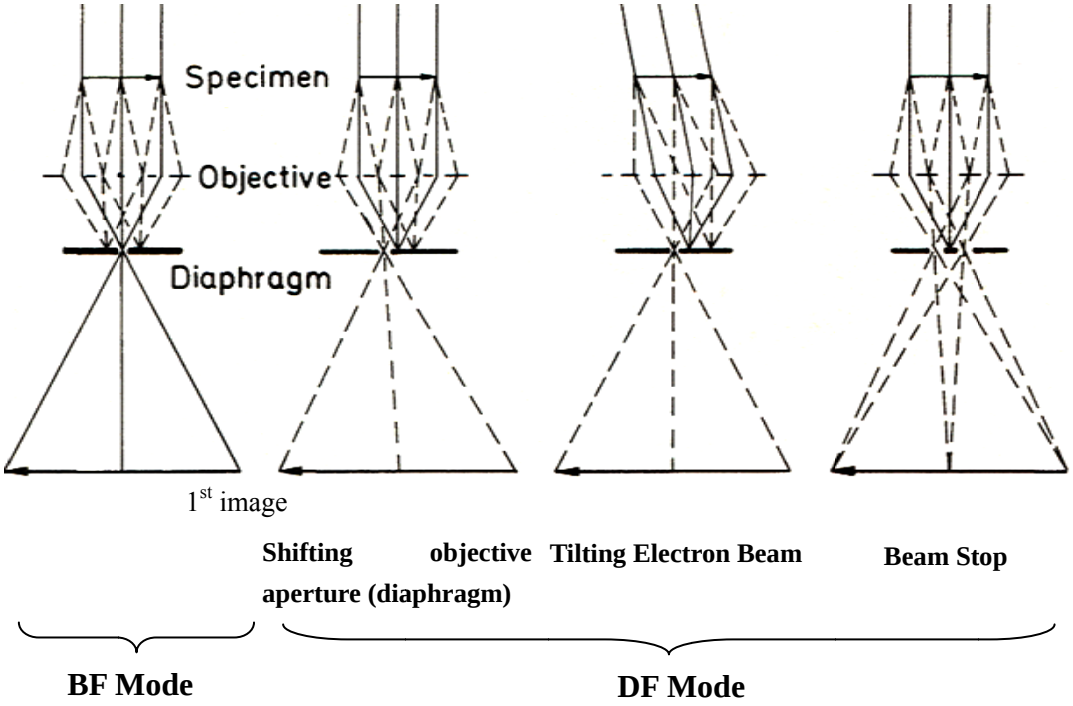

Fig. 3.8 BF and DF modes of TEM operation.

HRTEM is to use a larger objective aperture to allow the direct (bright field) beam and diffracted beams to pass and interfere for obtaining the phase contrast lattice structure information and forming image. This image is then magnified to display either on a fluorescent screen or to be detected by a sensor such as a CCD camera. The HRTEM system (Tecnai G2 F30 S-Twin and the operating voltage is 300kV) we used for cross-sectional observation of the EM-induced interdiffusion or typical failure slit is equipped with energy dispersive X-ray spectroscopy (EDX) analysis. EDX is the measurement of X-rays emitted during electron bombardment to determine the chemical composition of materials on the micro- and nano- scale. By determining the energies of the X-rays emitted from the area excited by the electron beam, the elements in the sample can be determined. The detection rate of these characteristic X-rays is

used to measure the amounts of elements. After the electron beam is rastered over the target area in the sample, EDX systems can acquire the X-ray maps showing elements spatial variation in the sample. It can detect the full range of elements from Boron (atomic no. 5) to Uranium (atomic no. 92). In this project, we use the cross-sectional TEM together with the EDX depth profiles to qualitatively characterize the interdiffusion behavior at the interfaces of the GMR ML or GMR SV devices.

3.3.2.3 Atomic Force Microscopy (AFM)

The Atomic Force Microscopy (AFM) is a high-resolution technique for atomic level surface characterization. The AFM system (Digital Instruments, Digital Instruments Nanoscope III (DI-3100) multimode scanning force microscope) is utilized in this study to generate images and information regarding surface roughness (RMS) and surface topography for the samples. AFM utilizes a probe, controlled by piezoelectric elements, to scan across the sample surface. This probe is a tip on the end of a cantilever that bends in response to the force between the sample and the tip. This force is an inter-atomic force called the van der Waals force. The deflection of the cantilever is then detected by the optical detection method where a fine laser spot is reflected from the back of the reflective cantilever and onto a position-sensitive photodiode. As the cantilever bends and thus the height of the tip changes, the position of the reflected spot will change as well. A schematic diagram of the AFM system is shown in Fig. 3.9. Generally, there are 3 different operational modes for the AFM, namely contact mode, non-contact mode and tapping mode. In this work, the tapping mode is utilized. In tapping mode, the cantilever is driven to oscillate up and down at

near its resonance frequency by a small piezoelectric element mounted in the AFM tip holder similar to non-contact mode. However, the amplitude of this oscillation is greater than 10 nm, typically 100 to 200 nm. Due to the interaction of forces acting on the cantilever when the tip comes close to the surface, Van der Waals force, dipole-dipole interaction, electrostatic forces and so on cause the amplitude of this oscillation to decrease as the tip gets closer to the sample. An electronic servo uses the piezoelectric actuator to control the height of the cantilever above the sample. The servo adjusts the height to maintain a set cantilever oscillation amplitude as the cantilever is scanned over the sample. A tapping AFM image is therefore produced by imaging the force of the intermittent contacts of the tip with the sample surface.

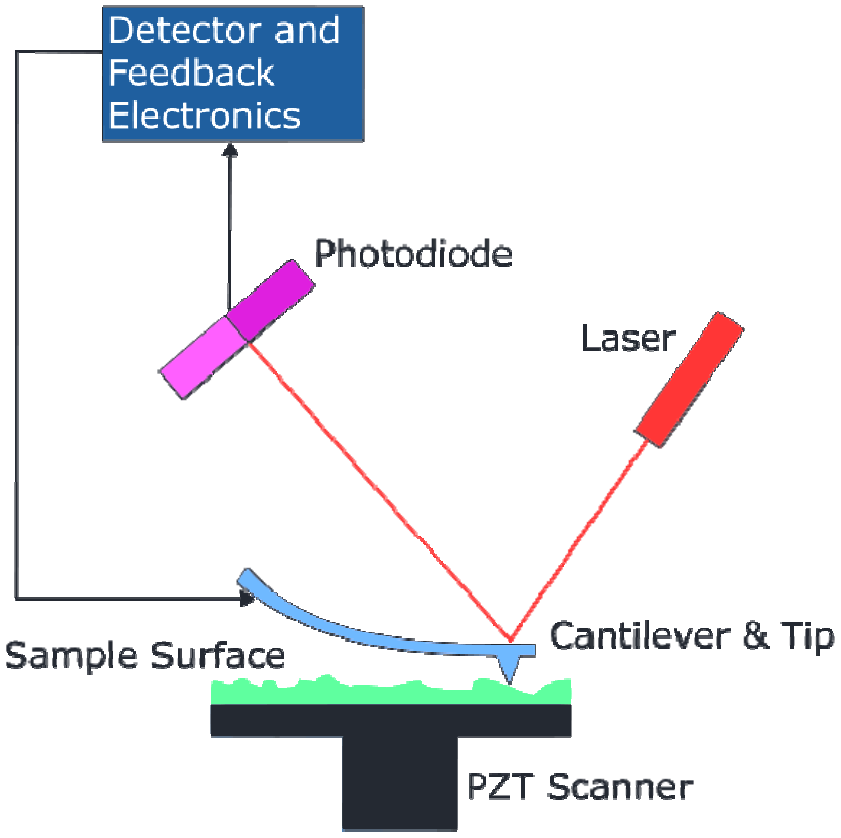

Fig. 3.9 Schematic diagram of AFM operation.

This method of "tapping" lessens the damage done to the surface and the tip compared to the amount done in contact mode. Tapping mode is gentle enough even for the visualization of supported lipid bilayers or adsorbed single polymer molecules (for instance, 0.4 nm thick chains of synthetic polyelectrolytes) under liquid medium. With proper scanning parameters, the conformation of single molecules can remain unchanged for hours (Roiter, 2005).

3.3.2.4 Auger Electron Spectroscopy (AES)

In Auger spectroscopy, the excitation source is a finely focused electron beam. Upon sample bombardment, a transfer of energy occurs which excites a core electron into an orbital of higher energy. Once in this excited state, the atom has two possible modes of relaxation: emission of a X-ray, or emission of an Auger electron. In both processes, the emitted particle will have an energy characteristic of the parent element. An energy spectrum of the detected electrons shows peaks assignable to the elements present. The ratios of the intensities of Auger electron peaks can provide a quantitative determination of surface composition.

The Auger multiprobe is capable of producing elemental composition spectra, surface images, selective elemental line scans and maps, and depth profiles. Imaging is achieved through detection of secondary, backscattered and Auger electrons. Elemental line scans detect concentrations along a line, while a map, which is considerably more time consuming, detects elemental distribution over an area. Auger analysis involves the top most 20 Å only, making it an extremely surface sensitive technique.

Auger depth-profiles are obtained by employing a controlled sputtering process

which enables elemental concentration to be plotted as a function of depth. “Sputtering” is a process in which an ion gun is used to remove a few angstroms of the top most surface of a sample. Sputtering and analysis are alternated until the desired depth is reached. Thicknesses in layered samples are calibrated by comparison to the sputtering rate of a known thickness of SiO_2. Auger depth profiling is well suited for conductive samples composed of thin MLs where thickness or interface properties must be determined.

3.3.3 Measurement of Magnetic Properties

3.3.3.1 Vibrating Sample Magnetometer (VSM)

All the M-H loops before and after EM testing in this project were measured by a vibrating sample magnetometer (VSM, Model is 886 from ADE Technologies) as shown in Fig. 3.10. A vibrating sample magnetometer is a scientific instrument that measures magnetic properties invented by Simon Foner at Lincoln Laboratory MIT and first introduced in his paper in 1959 (Foner, 1959). Using VSM it is possible to measure the total magnetic moment at a function of applied magnetic field, from which saturation magnetization, magnetic anisotropy, and exchange anisotropy of magnetic layers ca n be detected. VSM has a flexible design and combines high sensitivity with easy of sample mounting and exchange. Samples may be interchange rapidly even at any operating temperature. Measurements of magnetic moments as small as $5x10^{-5}$ emu are possible in magnetic fields from zero to 9 Tesla (or even higher). Maximum applied fields are reached using conventional laboratory electromagnets and superconducting solenoids, respectively. VSM normally is operated over a temperature

range of 2.0 to 1050 K. Powders, bulk and thin films can be measured and studied.

If a sample of any material is placed in a uniform magnetic field, created between the poles of an electromagnet, a dipole moment will be induced. If the sample vibrates with sinusoidal motion a sinusoidal electrical signal can be induced in suitable placed pick-up coils. The signal has the same frequency of vibration and its amplitude will be proportional to the magnetic moment, amplitude, and relative position with respect to the pick-up coils system. As we can see in Fig. 3.11, the sample is fixed to a small sample holder located at the end of a sample rod mounted in a electromechanical transducer. The transducer is driven by a power amplifier which itself is driven by an oscillator at a frequency of 90 Hertz. So, the sample vibrates along the Z axis

Fig. 3.10 Vibrating sample magnetometer (VSM) system used for measuring the magnetic properties.

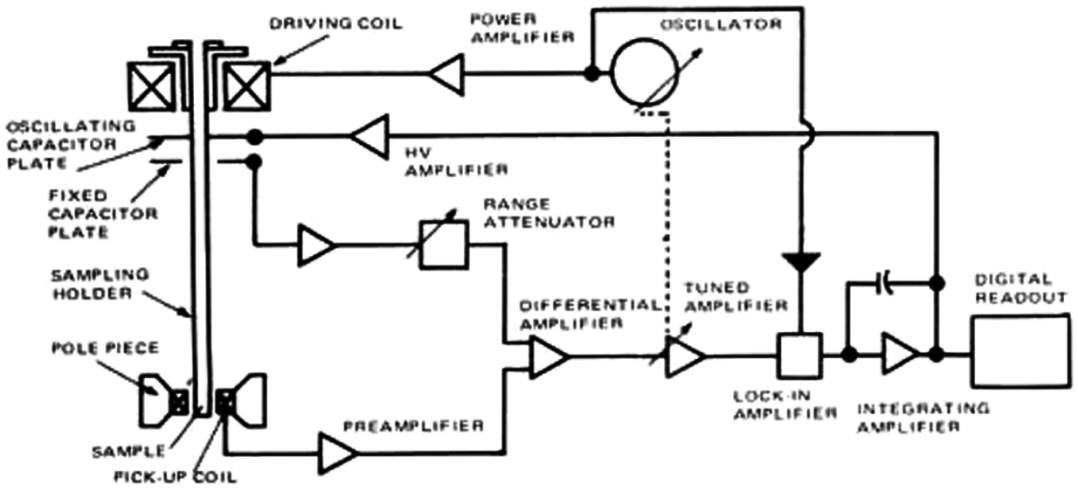

Fig. 3.11 block diagram of a VSM.

perpendicular to the magnetizing field. The latter induced a signal in the pick-up coil system that is fed to a differential amplifier. The output of the differential amplifier is subsequently fed into a tuned amplifier and an internal lock-in amplifier that receives a reference signal supplied by the oscillator. The output of this lock-in amplifier, or the output of the magnetometer itself, is a D.C. signal proportional to the magnetic moment of the sample being studied. The electromechanical transducer can move along X, Y and Z directions in order to find the saddle point (which Calibration of the vibrating sample magnetometer is done by measuring the signal of a pure Ni standard of known the saturation magnetic moment placed in the saddle point.

3.3.3.2 Four-point Probe CIP MR Measurement

A lab-built computer-controlled four point probe MR measurement system as shown in Fig. 3.12 is set up on the Micromanipulator Probe Station and used for rapid investigation of magnetoelectronic properties of patterned GMR SVSDs before and

after EM testing. This MR package consists of four probes, an MR signal processor unit, a data-acquisition card and software. In addition, this system can also be used to apply the combined electrical and magnetic stress during EM acceleration testing so as to mimic the working conditions close to what GMR read sensors are operated. This GMR measurement system can measure resistance between 0.1 and Mega Ohm, as a function of magnetic field. Sample can be manually loaded using the microscope attached to the Micromanipulator Probe Station. All the magnetoelectronic parameters including dR/R, coercivity, and exchange field from free and pinned layer can be extracted from the automatically recorded R-H curves.

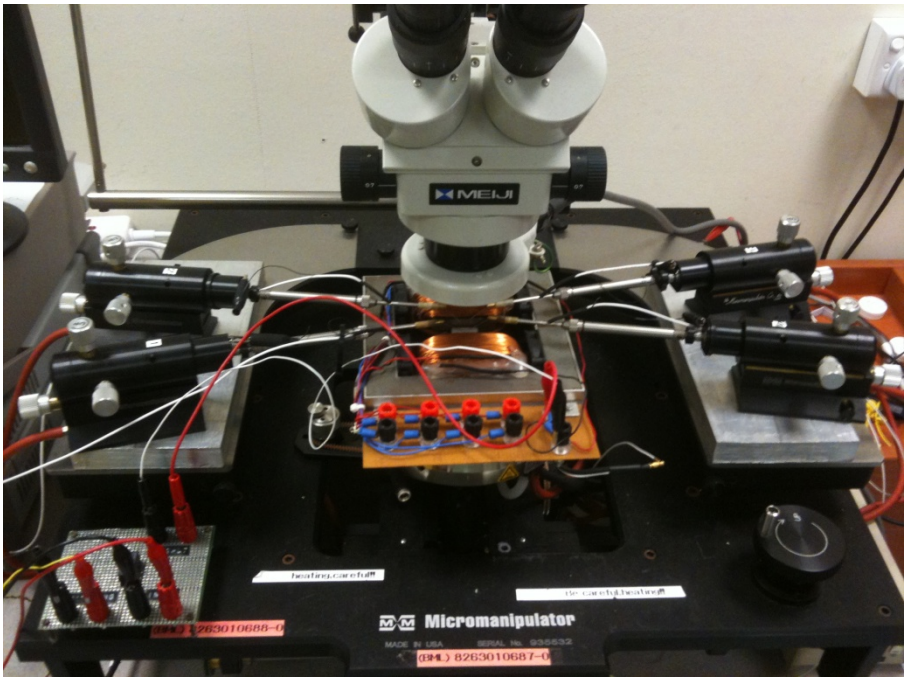

Fig. 3.12 Lab-built four point probe R-H measurement system.

References

Baibich, M.N., Broto, J.M., Fert, A., Nguyen Van Dau, F., Petroff, F., Eitenne, P.,

Creuzet, G., Friederich, A., and Chazelas, J. (1988). Giant Magnetoresistance of (001)Fe/(001)Cr Magnetic Superlattices. Phys. Rev. Lett. **61**, 2472-2475.

Chescoe, D., and Goodhew, P.J. (1990). The Operation of Transmission and Scanning Electron Microscopes. Royal Microscopical Society Handbooks, (Oxford University Press).

Foner, S. (1959). Versatile and Sensitive Vibrating-Sample Magnetometer. Rev. Sci. Instrum. **30**, 548-557.

Grünberg, P., Schreiber, R., Pang, Y., Brodsky, M.B., and Sowers, H. (1986). Layered magnetic structures: evidence for antiferromagnetic coupling of Fe layers across Cr interlayers. Phys. Rev. Lett. **57**, 2442-2445.

Holt, D.B., and Joy, D.C. (1989). SEM Microcharacterization of Semiconductors, Academic Press.

Lee, R.E. (1983). Scanning electron microscopy and x-ray microanalysis. (Prentice Hall).

Reimer, L. (1997). Transmission Electron Microscopy – Physics of Image Formation and Microanalysis, (Springer-Verlag, 4th ed.).

Roiter, Y, and Minko, S. (2005). AFM single molecule experiments at the solid-liquid interface: in situ conformation of adsorbed flexible polyelectrolyte chains. J. Am. Chem. Soc**. 127**, 15688-15689.

CHAPTER 4 ELECTROMIGRATION-INDUCED FAILURE CHARACTERISTICS OF FM/Cu/FM BASED SPIN-VALVE MULTI-LAYERS

4.1 Effects of Cu Inter-diffusion on the Electromigration Failure of FM/Cu/FM Tri-layers for Spin-valve Read Sensors

4.1.1 Introduction and Motivations

Recently, as the areal density of magnetic recording technology is being dramatically increased up to 1 Tera-bit/in^2 at an incredible rate of 120% per year (Weller, 2000), the required track width (sensor width), and sensor height of GMR SV read sensors for obtaining a reasonable signal-to-noise ratio (SNR) are being reduced down to the nano-scale dimensions. Correspondingly, the operating bias current density in the spin valve read sensors goes beyond as high as J=10^8 A/cm^2 (Bae, 2003). It is therefore that EM-induced failures are expected to be a crucial limitation of the reliability of such multi-layered magneto-electronic devices. In particular, the Cu inter-diffusion is considered to make the EM-induced failure of FM/Cu/FM trilayers in the SV read sensors more deteriorated due to high Cu solid solubility with Ni atoms and the lower activation energy of Cu compared to other magnetic materials such as NiFe, Co, and CoFe (Bae, 2002).

In this work, EM-induced failure (EIF) characteristics of FM/Cu/FM tri-layered structures, which are currently used in the GMR SV read sensors, were investigated by

considering the effects of Cu inter-diffusion to the top or bottom FM layer during electrical stressing on the EM-induced lifetime. In order to study the effects of "current sinking" and "Cu microstructure" on EM-induced lifetime in FM/Cu/FM tri-layered structures, Cu spacer thickness was changed from 1.8 to 4 nm. The relationship between the solid solubility of Cu with top or bottom FM layer and Cu inter-diffusion-induced EM accelerated failures were compared by using FM/Cu/FM tri-layered structures with different FM layers (FM: NiFe and Co). The reliability of FM/Cu/FM trilayers was determined by measuring EM-induced time-to-failure (TTF) and by calculating the corresponding mean-time-to-failure (MTTF, t_{50}). TTF in this report was defined as the time for the resistance of the trilayers to increase by 100%. The activation energy (E_a) of the FM/Cu/FM tri-layered structures was obtained by varying the ambient testing temperature from ambient temperature to 280 °C. The current density dependence factor "n" value for analyzing the contribution of joule heating to EIF was determined from the slope of a plot ln (J) vs. ln (time-to-failure (TTF)) at ambient temperature by changing the D.C. applied current density in the range of $2\times10^8 \sim 1.5\times10^9$ A/cm^2.

4.1.2 Experimental Works

All the FM/Cu/FM (FM: $Ni_{80}Fe_{20}$ or Co) and NiFe(2.5)/Co(0.5)/Cu(2)/Co(0.5)/NiFe(2.5 nm) magnetic multi-layered thin films were deposited on Si (100) substrate using a D.C. magnetron sputter under a basic pressure in the range of $1\times10^{-8} \sim 3\times10^{-8}$ Torr. Ar working gas pressure during deposition was kept at 2 mTorr. The deposition rate was varied from 0.29 Å/sec to 0.39 Å/sec depending on materials. The NiFe/Cu/NiFe and

NiFe/Co/Cu/Co/NiFe multi-layered thin films were patterned using standard electron beam lithography (EBL). The patterned device has geometry of 2 μm line-width and 20 μm line-length. In addition, in order to reduce the detrimental effects caused by the geometrically induced current crowding effect, the contact pads were designed to have a continuously shrunken width from 150 μm to 12 μm. The D.C. current with current density in the range of $1\times10^6 \sim 1\times10^9$ A/cm^2 was applied to the patterned GMR SV devices to measure the EM-induced failure lifetime (time-to-to failure, TTF, is defined as the time for the 100 % of resistance increase in the EM testing samples) and to determine the current density factor, n, which directly indicates the contribution of "Joule heating" to the EM-induced failures. Magnetic degradation caused by the EM-induced inter-diffusion was investigated by applying a constant current with 6×10^6 A/cm^2 current density to the NiFe(3)/Cu(t)/NiFe(3 nm) and NiFe(2.5)/Co(0.5)/Cu(t)/Co(0.5)/NiFe(2.5 nm) SV multi-layered thin films with different Cu spacer thickness. The SV-MLs for testing the EM-induced magnetic degradation had geometry of 0.75 mm line width and 10 mm line length. The time for applying electrical stress to the patterned GMR SV-MLs was controlled at 10 % of MTTF, t_{50}, to clearly observe the magnetic degradation due to electromigration. The M-H loops for the tested samples were measured by using a vibrating sample magnetometer (VSM) at ambient temperature. The change of interlayer coupling was confirmed by using a minor M-H loop. JEOL-6700 field-emission scanning electron microscope (FE-SEM) was used to topographically observe the different failure characteristics formed at the different current density ranges. AES depth profiles were

carried out at ambient temperature by using an auger microprobe with 10 kV, 10 nA e-beam as well as 2 keV, 1 μA Ar^+ ion beam at 2×2 mm^2 raster, and with sputtering rate of 4.82 nm/min relative to SiO_2. In order to analyze the inter-diffusion behavior of Cu spacer through the NiFe/Cu interfaces in the NiFe/(Co)/Cu/(Co)/NiFe GMR SV-MLs, four kinds of EM tested samples, before applying electrical stress, after applying electrical stress with current density of J = 5×10^7 A/cm^2 for 33 % of TTF, for 66 % of TTF, and for 99 % of TTF, were compared using an AES depth profile analysis. The bi-modal failure mechanism observed in the NiFe/Cu/NiFe SV-MLs was qualitatively and quantitatively confirmed by comparing AES depth profiles and by calculating current density factor, n, value for the samples electrically stressed under different current densities from 5×10^7 A/cm^2 to 9×10^7 A/cm^2 at ambient temperature.

4.1.3 Results and Discussion

4.1.3.1 EM-induced failure lifetime dependence on Cu spacer thickness

Figure 4.1 shows the effect of Cu spacer thickness on EM-induced time to failure (TTF) in NiFe(3nm)/Cu(t)/NiFe(3nm) tri-layers. As shown in Fig. 4.1 and Table 5-1, TTF of the NiFe/Cu/NiFe tri-layers was drastically decreased by increasing Cu spacer thickness. The decrease of TTF with increasing Cu spacer thickness can be explained in terms of the EM-induced Cu inter-diffusion characteristics owing to the variation of Cu microstructure and FM/Cu chemical interfaces resulted from the increase of Cu spacer thickness. In NiFe/Cu/NiFe tri-layers, EM-induced failure will be dominated by Cu EM due to its lower activation energy compared to NiFe (Bae, 2002) and “current sinking effect” that 2/3 of applied bias electrical current (J=3.3×10^8 A/cm^2 in Fig. 4.1) flows

through Cu spacer resulted from the film resistance difference (Gurney, 1997).

Table 4-1 Mean-time-to-failure (MTTF) of NiFe(3)/Cu(t)/NiFe(3)[nm] tri-layers with different Cu spacer thickness, stressed under the same D.C. current density ($J = 5\times10^8$ A/cm^2) at ambient temperature.

Cu thickness (nm)	4	3	2	1.8
t_{50} (hours)	6.06	16.22	36.21	47.84

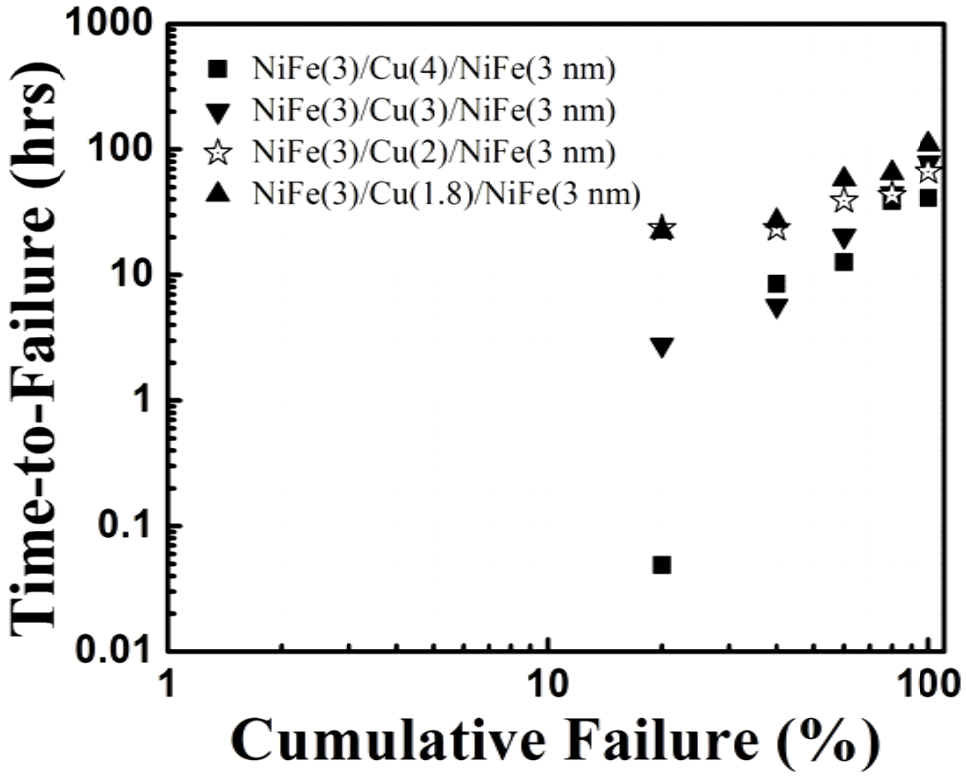

Fig. 4.1 TTF dependence on the Cu spacer thickness of NiFe(3)/Cu(t)/NiFe(3 nm) tri-layers, stressed under the same D.C. current density ($J = 5\times10^8$ A/cm^2) at ambient temperature.

With increasing Cu spacer thickness, Cu thin film spacer has irregular grain boundaries instead of grain clusters due to the crystal growth and FM/Cu interface has a rough surface due to the surface grooving caused by forming grains perpendicular to the film plane. Growth of grain boundaries in the thicker Cu spacer provides more diffusion paths for the Cu mass transport during electrical stressing (Bae, 2001) and the larger

interfacial roughness formed at FM/Cu interface induces to increase the possibility to form the Ni-Cu mixing regions that can provide more current paths from Cu to NiFe. These two physical reasons caused by increasing Cu spacer thickness result in accelerating EM failures in NiFe/Cu/NiFe tri-layers. According to the experimental results shown in Fig. 4.1 and Table 4-1, it can be concluded that the control of FM/Cu chemical interfaces owing to the Cu inter-diffusion and EM-induced failures in Cu spacer will be the crucial parameters in determining the electrical reliability of FM/Cu/FM tri-layer based GMR SV read sensors.

4.1.3.2 Effect of FM/Cu chemical interface on the EM lifetime

In order to confirm the contribution of FM/Cu chemical interfaces, we compared the TTF of Co/Cu/Co to that of NiFe/Cu/NiFe, because there is nearly no solid solubility between Co and Cu (Williams, 2001; Massalski, 1990). Figure 4.2 shows the cumulative percents vs. TTF of both NiFe/Cu/NiFe and Co/Cu/Co tri-layers under applied D.C. current density of 5×10^8 A/cm^2 at 100 °C. The MTTF (t_{50}) of NiFe(3)/Cu(2)/NiFe(3), and Co(3)/Cu(2)/Co(3) tri-layers is 70 minutes, and 107 minutes, respectively. The obvious shorter lifetime of NiFe/Cu/NiFe tri-layers compared to that of Co/Cu/Co tri-layers was mainly thought to be attributed to the formation of current paths resulted from Cu inter-diffusion into the top or bottom NiFe layer during electrical stressing caused by the Ni-Cu intermixing. According to the resistance change vs. time curves, the sharp resistance increase of the NiFe/Cu/NiFe tri-layers was due to the formation of voids (or cracks) during the EM-induced failure of the Cu spacer, while the hillocks (or whiskers) forming together with the formation of voids may provide

new mass transport paths for the inter-diffusion of the Cu atoms into the top or bottom NiFe layers. This is believed to be quite serious considering the high solid solubility of Cu atoms with Ni atoms (Massalski, 1990).

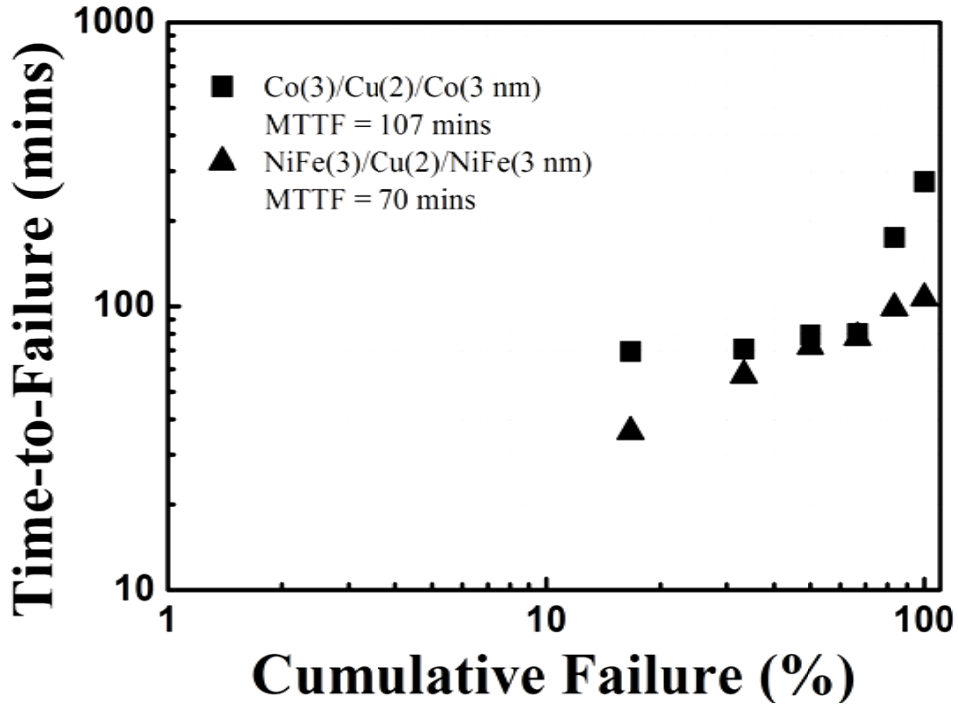

Fig.4.2 TTFs for Co(3)/Cu(2)/Co(3)[nm] and NiFe(3)/Cu(2)/NiFe(3 nm) stressed under the same D.C. current density ($J = 5\times10^8$ A/cm^2) at T = 100 °C.

Many newly generated mass transport (or current) paths toward the top and bottom NiFe layers may form and facilitate more D.C. current to pass through the NiFe layers after the EM-induced failure of the Cu spacer. This would accelerate the EM-induced failure of the top and bottom NiFe layers. However, on the contrary, in the case of Co/Cu/Co tri-layers, the immiscibility of Cu and Co atoms would restrain from forming a current (or mass transport) path to the Co layer caused by the Cu EM-induced failures. Most applied current would pass through the Co/Cu interface even after the EM-induced failure in the Cu spacer, and that is why the lifetime of Co/Cu/Co tri-layers is much

longer than that of NiFe/Cu/NiFe tri-layers.

4.1.3.3 Activation energy and current dependence factor, "n" values of NiFe(3)/Cu(2)/NiFe(3 nm) tri-layers

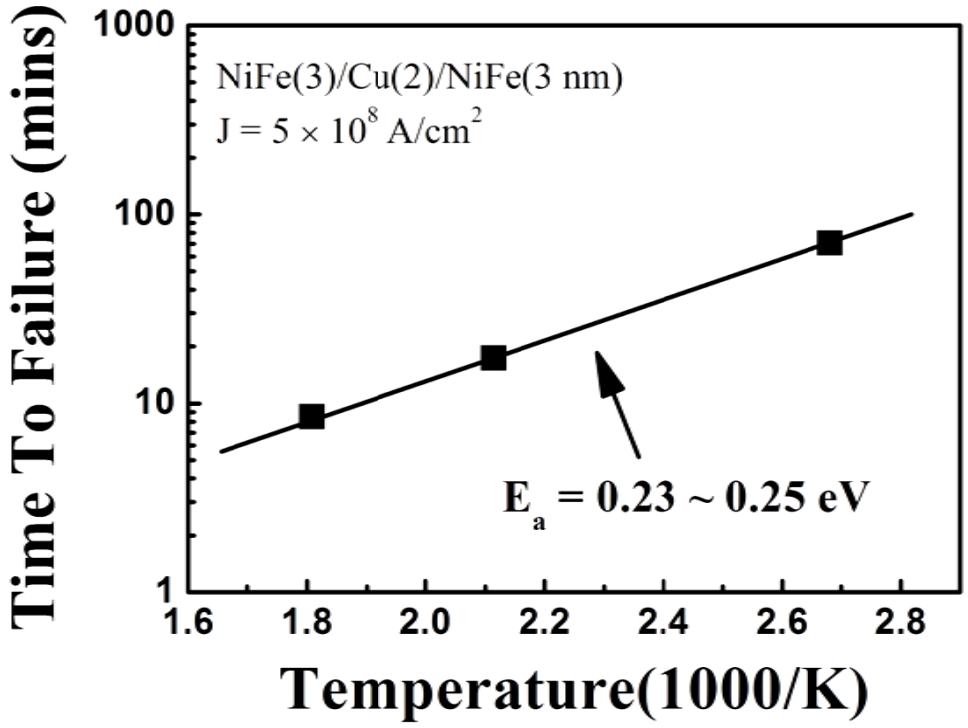

Fig. 4.3 TTF versus (1000/absolute temperature) plot for NiFe(3)/Cu(2)/NiFe(3 nm) tri-layered structures for determining the activation energy (E_a).

The activation energy related to diffusion process for NiFe(3)/Cu(2)/NiFe(3 nm) tri-layers was obtained by plotting a log (TTF) vs. (1/absolute temperature) plot as shown in Fig. 4.3. The activation energy obtained at constant D.C. current density of $J = 5\times10^8$ A/cm^2 was 0.23 ~ 0.25 eV, which lies in the range of the Cu (0.5±0.3 eV) single layered thin film activation energy (Poate, 1978). This means that the EM-induced failures of NiFe/Cu/NiFe tri-layers are dominantly controlled by the Cu spacer EM. In addition, this confirmed that the Cu spacer EM plays a key role in determining the electrical

reliability of FM/Cu/FM based GMR spin-valve read sensors.

The current dependence factor of "n" value in the "Black equation" (Black, 1969) was also determined from the slope of a plot ln (J) vs. ln (TTF) at constant temperature in NiFe/Cu/NiFe tri-layers under different constant D.C. current densities. As shown in Fig. 5-4, the determined n value was 1.23 ~ 1.32, which was found to be much smaller than the n value of 3.4 for Al-1%Ge-0.5%Cu, and 4.7 for Al-1%Si-0.5%Cu alloy single layers (Kuniko, 1994). Considering the joule heating effect, the extent of the temperature increase strongly depends on the applied current density since for the same ΔR, ΔT will be four times as high if the current density is doubled as shown in Eq. (4-1),

$$\Delta T = \frac{H_d (R_0 + \Delta R) J^2}{1 - H_d (R_0 + \Delta R) \alpha J^2} \tag{4-1}$$

where, H_d is the heat dissipation factor, R_0 is the initial resistance of the tri-layered thin films and α is the temperature coefficient. The lower current dependence factor value of NiFe/Cu/NiFe compared to the high conductivity materials such as Al alloys and Cu thin films is mainly though to be due to the higher resistivity of NiFe/Cu/NiFe tri-layers. Furthermore, it is confirmed that the contribution of joule heating during electrical stressing to the EM-induced failure in NiFe/Cu/NiFe tri-layers is less serious than that of high conductivity materials due to "current sinking effect".

4.1.3.4 Typical EM-induced failure characteristics observed in NiFe(3)/Cu(2)/NiFe(3 nm) tri-layers

Figure 4.5a shows the FESEM image of NiFe(3)/Cu(2)/NiFe(3) tri-layered structure, which was stressed at the ambient temperature of 200 °C with the D.C. constant current

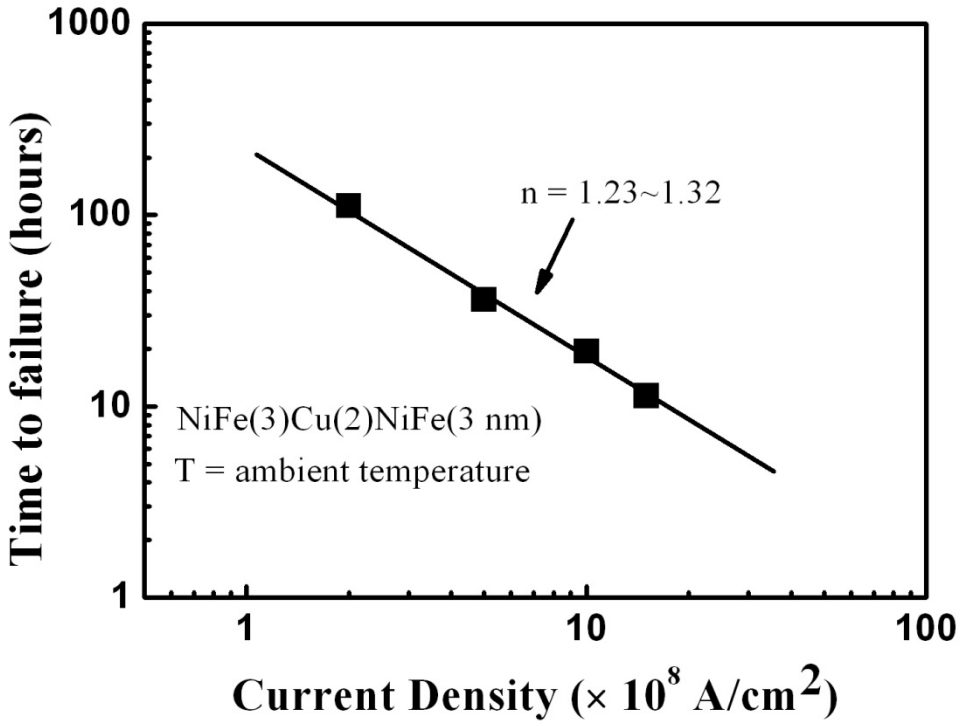

Fig.4.4 TTF of NiFe(3)/Cu(2)/NiFe(3)[nm] tri-layered structures stressed under different current densities.

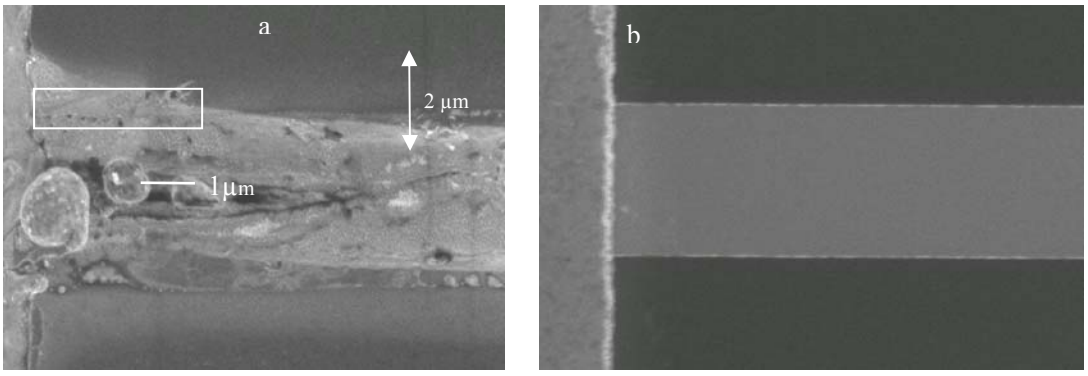

Fig.4.5 a) EM-induced failure (cracks marked within the rectangle) formed near the cathode region of NiFe(3)/Cu(2)/NiFe(3 nm) tri-layers., b) before stressing.

density of 5×10^8 A/cm^2 for 4 hours. The typical EM-induced failure (cracks) was observed near the cathode region of NiFe(3)/Cu(2)/NiFe(3) tri-layered structure. In Fig. 4.5b, the SEM image of such trilayered structure before stressing was shown for comparison.

4.1.4 Summary and Conclusions

EM-induced failure lifetime of FM/Cu/FM (FM: NiFe or Co) tri-layers, which are used in GMR spin-valve read sensors, has been investigated. NiFe/Cu/NiFe tri-layers show much shorter lifetime than that of Co/Cu/Co tri-layers. By decreasing the Cu spacer thickness, the lifetime of NiFe/Cu/NiFe tri-layers was dramatically increased. Experiment results in this work demonstrate that the reduction of Cu diffusion into the FM layer or controlling the chemical interface between FM and Cu spacer can be the best solution for enhancing the reliability of FM/Cu/FM based spin valve read sensors.

4.2 Electromigration-Induced Failure Characteristics of NiFe/(Co)/Cu/(Co)/NiFe Spin Valve Multi-layers

4.2.1 Introduction and Motivations

FM/Cu spacer/FM based giant GMR SV-MLs have drawn a great deal of attractions for the last two decades due to their technical promises for a variety of metallic based spintronic devices such as ultra high density of magnetic recording read sensors, GMR spin-valve transistors as well as logic devices and magnetic random access memories (MRAMs) (Jiang, 2005; Prinz, 1998; Shen, 1997; Monsma, 1995). However, recently, as the size of metallic based spintronic devices has been dramatically reduced down to a few hundred nano-meters, the research interests on the magnetic and electrical reliability of GMR spin-valve MLs directly relevant to the EM-induced failures are rapidly increased to successfully develop an extremely low dimensional device, which can produce a high SNR (Signal-to-Noise Ratio) and to maintain a high magneto-

electronic device stability. The operating (or biasing) current density of nano-scale spintronic devices is currently considered to exceed beyond $J = 1\times10^8$ A/cm^2 and the accordingly generated heating power is enormously high enough to accelerate the EM-induced failures. Thus, EM-induced failures and its underlying physics relevant to investigating the failure mechanism of GMR SV-MLs become a critical issue in characterizing the electrical and magnetic stability of spintronic devices.

EM or electrotransport is defined as a mass-transport caused by atomic migration in the metallic thin films under the applied biasing electrical stress (or field), which causes electro-static force (or electron wind force) in the metal stripe to activate atomic flux divergence due to temperature gradients and to induce thermal stress effects (Gupta, 1988). For the last few years, research activities on the EM and its failure characteristics of GMR spin-valve spintronic devices have been primarily focused on investigating the typical lifetime characteristics for the different single layered and double layered magnetic thin films (NiFe, CoFe, Co, NiFe/CoFe) in terms of film thickness dependence, current dependence factor relevant to Joule heating effects, activation energy for understanding an inter-diffusion phenomena, and geometrical effects including current crowding effects (Gangulee, 1974; Shingubara, 1999; Bae, 2002; Bae, 2001). However, different from high conductivity interconnection materials typically used in microelectronic devices or from single layered magnetic thin films, the GMR SV-MLs have a physically complicated structure, which is a FM/Cu/FM based multi-layered sandwich composed of alternatively deposited high (e.g. NiFe, Co or CoFe) and low activation energy materials (e.g. Cu) with different film resistivities (Hecker, 2002).

Therefore, EM-induced failure characteristics of GMR SV-MLs should be understood by considering two major physical parameters: (1) “current sinking effect” (Gurney, 1997) induced “Joule heating process” (or “thermal run-away process”) that is completely different modularity from those observed in the typical single layered thin films and (2) the existence of interfaces formed by the two layers with different activation energy and high solid solubility enabling to cause serious inter-diffusion problems. However, for the past few years, even though academia and industries involved in spintronics have already speculated that the EM-induced failures in the GMR SV multi-layered thin films would be distinctly differentiated from typical EM phenomenon, there has been no empirical activity to clarify an unknown physics on the EM failure mechanism in the GMR SV-MLs so far. Furthermore, no clear report on the physical relationship between the EM-induced failures and their physical contribution to the magnetic degradation in the GMR SV-MLs still trigger the research interests and curiosities to explore the electrical and magnetic reliability of GMR SV spintronic devices.

In this part of research work, EM-induced failure characteristics of patterned NiFe/Cu/NiFe GMR SV-MLs with or without Co insertion layer have been investigated by applying a constant D.C. current to explore the electrical and magnetic stability of GMR SV based spintronic devices. In order to control the inter-diffusion behavior between the Ni and Cu atoms through NiFe/Cu interface and to investigate the effects of EM-induced Cu inter-diffusion on the lifetime of NiFe/Cu/NiFe SV based spintronic devices, Co diffusion barrier was employed to insert at the interface between NiFe and

Cu layers. The magnetic degradation associated with the change of magnetic interlayer coupling, magnetic saturation moment, and magnetic reversal behavior caused by the EM-induced failures was investigated by applying constant D.C. current for 10% of mean time-to-failure (MTTF, t_{50}) to both NiFe/Cu/NiFe and NiFe/Co/Cu/Co/NiFe GMR SV-MLs. The diffusion behavior caused by EM in the patterned NiFe/(Co)/Cu/(Co)/NiFe GMR SV multi-layered devices and its physical contribution to the lifetime, and failure characteristics were analyzed by using an auger electron spectroscope (AES) depth profile as well as an energy dispersive X-ray (EDX) analysis, and a field emission scanning electron microscope (FE-SEM), respectively. In order to find the critical current density (J_c) for determining a "bi-modal EM failure characteristics", which describes two major failure modes relevant to (1) electro-static force (or "electron wind force" dominant EM failure characteristics resulting in typical failures such as voids or hillocks and (2) serious "Joule heating" dominant EM failures characteristics leading to catastrophic failures such as volcanic bumps at the cathode region (Zhang, 2007) and explosive cracking at the centers (Misra, 2006), in the NiFe/(Co)/Cu/(Co)/NiFe GMR SV-MLs, the applied current densities were changed from 1×10^6 to 1×10^8 A/cm^2. The current dependence factor, "n", considering all the experimentally determined physical parameters, was calculated from the "Black equation" (Black, 1969) to confirm a "bi-modal EM characteristic" in the GMR SV-MLs.

4.2.2 Results and Discussions

4.2.2.1 TTF of patterned NiFe(3)/Cu(2)/NiFe(3) SV-MLs at different current densities

Figure 4.6 shows the TTF of patterned Si/NiFe(3)/Cu(2)/NiFe(3 nm) SV-MLs electrically stressed at the different D.C. current densities varied from 5×10^7 A/cm^2 to 9×10^7 A/cm^2 at ambient temperature. The determined MTTF (t_{50}) values from the TTFs shown in Fig. 4.6 are summarized in Table 4-2. As can be seen in Fig. 4.6 and Table 4-2, EM-induced failure lifetime of the electrically stressed NiFe/Cu/NiFe SV-MLs had a strong dependence on the applied current density. Similar to the EM-induced failure characteristics of single layered high conductivity thin films such as Cu, Al, Al-Cu, and Al-Si alloys (Oates, 1995; Li, 2006; Witvrouw, 1999), MTTF including TTF of the NiFe/Cu/NiFe SV-MLs was monotonically decreased by increasing the applied current density. In addition, it was found that the contribution of "Joule heating effects" to the EM-induced failure lifetime was more significant at a higher current density above 7×10^7 A/cm^2. These results imply that EM-induced Cu spacer inter-diffusion or Cu spacer EM is directly relevant to determining the EM-induced failure characteristics of the patterned NiFe/Cu/NiFe SV-MLs, because Cu has lower activation energy than that of NiFe (Bae, 2002) and the "current sinking effects" describes that more than 2/3 of applied biasing current can flow through Cu spacer because the film resistance difference between NiFe and Cu layers are expected to be dominant in the patterned NiFe/Cu/NiFe SV-MLs (Gurney, 1997). More interestingly, considering this physical assumption, it can be speculated that Cu atoms (spacer) gained enough activation energy as well as Joule heating induced thermal energy under the applied electrical stress would

Table 4-2 Mean time-to-failure (MTTF, t_{50}) of patterned Si/NiFe(3)/Cu(2)/NiFe(3 nm) SV multi-layerd devices electrically stressed under the different current densities varied from J = 5 × 10^7 A/cm^2 to 9 × 10^7 A/cm^2 at ambient temperature.

J (10^7A/cm^2)	5	6	7	8	8.5	9
t_{50} (hours)	45.58	16.32	7.37	0.0088	0.0082	0.0075

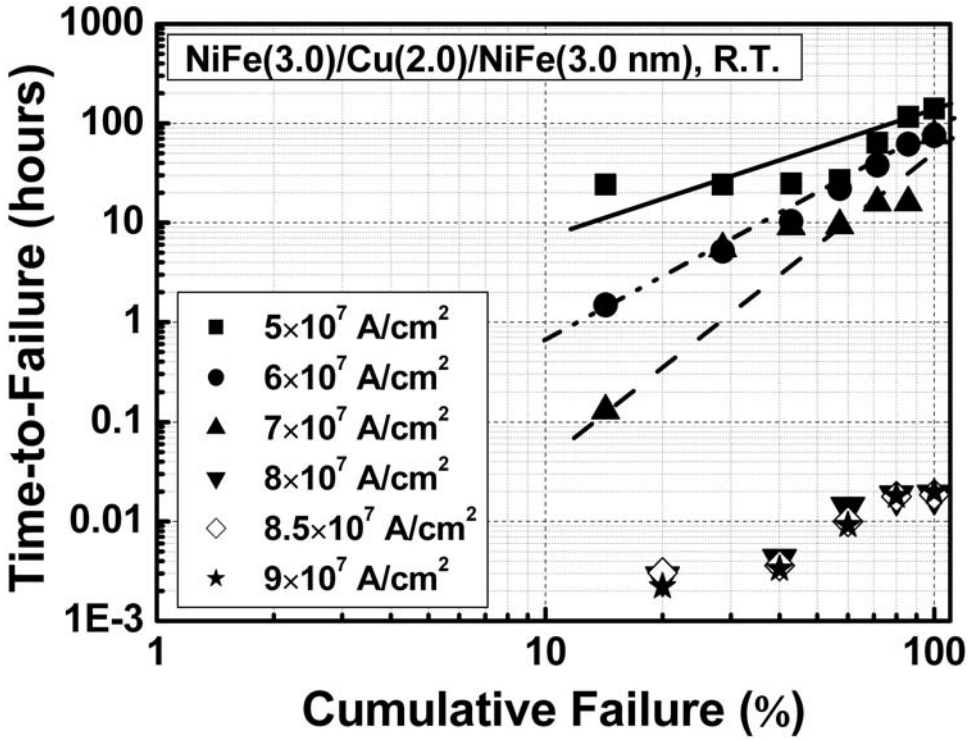

Fig. 4.6 Cumulative percent vs. time-to-failure (TTF) of patterned Si/NiFe(3)/Cu(2)/NiFe(3 nm) SV multi-layered devices electrically stressed under the different current densities J = 5 × 10^7 A/cm^2 ~ 9 × 10^7 A/cm^2 at ambient temperature.

first migrate or inter-diffuse into the NiFe through NiFe/Cu interfaces due to their high solid solubility with Ni atoms (Massalski, 1990). And then Ni-Cu inter-mixing regions formed at the NiFe/Cu interface or inside the NiFe resulted from the Cu EM or EM-induced Cu inter-diffusion would make a new shunting path for the biasing current from

Cu spacer into both top and bottom NiFe layers leading to accelerate the EM failures of patterned NiFe/Cu/NiFe SV-MLs.

4.2.2.2 Interfacial microstructure analysis of NiFe/Cu/NiFe SV-MLs

AES depth profiles for the patterned NiFe/Cu/NiFe SV-MLs before applying electrical stress and after being electrically stressed for 33 % of TTF, 66 % of TTF, and 99 % of TTF were compared to analyze the EM-induced Cu inter-diffusion behavior and its physical contribution to the EM-induced failure characteristics in the patterned NiFe/Cu/NiFe SV-MLs. Figure 4.7 shows the AES depth profiles obtained from the patterned Si/NiFe(3)/Cu(2)/NiFe(3 nm) SV multi-layered devices with 2 μm of line width and 20 μm of line length before applying electrical stress and after electrically stressed under the current density of $J = 5\times10^7$ A/cm^2. It was revealed that the surface of SV device before electrically stressed has already been oxidized to possibly form a kind of $NiFe_xO_y$ with approximately 0.72 nm of thickness (Fig. 4.7(a)). Moreover, as can be seen from Fig. 4.7(a) to Fig. 4.7(c), it was clearly observed that the Cu concentration peak has become lowering, as well as widening, and also its maximum peak position was shifting rightward (shifting toward Si substrate direction) by increasing the electrical stressing time up to 66 % of TTF. By considering the relationship between the sputter etch rate of AES and the shift of maximum Cu concentration peak observed from the “No stress” to the “electrically stressed for 66 % of TTF” SV multi-layered devices, it was assumed that approximately 0.24 nm-thick of Cu spacer was mostly inter-diffused into the bottom NiFe layer during electrical stressing mainly due to the EM of Cu spacer and a high solid solubility of Cu with Ni atoms (Massalski, 1990). In order to more

precisely analyze the EM-induced Cu spacer inter-diffusion behavior in the patterned

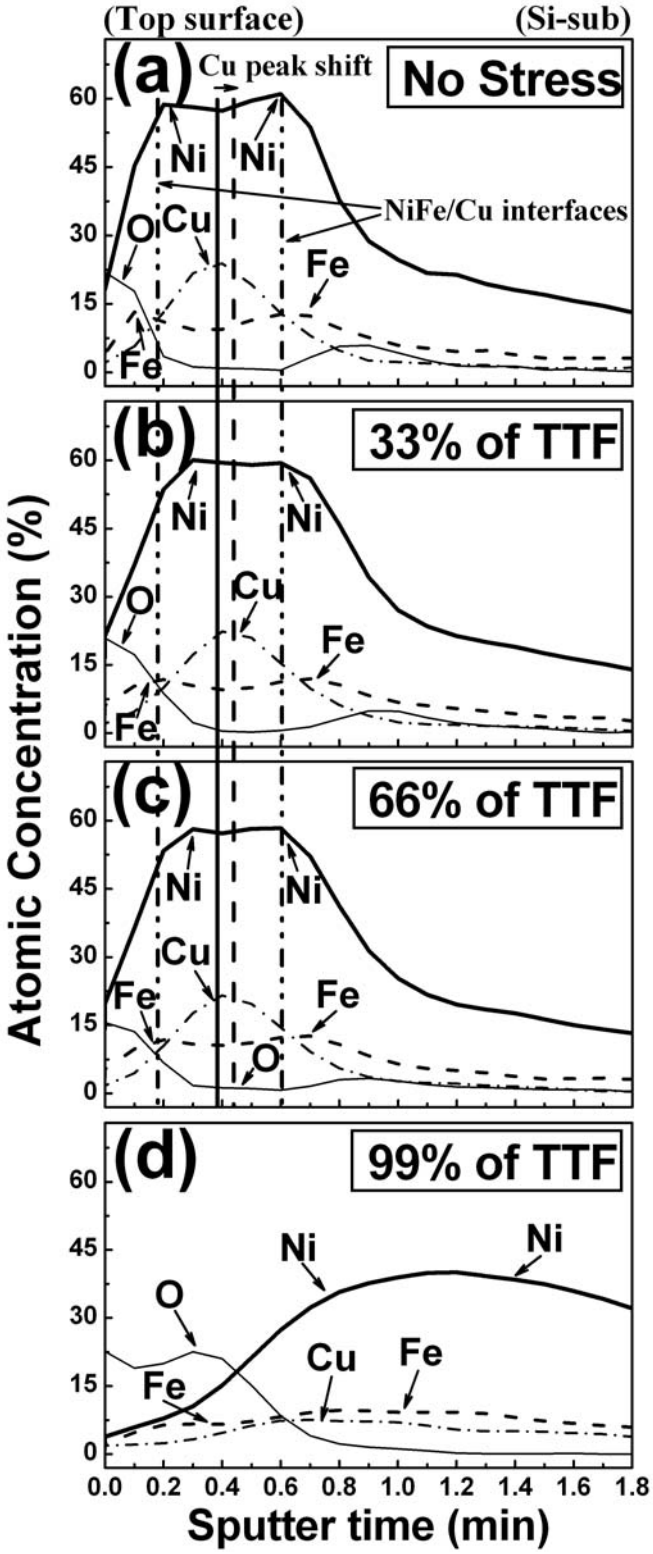

Fig. 4.7 AES depth profiles of patterned Si/NiFe(3)/Cu(2)/NiFe(3 nm) SV multi-layered devices: a) no stress; b) electrically stressed under J = 5 × 10^7 A/cm^2 for 33% of TTF; c) electrically stressed under J = 5 × 10^7 A/cm^2 for 66% of TTF; and d) electrically stressed under J = 5 × 10^7 A/cm^2 for 99% of TTF; all EM testing is at ambient temperature.

NiFe/Cu/NiFe SV multi-layered devices, energy dispersive x-ray analysis (EDX) was also employed. Figure 4.8 shows the EDX depth profiles of the patterned Si/NiFe(3)/Cu(2)/NiFe(3 nm) SV multi-layered devices before applying electrical stress and after electrically stressed for 33 % of TTF under $J = 5\times10^7$ A/cm^2 for comparison. As clearly seen in Fig. 4.8(b), Ni-Cu inter-mixing region was mostly formed at the bottom NiFe and Cu was more seriously inter-diffused into the bottom NiFe. This is thought to be primarily due to the possible formation of $NiFe_xO_y$ insulator that is resulted from the mixture of approximately 24 % of top NiFe with nature oxide (numerical calculation determined from Fig. 4.7(b)). The naturally formed $NiFe_xO_y$ insulator allows more shunting current into the bottom NiFe and gives rise to a passivation effect against EM leading to increase the threshold potential for the activation of Ni atoms to make substitutional inter-diffusion with the migrated Cu atoms from the spacer. The experimentally analyzed results shown in Fig. 4.7 and Fig. 4.8 strongly demonstrate that Cu EM and EM-induced Cu inter-diffusion dominantly determine the EM characteristics of patterned NiFe/Cu/NiFe SV-MLs or NiFe/Cu/NiFe SV based metallic spintronic devices. Figure 4.8(d) shows the AES depth profile for the completely failed NiFe(3)/Cu(2)/NiFe(3) SV-MLs, which has been electrically stressed for 99 % of TTF. It was clearly observed that there is no Cu spacer peak positioned in between top and bottom NiFe layers. This indicates that Cu was completely melted and then diffused into the bottom NiFe layer due to EM. The shift of Ni concentration peak to the Si substrate also provides strong physical evidence that completely inter-diffused Cu atoms into both the top and bottom NiFe layers change NiFe/Cu/NiFe SV multi-

layered structure into a possibly Ni-Fe-Cu alloyed single layered structure. Due to EM-induced Joule heating effects, the surface oxidation was severely accelerated to result in an increase in its thickness from 0.72 nm to 2.89 nm.

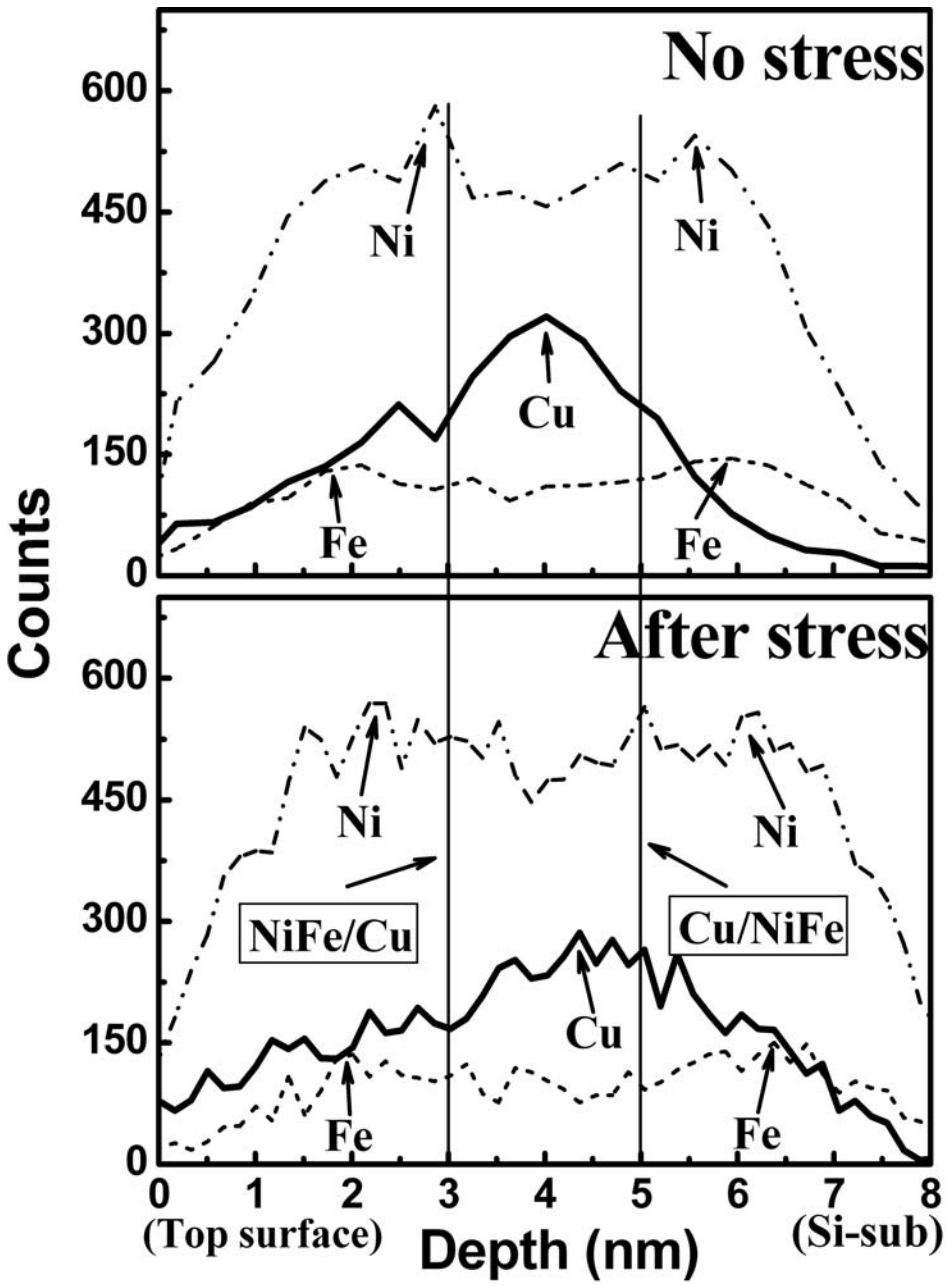

Fig. 4.8 EDX depth-profiles of the patterned Si/NiFe(3)/Cu(2)/NiFe(3 nm) SV multi-layered devices: (a) No electrical stress, and b) after electrically stressed for 33 % of TTF, under $J = 5 \times 10^7$ A/cm^2 at ambient temperature.

4.2.2.3 Bi-modal EM failure characteristics

Resistance change vs. time (ΔR-t) curves for the patterned NiFe(3)/Cu(2)/NiFe(3 nm) SV multi-layered devices with 2 μm of line width and 20 μm of line length used for AES depth profile analysis (see Fig. 4.7(b) ~ (d)) are shown in Fig. 4.9. According to the resistance change behavior with applying electrical stress time, it can be speculated that the EM induced lifetime of the patterned NiFe(3)/Cu(2)/NiFe(3 nm) SV multi-layered devices would be characterized by two specific failure regions depending on the applied stress time. The first one is before 66 % of TTF, which is considered as the time for building up the micro mass transport (current) paths between Cu and NiFe layers due to the EM-induced Cu inter-diffusion. In this time region, voids are first created due to the EM of Cu spacer and then grown up to form a crack, which can induce completely open failures in the Cu spacer. Melted and inter-diffused Cu atoms into both the top and bottom NiFe layers make up Ni-Cu intermixing regions both at the NiFe/Cu interface and in the NiFe layer. These would be considered as main shunting paths of the applied biasing current flowing through Cu into the NiFe layer during EM. The newly generated shunting paths along with the shrinkage of cross sectional area of the NiFe layer due to the formation of EM-induced voids give rise to a sudden increase of current density (so called by “current crowding effects”) and accordingly abrupt increase of local Joule heating temperature leads to the rapid acceleration of EM-induced failures in both the top and bottom NiFe layers. The second one is the time from 66 % of TTF to 99 % of TTF. In this time region, it is expected that most of applied biasing current would flow into both the top and bottom NiFe layers due to a lot of mass transport (or current) paths, which have already been built up during EM until

66 % of TTF, formed between the Cu and NiFe layers. For this time region, Cu spacer would be completely opened and diffused into the NiFe so that NiFe/Cu/NiFe SV multi-layered structures can be changed into a possibly Ni-Fe-Cu alloyed single layered structure and then eventually, Ni-Cu-Fe alloyed single layer would be electrically complete open with more than 100 % of resistance change. Experimental results relevant to the EM-induced electrical resistance change vs. applied stress time shown in Fig. 4.9 are agreed well with the AES depth profile analysis shown in Fig. 4.7 that EM-induced Cu inter-diffusion dominantly plays the most crucial role in determining the EM failure characteristics of metallic NiFe/Cu/NiFe based spintronic devices.

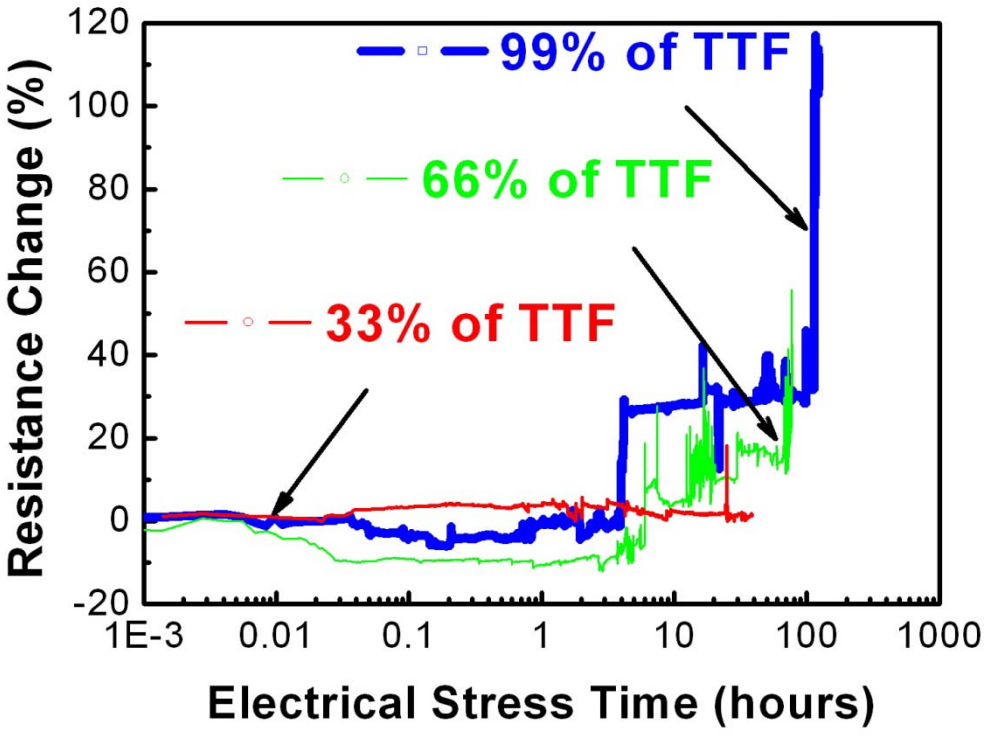

Fig. 4.9 Resistance change vs. time (ΔR-t) curves of the patterned Si/NiFe(3)/Cu(2)/NiFe(3 nm) SV mult-layered devices electrically stressed under the current density of J = 5 × 10^7 A/cm^2 at ambient temperature for 33% of TTF, 66% of TTF and 99% of TTF, respectively.

As clearly confirmed from Fig. 4.6 to Fig. 4.9, since the EM-induced failure

behavior of patterned NiFe/Cu/NiFe SV- MLs is dominantly determined by Cu spacer EM or EM-induced Cu inter-diffusion, it can be physically assumed that the patterned NiFe/Cu/NiFe SV multi-layered devices would exhibit different EM failure modes depending on the applied current density such as "bi-modal EM", which has been reported from the high conductivity thin films including Cu, Ag and Al (Misra, 2006; Zhang, 2007). Figure 4.10 shows the SEM images for the patterned NiFe(3)/Cu(2)/NiFe(3 nm) SV multi-layered devices before applying electrical stress and after completely EM-failed (100 % of resistance increase) under different current densities varied from $J = 5\times10^7$ to $J = 9\times10^7$ A/cm^2. According to the failure characteristics confirmed by SEM shown in Fig. 4.10, the critical current density (J_c) for such an obvious bi-modal failure mechanism was found to be determined at $J_c = 7\times10^7$ A/cm^2. As can be seen from Fig. 4.10(b) to (d), when $J \leq J_c$, the EM-failure was mainly caused by the electrostatic force (or electron wind force) accelerating an inter-diffusion through grain boundaries that leads to forming typical EM failures such as voids and hillocks. Whereas, as can be seen in Fig. 4.10(e) and (f), when $J>J_c$, a melting, vaporization, and solidification, which are dominantly accelerated by the Joule-heating, played more significant role and caused the catastrophic failures. It was also revealed that most of catastrophic failures occurred near the cathode region as clarified from Fig. 4.10(d) to (f). This is primarily thought to be due to the void formation at the cathode region, which causes the severe shrinkage of cross sectional area, in the SV multi-layered devices and correspondingly induced large current crowding and localized high Joule heating temperature. Proportionally increased number of volcanic bulbs as well as

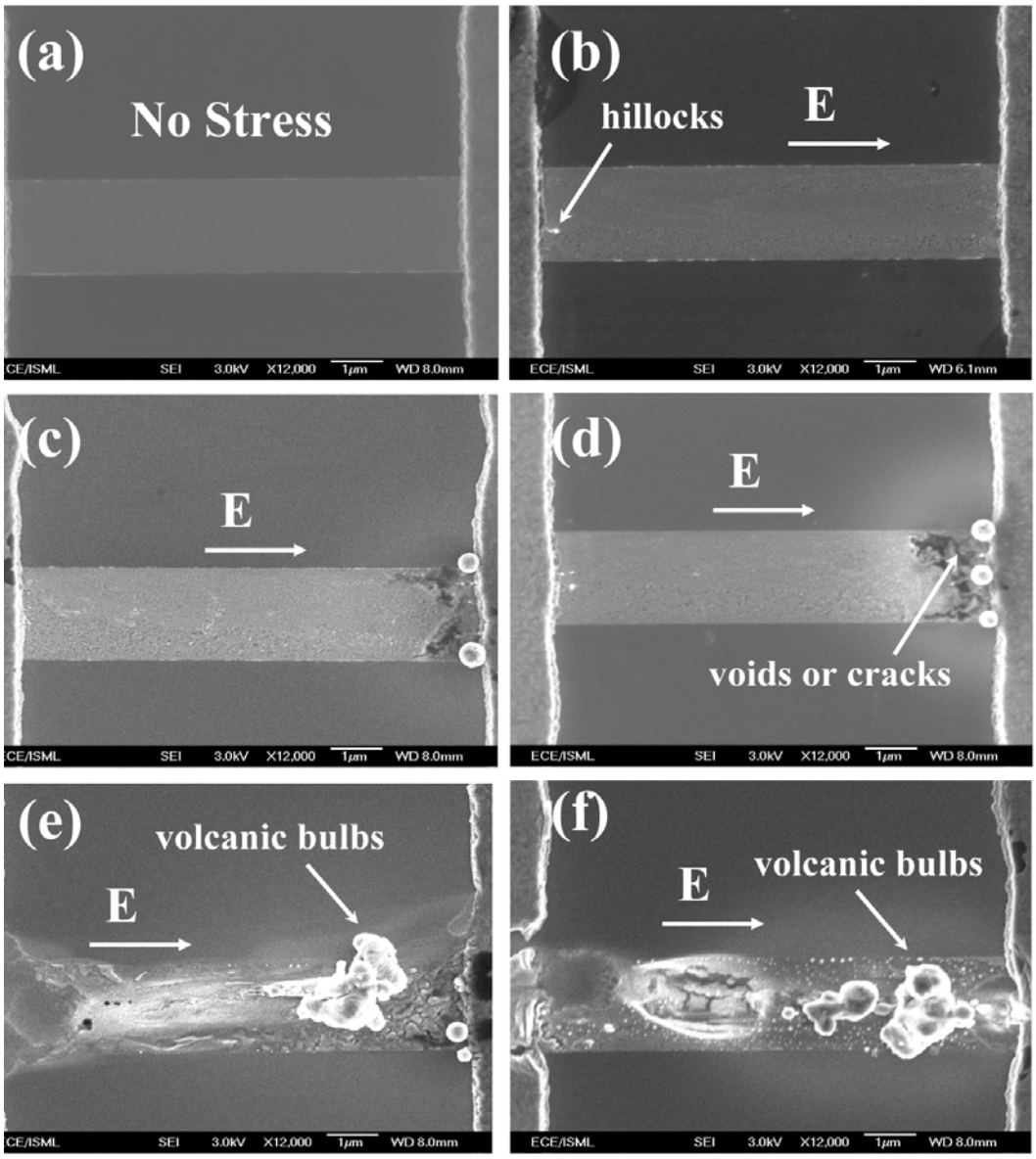

Fig. 4.10 SEM images of completely opened EM-induced failures for the patterned Si/NiFe(3)/Cu(2)/NiFe(3 nm) SV multi-layered electrically stressed under different current densities, a) no stress; b) $J = 5 \times 10^7$ A/cm^2; c) $J = 6 \times 10^7$ A/cm^2; d) $J = 7 \times 10^7$ A/cm^2; e) $J = 8 \times 10^7$ A/cm^2; and f) $J = 9 \times 10^7$ A/cm^2.

voids including cracks by increasing the applied current density directly demonstrates that the contribution of Joule heating to the EM-induced failures in the SV multi-layered devices become seriously dominant at a elevated current density beyond $J_c = 7\times10^7$ A/cm^2. In addition, this provides strong physical evidence that EM-induced failure mode of NiFe/Cu/NiFe SV multi-layered devices are closely followed by a “bi-modal

EM" similar to that observed in the Cu, or Al high conductivity thin films (Zhang, 2007; Misra, 2006). The "bi-modal EM characteristics" observed from the NiFe/Cu/NiFe SV multi-layered devices directly implies that Cu EM or EM-induced Cu inter-diffusion is dominantly relevant to the EM-induced failures in NiFe/Cu/NiFe SV-MLs. In order to further confirm the "bi-modal EM characteristics", the current dependence factor, "n", which directly describes how much the Joule heating contributes to the EM-induced failures was numerically determined from the "Black equation" (Black, 1969) in Eq. 4-2.

$$MTTF = A\frac{1}{j^n}\exp\left(\frac{E_a}{kT}\right) \tag{4-2}$$

Figure 4.11 shows the current dependence factor "n" values of the patterned NiFe(3)/Cu(2)/NiFe(3 nm) SV multi-layered devices determined from the slope of ln (TTF) vs. ln (J^{-1}) plot at ambient temperature. To obtain the "n" values, the applied current density was varied from J = 5×10^7 to J = 9×10^7 A/cm^2. As clearly confirmed in Fig. 4.11, the NiFe/Cu/NiFe SV-MLs had two different "n" values depending on the applied current density. At a lower current density range below J_c (J = $5\times10^7 \sim 7\times10^7$ A/cm^2), the "n" value was determined at 5.4. While, at a relatively high current density range above J_c (J = $8\times10^7 \sim 9\times10^7$ A/cm^2), the "n" value was determined at 1.3. Considering the physical relationship between the MTTF and the applied current density, J, described in the Black equation given by Eq. 4-2 (Black, 1969), the small "n" value indicates that EM-induced failure lifetime has a strong dependence on the applied current density. Furthermore, this clearly demonstrates that seriously high Joule heating temperature caused by the high current density dominantly accelerates the EM-induced failures, because the suddenly and sharply increased Joule heating temperature can

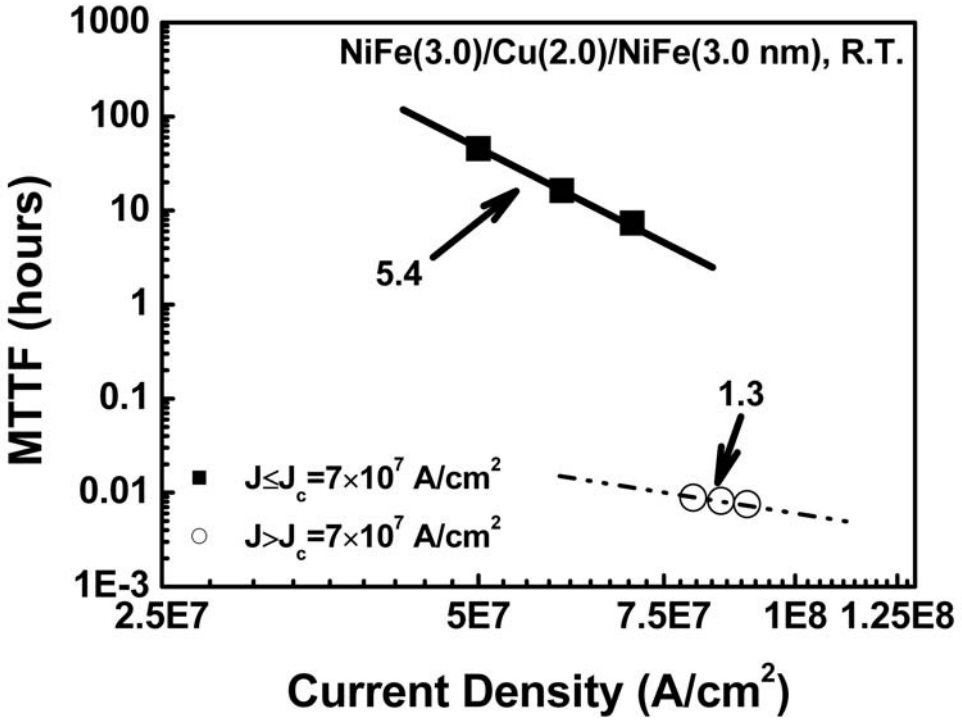

Fig. 4.11 Current dependence factor, n, values of the patterned Si/NiFe(3)/Cu(2)/NiFe(3 nm) SV mutli-layered devices determined from ln (MTTF) vs ln (J^{-n}) plot. The applied current densities to obtain the "n" vaule was varied from J = 5 × 10^7 A/cm^2 to J = 9 × 10^7A/cm^2 at ambient temperature.

provide the SV multi-layered devices with extremely high enough activation energy enabling to allow enormous atomic flux or flux divergence for the inter-diffusion in a very short time.

As can be understood by Eq. 4-2 and the Joule heating effect in Eq. 4-1, for the same ΔR, ΔT will be four times as high if the current density is doubled. Once the voids formed within the Cu thin films as a result of EM-induced failures and inter-diffusion into the NiFe layers, the actual cross-sectional area of the device would consequently shrink, and thus the real current densities passing through the devices should be rewritten as given by Eq. 4-3 (Venables, 1972),

$$j = \frac{j_0}{(1-p)} \tag{4-3}$$

where j_0 is the initial current density in the pore free stripe, p is the shrinkage percentage of cross-sectional area due to the EM-induced void formation. After the Cu spacer was completely opened at a high current density range, above J_c ($J = 8\times10^7 \sim 9\times10^7$ A/cm^2), the sudden increase of localized current density in both the top and bottom NiFe layers, which is named as the "current crowding effect", rapidly accelerated the EM-induced failures and eventually gave rise to the serious Joule heating induced temperature rise inside the NiFe layers. Such an abrupt increase of heating temperature induced a melting or vaporization in the patterned NiFe/Cu/NiFe SV multi-layered devices. This finally resulted in the volcanic failures in the blink of eye instead of the electrostatic force (or electron wind force) dominated EM-induced failures. The two distinctly different "n" values obtained from two different current density ranges, $J = 5\times10^7 \sim 7\times10^7$ A/cm^2 and $J = 8\times10^7 \sim 9\times10^7$ A/cm^2, directly imply that the EM failure behavior of NiFe/Cu/NiFe SV multi-layered devices are apparently followed by the "bi-modal EM failure mechanism". Figure 4.12 shows the AES depth profiles of patterned NiFe(3)/Cu(2)/NiFe(3 nm) SV multi-layered devices electrically opened (completely failed) under the different applied current densities varied from $J = 5\times10^7$ A/cm^2 to $J = 9\times10^7$ A/cm^2. As can be confirmed from Fig. 4.12(b) to Fig. 4.12(d), when the current densities, $J \leq J_c$ were applied, the completely failed devices still had clear Ni, Cu, and Fe atomic concentration peaks indicating that there is a NiFe/Cu/NiFe sandwich including a lot of Ni-Cu intermixing or a possibly Ni-Fe-Cu single layer (or two NiFe layers are attached each other after Cu completely inter-diffused into both the bottom and top NiFe layers). However, in contrast, as can be

confirmed from Fig. 4.12(e) to Fig. 4.12(f), when the current densities, $J>J_c$, were applied, the SV multi-layered devices showed almost zero Ni, Fe and Cu atomic concentration peaks except for the quite high oxygen atomic concentration peak indicating that most materials in the device have been vaporized during EM-induced failure process.

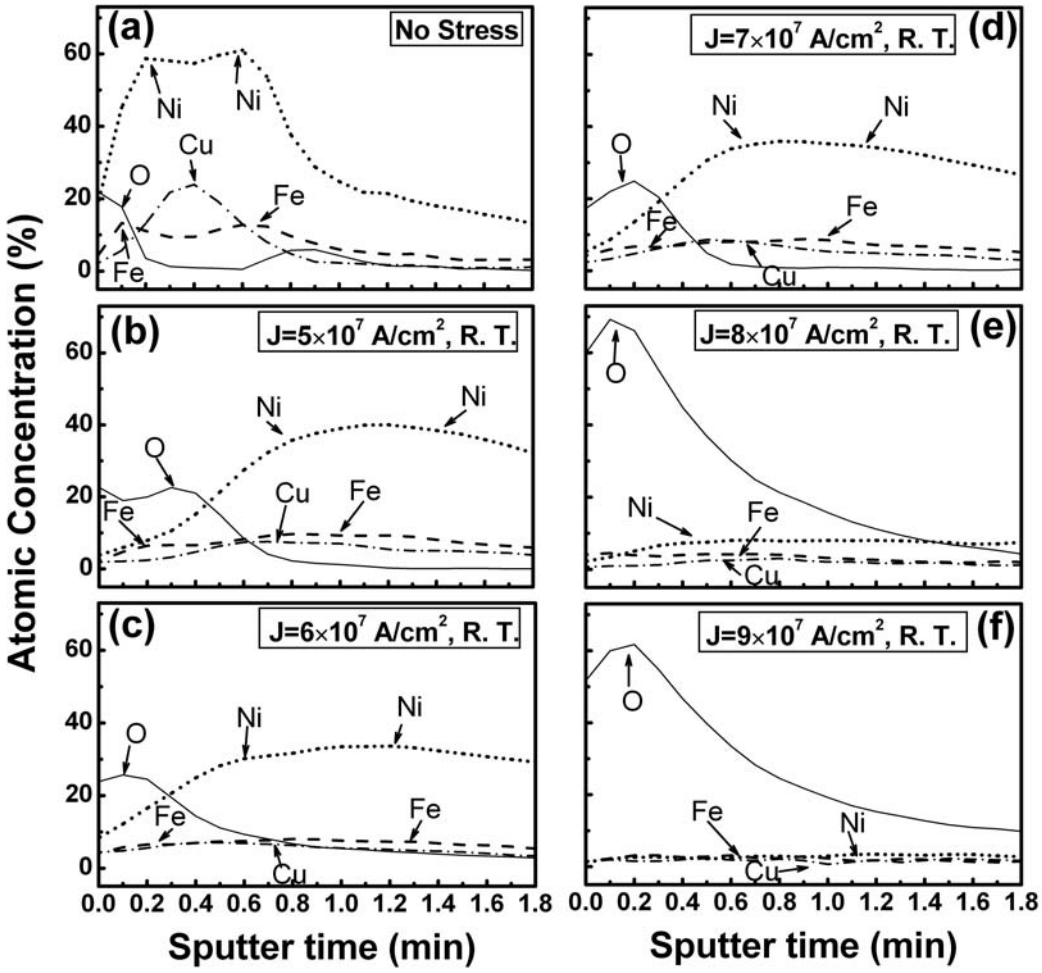

Fig. 4.12 Auger depth profiles for the patterned Si/NiFe(3)/Cu(2)/NiFe(3 nm) SV multi-layered devices, which were analyzed by FE-SEM as shown in Fig. 4.10.

4.2.2.4 Effect of an ultra-thin Co insertion layer on improving the EM reliability of NiFe/Cu/NiFe SV-MLs

As confirmed from Fig. 4.6 to Fig. 4.12, the EM-induced failure characteristics of patterned NiFe/Cu/NiFe SV multi-layered devices is dominantly determined by the Cu

spacer EM (or inter-diffusion). Accordingly, in order to control the Cu inter-diffusion or Cu inter-mixing with Ni atoms through NiFe/Cu interface, an ultra thin Co layer with 0.5 nm thickness was inserted at the interface between NiFe (both top and bottom layers) and Cu spacer. The main reason of using Co insertion is that Co has a very limited solid solubility with Cu that less than 1 at. % of Co can be mixed with Cu even at 400 ºC (Massalski, 1990). Figure 4.13 shows the TTF of patterned Si/NiFe(3)/Cu(2)/NiFe(3 nm) and NiFe(2.5)/Co(0.5)/Cu(2)/Co(0.5)/NiFe(2.5 nm) SV-MLs electrically stressed under the current density of $J = 8\times10^7$ A/cm^2 at ambient temperature. As can be seen in Fig. 4.13, the MTTF of SV multi-layered devices with Co insertion had 9.05 hours, while the SV multi-layered devices with no Co insertion had only 32 seconds of MTTF. The significantly increased EM-induced failure lifetime of NiFe/Co/Cu/Co/NiFe SV multi-layered devices compared to that of NiFe/Cu/NiFe is primarily thought to be due to the dramatic reduction of Cu inter-diffusion to both the top and bottom NiFe layers caused by the diffusion blocking effects of Co insertion layer. The experimental results shown in Fig. 4.13 indicates that controlling of Cu inter-diffusion behavior is the most crucial factor in determining the electrical reliability of NiFe/Cu/NiFe SV based spintronic devices and also it was clearly confirmed that the EM resistance of NiFe/Cu/NiFe SV based spintronic devices can be effectively improved if Cu diffusion blocking materials such as Co, and Co-Fe alloys are inserted at the NiFe and Cu interface.

SEM images shown in Fig. 4.14 further confirmed the diffusion barrier effect of such an ultra thin Co insertion layer. As shown in Fig. 4.14(a), the volcanic bulbs on

the surface of NiFe/Cu/NiFe SV multi-layered devices clearly demonstrated that there were Joule-heating induced catastrophic failures, however, after inserting an ultra thin Co diffusion barrier between Cu and NiFe layers, no volcanic bulbs was observed on the surface as shown in Fig. 4.14(b). The NiFe/Co/Cu/Co/NiFe SV multi-layered devices only showed typical EM-induced failures such as voids and hillocks including surface whiskers that are generally observed in the electrostatic force induced EM-induced failures. The detailed failure mechanism and the physical nature for the effectiveness of Co insertion on the improvement of EM-induced failure lifetime will be discussed in the following chapters.

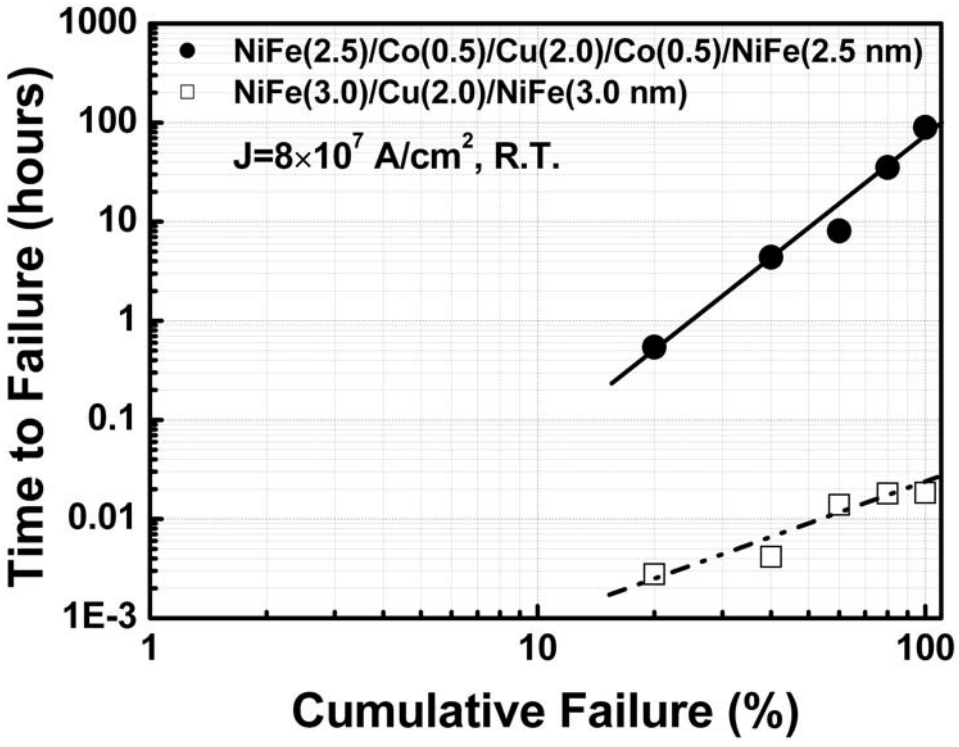

Fig. 4.13 Cumulative percent vs. TTF of the patterned Si/NiFe(3)/Cu(2)/NiFe(3 nm) and Si/NiFe(2.5)/Co(0.5)/Cu(2.0)/Co(0.5)/NiFe(2.5nm) SV multi-layered devices, which were electrically stressed under the current density of $J = 8 \times 10^7$ A/cm^2 at ambient temperature.

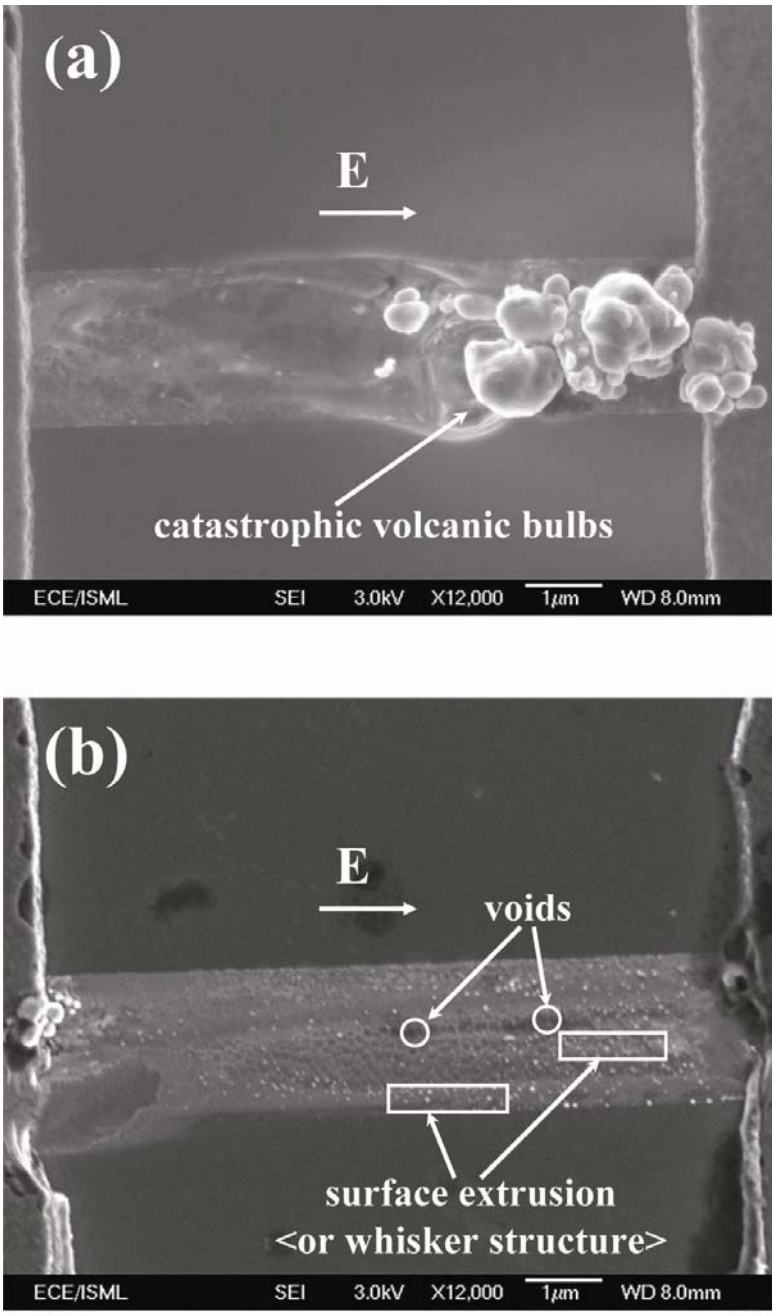

Fig. 4.14 SEM images for the EM-induced complete failures of (a) patterned Si/NiFe(3)/Cu(2)/NiFe(3 nm) SV multi-layered devices, and (b) patterned Si/NiFe(2.5)/Co(0.5)/Cu(2.0)/Co(0.5)/NiFe(2.5nm) SV multi-layered devices, electrically stressed under the current density of $J = 8 \times 10^7$ A/cm^2, at ambient temperature.

In order to investigate the magnetic instability of NiFe/Cu/NiFe based SV-MLs caused by the EM-induced failures, magnetic parameters including magnetic moment, and interlayer coupling field of the NiFe(3)/Cu(2)/NiFe(3 nm) and

NiFe(2.5)/Co(0.5)/Cu(2)/Co(0.5)/NiFe(2.5 nm) SV-MLs were compared by measuring M-H loops using a VSM. Figure 4.15 (a) and (b) show the hysteresis of NiFe(3)/Cu(2)/NiFe(3 nm) and NiFe(2.5)/Co(0.5)/Cu(2)/Co(0.5)/NiFe(2.5 nm) SV-MLs before applying electrical stress and after electrically stressed with J = 6×10^6 A/cm^2 at ambient temperature. In order to clearly compare the magnetic properties, the SV-MLs with geometry of 0.75 (W) × 10 (L) mm were used and the time for applying electrical stress was fixed at 12 hours, which is supposed as 10 % of MTTF obtained from the patterned SV multi-layered devices. The enlarged view of M-H loop of SV-MLs with and without Co insertion layer is showed in Fig.4-15 (c) and (d), respectively, for clearly comparing the reduction of magnetic moment and change of interlayer coupling field. As can be seen in Fig. 4.15(a) and (c), a 21 % degradation of magnetic moment and a serious change of interlayer coupling field (before stress: 1.8 Oe, and after stress: 0.5 Oe, determined from the minor M-H loop) were clearly observed in the electrically stressed NiFe(3)/Cu(2)/NiFe(3) SV-MLs, while there was almost no change of magnetic moment and interlayer coupling field in the NiFe(2.5)/Co(0.5)/Cu(2)/Co(0.5)/NiFe(2.5 nm) SV-MLs, as it is shown in Fig. 4.15 (b) and (d). The hysteresis losses indicated by black arrows in Fig. 4-15 (a) and (c) could be attributed to the incoherent spin alignment in the SV-MLs after electrical stress. The migrated Cu atoms scattered as nonmagnetic impurities in the NiFe layers. These scattered nonmagnetic impurities interacted with magnetic domains and weakened the spin-spin coupling in the NiFe layers. For NiFe/Co/Cu/Co/NiFe SV-MLs, small amounts of Cu atoms could diffuse into NiFe layer through the defects in Co insertion

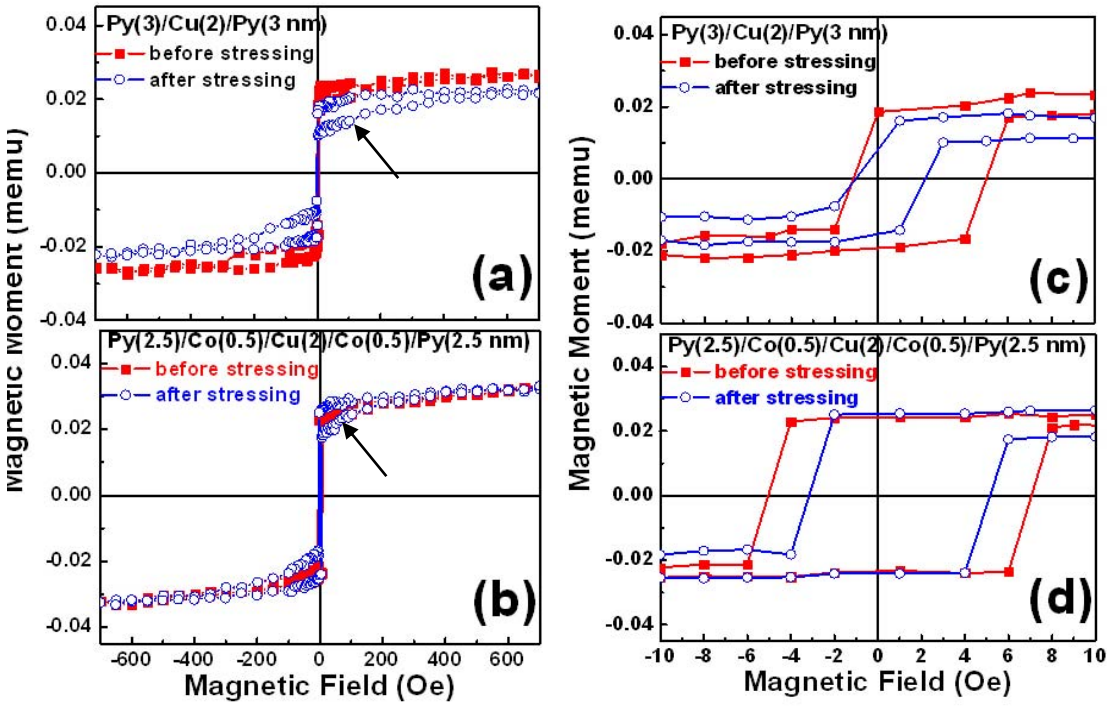

Fig. 4.15 M-H loops of (a) Si/NiFe(3)/Cu(2)/NiFe(3 nm) and (b) Si/NiFe(2.5)/Co(0.5)/Cu(2.0)/Co(0.5)/NiFe(2.5 nm) SV-MLs before applying electrical stress and after electrically stressed under J = 6 × 10^6 A/cm^2 for 12 hours at ambient temperature; (c) and (d) show the enlarged view of M-H loops showed in figure (a) and (b), respectively.

layer and therefore slight hysteresis loss is also observed on the M-H loop of NiFe/Co/Cu/Co/NiFe SV-MLs after electrical stress. (More analysis and discussion can be found in Chapter 5 and Chapter 6).

According to the EDX depth profiles and the cross sectional transmission electron microscope (XTEM) analysis as well as other more detailed experimental results (Jiang, 2008), the serious magnetic degradation of eclectically stressed NiFe/Cu/NiFe ML-SVs is dominantly due to the EM-induced Cu inter-diffusion (Cu EM) to both the top and bottom NiFe layers through the NiFe/Cu interfaces. The reduction of magnetic moment is attributed to the formation of Ni-Cu inter-mixing region in the NiFe and also the serious change of interlayer coupling field is thought to be due to the change

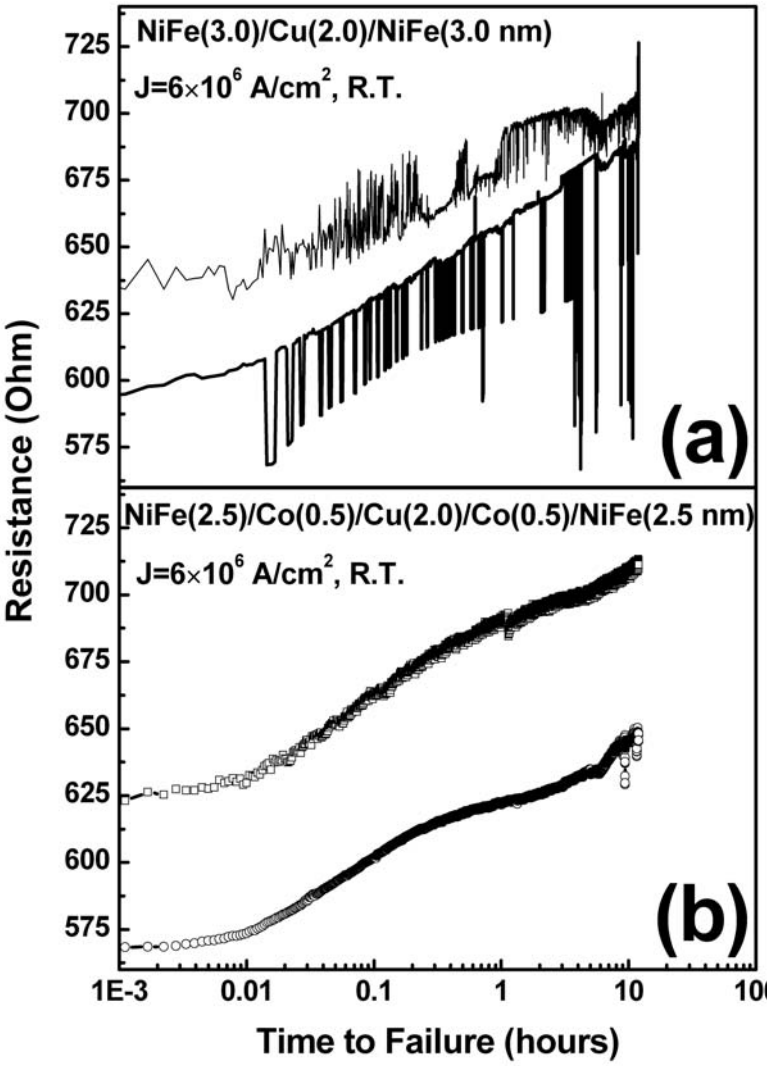

Fig. 4.16 Resistance change vs. stress time (R-t) curves for the (a) Si/NiFe(3)/Cu(2)/NiFe(3 nm), and (b) Si/NiFe(2.5)/Co(0.5)/Cu(2.0)/Co(0.5)/NiFe(2.5 nm) SV-MLs after applying D.C. current density of $J = 6 \times 10^6$ A/cm^2 to for 12 hours at R. T.

of Cu spacer thickness resulted from the EM-induced Cu inter-diffusion and accordingly the change of spin wave interaction along with the change of Cu impurity potential in the NiFe/Cu/NiFe SV-MLs (Jiang, 2008; Bruno, 1991).

Figure 4.16 shows the resistance-time (R-t) curves of electrically stressed NiFe(3)/Cu(2)/NiFe(3 nm) and NiFe(2.5)/Co(0.5)/Cu(2)/Co(0.5)/NiFe(2.5 nm) SV-MLs for 12 hours with $J = 6\times10^6$ A/cm^2 at ambient temperature. As can be seen in Fig. 4.16(a), a very serious resistance fluctuation (alternatively electrical open and short)

was observed in NiFe/Cu/NiFe SV-MLs with increasing time, while NiFe/Co/Cu/Co/NFe SV-MLs had a continuous and smooth increase of resistance without any severe fluctuation. By considering the resistivity value difference between NiFe and Ni-CuFe alloys, it can be speculated that the serious resistance fluctuation observed from the NiFe/Cu/NiFe SV-MLs is assumed to be due to the EM-induced Cu inter-diffusion resulting in the formation of Ni-Cu inter-mixing regions at the NiFe/Cu interfaces and in the NiFe layers.

4.2.3 Summary and Conclusions

The underlying EM-induced failure mechanism of patterned NiFe/Cu/NiFe SV multi-layered devices has been investigated in order to predict the electrical and magnetic stabilities of metallic SV based spintronic devices. It was clearly demonstrated that EM-induced Cu inter-diffusion (or Cu EM) through NiFe/Cu interfaces dominantly plays crucial role in determining the EM-induced failure characteristics in NiFe/Cu/NiFe SV multi-layered devices. It was found that EM-induced failure behavior in the NiFe/Cu/NiFe SV multi-layered devices with or without Co diffusion barrier was apparently followed by a “bi-modal EM-failure mechanism” depending on the applied current densities. By increasing the applied current density, their failure mechanism shifted from electrostatic force (or electron wind force) dominated EM-induced failures to the joule-heating dominated melting and vaporization-induced failures, which result in the volcanic-eruption characteristics. For the NiFe/(Co)Cu/(Co)/NiFe SV multi-layered devices, the critical current density for such

a "bi-modal failure mechanism" was determined at $J_c=7\times10^7$ A/cm^2. More interestingly, it was also confirmed that the magnetic instability of NiFe/(Co)/Cu/(Co)/NiFe SV multi-layered devices (or MLs) relevant to a serious reduction of magnetic moment (or anisotropy) and a severe change of magnetic interlayer coupling (or indirect exchange coupling) is directly affected by the EM-induced failures, especially by the EM-induced Cu inter-diffusion, which will be discussed in details in the next chapters.

In conclusion, it was demonstrated that EM-induced Cu spacer inter-diffusion to both the top and bottom NiFe magnetic layers is the most critical factor in characterizing the EM-induced failure lifetime of patterned NiFe/Cu/NiFe based metallic SV devices. Furthermore, controlling of EM-induced Cu inter-diffusion by inserting Co diffusion barrier at the interface between NiFe and Cu was found to be one of the most promising solutions to dramatically improve the electrical and magnetic stability of metallic NiFe/Cu/NiFe based spintronic devices.

References

Bae, S., Judy, J.H., Tsu, I.F., and Davis, M. (2003). Electrical reliability of tunneling magnetoresistive read heads. J. Appl. Phys. **94**, 7636-7645.

Bae, S., Judy, J.H., Tsu, I.-F., Davis, M., and Murdock, E.S. (2001). Dependence of electromigration-induced failure lifetimes on NiFe thin-film thickness in giant magnetoresistive spin-valve read heads. Appl. Phys. Lett. **79**, 3657-3659.

Bae, S., Tsu, I.F., Davis, M., Murdock, E.S., and Judy, J.H. (2002). Electromigration study of magnetic thin films for the electrical reliability of spin-valve read heads. IEEE

Trans. Magn. **38**, 2655-2657.

Black, J.R. (1969). Electromigration failure modes in aluminum metalization for semiconductor devices. Proc. IEEE **57**, 1587-1594.

Bruno, P., and Chappert, C. (1991). Oscillatory coupling between ferromagnetic layers separated by a nonmagnetic metal spacer. Phys. Rev. Lett. **67**, 1602-1605.

Gangulee, A., and d' Heurle, F.M. (1974). Electromigration and diffusion in Ni-Fe thin films. Jpn. J. Appl. Phys. **Suppl. 2**, 625-627.

Gurney, B.A., Speriosu, V.S., Wilhoit, D.R., Lefakis, H., Fontana, R.E., Jr., Heim, D.E., and Dovek, M. (1997). Can spin valves be reliably deposited for magnetic recording applications? (Invited) J. Appl. Phys. **81**, 3998-4003.

Gupta, D., and Ho, P.S. (1988). Diffusion phenomena in thin films and microelectronic materials. (New Jersay: Noyes Publications).

Jiang, J., Bae, S., and Ryu, H.J. (2009). Magnetic instability of giant magnetoresistance spin-valves due to electromigration-induced inter-diffusion. Thin Solid Film **517**, 5557-5562.

Jiang, J., Bae, S., and Ryu, H.J. (2008). Magnetic degradation of GMR spin-valve multi-layers due to EM induced failures. Intermag Europe 2008 Spain **AS-03**.

Jiang, Y., Yu, G.H., Wang, Y.B., Teng, J., Ochiai, T., Tezuka, N., and Inomata, K. (2005). Spin transfer in antisymmetric exchange-biased spin-valves. Appl Phys. Lett. **86**, 192515(1)-192515(3).

Kuniko, K., and Takamaro, K. (1994). Electromigration characteristics for Al-Ge-Cu. In Microelectronics Manufacturability, Yield, and Reliability. Vasquez, B., and

Kawasaki, H. Eds. Proc. SPIE **2334**, 4-12.

Li, Z., Christiansen, C., Gill, J., Sullivan, T., Yashchin, E., and Filippi, R. (2006). Threshold EM failure time and its statistics for Cu interconnects. J. Appl. Phys. **100**, 114516(1)-114516(10).

Massalski, T.B., Okamoto, H., Subramanian, P.R., and Kacprzak, L. (1990). Binary Alloy Phase Diagrams 2nd edn (Materials Park, OH: ASM International), p. 1182, p. 1444.

Misra, E., Theodore, N.D., Mayer, J.W., and Alford, T.L. (2006). Failure mechanisms of pure silver, pure aluminum and silver–aluminum alloy under high current stress. Microelectron. Reliab. **46**, 2096-2103. .

Monsma, D.J., Lodder, J.C., Popma, T.J.A., and Dieny, B. (1995). Perpendicular hot electron spin-valve effect in a new magnetic field sensor: the spin-valve transistor. Phys. Rev. Lett. **74**, 5260-5263.

Oates, S. (1995). Current density dependence of EM failure of submicron width, multilayer Al alloy conductors. Appl. Phys. Lett. **66**, 1475-1477.

Prinz, G.A. (1998). Measuring the spin polarization of a metal with superconducting point contact. Science **282**, 85-88.

Poate, J.M., Tu, K.N., and Mayer, J.W. (1978). Thin-Films-Inter-diffusion and Reactions. (New York: Wiley) p. 243.

Shen, J. (1997). Logic devices and circuits based on giant magnetoresistance. IEEE Trans. Magn. **33**, 4492-4497.

Shingubara, S., Takeda, Y., Sakaue, H., and Takahagi, T. (1999). Electromigration

reliability study of a GMR spin valve devices. Mater. Res. Symp. Proc. **563**. 145-150.

Venables, J.R., and Lye, R.G. (1972). A statistical model for electromigration-induced failures in thin film conductors. Proceedings of the 10th Annual Reliability Physics Symposium, 159-164.

Weller, D., Moser, A., Folks, L., Best, M.E., Lee, W., Toney, M.F., Schwickert, M., Thiele, J.U., and Doerner, M.F. (2000). High K_u materials approach to 100 Gbits/in^2. IEEE Trans. Magn. **36**, 10-15.

William, E.M. (2001). Thin Film Properties for MR Sensors. In Design and Analysis of Magnetoresistive Recording Heads-Thin Film Properties. (John Wiley & Sons, Inc.), p. 35.

Witvrouw, A., Bender, H., Roussel, P., and Maex, K. (1999). Modeling and microstructural characterization of incubation, time-dependent drift and saturation during EM in Al-Si-Cu stripes. Microelectron. Reliab. **39,** 1603-1616.

Zhang, H., Wang, G., and Cargill III, G.S. (2007). Local melting during EM in Cu conductor lines. J. Electron. Mater. **36**, 117-122.

CHAPTER 5 MAGNETIC INSTABILITY OF SPIN-VALVE MULTI-LAYERS DUE TO ELECTROMIGRATION-INDUCED INTER-DIFFUSION

5.1 Introduction and Motivations

Since the GMR effect was first discovered in the anti-ferromagnetically coupled Fe/Cr/Fe sandwiches (Grünberg, 1986), FM/metal spacer/FM based GMR MLs and GMR SVs with Cu spacer (Dutcher, 1988; Binasch, 1989) have been paid considerable attention for their applications in various spintronic devices such as magnetic recording read sensors and magnetic random access memories (Daughton, 1992; Reiss, 2003). In particular, technical interests on the FM/Cu/FM based MLs, more specifically NiFe/Cu/NiFe based GMR SV devices have been dramatically increased for the past few years due to their higher magnetic sensitivity, smaller saturation magnetic field and negligibly small hysteresis loss (Reiss, 2003; Ene, 2005). However, magnetic instability of NiFe/Cu/NiFe based GMR SV-MLs possibly caused by geometrical, electrical, and thermally-induced stress effects was considered as the most serious problem to be overcome for achieving a higher performance of such spintronic devices (Ene, 2005; Bae, 2002; Hecker, 2002). Accordingly, in order to investigate the effects of thermally induced inter-diffusion on the magnetic stability of GMR SV-MLs, extensive studies have been focused on finding out a physical nature of thermally-induced magnetic degradation in the GMR SV spintronic devices (Ene, 2005; Hecker, 2002; van Loyen, 2000). Furthermore, as the operating (or biasing) current density is

rapidly increased beyond $J=1\times10^8$ A/cm^2 with increasingly scaling-down of device geometry in the advanced nano-scale GMR spintronic devices, electrical stress effects, especially, magnetic degradation due to the electromigration (EM)-induced failures or inter-diffusion in the NiFe/Cu/NiFe based GMR SVs becomes more critical in estimating the magnetic stability of GMR based spintronic devices (Bae, 2002; Neamtu, 1999).

In this chapter, magnetic degradation of NiFe/Cu/NiFe based GMR SV-MLs was experimentally investigated by considering the EM-induced failures or inter-diffusion between the magnetic layer and Cu spacer, which has a smaller activation energy compared to the magnetic thin films (Bae, 2002). In order to clearly verify the physical nature of magnetic degradation in the GMR SV-MLs caused by EM, an ultra thin Co diffusion barrier was employed to control the Cu diffusion behavior through NiFe/Cu interfaces resulting in Ni-Cu intermixing in the NiFe/(Co)/Cu/(Co)/NiFe GMR SV multi-layered based devices. In addition, diffusion behavior of Cu and its physical effects on the magnetic degradation in SV-MLs with or without Co diffusion barrier were analyzed and confirmed by using an Energy Dispersive X-ray Analysis (EDX) and a cross sectional transmission electron microscopy (XTEM).

5.2 Experimental Works

All the NiFe(3.0)/Cu(t)/NiFe(3.0 nm) and NiFe(2.5)/Co(0.5)/Cu(t)/Co(0.5)/NiFe(2.5 nm) (t = 1.8~3.2nm) SV-MLs with the geometry of 0.75 (W) × 10 (L) mm were sputtered on Si (100) substrate at the base pressure of $1\times10^{-8} \sim 3\times10^{-8}$ Torr. Ar working

gas pressure during deposition was fixed at 2mTorr. To study the effect of EM-induced Ni-Cu inter-diffusion on the magnetic stability of NiFe/Cu/NiFe (with or without an ultra thin Co diffusion barrier) multilayers, M-H loops before and after electrically stressed under constant D.C. were measured by a vibrating sample magnetometer (VSM). All the samples were stressed with D.C. biasing current applied in the plane of testing samples and the current density was fixed at $J = 6\times10^6$ A/cm^2 for 12 hours, below 10 % of mean time-to-failure (MTTF), and their resistance (R) vs. time (t) curves were determined using a computer-controlled probe station. The contribution of electrical stress induced heating temperature rise during EM test was analyzed by measuring the temperature coefficient of resistance values of SV-MLs. The Ni-Cu inter-diffusion behavior through the NiFe/Cu interfaces was qualitatively characterized by XTEM and nano-beam EDX with a nominal beam size of 2 nm attached to the TEM. For further confirmation of EM-induced Cu inter-diffusion through the NiFe/Cu interfaces, the change of surface roughness was analyzed using an atomic force microscope (AFM).

5.3 Results and Discussion

5.3.1 Characterization of Magnetic Degradation Dependent on Cu Spacer Thickness and Diffusion Barriers

Figure 5.1 shows the Magnetic moment (M)-Magnetic field (H) loops of NiFe(3.0)/Cu(t)/NiFe(3.0 nm) and NiFe(2.5)/Co(0.5)/Cu(t)/Co(0.5)/NiFe(2.5 nm) (t=1.8, 2.3, and 3.2 nm) GMR SV-MLs before and after applying electrical stress. An

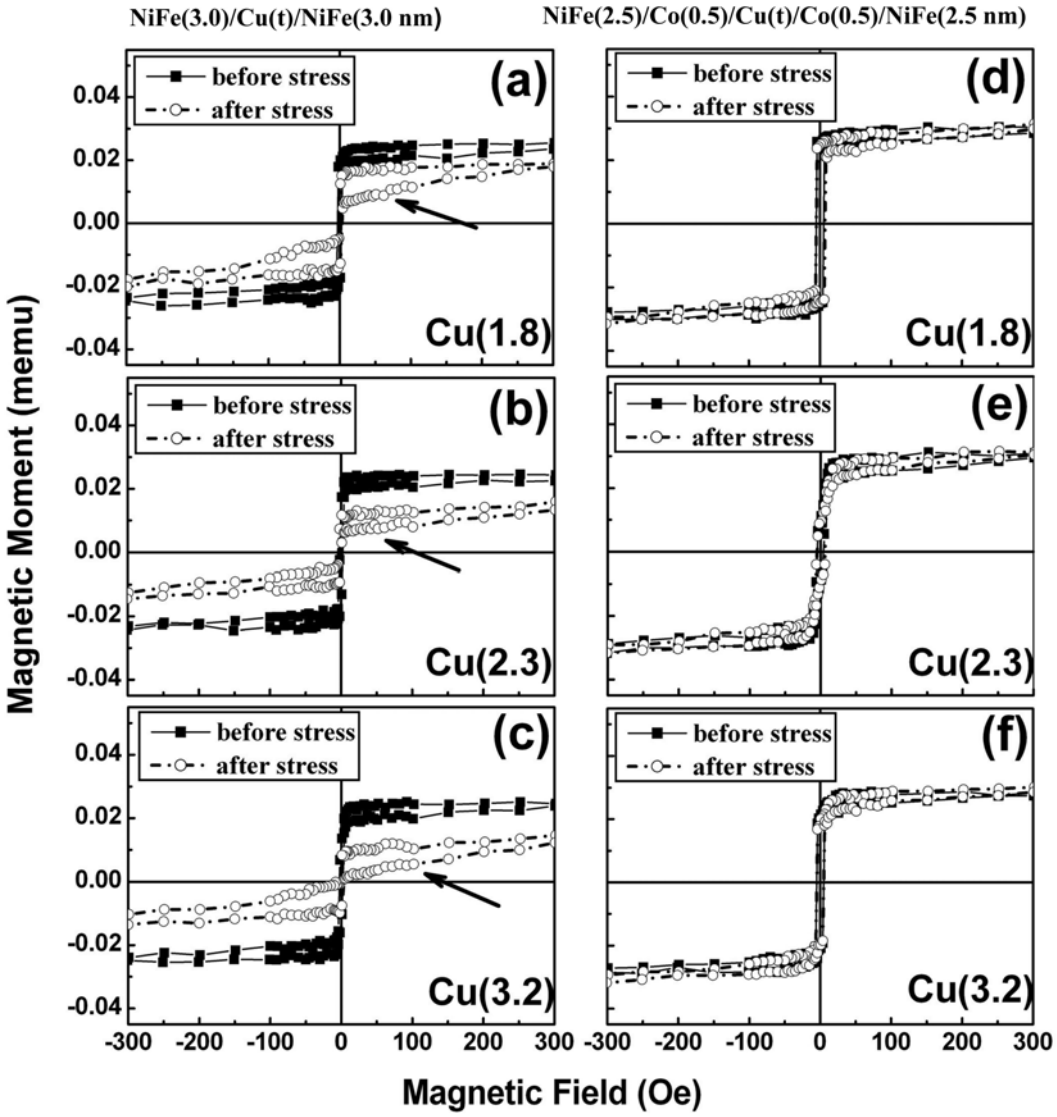

Fig.5.1 M-H loops of Si/NiFe(3.0)/Cu(t)/NiFe(3.0 nm) and Si/NiFe(2.5)/Co(0.5)/Cu(t)/Co(0.5)/NiFe(2.5 nm) GMR SV-MLs with different Cu spacer thickness. Constant D.C. current density of $J = 6\times10^6$ A/cm^2 was applied to the EM test samples for 12 hours.

ultra thin Co diffusion barrier inserted at NiFe/Cu interfaces was used to control the Cu diffusion to the NiFe due to very low solid solubility between Cu and Co as few as below 1 at. % (Massalski, 1990) up to 400 ºC in contrast to the well miscible Ni-Cu binary alloy system. Although 0.5-nm Co interlayer is not a continuous film, from the viewpoint of thermodynamics, Co atoms are deposited at NiFe/Cu interfaces to effectively reduce the Ni-Cu intermixing by taking over the counterpart sites of Ni

atoms involved in the EM-induced Cu inter-diffusion. The D.C. current density was fixed at $J = 6\times10^6$ A/cm^2. In order to clearly observe the magnetic degradation caused by the EM-induced inter-diffusion or failures, the stressing time was fixed at 12 hours, below 10 % of MTTF, which is determined from the micro-patterned NiFe/(Co)/Cu/(Co)/NiFe SV multi-layered based devices (MTTF, t_{50} = 120 ± 20 % hours at $J=6\times10^6$ A/cm^2). As can be clearly seen in Fig. 5.1(a), (b) and (c), a dramatic degradation of magnetic moment was observed in the electrically stressed NiFe/Cu/NiFe SV-MLs, while there was no obvious change of magnetic moment in the NiFe/Co/Cu/Co/NiFe SV-MLs (Fig. 5.1(d), (e), and (f)). In addition, the reduction of magnetic moment in the electrically stressed NiFe/Cu/NiFe SV-MLs was revealed to become serious by increasing Cu spacer thickness (reduction rate was increased from 23 to 41 %). Figure 5.2(a) and (b) shows the R-t curves for the electrically stressed NiFe/(Co)/Cu(t)/(Co)/NiFe SV-MLs for 12 hours under the D.C. current density of $J = 6\times10^6$ A/cm^2. Both SV-MLs showed increasing trend of resistance with increasing stress time. However, NiFe/Cu/NiFe SV-MLs showed a very serious resistance fluctuation with increasing time (supposed to be alternatively electrical open and short), whereas, NiFe/Co/Cu/Co/NiFe SV-MLs showed a continuous and gentle increase of resistance without any severe fluctuation.

By considering that the resistance change of SV-MLs under the applied D.C. constant current is directly due to the EM-induced atomic movements in the thin films, the dramatic reduction of magnetic moment and the serious fluctuation of resistance shown in Fig. 5.1 and Fig. 5.2 can be understood in terms of EM-induced inter-

diffusion or failures. For NiFe/Cu/NiFe SV-MLs, EM-induced failures (EIFs) or inter-diffusion would be dominated by EM in Cu spacer due to its lower activation energy

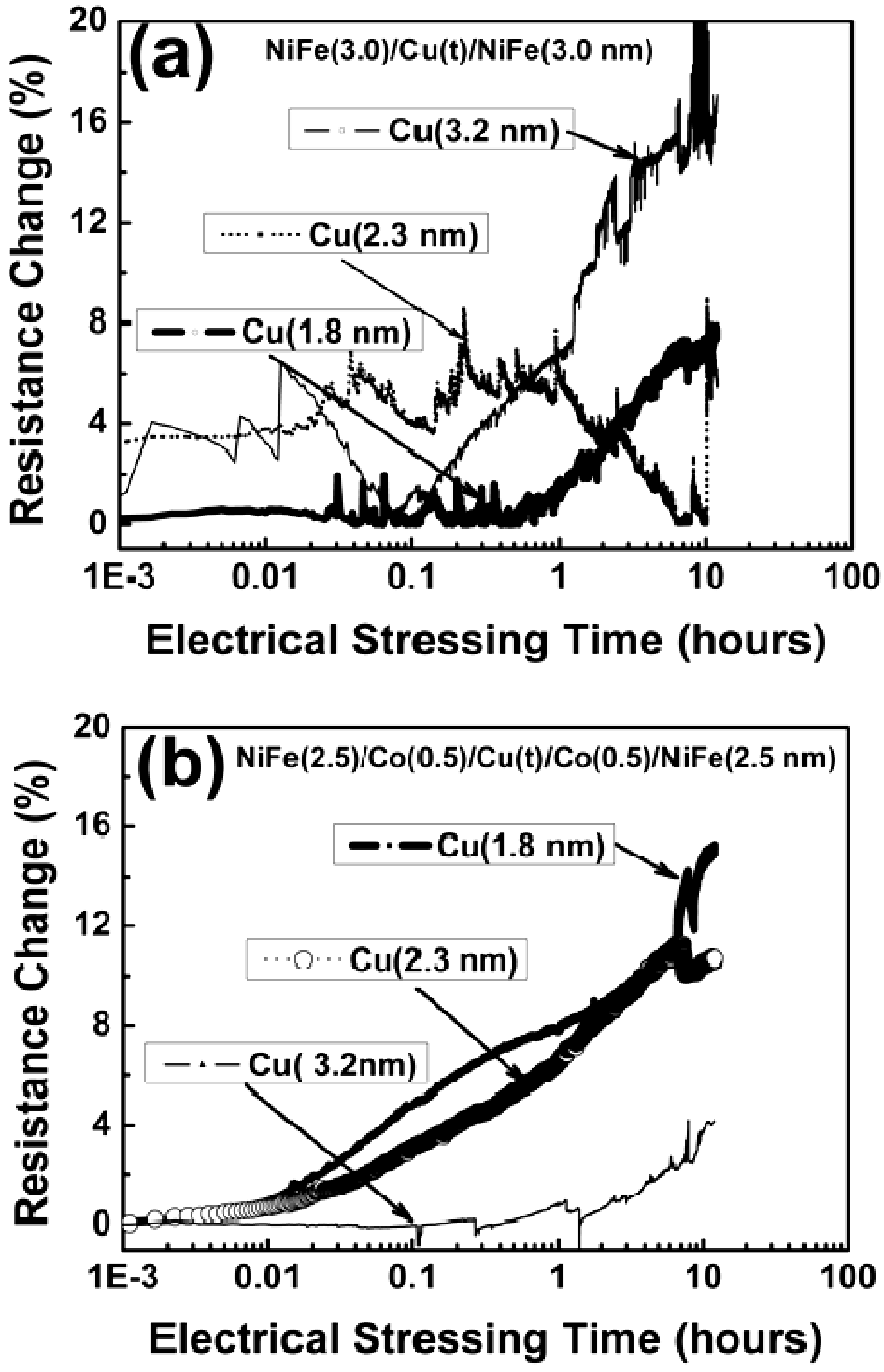

Fig. 5.2 Resistance vs. stress time (R-t) curves for the Si/NiFe(3.0)/Cu(t)/NiFe(3.0 nm) and Si/NiFe(2.5)/Co(0.5)/Cu(t)/Co(0.5)/NiFe(2.5 nm) GMR SV-MLs with different Cu spacer thickness. The applied D.C. current was fixed at $J = 6\times10^6$ A/cm^2.

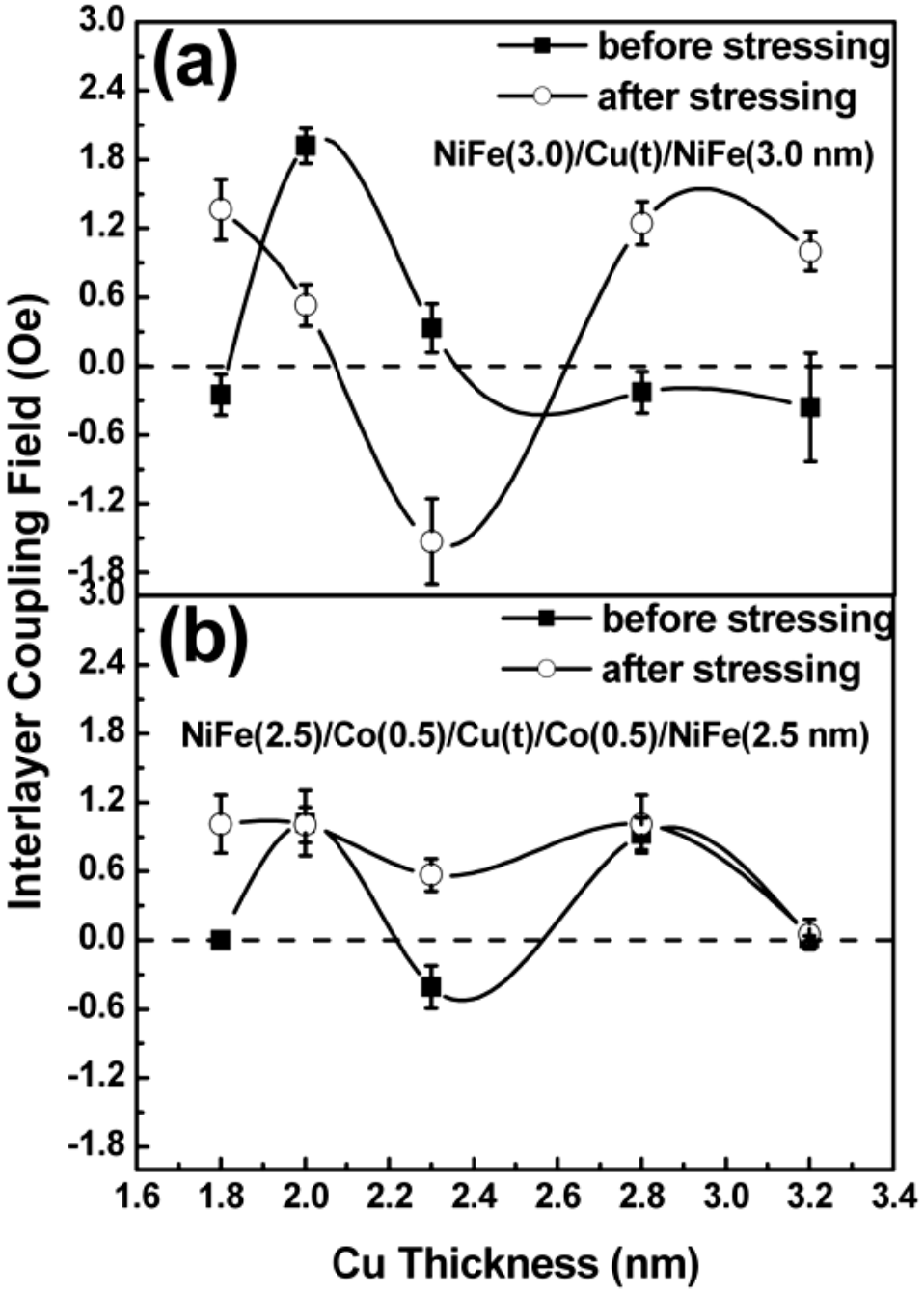

Fig. 5.3 Variation of interlayer coupling field and its oscillation period for (a) Si/NiFe(3.0)/Cu(t)/NiFe(3.0 nm) and (b) Si/NiFe(2.5)/Co(0.5)/Cu(t)/Co(0.5)/NiFe(2.5 nm) GMR SV-MLs with different Cu spacer thickness before and after applied electrical stress under $J=6\times10^6$ A/cm^2 for 12 hours at ambient temperature.

(0.5 ± 0.2 eV) compared to that of NiFe (0.8 ± 0.15 eV) (Bae, 2002) and "current sinking effects" that 2/3 of applied sensing current flows through Cu spacer because of

the film resistance difference (Gurney, 1997). Based on this physical assumption, EIFs of NiFe/Cu/NiFe SV-MLs can be supposed to first occur in the Cu spacer. Cu atoms gained enough activation energy from the applied electrical stress as well as its induced joule heating would migrate through NiFe/Cu interfaces and then the diffused Cu atoms easily form a Ni-Cu intermixing region at the NiFe/Cu interfaces or inside the NiFe layer due to their high solid solubility with Ni atoms (Jiang, 2007). This intermixed Ni-Cu alloy or intermixing region would be a main reason for the serious reduction of magnetic moment in the electrically stressed NiFe/Cu/NiFe SV-MLs, because Ni-Cu intermixing region has a very weak magnetic moment (significantly reduced magnetic moment, or zero magnetic moment at the $Ni_{40}Cu_{60}$ alloy composition) (Parra, 1980). The increase on the reduction rate of magnetic moment by increasing Cu spacer thickness in the NiFe(3.0)/Cu(t)/NiFe(3.0 nm) SV-MLs is primarily thought to be due to the increase on the total amounts of EM-induced Cu diffused atoms as well as a rougher NiFe/Cu interface caused by the change of Cu microstructure that possibly induces the increase of Cu inter-diffusion paths at the NiFe/Cu interface (Jiang, 2007). Moreover, by considering the EM-induced Cu inter-diffusion to the NiFe magnetic layer under constant D.C. stress, the electrical open (or suddenly increase of resistance) shown in Fig. 5.2(a) can be supposed to be due to the accelerated EIF in the Cu spacer, while the subsequent resistance decrease could be attributed to the formation of Ni-Cu alloy, which reduces the resistance of NiFe thin films. As clearly confirmed in Fig. 5.1 and Fig. 5.2, there was no obvious change of magnetic moment and resistance fluctuation in the electrically stressed

NiFe(2.5)/Co(0.5)/Cu(t)/Co(0.5)/NiFe(2.5 nm) SV-MLs. This strongly implies that the serious magnetic degradation of the electrically stressed NiFe/Cu/NiFe SV-MLs is directly relevant to EM-induced Cu spacer inter-diffusion to the NiFe magnetic layers.

Another interesting phenomenon relevant to the change of magnetic reversal (or appearing double hysteresis) indicated by the arrows in Fig. 5.1 was observed in the electrically stressed NiFe(3.0)/Cu(t)/NiFe(3.0 nm) SV-MLs. This can also be considered as physical evidence that EM-induced Cu inter-diffusion to the NiFe is directly responsible for the magnetic instability of NiFe/Cu/NiFe SV-MLs. In the NiFe FM thin films, the adjacent magnetic spins should be aligned parallel due to ferromagnetic exchange energy and rotate coherently by the applied external magnetic field. However, after applying electrical stress, EM-induced Cu diffused atoms were migrated into the NiFe and then scattered as nonmagnetic impurities or formed Ni-Cu intermixing in the NiFe layers. These scattered nonmagnetic impurities or nonmagnetic Ni-Cu intermixing would weaken the strength of spin-spin coupling in the NiFe (or spin aligned more incoherently) due to the reduction of inter-granular exchange coupling caused by the nonmagnetic impurities. This would be the physical reason for producing the incoherent magnetic reversal (or double hysteresis) in the electrically stressed NiFe/Cu/NiFe SV-MLs as shown in Fig. 5.1. The scattered nonmagnetic Cu atoms or Ni-Cu intermixing in the NiFe due to EM-induced inter-diffusion or failures are also assumed to change the spin wave interaction between two NiFe layers separated by Cu spacer due to the possible interference caused by the phonon wave generated from nonmagnetic impurities or Ni-Cu intermixing in the NiFe. Change of

spin wave interaction as well as the change of Cu impurity potential due to the EM-induced Cu inter-diffusion to the NiFe in the electrically stressed NiFe(3.0)/Cu(t)/NiFe(3.0 nm) SV-MLs are assumed to change the interlayer (indirect exchange) coupling field and its RKKY type of oscillation frequency in SV-MLs (Bruno, 1991).

5.3.2 Interlayer Coupling Characteristics of Electrically Stressed NiFe/Cu/NiFe versus NiFe/Co/Cu/Co/NiFe SV-MLs

Figure 5.3 shows the interlayer coupling field and its oscillation frequency determined from the minor M-H loops of the NiFe(3.0)/Cu(t)/NiFe(3.0 nm) and NiFe(2.5)/Co(0.5)/Cu(t)/Co(0.5)/NiFe(2.5 nm) (t=1.8, 2.0, 2.3, 2.8 and 3.2nm) GMR SV-MLs before and after applying electrical stress. As it is clearly seen in Fig. 5.3(a) and (b), M-H loops of NiFe/Cu/NiFe SV-MLs showed a serious change in both interlayer coupling field and its oscillation frequency after applying electrical stress. However, only small change of interlayer coupling field was observed in the NiFe/Co/Cu/Co/NiFe SV-MLs. No obvious change of interlayer coupling field as well as its oscillation frequency implies that there was no severe EM-induced Cu inter-diffusion in the NiFe/Co/Cu/Co/NiFe SV-MLs due to the significant blocking effect of Cu diffusion at the NiFe/Cu interface by Co diffusion barrier. It is generally considered that the interlayer coupling field is originated from two different physical natures: (1) Néel-type topological coupling (correlated waviness or “orange-peel” coupling), which is magnetostatic nature, and usually favors a ferromagnetic configuration (Kools, 1995; Egelhoff, 1996), while (2) oscillatory exchange coupling (similar to RKKY-type

oscillation, indirect exchange interaction) due to an exchange based mechanism influenced by the Fermi surface of the spacer material, and favoring ferro or anti-ferromagnetic coupling depending on the spacer thickness (Leal, 1996). Considering these physical natures, the change of interlayer coupling field for the NiFe(3.0)/Cu(2.0)/NiFe(3.0 nm) and NiFe(2.5)/Co(0.5)/Cu(2.0)/Co(0.5)/NiFe(2.5 nm) SV-MLs before and after applying electrical stress shown in Fig. 5.3 were analyzed in terms of the interlayer coupling energy, which is composed of topological and RKKY type of exchange energy. The topological coupling energy per unit area of the SV-MLs before and after applied electrical stress was determined from the Eq. 5-1 (Williams, 2001). All the physical parameters used for Eq. 5-1 were experimentally determined. The details are summarized in Table 5-1.

$$E_{topo} = \frac{\pi^2}{\sqrt{2}} \frac{h^2}{\lambda} M^2 \exp\left(\frac{-2\pi\sqrt{2} t_S}{\lambda} \right) \tag{5-1}$$

where h is the waviness amplitude (or surface roughness) of each film, λ is the wavelength of the surface variations and t_s is the spacer thickness. The former two parameters, h and λ, were determined by the surface roughness and cross sectional images of SV-MLs analyzed by AFM as shown in Fig. 5.4, and the real spacer thickness t_s of the electrically stressed NiFe(3.0)/Cu(2.0)/NiFe(3.0 nm) SV-MLs analyzed by AES depth profile was determined at 2.26 nm (Jiang, 2008) considering the inter-diffusion at NiFe/Cu interfaces, which leads to the formation of Ni-Cu nonmagnetic intermixing region. Assuming the top and bottom FM layers are uniformly saturated, the magnetization, M_{FM}, can be calculated from the corresponding magnetic moment (Jiang, 2008) as well as the total volume of FM layers.

Due to the surface oxidation of top FM layer, the total FM layer thickness including

Table 5-1 Experimentally determined physical parameters for calculating the topological energy of testing samples S1~S4. S1: Si/NiFe(3.0)/Cu(2.0)/NiFe(3.0 nm) GMR SV-MLs, before electrical stress; S2: Si/NiFe(3.0)/Cu(2.0)/NiFe(3.0 nm) GMR SV-MLs after electrical stress; S3: Si/NiFe(2.5)/Co(0.5)/Cu(2.0)/Co(0.5)/NiFe(2.5 nm) GMR SV-MLs, before electrical stress; S4: Si/NiFe(2.5)/Co(0.5)/Cu(2.0)/Co(0.5)/NiFe(2.5 nm) GMR SV-MLs, after electrical stress. (in the Table, λ is the wavelength of the surface variations, h is the waviness amplitude (or surface roughness) of each film, M is the magnetization of FM layers, t_{FM} is the total thickness of FM layers, t_s is the spacer thickness and E_{topo} is the topological coupling energy per unit area of the SV-MLs).

Symbol	S1	S2	S3	S4
λ	77.5 nm	118.4 nm	75.1 nm	111.3 nm
h	0.199 nm	0.508 nm	0.243 nm	0.294 nm
M	654×10^3 A/m	582×10^3 A/m	804×10^3 A/m	795×10^3 A/m
t_{FM}	5.28 nm	5.02 nm	5.42 nm	5.42 nm
t_s	2.0 nm	2.26 nm	2 .0 nm	2.0 nm
E_{topo}	0.00012 ergs/cm^2	0.00044 ergs/cm^2	0.00028 ergs/cm^2	0.00029 ergs/cm^2

top and bottom FM layers for the SV-MLs before electrical stress was assumed as 5.28 nm, and 5.42 nm for the NiFe(3.0)/Cu(2.0)/NiFe(3.0), and NiFe(2.5)/Co(0.5)/Cu(2.0)/Co(0.5)/NiFe(2.5 nm) SV-MLs, respectively (Jiang, 2008). For the electrically stressed NiFe(3.0)/Cu(2.0)/NiFe(3.0 nm) SV-MLs, the FM layer thickness was reduced to be 5.02 nm (Jiang, 2008) , which is primarily thought to be due to the formation of Ni-Cu intermixing. The calculated topological energy value for the NiFe(3.0)/Cu(2.0)/NiFe(3.0 nm) SV-MLs before electrical stress was determined at 0.00012 ergs/cm^2, while, it was 0.00044 ergs/cm^2 for the electrically stressed NiFe(3.0)/Cu(2.0)/NiFe(3.0 nm) SV-MLs. However, for the NiFe(2.5)/Co(0.5)/Cu(2.0)/Co(0.5)/NiFe(2.5 nm) SV-MLs before, and after applying electrical stress, the topological energy value was determined at 0.00028 and 0.00029

ergs/cm^2, respectively, which is quite close to each other. The calculation of topological coupling energy directly demonstrates that the severe change of interlayer coupling field for the electrically stressed NiFe(3.0)/Cu(2.0)/NiFe(3.0 nm) SV-MLs is closely relevant to the change of nonmagnetic spacer thickness and interfacial roughness mainly caused by the EM-induced Cu inter-diffusion.

Another possible physical reason for the change of interlayer coupling field and its oscillation frequency was considered from the oscillatory interaction, which can be determined from Eq.5-2.

$$E_{ex} = \frac{E_0}{\left(k_0 t_s\right)^2} \sin\left(\frac{2\pi t_s}{\Lambda} + \phi\right) \tag{5.2}$$

where E_0 is surface energy relevant to conduction electron potential, k_0 is wave number, ϕ is phase shift and Λ is the oscillatory coupling frequency, which is drastically influenced by the topological properties of the spacer Fermi surface. As clearly seen in Fig. 5.3(a), the oscillatory coupling frequency, Λ , of the NiFe(3.0)/Cu(2.0)/NiFe(3.0 nm) SV-MLs before and after applied electrical stress has been obviously changed. Due to the inter-diffusion through NiFe/Cu interfaces, the migrated Ni atoms inside the Cu spacer behave as a magnetic impurity to change the conduction electron potentials. This causes the shift of oscillatory frequency. The oscillation frequency is determined by the wave vector at the Fermi surface, which is strongly affected by the effective impurity potential in the nonmagnetic spacer. The EM-induced Cu inter-diffusion is involved in resulting in the inter-diffusion of Ni atoms into the Cu spacer as well. It leads to inducing the $3d$ band of Ni to be split up into a majority band lying completely below the Fermi level E_F and a minority band

intersecting E_F . Therefore, the impurity potential variation due to the magnetic impurity Ni in a nonmagnetic Cu spacer would have a strong effect on the oscillation frequency Λ of the interlayer coupling (Hartmann, 1999). Moreover, as can be seen from the Eq. 5-2, the change of nonmagnetic spacer thickness, t_s , possibly caused by EM induced Cu spacer inter-diffusion, is also closely related to the change of oscillatory exchange coupling energy.

5.3.3 Surface and Interfacial Characterization of Electrically Stressed NiFe/Cu/NiFe versus NiFe/Co/Cu/Co/NiFe SV-MLs

The change of nonmagnetic spacer thickness was confirmed by AFM image analysis as shown in Fig. 5.4. For the NiFe(3.0)/Cu(2)/NiFe(3.0 nm) SV-MLs, it showed a change of surface roughness from $R_{ms,bf}$ = 0.199 nm (before stress) to $R_{ms,af}$ = 0.508 nm (after stress, 155% increase). However, for the NiFe(2.5)/Co(0.5)/Cu(2)/Co(0.5)/NiFe(2.5 nm), it showed a change of surface roughness from $R_{ms,bf}$ = 0.243 nm (before stress) to $R_{ms,af}$ = 0.294 nm (after stress, 21 % increase). The apparent small variation of surface roughness in the NiFe(2.5)/Co(0.5)/Cu(2.0)/Co(0.5)/NiFe(2.5 nm) SV-MLs after applying electrical stress indirectly indicates that there was no serious EM-induced Cu inter-diffusion because of controlling Ni-Cu inter-diffusion by the Co diffusion barrier. Consequently, the variation on the oscillatory exchange coupling energy and the oscillatory frequency for the electrically stressed NiFe(3.0)/Cu(2.0)/NiFe(3.0 nm) SV-MLs are directly associated with the EM-induced Cu spacer inter-diffusion.

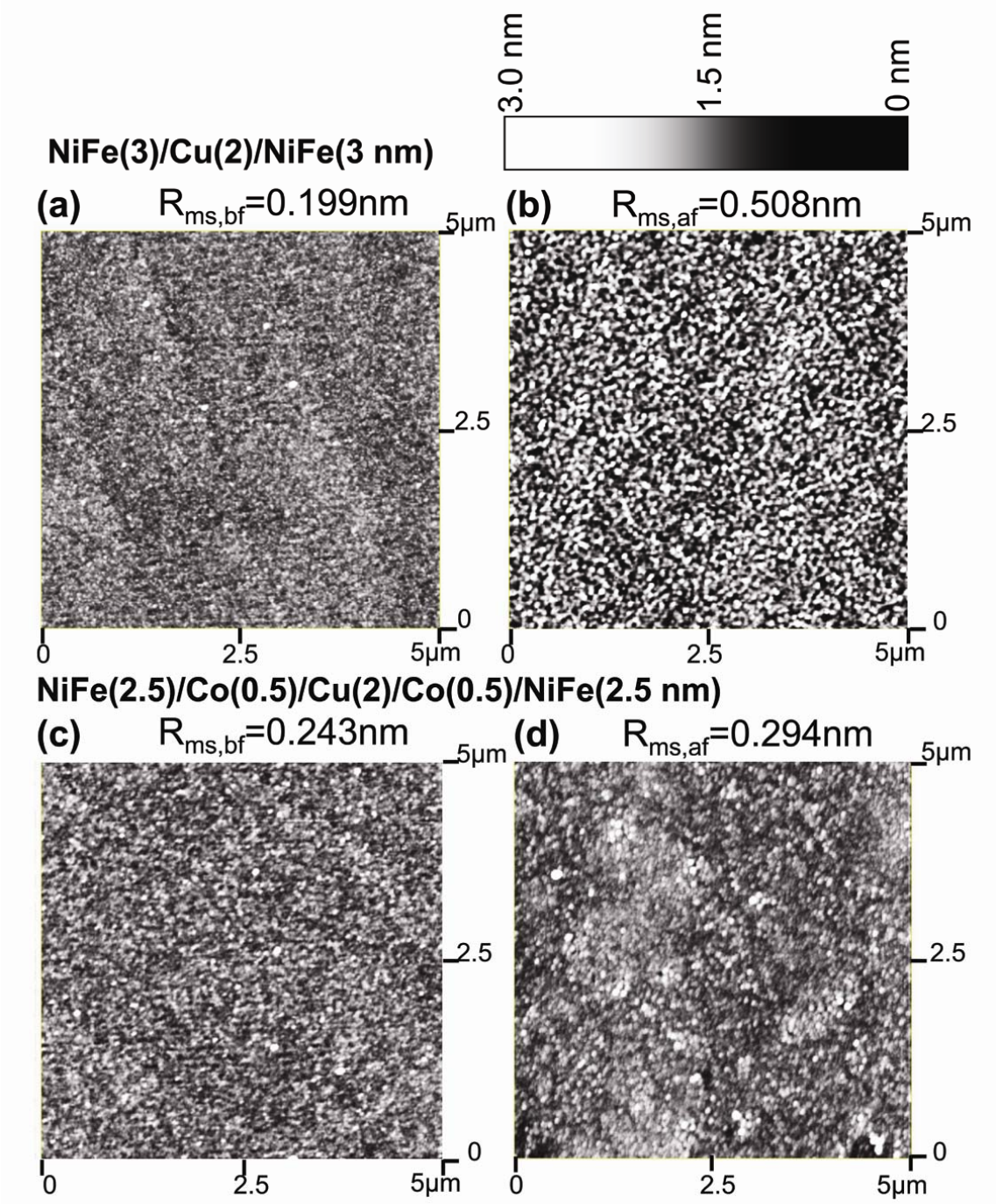

Fig. 5.4 AFM images of GMR SV-MLs electrically stressed under J=6×10^6 A/cm^2 for 12 hours at ambient temperature: (a) Si/NiFe(3.0)/Cu(2.0)/NiFe(3.0nm) MLss, before stress; (b) Si/NiFe(3.0)/Cu(2.0)/NiFe(3.0nm) MLs, after stress; (c) Si/NiFe(2.5)/Co(0.5)/Cu(2.0)/Co(0.5)/NiFe(2.5 nm MLs, before stress: and (d) Si/NiFe(2.5)/Co(0.5)/Cu(2.0)/Co(0.5)/NiFe(2.5 nm) MLs, after stress.

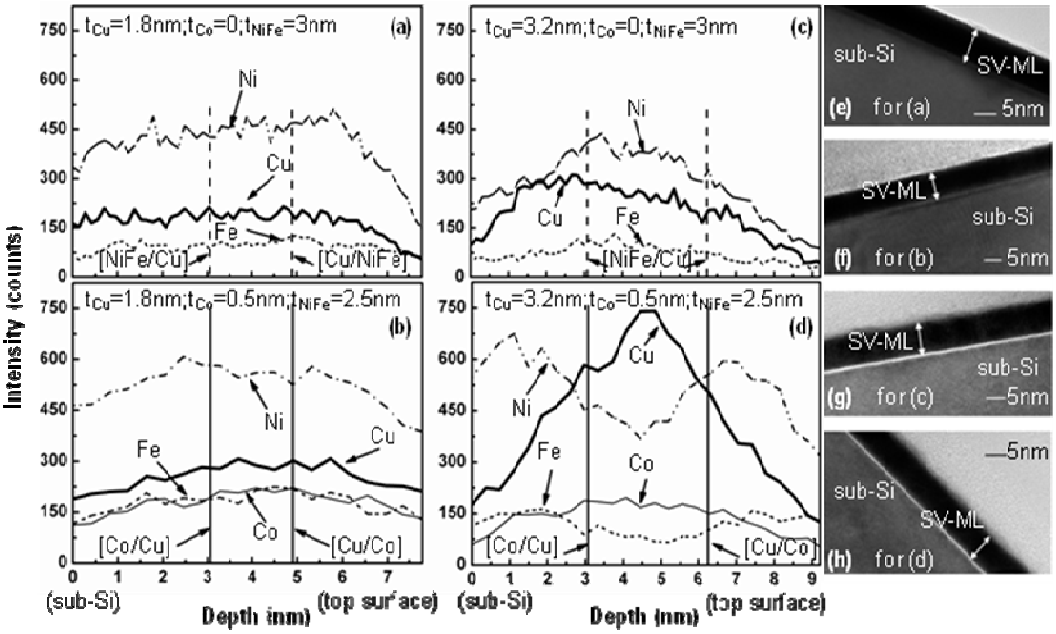

Fig. 5.5 EDX depth-profile for the electrically stressed Si/NiFe(3.0)/Cu(t)/NiFe(3.0 nm) [(a) t_{Cu} = 1.8 nm and (c) t_{Cu} = 3.2 nm] and Si/NiFe(2.5)/Co(0.5)/Cu(t)/Co(0.5)/NiFe(2.5 nm) [(b) t_{Cu} = 1.8 nm and (d) t_{Cu} = 3.2 nm] GMR SV-MLs (scanning direction was from bottom to top) at the current density of J = 6×10^6 A/cm^2 for 12 hours. XTEM images shown in Fig. (e) through (h) corresponding to the samples analyzed in Fig. (a) through (d), respectively.

XTEM and EDX analysis shown in Fig. 5.5 give strong evidence that the EM-induced Cu inter-diffusion through the NiFe/Cu interfaces is the main reason for the magnetic degradation of electrically stressed NiFe/Cu/NiFe SV-MLs at J = 6×10^6 A/cm^2. As can be seen in Fig. 5, even though no apparent EIFs such as voids or hillocks were observed in the XTEM images due to their incomplete lifetime, considerably large amount of EM-induced Cu inter-diffusion into the bottom NiFe layer was clearly confirmed by EDX in the NiFe/Cu/NiFe (Fig. 5-(a) and (c)), but not in the NiFe/Co/Cu/Co/NiFe SV-MLs (Fig. 5-(b) and (d)). For the clear observation of Ni-Cu intermixing mostly occurring toward the bottom NiFe and more serious Cu diffusion to the bottom NiFe, it is thought to be due to the natural oxidation and

possibly formed NiFexOy insulator on the surface of top NiFe, which resulted in inducing more shunting current into the bottom NiFe and to give rise to the passivation effects against electromigration to the top NiFe.

5.4 Summary and Conclusions

EM-induced magnetic failures in NiFe/(Co)/Cu/(Co)/NiFe GMR SV-MLs have been investigated to estimate the magnetic stability of GMR SV-MLs. It was clearly confirmed that EM-induced Cu inter-diffusion or failure is the most fatal problem to give rise to the magnetic degradation of NiFe/Cu/NiFe based GMR SV-MLs under electrical stressing. However, an ultra thin Co diffusion barrier inserted at the NiFe/Cu interfaces was found to be promisingly effective to improve the magnetic stability of NiFe/Cu/NiFe based SV-MLs against electromigration due to its significant blocking effects on Cu inter-diffusion.

References

Bae, S., Tsu, I.F., Davis, M., Murdock, E.S., and Judy, J.H. (2002). Electromigration study of magnetic thin films for the electrical reliability of spin-valve read heads. IEEE Trans. Magn. 38, 2655-2657.

Binasch, G., Grünberg, P., Saurenbach, F., and Zinn, W. (1989). Enhanced magnetoresistance in layered magnetic structures with antiferromagnetic interlayer exchange. Phys. Rev. B **39**, 4828-4830.

Bruno, P., and Chappert, C. (1991). Oscillatory coupling between ferromagnetic layers

separated by a nonmagnetic metal spacer. Phys. Rev. Lett. **67**, 1602-1605.

Daughton, J.M. (1992). Magnetoresistive memory technology. Thin Solid Films **216**, 162-168.

Dutcher, J.R., Heinrich, B., Cochran, J.F., Steigerwald, D.A. and Egelhoff Jr., W.F. (1988). Magnetic properties of sandwiches and superlattices of fcc Fe(001) grown on Cu(001) substrates. J. Appl. Phys. **63**, 3464-3466.

Egelhoff, W., Chen,P., Powell,C., Stiles,M., McMichael,R. (1996). Growth of giant magnetoresistance spin valves using indium as a surfactant. J. Appl. Phys. **79**, 2491-2496.

Ene, C.B., Schmitz, G., Kirchheim, R., and Hütten, A. (2005). Stability and thermal reaction of GMR NiFe/Cu thin films. Acta Mater. **53**, 3383-3393.

Grünberg, P., Schreiber, R., Pang, Y., Brodsky, M.B., and Sowers, H. (1986). Layered magnetic structures: evidence for antiferromagnetic coupling of Fe layers across Cr interlayers. Phys. Rev. Lett. **57**, 2442-2445.

Gurney, B.A., Speriosu, V.S., Wilhoit, D.R., Lefakis, H., Fontana, R.E., Jr., Heim, D.E., and Dovek, M. (1997). Can spin valves be reliably deposited for magnetic recording applications? (Invited) J. Appl. Phys. **81**, 3998-4003.

Hecker, M., Tietjen, D., Wendrock, H., Schneider, C.M., Cramer, N., Malkinski, L., Camley, R.E., and Celinski, Z. (2002). Annealing effects and degradation mechanism of NiFe/Cu GMR multilayers. J. Magn. Magn. Mater. **247**, 62-69.

Hartmann, U. (1999). Magnetic Multilayers and Giant Magnetoresistance: Fundamentals and Industrial Applications. (Berlin: Springer), 184-190.

Jiang, J., Bae, S., and Kim, S.W. (2007). Effects of Cu inter-diffusion on the electromigration failure of FM/Cu/FM tri-layers for spin valve read sensors. IEEE Trans. Magn. **43**, 2836-2838.

Jiang, J., Bae, S. and Ryu, H.J. (2008). Magnetic instability of giant magnetoresistance spin-valve MLs due to electromigration-induced inter-diffusion. IEEE Trans. Dev. Mater. Reliab. **8**, 680-688.

Kools, J., Rijks, T., Veirman, A., Coehoorn, R. (1995). On the ferromagnetic interlayer coupling in exchange-biased spin-valve multilayers. IEEE Trans. Magn. **31**, 3918-3920.

Leal, J.L., Kryder, M.H. (1996). Oscillatory interlayer exchange coupling in $Ni_{81}Fe_{19}$/Cu/$Ni_{81}Fe_{19}$/$Fe_{50}Mn_{50}$ spin valves. J. Appl. Phys. **79**, 2801.

Massalski, T.B., Okamoto, H., Subramanian, P.R., and Kacprzak, L. (1990). Binary Alloy Phase Diagrams 2nd edn (Materials Park, OH: ASM International), p. 1182, p. 1444.

Neamtu, J., Volmer, M., and Coraci, A. (1999). Magnetoresistive properties and microstructure of NiFe thin films and NiFe(t)/Cu(s)/NiFe(t) multilayer films Thin Solid Films **343-344**, 218-221.

Parra, R.E., and Medina, R. (1980). Magnetic-environment model of Ni-Pt and Ni-Pd alloys. Phys. Rev. B **22**, 5460-5470.

Reiss, G., Brückl, H., Hütten, A., Schmalhorst, J., Justus, M., Thomas, A., and Heitmann, S. (2003). Spintronics and its applications. Phys. Stat. Sol. (b) **236**, 289-302.

Williams, E.M. (2001). Design and Analysis of Magnetoresistive Recording Heads. (New York: John Wiley & Sons, Inc.), p. 34-35.

van Loyen, L., Elefant, D., Tietjen, D., Schneider, C.M., Hecker, M., and Thomas, J. (2000). Annealing of $Ni_{80}Fe_{20}$/Cu and Co/Cu multilayers**.** J. Appl. Phys. **87**, 4852-4854.

CHAPTER 6 EFFECTS OF CONTROLLING ELECTROMIGRATION-INDUCED INTER-DIFFUSION ON THE MAGNETIC AND ELECTRICAL STABILITY OF GMR SPIN-VALVE DEVICES

6.1. Introduction and Motivations

NiFe/Cu/NiFe($Ni_{81}Fe_{19}$)/(Mn-based anti-ferromagnetic layer, Mn-AFM) exchange biased GMR (EBGMR) spin-valves (SV) have been paid considerable attention in the various metallic spintronics devices such as a GMR magnetic read sensor and an in-vitro GMR biosensor (Parkin,1994; Wang, 2008; Daughton, 1992) due to a high sensitivity at a low switching magnetic field and an extremely small hysteresis (Parkin,1992). However, as the device size has been dramatically scaled-down to achieve an extremely high information storage density and to realize an ultra large scale integrated sensor array, the operating current density allowing for a reasonably high SNR (Signal-to-Noise Ratio) is subsequently increased beyond $J = 1 \times 10^8$ A/cm^2 (Childress, 2005). This abruptly increased operating current density gives rise to a severe reliability problem relevant to the magnetic (Jiang, 2009) and electrical (Kos, 1997) degradation of NiFe/Cu/NiFe/FeMn based EBGMR SV spintroincs devices (SVSDs) primarily due to EM and thermally-induced inter-diffusion, thermomigration (TM), across the GMR SV multi-layer (ML) interfaces driven by the temperature gradient resulted from the different film resistivity of each layer (Huang, 1993; Zeng, 2009). In particular, as the EM and TM accelerated Cu inter-diffusion at the

NiFe/Cu/NiFe interfaces and the Mn atomic inter-diffusion induced at the NiFe/Mn-AFM interface have been demonstrated to be the main physical reasons for the MR and magnetic degradation of NiFe/Cu/NiFe/Mn-AFM EBGMR SVSDs (Jiang, 2009; Anderson, 2000; Saito, 1998), the research activities to find a promising solution for effectively controlling the Cu spacer inter-diffusion as well as to explore its physical effects on the Mn atomic inter-diffusion behavior under high current densities are urgently required to achieve high electrical and magnetic stability of NiFe/Cu/NiFe/Mn-AFM based GMR SVSDs for advanced spintronics applications.

In this study, we present the effects of controlling Cu spacer inter-diffusion by Co and $Co_{90}Fe_{10}$ diffusion barriers, which are inserted at the NiFe/Cu interfaces, on the EM and TM-induced electrical and magnetic degradation of NiFe/Cu/NiFe/Mn-AFM based GMR SVSDs operating at the high current densities ranging from $J = 2.5 \times 10^7$ A/cm^2 to $J = 9 \times 10^7$ A/cm^2. The main reason for choosing Co and CoFe as the diffusion barrier to control the Cu spacer inter-diffusion is that they have both a very limited solid solubility with Cu, e.g. below 1 at.% of Cu inter-mixing with Co up to 400 °C (Massalski, 1990), and a higher activation energy than that of NiFe and Cu thin films (Bae, 2002)**.** The effects of diffusion barrier on the EM and TM-induced Cu spacer inter-diffusion behavior was first studied from the patterned NiFe/(Co)/Cu/(Co)/NiFe magnetic multi-layered devices (MMLD). In order to verify the physical effects of Co diffusion barrier on the EM and TM-induced failure lifetime and the magnetic degradation occurred in the patterned NiFe/(Co)/Cu/(Co)/NiFe MMLDs, the Cu inter-diffusion behavior through NiFe/Cu interfaces was explored by

changing the Co insertion layer thickness from 0 to 0.9 nm. In addition, the EM and TM accelerated Cu spacer inter-diffusion behavior and its physical correlation with the EM and TM-induced failure characteristics of the patterned MMLDs with or without Co diffusion barrier were analyzed and confirmed by using a nano-beam energy dispersive X-ray analysis (EDX), and a cross sectional transmission electron microscopy (XTEM), respectively. After investigating the effects of controlling Cu spacer inter-diffusion on the EM and TM-induced electrical and magnetic stability of the MMLDs, its physical effects on the magnetic degradation, particularly the variation of both GMR performance relevant to interfacial spin dependent scattering and exchange bias field associated with the acceleration or deceleration of Mn atomic inter-diffusion, were further studied using Si/Ta/NiFe/Cu/NiFe/FeMn/Ta based EBGMR top SVSDs (TSVSD). The TSVSDs were electrically stressed under the applied D.C. current density of $J = 2.5\times10^7$ A/cm^2 (I = 16.5 ~ 17.25 mA) at ambient temperature and two diffusion barriers, Co and $Co_{90}Fe_{10}$, were inserted at the NiFe/Cu interfaces, i.e. NiFe/Cu/NiFe/FeMn (denoted by NiFe-TSVSD), NiFe/Co/Cu/Co/NiFe/FeMn (denoted by Co-TSVSD) and NiFe/CoFe/Cu/CoFe/NiFe/FeMn (denoted by CoFe-TSVSD), respectively.

6.2 Experimental Works

All the NiFe(3.0-t)/Co(t)/Cu(2)/Co(t)/NiFe(3.0-t nm) magnetic MLs and the Ta(4.5)/NiFe(3.3)/[Co(0.77) or CoFe(0.77)]/Cu(2.4)/[Co(0.77) or CoFe(0.77)]/NiFe(3.3)/FeMn(15)/Ta(4.5 nm) EBGMR top SV-MLs were deposited on

the Si (100) substrate using a D.C. magnetron sputtering. The Ar working gas pressure during deposition was kept at 2 mTorr. The magnetic MLs as well as the EBGMR top SV-MLs were patterned using standard electron beam lithography (EBL) and a photolithography. The patterned MMLDs and the EBGMR SVSDs have geometry of 2μm - width and 20 μm - length (see the inset in Fig. 1) The detailed testing conditions, test structure fabrication procedures, and the definition of TTF and MTTF has been described in Chapter 3. The activation energy, "E_a", directly related to the EM and TM-induced inter-diffusion process of the devices was obtained based on the "Black equation" (Black, 1969) given by Eq. 6-1 by measuring the failure lifetime at various temperature from ambient temperature (R.T) to 280 °C.

$$MTTF = A\frac{1}{j^n}\exp(\frac{E_a}{kT}) \tag{6-1}$$

In addition, the current density factor, "n", value describing the contribution of joule heating to the EM and TM-induced failures was determined from the slope of a plot ln (J) vs. ln (MTTF) at ambient temperature by changing the applied current density. The magnetic and the GMR properties of the patterned MMLDs and the EBGMR SVSDs were measured using a vibrating sample magnetometer (VSM), and a computer controlled micro-probe station, respectively. A high resolution of transmission electron microscope (HR-TEM) was used to analyze the EM and TM-induced failures of the ML as well as the EBGMR SVSDs and an EDX (with a nominal beam size of 2 nm attached to this TEM) depth profiling was employed to study the EM and TM-induced Cu spacer inter-diffusion behavior and the degree of Ni-Cu intermixing of the electrically stressed MMLDs.

6.3 Results and Discussion

6.3.1 Dependence of Lifetime on the Co Diffusion Barrier Thickness

Figure 6.1 shows the dependence of TTF and MTTF on the Co diffusion barrier thickness in the patterned Si/NiFe(3.0-t)/Co(t)/Cu(2)/Co(t)/NiFe(3.0-t nm) [t = 0 ~ 0.9 nm] MMLDs. As can be clearly seen in Fig. 6.1, the MTTF of patterned Si/NiFe(3.0-t)/Co(t)/Cu(2)/Co(t)/NiFe(3.0-t nm) MMLDs determined at the applied D.C. current density of J = 7×10^7 A/cm^2 was drastically increased from 7.28 hours (t_{Co} = 0 nm) to 50.68 hours (t_{Co} = 0.9 nm). In addition, it was clearly observed that the patterned Si/NiFe(3.0-t)/Co(t)/Cu(2)/Co(t)/NiFe(3.0-t nm) MMLDs with t_{Co} > 0.5 nm have a high magnetic stability, i.e. no severe change of saturation magnetic moment and interlayer coupling field (Jiang, 2009). Even though the TTF was increased by increasing the Co diffusion barrier thickness, the distinct improvement of TTF was observed when the Co thin film has a thickness beyond 0.5 nm. This indicates that at least two mono layers of Co atoms are essentially required to make an effective diffusion barrier to block the EM and TM-induced Cu spacer inter-diffusion to the NiFe magnetic layers as well as to build up a stable crystalline structure of Co, which can contribute to the improvement of activation energy, E_a, in the Si/NiFe(3.0-t)/Co(t)/Cu(2)/Co(t)/NiFe(3.0-t nm) MMLDs.

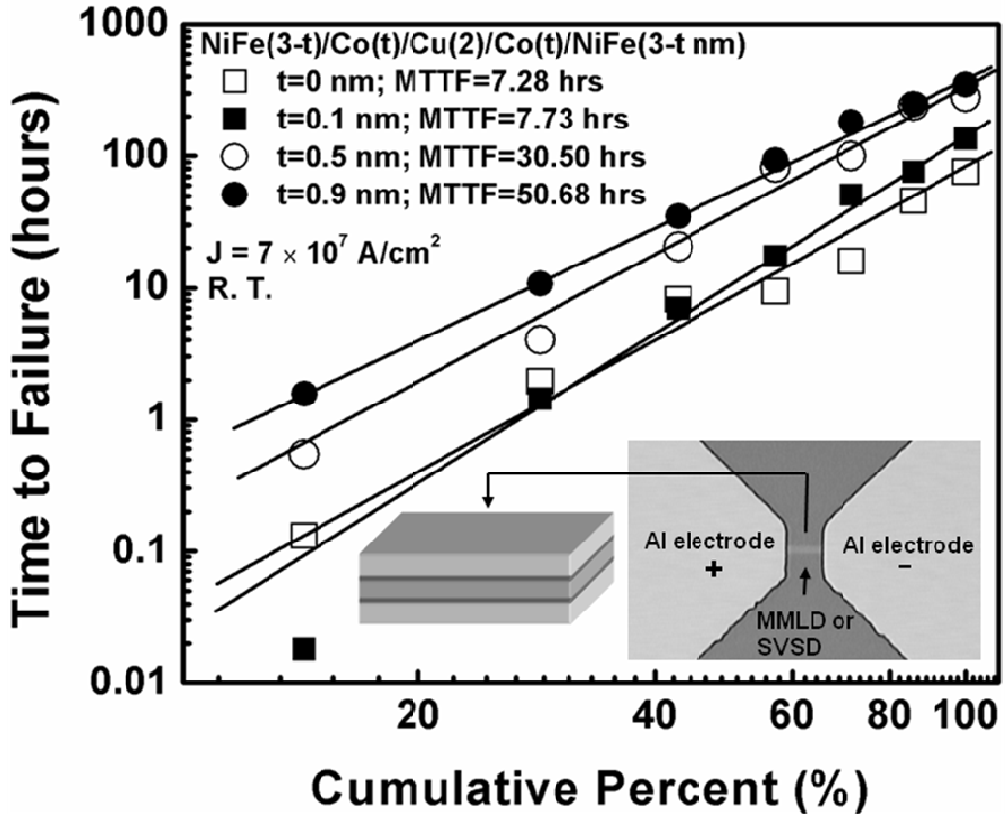

Fig. 6-1 Time-to-failure (TTF) vs. cumulative percent of Si/NiFe(3-t)/Co(t)/Cu(2)/Co(t)/NiFe(3-t nm) [t = 0~0.9 nm] MMLDs under the applied D.C. constant current density of 7×10^7 A/cm^2 at AMBIENT TEMPERATURE. [The insert is the top-view image of the MMLDs (or EBGMR SVSDs) as well as the cross-sectional MMLDs (or EBGMR SVSDs) structure]

6.3.2 Activation Energy and Current Dependence Factors

In order to quantitatively verify the effects of Co diffusion barrier on the control of Cu spacer inter-diffusion directly relevant to the EM and TM-induced failures of NiFe/(Co)/Cu/(Co)/NiFe MMLDs, the E_a, describing the inter-diffusion behavior, was determined by plotting a ln (MTTF) vs. (1000/T) plot as shown in Fig. 6.2. The applied current density to determine E_a was kept at J= 5×10^7 A/cm^2 and the temperature was changed from AMBIENT TEMPERATURE to 280 °C. The E_a value for the NiFe(3)/Cu(2)/NiFe(3 nm) MMLDs was determined at 0.52 ± 0.2 eV, which lies within the range of E_a value for the Cu (0.5 ± 0.3 eV) single layered thin films (Bae, 2002).

While, the NiFe(2.5)/Co(0.5)/Cu(2)/Co(0.5)/NiFe (2.5 nm) MMLDs had a significantly enhanced E_a value of 1.17 ± 0.16 eV, which lies in between that of NiFe (0.8 ± 0.15 eV) and Co (1.4 ± 0.2eV) single layered thin films (Bae, 2002). The remarkably increased E_a value close to that of NiFe or Co thin film directly implies that the EM and TM-induced failure mechanism of the MMLDs with a 0.5 nm Co diffusion barrier is dominantly determined by either the EM and TM-induced failure of the Co or NiFe thin films instead of EM and TM-induced Cu inter-diffusion. This result strongly demonstrates that controlling of EM and TM-accelerated Cu spacer inter-diffusion behavior by the Co diffusion barrier plays a critical role in characterizing the magnetic and electrical stability of NiFe(2.5)/Co(0.5)/Cu(2)/Co(0.5)/NiFe (2.5 nm) MMLDs operated at high current densities.

The "n" value of the Si/NiFe/(Co)/Cu/(Co)/NiFe MMLDs in the "Black equation" (Black, 1969) was determined from the slope of a plot ln (MTTF) vs. ln (J) at ambient temperature. The applied D.C. current density was varied from J = 5×10^7 to 9×10^7 A/cm^2 at AMBIENT TEMPERATURE As shown in Fig. 6.3, the MTTF of NiFe(2.5)/Co(0.5)/Cu(2)/Co(0.5)/NiFe (2.5 nm) MMLDs was monotonically decreased by increasing the current density and the "n" value graphically determined was 6.1, which is a larger than that of NiFe(3)/Cu(2)/NiFe(3 nm) MMLD. The large "n" value indicates that the contribution of joule heating and the correspondingly accelerated EM and TM-induced Cu inter-diffusion to the device failures is very limited. Thus, the

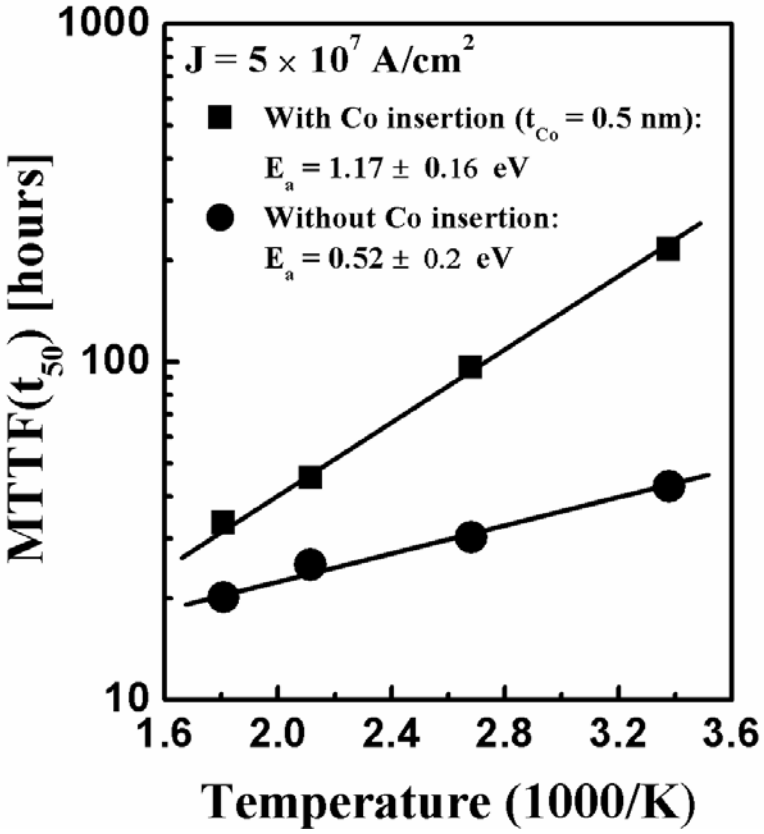

Fig 6.2 MTTF vs. (1000/T) plot for the Si/NiFe(3-t)/Co(t)/Cu(2)/Co(t)/NiFe(3-t nm) MMLDs [t = 0 or 0.5 nm] to determine the activation energy value, E_a.

NiFe(2.5)/Co(0.5)/Cu(2)/Co(0.5)/NiFe (2.5 nm) MMLDs have a high thermal and electrical stability even at the applied D.C. current density beyond J = 1×10^8 A/cm^2. In contrast, the NiFe(3)/Cu(2)/NiFe(3 nm) MMLDs had a very small as well as discrete "n" values depending on the applied D.C. current density. The "n" value determined at the low current density region below J = 7 × 10^7 A/cm^2 was 5.4. However, the "n" value determined at the high current density region above below J = 8 × 10^7 A/cm^2 was 1.3, which is very small similar to those obtained from Al (n = 1.5) (Attardo, 1970) and Al-1%Si, or Al-0.5%Si-0.5%Cu (n = 1.7) (Danso, 1981). The discrete and small "n" value at the applied current density beyond J = 8 × 10^7 A/cm^2 demonstrates that the

EM and TM-accelerated Cu inter-diffusion at the NiFe/Cu interfaces due to the high temperature gradient resulted from the suddenly increased joule heating in the Cu spacer is dominantly responsible for the electrical and magnetic degradation of NiFe(3)/Cu(2)/NiFe(3 nm) MMLDs.

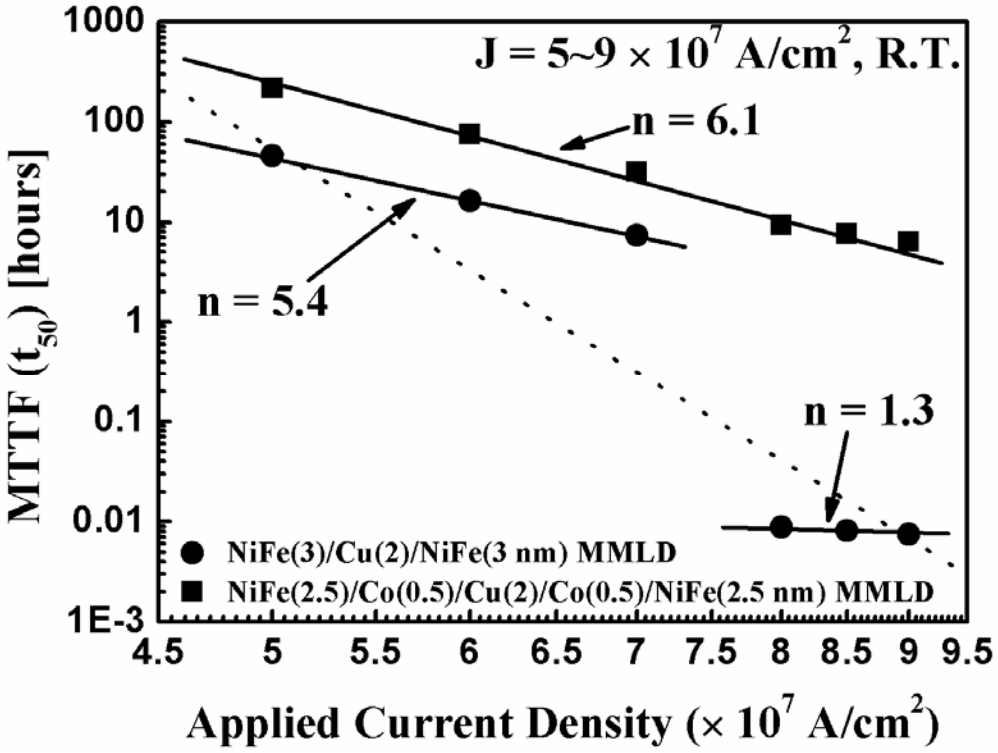

Fig. 6.3 ln (MTTF) vs. ln (J) plots of Si/NiFe(3-t)/Co(t)/Cu(2)/Co(t)/NiFe(3-t nm) MMLDs [t = 0 or 0.5 nm] to determine the "n" value. The applied current density was changed from J = 5×10^7 A/cm^2 to J = 9×10^7A/cm^2 at ambient temperature.

6.3.3 Current Shunting Path and Self-healing Process Model

The physical mechanisms responsible for the higher electrical stability of NiFe/Co/Cu/Co/NiFe MMLDs can be explained by considering physical models based on current transport theory in magnetic MLs (Hartmann, 1999) and inter-diffusion mechanism: (1) current shunting path model, and (2) self-healing process model. To interpret the current shunting path model, two physical prerequisites, which are the

lower activation energy of Cu compared to that of NiFe or Co (Bae, 2002) and the "current sinking effects" describing that more than 2/3 of applied current would flow through the Cu spacer in the NiFe/(Co)/Cu/(Co)/NiFe MMLDs due to the film resistivity difference between the NiFe (or Co) and Cu layers, should be considered (Gurney, 1997). According to Zhang's report (Zhang, 2006) and Chang's calculation (Chang, 2003), the suddenly increased local temperature at a void site due to the "current crowding effect" would be high enough to cause the local melting of Cu spacer in the NiFe/Cu/NiFe MMLDs. At this situation, if there is no diffusion barrier, the melted Cu atoms due to the suddenly increased joule heating would rapidly migrate to form Cu-Ni intermixing regions both in the NiFe layer and at the NiFe/Cu interfaces due to a high solid solubility between the Cu and Ni atoms (Massalski, 1990). These Ni-Cu intermixing regions provide shunting current paths to diverge from the Cu spacer towards the NiFe layers because of their lower electrical resistivity than that of pure NiFe thin films. In addition, the subsequently increased current density in the NiFe layers due to the increase of Ni-Cu intermixing shunting paths leads to accelerating EM-induced failures of NiFe layers resulting in the magnetic degradation as well as the shorter lifetime of NiFe/Cu/NiFe MMLDs (Jiang, 2009; Kos, 1997). In contrast, for the NiFe/Co/Cu/Co/NiFe MMLDs, the current density in the NiFe/Co layers under the electrical stressing would be almost constant due to the very limited Ni-Cu intermixing current shunting paths resulted from the restrained Cu spacer inter-

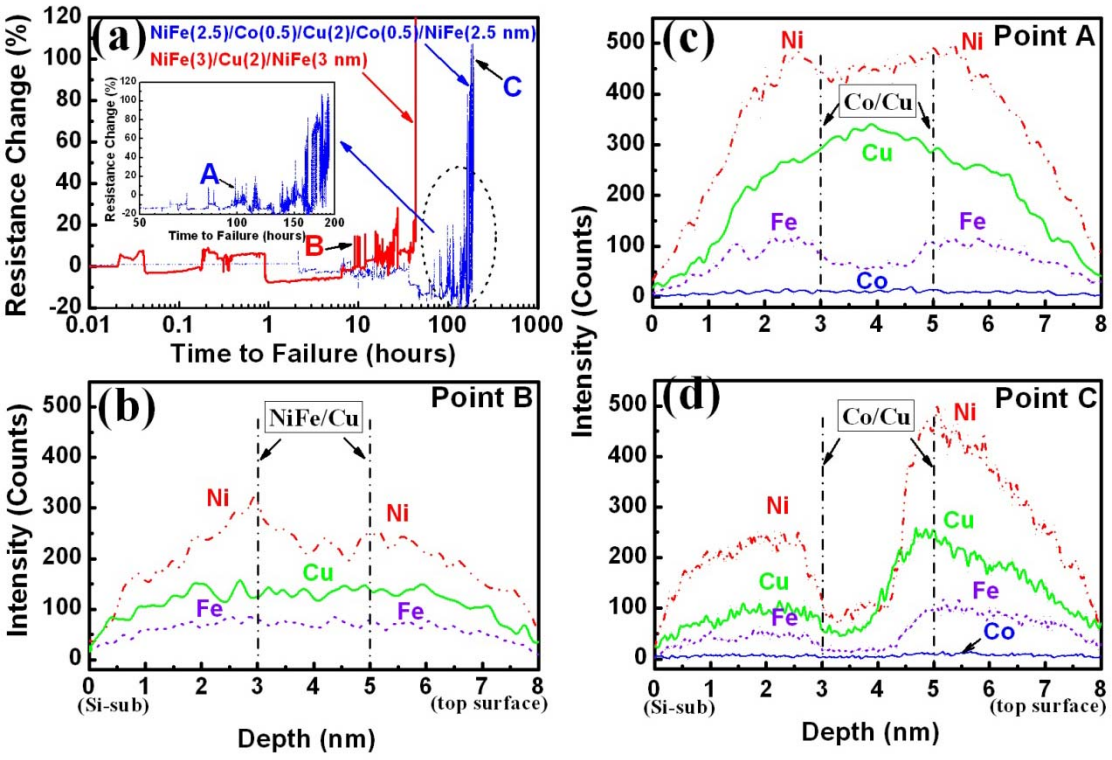

Fig. 6.4 (a) Resistance vs. electrical stressing time (R-t) curves for the Si/NiFe(2.5)/Co(0.5)/Cu(2)/Co(0.5)/NiFe(2.5 nm) MMLDs. The applied D.C. current density was fixed at J = 5 × 10^7 A/cm^2, at ambient temperature. Figures (b)~(d) show the EDX depth profiles for the electrically stressed MMLDs corresponding to the different TTFs indicated in Fig. 4-(a) [(b) t_{Co} = 0 nm, point B; (c) t_{Co} = 0.5 nm, point A; (d) t_{Co} = 0.5 nm, point C].

diffusion controlled by the Co diffusion barrier. By considering this different "current shunting path modality" directly relevant to the EM and TM-induced Cu inter-diffusion behavior, it can be understood that the NiFe/Co/Cu/Co/NiFe MMLDs would have much higher electrical and magnetic stability than that of NiFe/Cu/NiFe MMLDs.

Another reason is regarded to the "self-healing process model". Figure 6.4 shows the resistance vs. time (R-t) curves and the nature of Cu spacer inter-diffusion behavior, which is determined using an EDX depth profiling, of the MMLDs with and without 0.5-nm-thick Co diffusion barrier. As shown in Fig. 6.4(a) (indicated by the point A and B), the time for 10 % resistance change, which is generally considered as the TTF

for the GMR magnetic recording read sensors, of the MMLDs with, and without 0.5-nm-thick Co diffusion barrier was 9.7 and 98.6 hours, respectively. In addition, the NiFe(2.5)/Co(0.5)/Cu(2)/Co(0.5)/NiFe(2.5 nm) MMLDs exhibited an obvious resistance fluctuation before reaching the complete EM and TM-induced failures (see the inset of Fig. 6.4(a)). The resistance fluctuation indicates that the Cu spacer is undergoing an alternative electrical open (resistance increase) and electrical short, reconnection, (resistance decrease) process (Zhang, 2007) during applying the electrical stress. If the EM and TM-induced slit or crack voids are rapidly propagated along the Cu spacer under a high D.C. current density, it leads to completely break or melt the Cu spacer resulting in less current flowing into the Cu spacer. Thus, the melted Cu spacer would be quenched due to the suddenly dropped joule heating caused by the electrically opened Cu spacer (Sun, 2002). However, during this quenching process, the migration of locally melted Cu atoms to the NiFe layers is strictly limited by the two Co diffusion barriers so that they could be solidified and subsequently make reconnection. At this situation, the device resistance of NiFe(2.5)/Co(0.5)/Cu(2)/Co(0.5)/NiFe(2.5 nm) MMLDs would almost revert to the original value and maintain until the reconnected Cu spacer is re-opened by the EM and TM-induced failures at the same current density. This “self-healing process” of Cu spacer induced by the Co diffusion barrier would be continued until the NiFe/Co layers are electrically and completely opened by the EM and TM-induced failures. This process eventually leads to the apparent improvement of electrical and magnetic (Jiang, 2009) stability of NiFe(2.5)/Co(0.5)/Cu(2)/Co(0.5)/NiFe(2.5 nm) MMLDs. The EDX

depth profiles of MMLDs electrically stress for the time of 10% resistance change) shown in Figs. 6.4(b) and (c) clearly demonstrate that the Co diffusion barrier successfully controls the Cu atomic inter-diffusion to the NiFe layers resulting in reducing the Ni-Cu intermixing as well as in inducing the Cu spacer "self-healing process".

6.3.4 Interfacial Analysis of Electrically Stressed NiFe/(Co)/Cu/(Co)/NiFe MMLDs

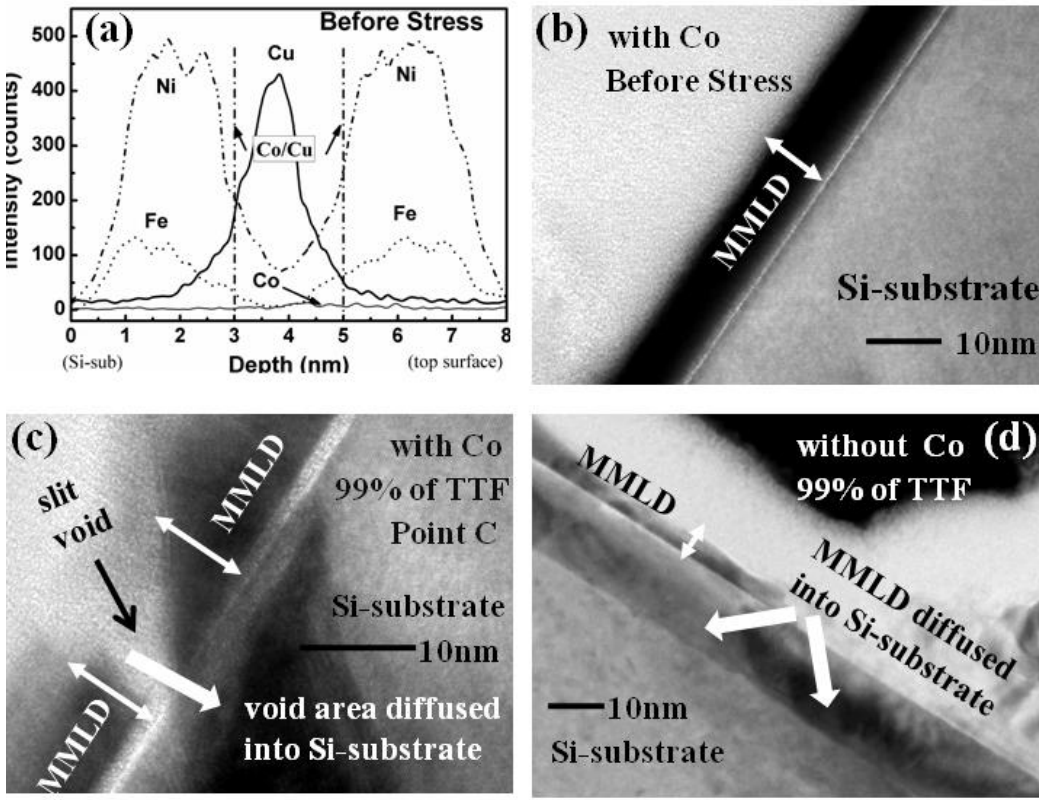

Fig. 6.5 (a) EDX depth profile of the Si/NiFe(2.5)/Co(0.5)/Cu(2)/Co(0.5)/NiFe(2.5 nm) MMLD before applying electrical stress and XTEM images for: (b) Si/NiFe(2.5)/Co(0.5)/Cu(2)/Co(0.5)/NiFe(2.5 nm) MMLD before applying electrical stress, (c) Si/NiFe(2.5)/Co(0.5)/Cu(2)/Co(0.5)/NiFe(2.5 nm) MMLD at 99.9 % of TTF, electrically stressed under the current density of $J = 5 \times 10^7$ A/cm^2 at ambient temperature, and (d) Si/NiFe(3)/Cu(2)/NiFe(3 nm) MMLD at 99.9% of TTF, electrically stressed under the current density of $J = 5 \times 10^7$ A/cm^2, ambient temperature.

Figures 6.5(c), and (d) show the XTEM images of completely failed MMLDs with and without Co diffusion barriers. As clearly seen in Fig. 6.5(c) and (d), the NiFe/Cu/NiFe MMLD was mostly diffused into the Si substrate at its final failure stage, while the NiFe/Co/Cu/Co/NiFe MMLD showed a typical slit void failure. The gradual inter-diffusion of NiFe/Cu/NiFe MMLD under the electrical stress indicates that the NiFe/Cu/NiFe MLs were possibly changed into a single layered Ni-Cu-Fe alloy after the EM and TM-induced Ni-Cu inter-diffusion (or intermixing). The rapidly increased local temperature due to the suddenly increased current density induced by the reduction of film thickness accelerates the inter-diffusion of Ni-Cu-Fe alloy to the Si substrate due to a high solid solubility of Cu-Si (Massalski, 1990). In contrast, although the Co diffusion barrier remarkably enhanced the EM and TM-induced failure lifetime of NiFe/(Co)/Cu/(Co)/NiFe MMLDs due to the effective blocking of Cu inter-diffusion, the EM and TM-induced voids (or cracks) in the Cu spacer cannot be reversibly recovered during the “self-healing process”. The stress-induced lattice expansion during solidification of melted Cu atoms would create undesirable defects at the Cu and Co diffusion barrier interfaces. The small amounts of Cu atoms inter-diffused through the defects possibly induce Ni-Cu intermixing in the NiFe layers, which is considered as the prime path of shunting current from the Cu spacer to the NiFe/Co layers. This possible failure mechanism eventually results in the formation of a local slit void (or crack) due to the EM and TM-induced failures in the Co/NiFe layers after electrically stressing such a long time as clearly shown in both the EDX spectrum (Fig. 6.4(d)) and the XTEM image (Fig. 6.5(c)).

6.3.5 Effect of FM/Cu interfaces on the Magnetic Degradation

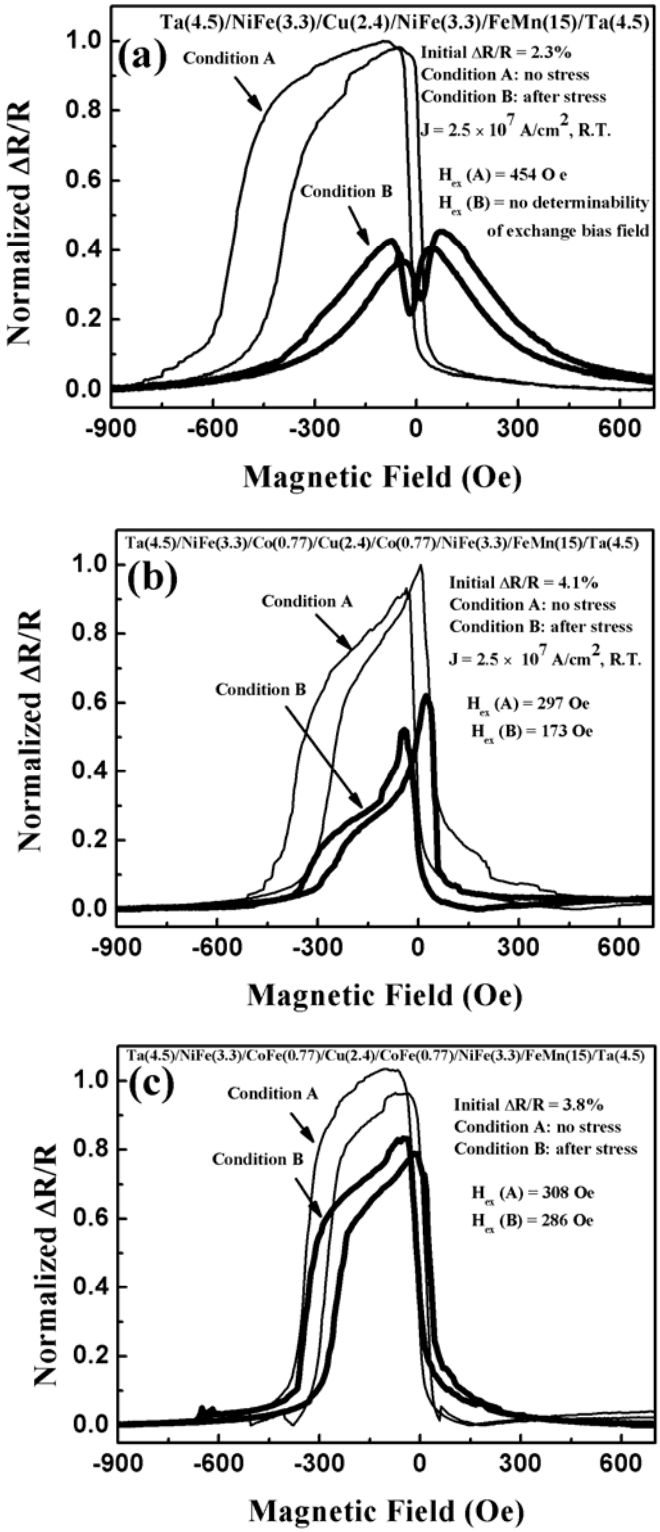

Fig. 6.6 Normalized MR curves (R-H curves) of top FeMn EBGMR SVSDs before and after electrically stressed. (a) NiFe-TSVSD, (b) Co-TSVSD, and (c) CoFe-TSVSD. A J = 2.5 × 10^7 A/cm^2 of D.C. constant current density was applied to the SDSDs for 9 hours at ambient temperature.

After verifying that controlling of EM and TM-induced Cu spacer inter-diffusion is the most critical factor in characterizing the electrical and magnetic stability of MMLDs, the FeMn EBGMR SVSDs with NiFe/Cu/NiFe based MLs were employed to explore the effects of controlling EM and TM-induced Cu spacer inter-diffusion on the magnetic degradation, especially to find out its physical effects on the acceleration or deceleration of Mn atomic inter-diffusion, and the variation of interfacial spin dependent scattering that are relevant to the exchange bias field, and the GMR performance, respectively. Three kinds of top EBGMR SVSDs, e.g. NiFe-TSVSDs, Co-TSVSDs and CoFe-TSVSDs, were compared to study the GMR performance and other magnetic properties.

Figure 6.6 shows the normalized MR curves (R-H curves) for the three top EBGMR SVSDs electrically stressed for 9 hours under the applied current density of $J = 2.5 \times 10^7$ A/cm^2 ($I = 16.5 \sim 17.25$ mA) at ambient temperature. As can be clearly seen in Fig. 6.6(a), the NiFe-TSVSD showed a severe magnetic degradation, i.e. almost zero exchange bias field (only showed a magnetic coercivity difference between NiFe free and NiFe pinned layers) and a 54 % of MR degradation. In contrast, the Co-TSVSD (Fig. 6.6(b)), and CoFe-TSVSD (Fig. 6.6(c)) showed a relatively small reduction in both GMR ratio (38 %, and 19 %, respectively), and exchange bias field (42 %, and 7 %, respectively). The remarkably improved magnetic stability of Co-TSVSD and CoFe-TSVSD compared to that of NiFe-TSVSD can be elucidated by considering two physical factors, which are closely relevant to the EM and TM-induced Cu spacer inter-diffusion: (1) the reduced Mn atomic inter-diffusion through NiFe/FeMn interface,

and (2) the improved interfacial spin dependent scattering at the Cu/(Co, CoFe)/NiFe interfaces. Figure 6.7(a) shows the temperature distribution profiles of NiFe-TSVSDs before and after electrical stress at J = 2.5 × 10^7 A/cm^2. The temperature distribution profiles were numerically calculated by considering the thermally-induced mass transport models and all the experimentally determined physical parameters (Zeng, 2009). The change of electrical resistivity of NiFe pinned layer due the Cu spacer inter-diffusion was determined from the EDX depth profiling results. Around 0.5 nm thick Cu spacer was approximately inter-diffused into the NiFe to form Ni-Cu intermixing (Brückner, 2000).

6.3.6 Theoretical Prediction of the Temperature Gradient and Mn Atomic Flux

In order to analyze the different temperature rise and current distribution inside the TSVSDs, 3D electrical-thermal calculations of GMR SV devices were done using a numerical finite element method by solving following equations:

$$\nabla \bullet J = 0$$

$$J = -\sigma \nabla \phi \tag{6-2}$$

and Joule's law of heating

$$Q = \sigma (\nabla \phi)^2 \tag{6-3}$$

where σ is the electrical conductivity and ϕ is the electric potential. The electrical conductivity is temperature dependent as it is described in Eq. (6-4).

$$\sigma(T) = \frac{\sigma_0}{1 + \alpha T} \tag{6-4}$$

where σ_0 is the electrical conductivity at ambient temperature (300 K) and α is the temperature coefficient of resistivity (TCR). The temperature profiles of CIP and CPP GMR SV read sensor were extracted from the central region (0, 0, Z) of the GMR TSVSDs, where Z was varied from the bottom to the top of the device. The temperature gradient, ∇T , generated in the TSVSD is defined as $\partial T / \partial x$. Because of this temperature gradient, the total atomic flux of thermally induced inter-diffusion, thermomigration (TM) can be calculated using Eq. (6-5) (Ragone, 1995).

$$J_{TM} = N_a v_{TM} = -\frac{N_a D(T) Q^*}{kT^2} \nabla T \tag{6-5}$$

where Q^* is the heat of transport, N_a is the atomic concentration, $D(T)$ is the diffusivity, and k is the Boltzman constant. The thermal energy change by the driving force of TM in an atomic jump distance (d) can be expressed as in Eq. (6-6) (Huang, 2006).

Figure 6.7 shows the temperature distribution profiles of top FeMn EBGMR SVSDs numerically calculated based on the above thermally-induced mass transport models. As can be seen in Fig. 6.7(a), the temperature at the NiFe/FeMn interface was increased from 313.99 K (before electrical stressing, no EM and TM-induced Cu inter-diffusion) to 315.54 K (after electrical stressing for 9 hours, EM and TM-induced Cu inter-diffusion). Correspondingly, the increased temperature gradient from 20.5 °C/μm to 24.4 °C/μm led to the increase of Mn atomic flux across the NiFe/FeMn interface from 8.39×10^{11} $m^{-2}s^{-1}$ to 1.23×10^{12} $m^{-2}s^{-1}$. These results demonstrate that the controlling of Cu spacer inter-diffusion obviously influence on the control of Mn atomic inter-diffusion because it can directly control the degree of NiFe film resistivity

resulting in the change of SVSD temperature as well as the temperature gradient at the NiFe/FeMn interface. It is well known that the interfacial exchange energy formed at the NiFe/FeMn interface depends on the exchange stiffness of FeMn layer, which is closely relevant to the Mn atomic concentration.(Skomski, 2008) By considering this physical concept, the severe reduction of exchange bias field observed from the electrically stressed NiFe-TSVSDs can be understood that this is resulted from the degradation of exchange stiffness in the FeMn pinning layer due to the reduction of Mn concentration accelerated by the EM and TM-induced Cu spacer inter-diffusion. In addition, the degradation of NiFe magnetic properties due to the inter-diffusion induced Mn and Cu atomic mixtures with Ni atoms would be thought to be another physical reason responsible for the reduction of exchange bias field.

In contrast, as can be seen in Fig. 6.7(b), the Co-TSVSD, and the CoFe-TSVSD under the same electrical stressing conditions showed a lower temperature gradient of 22.4 °C/μm, and 16.9 °C/μm, respectively at the NiFe/FeMn interface and correspondingly, a smaller Mn atomic flux of 1.1×10^{12} $m^{-2}s^{-1}$, and 6.44×10^{11} $m^{-2}s^{-1}$, respectively. The obvious reduction of temperature gradient and the Mn atomic flux across the NiFe/FeMn interface are supposed to be due to the reduction of EM and TM-induced Cu spacer inter-diffusion controlled by the Co and CoFe diffusion barriers. Furthermore, this result strongly indicates that the EM and TM-induced Cu spacer inter-diffusion should be considered as one of the most crucial physical parameters in controlling the magnetic degradation of Mn-AFM-based EBGMR SVSDs operating at high current density. It was also found that the control of Cu spacer inter-diffusion by

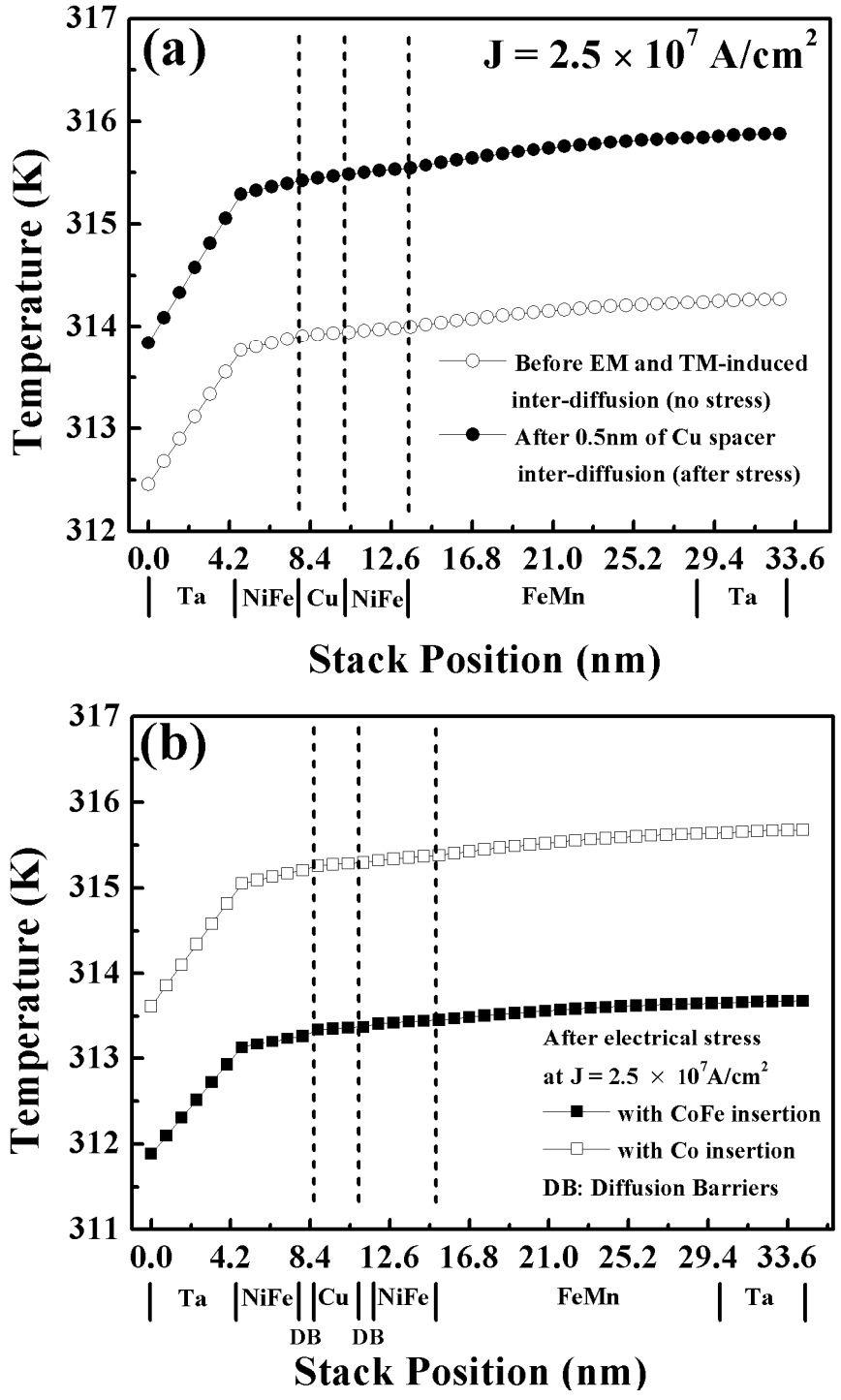

Fig. 6.7 Temperature distribution profiles of top FeMn EBGMR SVSDs numerically calculated based on the thermally-induced mass transport models. (a) Si/Ta(4.5)/NiFe(3.3)/Cu(2.4)/NiFe(3.3)/FeMn(15)/Ta(4.5 nm) top EBGMR SVSDs before and after electrically stressed at J = 2.5 × 10^7 A/cm^2, and (b) Si/Ta(4.5)/NiFe(3.3)/[Co(0.77) or CoFe(0.77)]/Cu(2.4)/[Co(0.77) or CoFe(0.77)]/NiFe(3.3)/FeMn(15)/Ta(4.5 nm) Top EBGMR SVSDs after electrically stressed at J = 2.5 × 10^7 A/cm^2.

Co and CoFe diffusion barriers apparently improved the MR degradation as shown in Fig. 6.6. According to the spin-polarized electron transport theory in magnetic MLs (Hartmann, 1999), it can be interpreted that the small degradation of interfacial spin-dependent scattering due to the well-maintained smooth interface resulted from the reduction of Ni-Cu magnetically dead regions caused by the effectively blocked Cu inter-diffusion (Jiang, 2009) is the main physical reason for the improvement of MR degradation. In addition, the well-maintained exchange-bias coupling at the NiFe/FeMn interface as a result of controlled Cu spacer inter-diffusion is another possible reason for the small reduction of MR degradation because it allows for a strong anti-parallel spin state in the EBGMR SVSDs during free layer magnetic reversal. As can be interestingly seen in Figs 6.6(a) and (b), although the Co and the CoFe have a similar solid solubility with Cu spacer, the CoFe-TSVSD showed a higher magnetic stability than that of Co-TSVSD. The lower device temperature as well as the smaller temperature gradient generated at the Cu/CoFe interface as shown in Fig. 6.7(b) due to the lower resistivity of CoFe ($\rho_{Co_{90}Fe_{10}}$ = ~ 20 μΩ-cm) compared with that of Co (ρ_{Co} = ~ 450 μΩ-cm) in thin film ((Jarratt,1997; Ko, 2003), and the more effectively controlled Cu spacer inter-diffusion due to the insolubility of both Co and Fe with Cu (Huang, 2003) are assumed to be the main physical reason for the technical promises of CoFe diffusion barrier for successfully controlling the magnetic degradation of EBGMR SVSDs.

6.4 Summary and Conclusions

The effects of controlling Cu spacer inter-diffusion by diffusion barriers on the EM and TM-induced magnetic and electrical degradation of NiFe/Cu/NiFe based MMLDs and top FeMn EBGMR SVSDs were investigated under the high applied D.C. current density. It was clearly demonstrated that the controlling of Cu spacer inter-diffusion by the ultra-thin Co and CoFe diffusion barriers plays a dominant role in determining the magnetic and electrical degradation of NiFe/Cu/NiFe based MMLDs and top FeMn EBGMR SVSDs. Furthermore, it was found that the CoFe diffusion barrier is more promising to control the EM and TM-induced Cu spacer inter-diffusion resulting in maintaining both a high GMR performance and a large exchange bias field of the electrically stressed FeMn EBGMR SVSDs. According to the experimentally and theoretically analyzed results, the effectively reduced Mn atom inter-diffusion at the NiFe/FeMn interface and the well-maintained interfacial spin-dependent scattering resulted from the control of Cu spacer inter-diffusion were the main physical reasons for the significantly improved magnetic and electrical stability of top FeMn EBGMR SVSDs operating at high current density.

EM-induced magnetic failures in NiFe/(Co)/Cu/(Co)/NiFe GMR SV MLs have been investigated to estimate the magnetic stability of GMR SV MLs. It was clearly confirmed that EM-induced Cu inter-diffusion or failure is the most fatal problem to give rise to the magnetic degradation of NiFe/Cu/NiFe based GMR SV MLs under electrical stressing. However, an ultra thin Co diffusion barrier inserted at the NiFe/Cu

interface was found to be promisingly effective to improve the magnetic stability of NiFe/Cu/NiFe based SV MLs against electromigration due to its significant blocking effects of Cu diffusion.

References

Anderson, G.W., Pakala, M., and Huai, Y.M. (2000). Spin-valve thermal stability: interdiffusion versus exchange biasing. IEEE Trans. Magn. **36**, 2605.2607.

Attardo, M.J., and Rosenberg, R. (1970). Electromigration damage in aluminum film conductors. J. Appl. Phys. **41**, 2381.

Bae, S., Judy, J.H., Tsu, I.F., and Murdock, E.S. (2001). Electromigration-induced failure of single layered NiFe Permalloy thin films for a giant magnetoresistive read head. J. Appl. Phys. **90**, 2427-2432.

Bae, S., Tsu, I.F., Davis, M., Murdock, E.S., and Judy, J.H. (2002). Electromigration study of magnetic thin films for the electrical reliability of spin-valve read heads. IEEE Trans. Magn. **38**, 2656.2657.

Black, J.R. (1969). Electromigration failure modes in aluminum metalization for semiconductor devices. Proc. IEEE **57**, 1587-1594.

Brückner, W., Baunack, S., Hecker, M., Mönch, J.I., van Loyen, L., and Schneider, C.M. (2000). Interdiffusion in NiFe/Cu/NiFe trilayers: possible failure mechanism for magnetoelectronic devices. Appl. Phys. Lett. **77**, 358-360.

Chang, C.W., Gan, C.L., Thompson, C.V., Pey, K.L., Choi, W.K., and Chua, M.H. (2003). Joule heating-assisted electromigration failure mechanisms for dual damascene Cu/SiO_2 interconnects. IEEE Proceedings of the 10th IPFA (Piscataway, New Jersey: IEEE), p. 69.

Childress, J.R., and Fontana Jr., R. E. (2005). Magnetic recording read head sensor technology. Comptes Rendus – Physique **6**, 997-1012.

Danso, K.A., and Tullos, L. (1981). Thin film metallization studies and device lifetime prediction using Al-Si and Al-Cu-Si conductor test bars. Micro-electronics Reliab. **21**, 513-527.

Daughton, J.M. (1992). Magnetoresistive memory technology. Thin Solid Films **216**, 162-168.

Gurney, B.A., Speriosu, V.S., Wilhoit, D.R., Lefakis, H., Fontana, R.E., Jr., Heim, D.E., and Dovek, M. (1997). Can spin valves be reliably deposited for magnetic recording applications? (Invited) J. Appl. Phys. **81**, 3998-4003.

Hartmann, U. (1999). Magnetic Multilayers and Giant Magnetoresistance: Fundamentals and Industrial Applications. (Berlin: Springer), 184-190.

Huang, A.T., Gusak, A.M., and Tu, K.N. (2006). Thermomigration in SnPb composite flip chip solder joints. Appl. Phys. Lett. **88**, 141911-(1-3).

Huang, R.T., Chen, F.R., Kai, J.J., Kai, W., Tsu, I.F., and Mao, S. (2003). Diffusion behavior in spin valves studied by high resolution transmission electron microscopy and nanobeam technique. J. Magn. Magn. Mater. **260**, 28-36.

Huang, T.C., Nozieres, J.P., Speriosu, V.S., Gurney, B.A., and Lefakis, H. (1993). Effect of annealing on the interfaces of giant‐magnetoresistance spin-valve structures. Appl. Phys. Lett. **62**, 1478-1480.

Jarratt, J.D., Klemmer, T.J., and Barnard, J.A. (1997). Electrical resistivity in sputtered $Co_{90}Fe_{10}$/Ag GMR multilayers. J. Appl. Phys. **81**, 5793-5795.

Jiang ,J., Bae,S., and Ryu,H. (2009). Magnetic instability of giant magnetoresistance spin-valve due to electromigration-induced inter-diffusion. Thin Solid Films **517**, 5557-5562.

Ko, Y.K., Park, D.S., Seo, B.S., Yang, H.J., Shin, H.J., Kima, J.Y., Lee, J.H., Lee, W.H., Reucroft, P.J., and Lee, J.G. (2003). Studies of cobalt thin films deposited by sputtering and MOCVD. Mater. Chem. Phys. **80**, 560-564.

Kos, A.B., Russek, S.E., Kim, Y.K., and Cross, R.W. (1997). High current density measurements of giant magnetoresistive spin-valves for magnetic recording and sensor applications. IEEE Trans. Magn. **33**, 3541-3543.

Massalski, T.B., Okamoto, H., Subramanian, P.R., and Kacprzak, L. (1990). Binary Alloy Phase Diagrams 2nd edn (Materials Park, OH: ASM International), p. 1182, p. 1444.

Parkin, S.S.P. (1992). Oscillations in giant magnetoresistance and antiferromagnetic coupling in $[Ni_{81}Fe_{19}/Cu]_N$ multilayers. Appl. Phys. Lett. **60**, 512-514.

Parkin, S.S.P. (1994). Magnetic coupling and magnetoresistance, in Ultrathin Magnetic Structures II, Heinrich, B., and Bland, J.A.C. ed. (Berlin: Springer), p. 148-186.

Ragone, D.V. (1995). Thermodynamics of Materials. (New York: Wiley). Vol. **2**, Chap. 8.

Saito, A.T., Twasaki, H., Kamiguchi, Y., Fuke, H.N.,and Sahashi, M. (1998). Activation energy of interdiffusion and interface structure for CoFe/Cu spin-valves. IEEE Trans. Magn. **34**, 1420-1422.

Skomski, R. (2008). Simple Models of Magnetism. (Oxford, New York: University Press). P. 118-120.

Sun, Y.H., Zhou, P., Kim, D.Y., Goodson, K.E., and Wong, S.S. (2002). IEEE 40th Annual International Reliability Physics Symposium (Piscataway, New Jersey: IEEE), p. 435.436.

Wang, S.X., and Li, G.X. (2008). Advances in giant magnetoresistance biosensors with magnetic nanoparticle tags: Review and outlook. IEEE Trans. Magn. **44**, 1687-1702.

Zeng, D.G., Chung, K.W., and Bae, S. (2009). Thermomigration-induced magnetic degradation of current perpendicular to the plane GMR spin-valve read sensors operating at high current density. J. Appl. Phys. **106**, 113908(1)-113908(6).

Zhang, H.Q, Wang, G., and Cargill III, G.S. (2006). Electrical resistance anomalies during electromigration testing of Cu conductor lines: examples of local melting? MRS Symp. Proc. **914**, 0914-F06-08.

Zhang, H., Wang, G., and Cargill III, G.S. (2007). Local melting during electromigration in Cu conductor lines. J. Electron. Mater. **36**, 117-122.

CHAPTER 7 HALL EFFECT-INDUCED ACCELERATION OF ELECTROMIGRATION FAILURES IN SPIN-VALVES MULTI-LAYERS UNDER MAGNETIC FIELD

7.1 Introduction

Recently, research interests on the electrical and magnetic reliability of giant magnetoresistance spin valves (GMR SVs) and magnetic tunnel junctions (MTJs) induced by electromigration (EM) failures have been dramatically increased in the applied spintronics devices, such as GMR SV read sensors and a toggle switching GMR or MTJ based magnetic random access memories (MRAM), due to the geometrically-induced high operating current density, $J > 2\times10^7$ A/cm^2, and the structurally-induced extremely large local temperature gradient in the multi-layered thin films (Ho, 1989; Shingubara, 1999; Rosenberg, 2000; Bae, 2001). Accordingly, systematic studies of EM-induced magnetic and electrical degradations of magnetic thin films (Bae, 2002), SV multi-layers (SV-MLs), GMR SVs, and MTJs (Bae, 2003; Ventura, 2005; Guarisco, 2008; Thiyagarajah, 2009; Jiang, 2010; Yang, 2010) have been intensively done for the last ten years to understand the EM-induced failure mechanism and to find effective solutions enabling to improving the reliability of GMR SV and MTJ based spintronics devices. However, all the research activities have been made so far entirely focused on studying the physical mechanism responsible for the EM-induced failures under the accelerated electrical stress and different ambient

temperature conditions, there has been no report on the physical effects of applied magnetic field including DC and pulsed DC magnetic fields on the EM-induced failure lifetimes and its characteristics, although all of the GMR SVs, SV-MLs, and MTJ based spintronics devices are operated by an externally applied magnetic field (Chappert, 2007).

In this chapter, we report on the EM-induced failure characteristics and newly developed physical mechanism (model) of SV-ML devices stressed by both magnetic field and constant D.C. current. The effects of magnetic fields on the EM-induced failure characteristics were systematically investigated by measuring the mean-time-to-failure (MTTF) of SV-ML devices under the different DC magnetic fields and pulsed DC magnetic fields with different duty factors. In order to precisely understand the physical nature of EM-induced failure mechanism of SV-ML devices under magnetic field, a theoretical model describing electron & mass transport, joule heating, and thermal (local temperature) gradient in the SV-ML devices under both electric and magnetic field was developed based on the Boltzmann transport equation. The physical validity of the proposed model was verified by both experimental works and numerical calculations.

7.2 Experimental Works

The NiFe(3)/Co(0.5)/Cu(2)/Co(0.5)/NiFe(3 nm) SV-MLs commonly used as a part of GMR SV devices were deposited on Si (100) substrate using a DC magnetron sputter. The Ar working gas pressure during sputtering was kept at 2 mTorr. The SV-ML devices

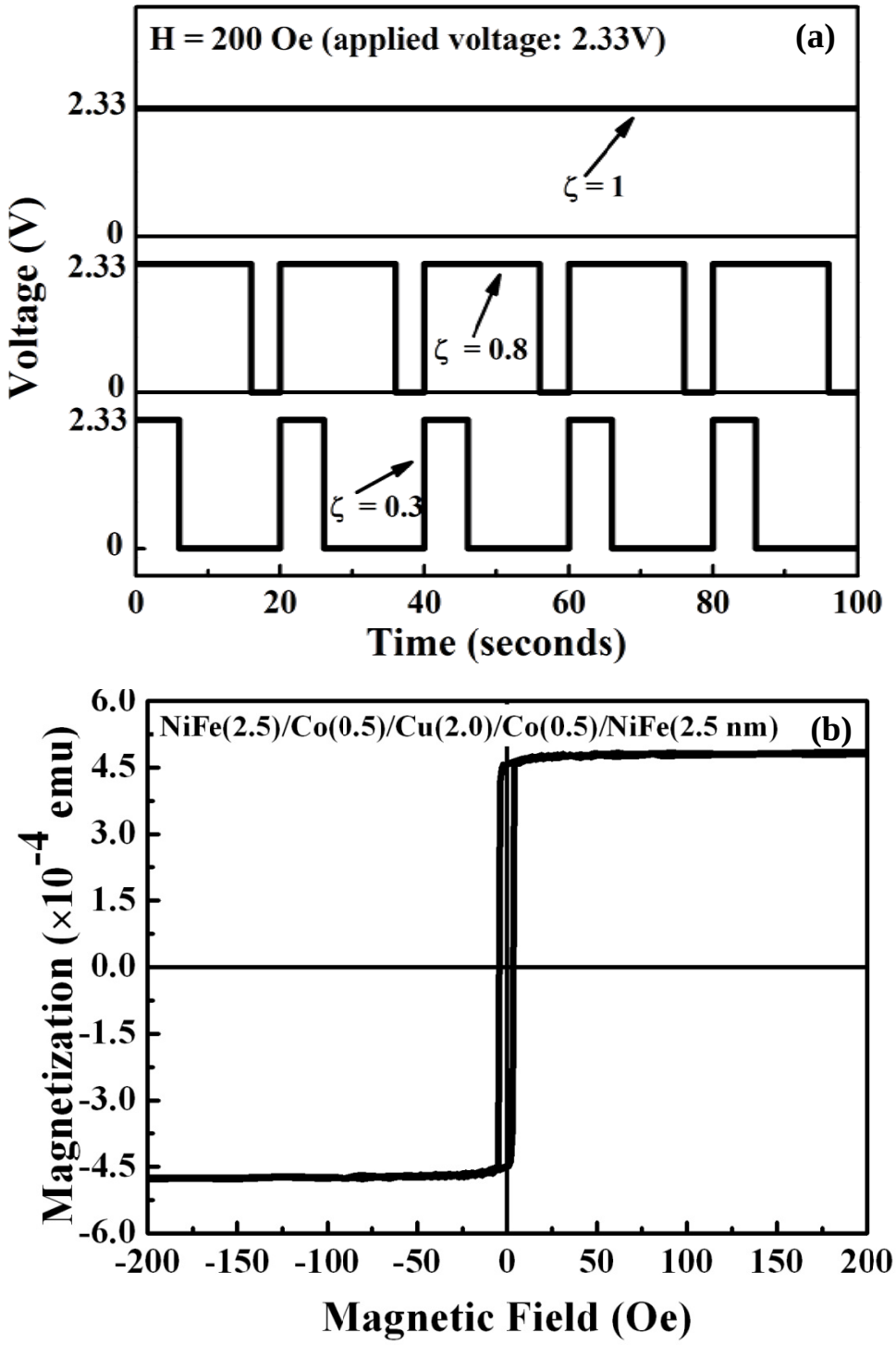

Fig. 7.1 (a) Applied magnetic fields with different duty factors controlled by an electromagnet to the SV-MLs devices, and (b) a M-H loop of NiFe(2.5)/Co(0.5)/Cu(2)/Co(0.5)/NiFe(2.5 nm) SV-MLs.

with a width of 2μm and a length of 20μm were patterned using standard electron beam lithography and photolithography and etched by an ion miller etching system. An

electromagnet precisely calibrated was used to apply DC magnetic fields or pulsed DC magnetic fields with different duty factors (see Fig. 7.1(a)) to the SV-ML devices electrically stressed by a constant DC current fixed at $J = 5\times10^7$ A/cm^2. The applied DC magnetic field was changed from 200 Oe to 600 Oe and the duty factor of the pulsed DC magnetic field, which is orthogonally applied to the electric field (considering device operating conditions for a real GMR SV read sensor and a toggle switching MRAM), was changed from 0.3 to 1 (constant cycle time of 20 seconds) at the fixed magnetic filed of 200 Oe. In order to exclude the influence of interlayer coupling and magnetostatic coupling energy, which are formed in the SV-ML devices, on the EM-induced change of resistance under both magnetic and electric fields, the applied magnetic field was controlled to be larger than the saturation magnetic field of the SV-ML devices (see Fig. 7.1(b)). The time-to-failure (TTF) and the mean-time-to-failure (MTTF, t_{50}) were defined as the time for the resistance of the devices to increase by 100 % and the exponential of the mean of the logarithm of TTFs, respectively (Bae, 2001). The EM-induced failures were analyzed using high resolution transmission electron microscopy (HR-TEM).

7.3 Results and Discussion

7.3.1 Failure Characteristics and Lifetime Dependence on the Applied Magnetic Field Amplitude and Duty Factor

Figures 7.2(a) and 7.2(c) show the electrical resistance change vs. time for SV-ML

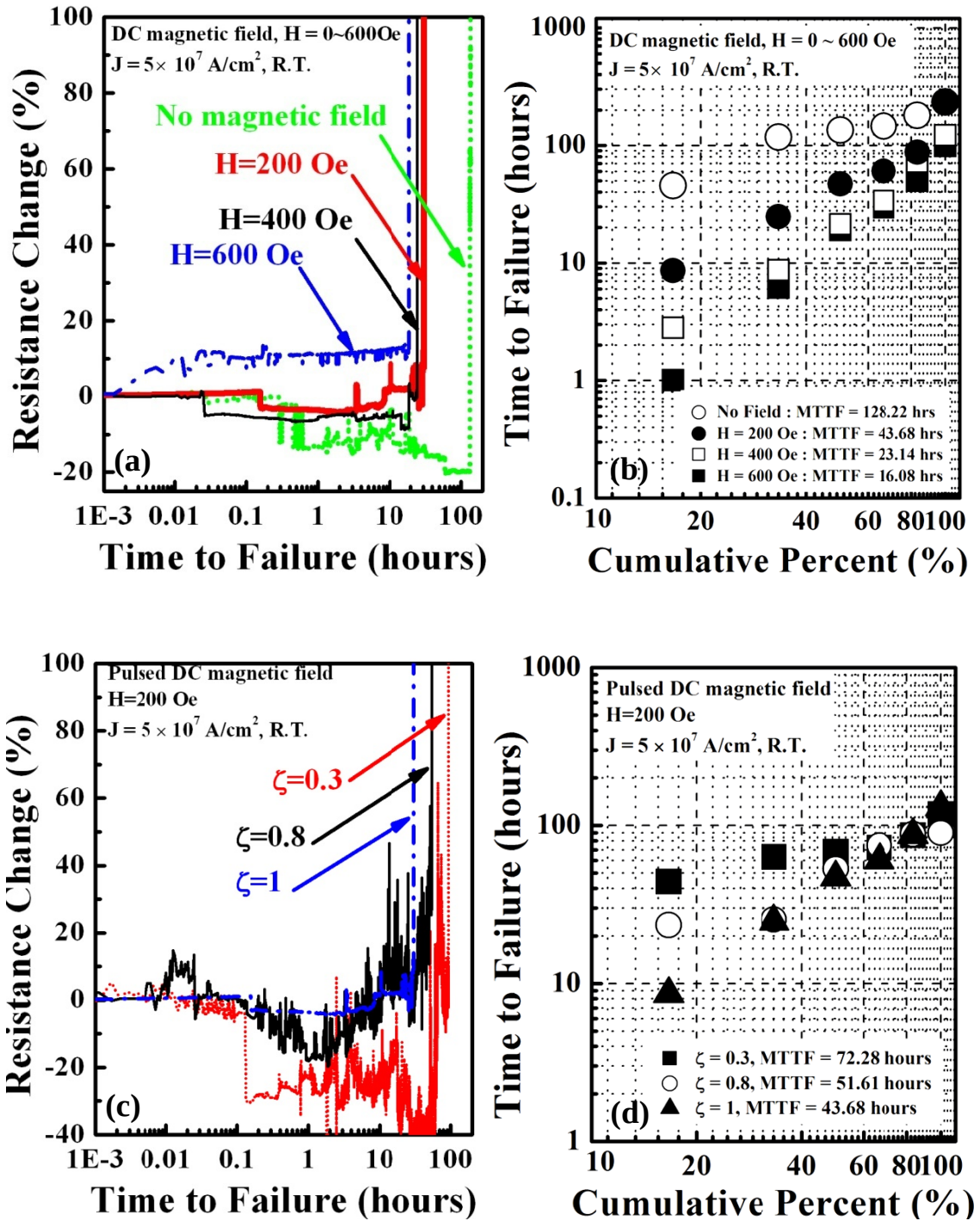

Fig. 7.2 The dependence of applied D,C, and pulsed D.C. magnetic fields on the EM-induced failure characteristics of SV-ML devices electrically stressed by a constant D.C. current density of J = 5 × 10^7 A/cm^2. The D.C. magnetic field orthogonally applied to the electrical current was changed from 0 to 600 Oe and the duty factor (ζ) of pulsed D.C. was varied from 0.3 to 1 at the fixed magnetic field of 200 Oe. (a) electrical resistance change (ΔR) vs. time (t) curves at the different D.C. magnetic field, (b) cumulative percent vs. TTF curves at the different D.C. magnetic field, (c) ΔR vs. t curves at the different pulsed D.C. magnetic field (different duty factors), and (d) cumulative percent vs. TTF curves at the different pulsed D.C. magnetic field (different duty factors).

devices stressed by both electric and magnetic fields. The current density applied to the SV-ML devices was constant kept at $J = 5\times10^7$ A/cm^2 and the applied DC magnetic field (see Fig. 7.3(b)) was varied from 200 Oe to 600 Oe. The pulsed DC magnetic field was kept constant at 200 Oe with different duty factors of 0.3, 0.8, and 1, respectively. As shown in Fig. 7.2(a) and 7.2(c), the EM-induced failure lifetime of SV-ML devices had a strong dependence on the strength and duty factor of the applied magnetic field. In order to obtain a full picture of the dependence of MTTF on the applied magnetic field, the cumulative failure percent with different field strengths and duty factors was determined based on the TTF of the SV-ML devices, as shown in Fig. 7.2(b), and 7.2(d), respectively. As can be clearly seen in Fig. 7.2(b), the MTTF of SV-ML devices electrically stressed at the current density of $J = 5\times10^7$ A/cm^2 was inversely proportional to the applied magnetic field. A significant decrease of MTTF from 128.22h to 16.08h was observed by increasing the DC magnetic field from 0 to 600 Oe. In order to investigate the effects of magnetic field on the EM-induced failure lifetime characteristics in an environment more close to GMR SV read sensor or GMR SV MRAM operating conditions, the duty factor of the pulsed DC magnetic field was changed from 0.3 to 1 at the fixed field of 200 Oe, as shown in Fig. 7.2(d). It was clearly revealed that the MTTF was monotonically decreased by increasing the duty factor of the pulsed DC magnetic field. All the experimentally analyzed results shown in Fig. 7.2 demonstrated that EM-induced failures of SV-ML devices are severely accelerated by the externally applied magnetic field. Furthermore, these results strongly indicate that the EM-induced failure characteristics of GMR SV and SV-MLs based

spintronics devices must be differently interpreted from other electronic devices due to the externally applied magnetic field for device operation.

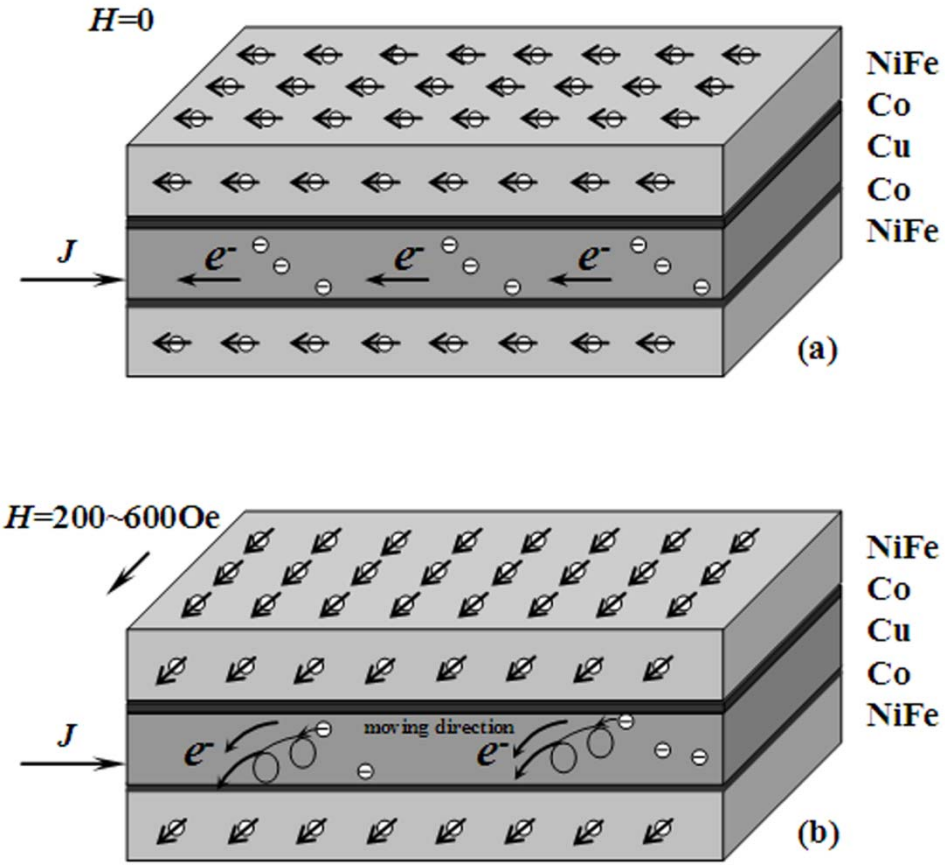

Fig. 7.3 Schematic illustrations of electrons' motion in the SV-ML devices under (a) electrical field (E_x or J_x) & no magnetic field (H = 0), and (b) electrical field (E_x or J_x) & magnetic field (H_y = 200 ~ 600 Oe)

7.3.2 Physical Model

The dramatic decrease in MTTF of SV-ML devices under magnetic field can be assumed to be originated from the geometrically-induced Hall-effect, which can exert an extra Lorentz force to the perpendicular-to-the-film-plane (z) direction (see Fig. 7.3(b)) possibly responsible for the acceleration of atomic diffusion (migration). Based

on this physical assumption, a theoretical model was developed to study the physical nature of the severe acceleration of EM-induced failures in SV-MLs devices under magnetic field. In this model, it was considered that the accelerated atomic migration is mainly occurred in the Cu spacer region due to the "current sinking effect" describing that the operation current of SV-ML devices (or GMR SV devices) would be concentrated on the Cu spacer because of its lowest electrical resistivity compared to other magnetic layers (Zeng, 2010). In order to analyze the electron transport properties of the SV-ML devices under the both electric and magnetic fields (E_x, H_y), as illustrated in Fig. 7.3(b), the distribution function of electrons in a steady state is expressed based on the Boltzmann equation (Mayadas, 1970).

$$\frac{f_1}{\tau} - \frac{eH}{m^*}\left(v_z \frac{\partial f_1}{\partial v_x} - v_x \frac{\partial f_1}{\partial v_z}\right) = \frac{e}{m^*}\left(E_x \frac{\partial f_0}{\partial v_x} + E_z \frac{\partial f_0}{\partial v_z}\right) \tag{7-1}$$

Where, m^* is the effective mass, τ is the effective relaxation time of conduction electrons, f_0 is the Fermi function given by $1/\{e^{(E-\xi)/kT}+1\}$ (ξ being the Fermi energy level), f_1 is the deviation of electron distribution function f ($f = f_0+f_1$), and v_x, v_z are the x and z component of electron velocity v. In order to obtain the current densities in the x direction due to E_x and z direction induced by Hall effect (or Lorenz force), the Boltzmann equation needs to be solved by assuming a solution of the form,

$$f_1 = (C_1 v_x + C_2 v_z)\partial f_0 / \partial v \tag{7-2}$$

Where, C_1 and C_2 are functions of v. Substituting Eq. (7-2) into Eq. (7-1), the Boltzmann equation becomes two simultaneous equations, given by Eq. (7-3) and (7-4),

$$\frac{C_1}{\tau} + \frac{eH}{m^*} C_2 = \frac{e}{m^* v} E_x \tag{7-3}$$

$$\frac{C_2}{\tau} - \frac{eH}{m^*} C_1 = \frac{e}{m^* v} E_z \tag{7-4}$$

In Fuchs' model (Fuchs, 1938), a conduction electron colliding with the interface/surface is scattered specularly with a probability of p and diffusely with a probability of 1-p. In the presence of both bulk and interface scatterings, we may define an effective relaxation time (τ) (Tellier, 1978),

$$\tau \cong \frac{l}{v} = \frac{l_0[1 + \frac{1-p}{k}\frac{|v_z|}{v}]^{-1}}{v} \tag{7-5}$$

Where, l_0 is the mean free path, $v_z = v\cos\theta$. The effective relaxation time depends on the angle of incidence θ, specularity parameter p and the reduced film thickness k ($k=a/l_0$, a is the film thickness). Substituting Eq. (7-5) and (7-4) into Eq. (7-3), we can obtain,

$$C_1 = \frac{el_0}{m^* v^2} \frac{E_x(1 + |\cos\theta|\mu^{-1}) - \alpha E_z}{[1 + |\cos\theta|\mu^{-1}]^2 + \alpha^2} \tag{7-6}$$

$$C_2 = \frac{el_0}{m^* v^2} \frac{E_z(1 + |\cos\theta|\mu^{-1}) + \alpha E_x}{[1 + |\cos\theta|\mu^{-1}]^2 + \alpha^2} \tag{7-7}$$

Where, $\alpha=l_0/r$ (r is the radius of the circular orbit of an electron in a magnetic field $r = m^* v / eH$), and $\mu=k/(1-p)$. Having the determined solution of the transport equation, the current density in the current flowing (x) direction, and the current density induced by the Hall effect in the perpendicular-to-the-film-plane (z) direction, which is designated as J_x, and J_z, respectively, can be determined as Eq. (7-8) (Sondheimer, 1950),

$$J_x = -2e(\frac{m^*}{h})^3 \iiint v_x f dv_x dv_y dv_z$$

$$J_z = -2e(\frac{m^*}{h})^3 \iiint v_z f dv_x dv_y dv_z \tag{7-8}$$

Substituting Eq. (7-2) into Eq. (7-8), J_x and J_z becomes

$$J_x = -2e(\frac{m^*}{h})^3 \iiint C_1 v_x{}^2 \frac{\partial f_0}{\partial v} dv_x dv_y dv_z \tag{7-9}$$

and

$$J_z = -2e(\frac{m^*}{h})^3 \iiint C_2 v_z{}^2 \frac{\partial f_0}{\partial v} dv_x dv_y dv_z \tag{7-10}$$

Introducing the polar coordinates (v, θ, φ) in the v-space where $v_z = v\cos\theta$, the total current densities in the x and z directions, J_x and J_z , can be expressed as,

$$J_x = -2e(\frac{m^*}{h})^3 v^4 \int_0^{2\pi} \cos^2\varphi \, d\varphi \times \int_0^{\pi} C_1 \sin^3\theta \, d\theta \tag{7-11}$$

and

$$J_z = -2e(\frac{m^*}{h})^3 v^4 \int_0^{2\pi} d\varphi \times \int_0^{\pi} C_2 \cos^2\theta \sin\theta \, d\theta \tag{7-12}$$

Integrating over θ and φ, we can obtain,

$$J_x = \frac{3}{2}\sigma_0 (A_1 \cdot E_x - \alpha B_1 \cdot E_z) \tag{7-13}$$

and

$$J_z = \frac{3}{2}\sigma_0 (A_2 \cdot E_z + \alpha B_2 \cdot E_x) \tag{7-14}$$

With

$$A_1 = -\frac{1}{2}\mu + \mu^2 + \frac{\mu}{2}(1-\mu^2+\alpha^2\mu^2)\ln\left[\frac{(1+\mu^{-1})^2+\alpha^2}{1+\alpha^2}\right] - 2\alpha\mu^3 \tan^{-1}(\frac{\alpha}{\mu}\frac{1}{\alpha^2+1+\mu^{-1}})$$

$$B_1 = -\mu^2 + \mu^3 \ln\left[\frac{(1+\mu^{-1})^2+\alpha^2}{1+\alpha^2}\right] + \frac{\mu}{\alpha}(1-\mu^2+\alpha^2\mu^2)\tan^{-1}(\frac{\alpha}{\mu}\frac{1}{\alpha^2+1+\mu^{-1}}) \tag{7-15}$$

and

$$A_2 = \mu - 2\mu^2 + \mu(\mu^2 - \alpha^2\mu^2)\ln\left[\frac{(1+\mu^{-1})^2+\alpha^2}{1+\alpha^2}\right] + 4\alpha\mu^3\tan^{-1}\left(\frac{\alpha}{\mu}\frac{1}{\alpha^2+1+\mu^{-1}}\right)$$

$$B_2 = 2\mu^2 - 2\mu^3\ln\left[\frac{(1+\mu^{-1})^2+\alpha^2}{1+\alpha^2}\right] + \frac{2\mu}{\alpha}(\mu^2-\alpha^2\mu^2)\tan^{-1}\left(\frac{\alpha}{\mu}\frac{1}{\alpha^2+1+\mu^{-1}}\right) \quad (7\text{-}16)$$

Eqs. (7-14) and (7-16) clearly demonstrate that in the absence of a magnetic field, J_z becomes zero since H=0, α=0, and E_z=0, as schematically illustrated in Fig. 7.3(a); while in the presence of a magnetic field, there exists an induced current (J_z) in the perpendicular-to-the-film-plane (z) direction due to the curling motion of electrons caused by Lorentz force due to the Hall effect, as schematically illustrated in Fig. 7.3(b). In order to calculate and compare the Joule heating generated in the SV-MLs devices both in the presence and in the absence of a magnetic field, the electrical conductivity needs to be calculated according to the definition (Sondheimer, 1950) given by Eq. (7-17),

$$\sigma_F = \left.\frac{J_x}{E_x}\right|_{J_z=0} = \frac{3}{2}\sigma_0\frac{A_1A_2+\alpha^2B_1B_2}{A_2} \quad (7\text{-}17)$$

Where, σ_0 is the conductivity of bulk metal ($\sigma_0 = ne^2l_0/m^*v$). In the absence of a magnetic field (H=0, α=0), Eq. (7-15) could be simplified by Eq. (7-18),

$$A_1' = A_1 = -\frac{1}{2}\mu + \mu^2 + \mu(1-\mu^2)\ln(1+\mu^{-1}) \quad (7\text{-}18)$$

The electrical conductivity becomes $\sigma_F' = 3\sigma_0 A_1'/2$. If the Hall-effect is not taken into consideration, the Joule heating Q under only electrical stress is given by [14],

$$Q = \sigma(\nabla\Phi)^2 \quad (7\text{-}19)$$

Where, σ is the electrical conductivity and Φ the electrical potential. However, in the presence of externally applied magnetic field, the Joule heating Q considering the duty

factor (ζ) of the pulsed DC magnetic field can be modified as;

$$Q = \zeta\sigma_F(\nabla\Phi)^2 + (1-\zeta)\sigma_F'(\nabla\Phi)^2 \tag{7-20}$$

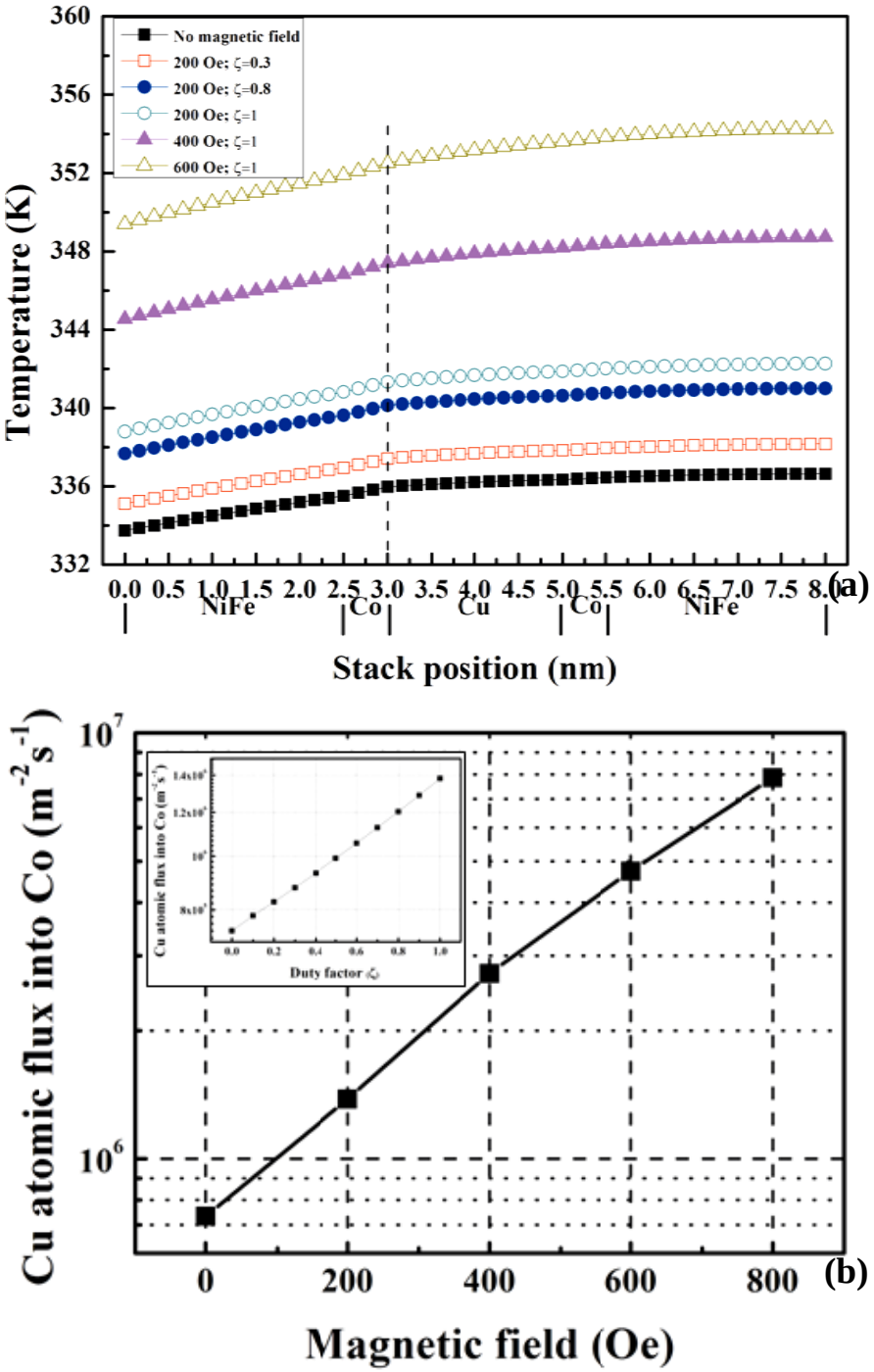

Fig. 7.4 (a) Temperature distribution profiles, and (b) Cu atomic flux into the bottom Co layer in the SV-ML devices electrically stressed by a constant D.C. current density of J = 5 × 10^7 A/cm^2 with or without magnetic field including pulsed D.C. magnetic field with different duty factors.

Based on Eqs. (7-13) ~ (7-20), we can conclude that the Joule heating generated in the SV-Ml devices under both magnetic and electrical stress is directly relevant to the strength and ζ of the magnetic field. In order to numerically confirm the change of Joule heating and temperature gradient inside the SV-ML devices due to the Hall-effect, the temperature distribution profiles of the SV-ML devices electrically stressed by a J = 5×10^7 A/cm^2 with different DC magnetic fields and pulsed DC magnetic field with different duty factors were calculated by considering Eq. (7-20) and thermally-induced mass transport models (Zeng, 2010). The temperature gradient related to the internal Joule heating in the (+z) direction (see Fig. 7.3(b)) is defined as the temperature variation in an infinitesimal distance $\nabla T = \Delta T / \Delta Z$. As can be seen in Fig. 7.4(a), the temperature and temperature gradient at the bottom Cu/Co interface were obviously increased by increasing the magnetic fields and the duty factor of the pulsed DC magnetic field, resulting in an increase of Cu atomic flux into the bottom Co layer, as shown in Fig. 7.4(b). In addition, it was revealed that the temperature (temperature gradient ∇T) at the interface of Cu/Co was increased from 335.9K (~6.0×10^6 °C/cm) to 352.5K (~9.9×10^6 °C/cm) and the Cu atomic flux into Co was correspondingly increased from 7.3×10^5 m^{-2}s^{-1} to 7.85×10^6 m^{-2}s^{-1} by increasing the DC magnetic field from 0 to 600 Oe, leading to an increase of temperature gradient of around 65 % and Cu atomic flux into bottom Co layer of approximately ten-fold. Furthermore, the Cu atomic flux was found to increase from ~ 7.8×10^5 m^{-2}s^{-1} to ~1.29×10^6 m^{-2}s^{-1} when the duty factor of the pulsed DC magnetic field was increased from 0.1 to 0.9. These results indicate that the additionally increased Joule heating due to the abruptly

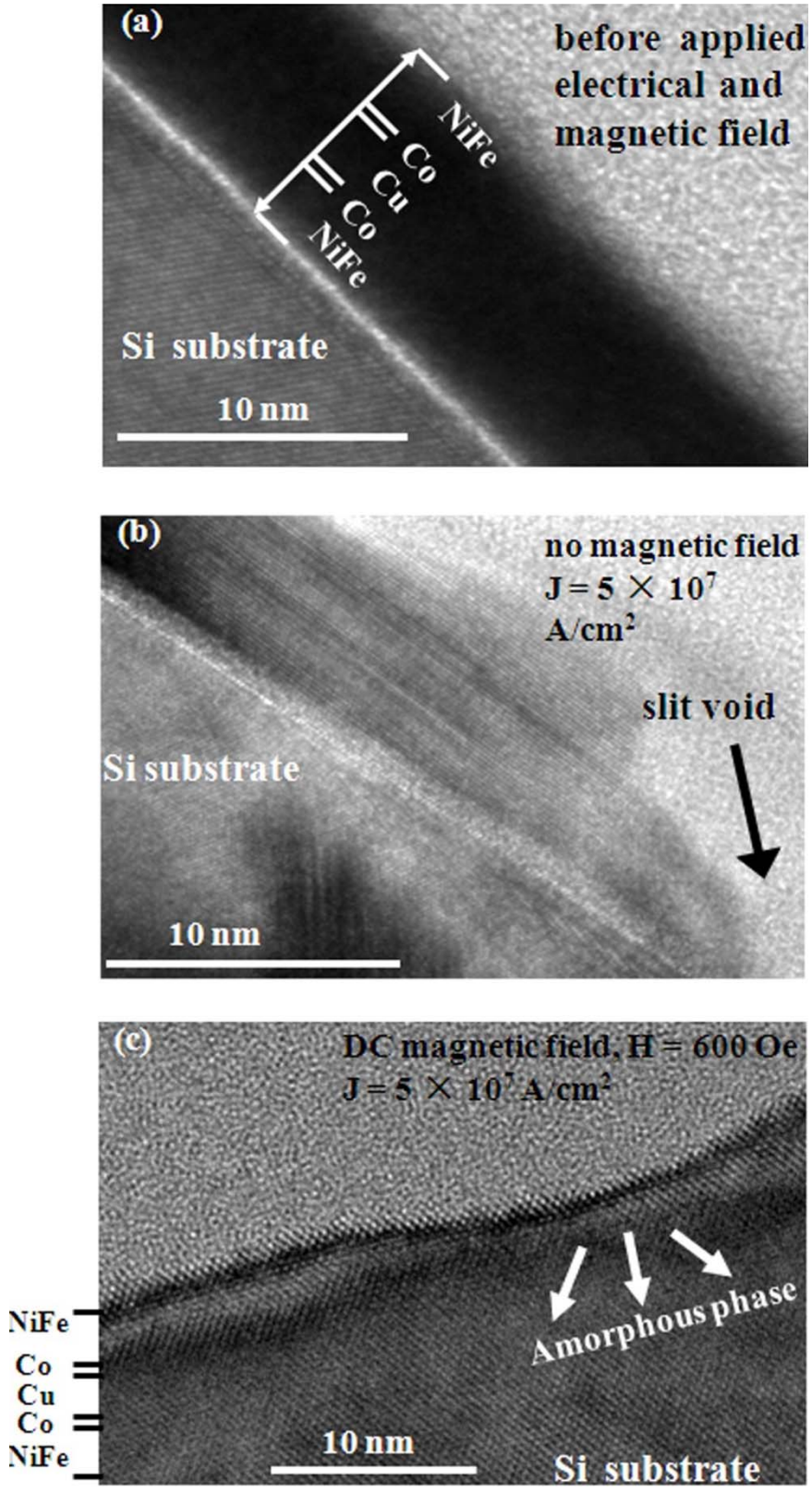

Fig. 7.5 HR-TEM images for the SV-ML devices (a) before applying electrical stress, (b) after complete failure under the applied current density 5×10^7 A/cm^2 and zero magnetic field (99 % of TTF), and (c) after failure under the both applied current density 5×10^7 A/cm^2 and a 600 Oe of magnetic field (99 % of TTF).

increased local current density induced by Hall effect (Lorenz force) is directly responsible for the large increment of the temperature gradient resulting in accelerating the driving force for mass transport (or atomic flux) in the SV-ML devices.

7.3.3 Failure Analysis Using XTEM

In order to experimentally confirm the physical validity of the above theoretical model, the failure analysis for the EM tested SV-ML devices was carried out using a HR-TEM as shown in Fig. 7.5. As can be clearly seen in Fig. 7.5(b) and 7.5(c), the SV-ML devices under only electrical stress showed a typical slit void failure; while the SV-ML devices stressed by both magnetic field and electrical current showed completely different failure modality. As indicated in Fig. 7.5(c) (white arrow), a few of amorphous regions were found at the Cu/Co interface and underneath of the Cu spacer. The underlying mechanisms responsible for the different failure characteristics can be interpreted in terms of "current sinking" and Hall effects. In the absence of magnetic field, EM-induced Cu spacer diffusion was found to be primarily responsible for the formation of voids (or cracks) due to the "current sinking effect". The initial voids formed at the Cu spacer or Cu/Co interfaces would increase the local current density and Joule heating, thus leading to a shunting current from Cu spacer to the Co/NiFe layers and eventually resulting in the formation of a local slit void. On the other hand, in the presence of the magnetic field, the Lorentz force would exert a curling motion of electrons, which induces an extra current towards the (+z) direction (see Fig. 7.3(b) & Eq. (7-14)). This Hall effect-induced additional current would become more accelerated when passing through the regions with high density of dislocations or

defects (Sondheimer, 1950), such as the interface of Cu/Co, thus giving rise to a abrupt increase of local Joule heating ,which in turn accelerates the electron-phonon scattering Kittel, 2004). Subsequently, this suddenly increased Joule heating and electron-phonon scattering would provide suddenly melted Cu atoms with extra activation energy to jump into or even through the adjacent Co layer and then to mingle with it. Eventually, after sudden quenching due to electrical open at the local region, amorphous phase of a Ni-Cu-Fe mingled with small percent of amorphous Co-Cu alloy were formed, because there is no enough time for recrystallization (Massalski, 1990; Li, 2001).

7.4 Summary and Conclusions

In summary, it was found that EM-induced failures of SV-ML devices were severely accelerated by the applied magnetic field. The theoretical analysis results confirmed that Hall effect-induced Lorentz force driven to the perpendicular-to-the-film-plane direction is primarily responsible for the severe acceleration of EM failures due to its dominant contribution to abruptly increasing local temperature and current density. The good agreement between experimental observation and theoretical works apparently demonstrated that the physical nature of EM-induced failures of SV-ML or GMR SV spintronics devices is completely different from that of conventional electronic devices due to the applied magnetic fields for device operation.

References

Bae, S., Judy, J.H., Tsu, I.-F., Davis, M., and Murdock, E.S. (2001). Dependence of

electromigration-induced failure lifetimes on NiFe thin-film thickness in giant magnetoresistive spin-valve read heads. Appl. Phys. Lett. **79**, 3657-3659.

Bae, S., Judy, J.H., Tsu, I.F., and Murdock, E.S. (2001). Electromigration-induced failure of single layered NiFe Permalloy thin films for a giant magnetoresistive read head. J. Appl. Phys. **90**, 2427-2432.

Bae, S., Tsu, I-F., Davis, M., Murdock, E.S., Judy, J.H. (2002). EM study of magnetic thin Films for the electrical reliability of spin-valve read heads. IEEE Trans. Magn. **38**, 2655 - 2657.

Bae, S., Judy, J.H., Tsu, I.F., and Davis, M. (2003). Electrical reliability of tunneling magnetoresistive read heads. J. Appl. Phys. **94**, 7636-7645.

Chappert, C., Fert, A., van Dau, F.N. (2007). The emergence of spin electronics in data storage. Nature Materials **6**, 813-823.

Dugdale, J.S., and Basinski, Z.S. (1967). Mathiessen's Rule and Anisotropic Relaxation Times. Phys. Rev. **157**, 552-560.

Fuchs, K. (1938). The conductivity of thin metallic films according to the electron theory of metals. Proc. Cambridge Phil. Soc. **34**, 100-108.

Guarisco, D. (2008). Resilience of tunneling magnetoresistive heads against electrical overstress. J. Appl. Phys. **103**, 07F535.

Ho, P.S., and Kwok, T. (1989). Electromigration in metals. Rep. Prog. Phys. **52**, 301-348.

Jiang, J. Zeng, D.G., Ryu, H., Chuang, K.W., and Bae, S. (2010). Effects of controlling Cu spacer inter-diffusion by diffusion barriers on the magnetic and electrical stability of GMR spin-valve devices", J. Magn. Magn. Mater. **322**, 1834-1840.

Kittel, C. (2004). Introduction to Solid State Physics. (New York: Wiley), Chap. 4.

Massalski, T.B., Okamoto, H., Subramanian, P.R., Kacprzak, L. (1990). Binary Alloy Phase Diagram, 2nd edn. (OH: ASM International, Materials Park).

Li, Z.F., and Liu, B.X. (2001). Irradiation-induced amorphization and growth of dodecagonal phase in an immiscible Co–Cu systemNulc. Instru. and Meth. Phys. Rev. B **178**, 224-228.

Mayadas, A.F., and Shatzkes, M. (1970). Electrical-Resistivity Model for Polycrystalline Films: the Case of Arbitrary Reflection at External Surfaces. Phys. Rev. B **1**, 1382-1389.

Rosenberg, R., Edelstein, D.C., Hu, C.K., and Rodbell, K.P. (2000). Copper Metalization for high performance silicon technology. Annu. Rev. Mater. Sci. **30**, 229-262.

Shingubara, S., Takeda, Y., Sakue, H., Takehagi, T., and Verbruggen, A.H. (1999). Electromigration reliability study of a GMR spin valve device. Mater. Res. Soc. Symp. Proc. **563**, 145-153.

Sondheimer, E.H. (1950). The Influence of a Transverse Magnetic Field on the Conductivity of Thin Metallic Films. Phys. Rev. **80**, 401-406.

Tellier, C.R., Rabel, M., and Tosser, A.J. (1978). Hall coefficient of thin films in a mean free path model. J. Phys. F: Metal Phys. **8**, 2357-2363.

Thiyagarajah, N. Joo, H.W., and Bae, S. (2009). High magnetic and thermal stability of nano-patterned [Co/Pd] based pseudo spin-valves with perpendicular anisotropy for 1Gb MRAM. Appl. Phys. Lett. **95,** 232513-(1-3).

Ventura, J., Sousa, J.B., Liu, Y., Zhang, Z., and Freitas, P.P. (2005). Electromigration in

thin tunnel junctions with ferromagnetic/nonmagnetic electrodes: nanoconstrictions, local heating, and direct and wind forces. Phys. Rev. B **72**, 094432-(1-7).

Yang, T., Otagiri, M., and Kanai, H., and Uehara, Y. (2010). Barrier degradation of tunneling magnetoresistance device with MgO barrier and low resistance-area product. J. Magn. Magn. Mater. **322**, L53-L56.

Zeng, D.G., Chuang, K.W., Judy, J.H., and Bae, S. (2010). Numerical simulation of current density induced magnetic failure for giant magnetoresistance spin valve read sensors. J. Appl. Phys. **108**, 023903-(1-5).

CHAPTER 8 CONCLUSION AND SUGGESTED FUTURE WORKS

8.1 Conclusions

The minimum lifetime of hard disk drives is required to be 5 years. As giant GMR SV thin films are implemented in high-density magnetic recording heads, electromigration of metals and EM-induced inter-diffusion between thin layers of magnetic and non magnetic materials has become one of the crucial factors limiting the reliability of GMR SV MLs and devices, because EM can lead to discontinuity of metallic thin films with resistance being increased by an unacceptable amount or even total melting of device metallurgy, and inter-diffusion may cause a reduction of output signal and degradation of magnetic performance. The work reported in this thesis focused on the detrimental effect of electromigration (EM) and EM-induced inter-diffusion in the electrical and magnetic reliability of FM/Cu/FM based magnetic MLs and FM/Cu/FM/FeMn based GMR SV devices. The major findings and conclusions are summarized as follows.

(1) It is found that the lifetime of patterned NiFe/Cu/NiFe tri-layers was dramatically increased by decreasing the Cu spacer thickness, because thicker Cu spacers have irregular grain boundaries (GBs) providing more diffusion paths and increased NiFe/Cu interfacial roughness favors the formation of Ni-Cu intermixing region. The obvious shorter lifetime of NiFe/Cu/NiFe tri-layers compared to that of Co/Cu/Co tri-layers was mainly thought to be attributed to the formation of current paths resulted from the EM-induced Cu inter-diffusion into the top or bottom NiFe

layer during electrical stressing caused by the Ni-Cu intermixing. It is suggested that controlling the Cu spacer inter-diffusion and chemical roughness at the FM/Cu interface is crucial in determining the electrical reliability of FM/Cu/FM based GMR SV read sensors.

(2) The failure mechanism of patterned NiFe/Cu/NiFe SV tri-layered devices showed a "bi-modal failure characteristics". The critical current density (J_c) for such a bi-modal failure mechanism was found to be determined at $J_c = 7\times10^7$ A/cm^2. When $J \le J_c$, the failure was mainly caused by the electrostatic force (or electron wind force) accelerating an inter-diffusion through grain boundaries that leads to forming typical EM failures such as voids and hillocks. While, when $J > J_c$, a melting or a vaporization dominantly accelerated by the Joule-heating played more significant role and caused the catastrophic failures. In addition, the "n" values measured at different current density range are quite different. At a lower current density range below J_c, the "n" value was determined at 5.4, whereas, at a relatively high current density range above J_c, the "n" value was 1.3 only. The small "n" value indicates that the EM-induced failure lifetime strongly depends on the applied current densities and also demonstrates that Joule heating dominantly accelerates the EM-induced failures when the biasing current density is beyond J_c.

(3) EM and inter-diffusion induced degradation of magnetic properties of the NiFe/(Co)/Cu/(Co)/NiFe SV-MLs has been investigated. Electrically stressed NiFe/Cu/NiFe SV-MLs showed a dramatic reduction of magnetic moment up to 41%, and a shift of interlayer coupling characteristics. The reduction rate of

magnetic moment was increased from 23% to 41% by increasing Cu spacer thickness. By comparison, no obvious magnetic degradation was observed in the NiFe/Co/Cu/Co/NiFe SV-MLs. It was experimentally confirmed that the magnetic degradation of the NiFe/Cu/NiFe SV-MLs is primarily due to the formation of Ni-Cu intermixing caused by the EM-induced Cu spacer inter-diffusion. Furthermore, it was demonstrated that an ultra thin Co diffusion barrier at the NiFe/Cu interface is promisingly effective to improve the magnetic stability of NiFe/(Co)/Cu/(Co)/NiFe SV-MLs against EM.

(4) An ultra thin Co or CoFe diffusion barrier inserted at the NiFe/Cu interfaces was revealed to effectively control the electrical and magnetic stability of NiFe/Cu/NiFe/FeMn based GMR SV spintronics devices (SVSDs) operating at high current density. It was found that the activation energy, E_a, related to the EM-induced inter-diffusion process for the patterned NiFe(3)/Cu(2)/NiFe(3 nm) magnetic multi-layered devices (MMLD) was remarkably increased from 0.52 ± 0.2 eV to 1.17 ± 0.16 eV after the insertion of a 0.5-nm Co diffusion barrier at the NiFe/Cu interfaces. The optimized thickness of Co diffusion barrier is determined to be 0.5 nm or beyond. This implies that the minimum of two monolayers of Co atoms is essentially required for an effective blocking effect.

(5) The dramatically reduced “current shunting paths” from the Cu spacer to the NiFe thin films and the development of “self-healing process” resulted from the effectively restrained Cu inter-diffusion (inter-mixing with Ni atoms) due to the

diffusion barriers were found to be primarily responsible for the improvement of electrical and magnetic stability of NiFe/Co/Cu/Co/NiFe MMLD.

(6) The investigation on the effects of controlling Cu spacer inter-diffusion by diffusion barriers on the EM and thermomigration (TM)-induced magnetic degradation was carried out for the NiFe/(Co or $Co_{90}Fe_{10}$)/Cu/(Co or $Co_{90}Fe_{10}$)/NiFe/FeMn top exchange biased GMR (EBGMR) SVSDs electrically stressed under the applied D.C. current density of $J = 2.5 \times 10^7$ A/cm^2 (I = 16.5 ~ 17.25 mA). It was clearly confirmed that the Co and the CoFe diffusion barriers effectively control the Cu spacer inter-diffusion resulting in a smaller reduction in both GMR ratio and exchange bias field of the EBGMR SVSDs. Furthermore, it was obviously observed that the effects of CoFe diffusion barrier on controlling the Cu spacer inter-diffusion are more significant than that of Co. The effectively reduced Mn atomic inter-diffusion at the NiFe/FeMn interface and the well maintained interfacial spin dependent scattering resulted from the control of EM and TM-induced Cu spacer inter-diffusion were the main physical reasons for the significant improvement of magnetic and electrical degradation of top EBGMR SVSDs.

(7) The EM-induced failure in MMLDs was severely accelerated by an external magnetic field orthogonally applied to the electrical field. The significant decrease of MTTF was found in the NiFe/Co/Cu/Co/NiFe MMLDs by increasing the DC magnetic field from 0 to 600 Oe and by increasing the duty factor from 0.3 to 1.

The theoretical calculation and thermo-electrical simulation numerically confirmed the contribution of Hall effect-induced Lorentz force to the additional current density in the perpendicular-to-the-plane direction and abruptly increasing local temperature gradient. The calculated increase of temperature gradient at the Cu/Co interfaces is up to 65% when the applied magnetic field is increased from 0 to 600, which leads to an increase of Cu atomic flux to the bottom Co layer by ~ ten-fold. HRTEM images also showed that EM-induced failure of SV-MLs in the presence of magnetic field is completely different from that in the absence of magnetic field. The good agreement between experimental observation and theoretical works apparently demonstrated that the EM-induced degradation of SV-ML or GMR SV spintronics devices would be more serious than that of conventional electronic devices due to the applied magnetic fields during device operation.

8.2 Suggestions for Future Work

(1) In this work, we have already demonstrated that the atomic diffusion of Mn atoms to Cu spacer with the aid of Ni-Cu intermixing at high electrical stress would not only cause a reduction in the spin-dependent scattering at the NiFe/Cu or Co(Fe)/Cu interfaces, it also leads to the deterioration of exchange-bias coupling which weaken a complete anti-parallel spin state between the pinned and free layers. The activation energies of interdiffusion for CoFe-FeMn SVs and CoFe-IrMn SVs were determined at 2.16 and 2.49 eV, respectively (Saito, 1998). CoFe-IrMn SVs also showed better thermal stability in comparison with CoFe-FeMn SVs during Saito et.al.'s annealing

experiment with the annealing temperature increased from 210 to 285 °C. It indicates that replacing the FeMn by IrMn as AFM layer may further enhance the EM reliability of NiFe/(Co or CoFe)/Cu/(Co or CoFe)/NiFe/Mn-AFM GMR SV devices operated at high current density, but more systematic and quantitative experimental works are needed to verify this assumption and to find out the physical reason behind it.

(2) The Hall effect accelerated EM failure model that has been developed in this thesis is new and well fits the experimental works which have been done for the NiFe/Co/Cu/Co/NiFe SV MLs. Orthogonal pulsed magnetic field and electrical field concurrently applied to the EM testing samples closely simulate the real working conditions of GMR read heads. Therefore, it is recommended that systematic and quantitative studies be made of the contributions of Hall effect in the EM phenomenon of CoFe-TSVSDs. Understanding these failure mechanisms and therefore providing the possibilities of optimizing the GMR head reliability is of great practical concern. Systematic incremental values of external magnetic field strength below the interlayer coupling field might be applied. Lifetime measurement under the concurrent electrical and pulsed magnetic field with different duty factors would also be carried out. Magnetic performance of these CoFe-TSVSDs stressed at different EM testing conditions needs to be measured. The well agreement of numerical simulation with experimental measurement and characterization of these SVSDs will advance our understanding of the complete picture of mass transport during EM of GMR read heads and to provide a strong proof to support the model.

LIST OF PUBLICATIONS

Journal articles

1. Jing Jiang, Seongtae Bae, and Sunwook Kim, "Effects of Cu inter-diffusion on the electromigration failure of FM/Cu/FM tri-layers for spin valve read sensors", *IEEE Trans. Magn.,* **43**, 2836-2838 (2007)
2. Jing Jiang, Seongtae Bae, and Hojun Ryu, "Magnetic instability of giant magnetoresistance spin-valve multi-layers due to electromigration-induced inter-diffusion", *IEEE Trans. Dev. Mater. Reliab.*, **8**, 680-688 (2008)
3. Jing Jiang, Seongtae Bae, and Hojun Ryu, "Magnetic instability of giant magnetoresistance spin-valves due to electromigration-induced inter-diffusion", *Thin Solid Film* (impact factor: 1.727) **517**, 5557-5562 (2009)
4. Jing Jiang, Ding Gui Zeng, Hojun Ryu, Kyung-Won Chung, and Seongtae Bae, "Effects of controlling Cu spacer inter-diffusion by diffusion barriers on the magnetic and electrical stability of GMR spin-valve devices", J. Magn. Magn. Mater. **322**, 1834-1840 (2010)
5. Jing Jiang, Ding Gui Zeng, Kyung-Won Chung, Jongryoul Kim, and Seongtae Bae, "Hall effect-induced acceleration of electromigration failures in spin valve multi-layers under magnetic field", Appl. Phys. Lett., 98, 162504-(1-3) (2011)

Conference Presentations

1. Jing Jiang, Sunwook Kim, and Seongtae Bae, "Effects of Cu interdiffusion on electromigration failure of FM/Cu/FM tri-layers for spin valve read sensors", 10th Joint MMM–Intermag Conference, January 7-11th, 2007, Baltimore, Maryland, USA
2. Jing Jiang, Seongtae Bae, and Hojun Ryu, "Magnetic instability of giant magnetoresistance spin-valve multi-layers due to electromigration-induced inter-diffusion", Intermag 2008 conference proceedings, May 4-8th, 2008, Madrid, Spain
3. Jing Jiang, Seongtae Bae, and Hojun Ryu, "Significant enhancement of electromigration-induced failure lifetime due to an ultra-thin Co insertion at the NiFe/Cu/interface in GMR spin-valve multi-layered devices", 53rd Conference on Magnetism and Magnetic Materials, November 10-14th, 2008, Austin, Texas, USA